NASA SP-5102

TECHNOLOGY UTILIZATION

TECHNOLOGY OF FORCED FLOW AND ONCE-THROUGH BOILING

A SURVEY

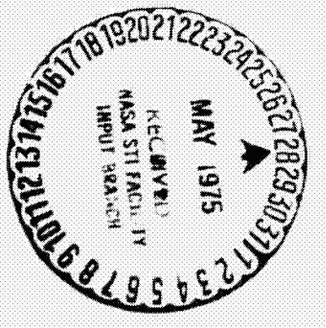

NATIONAL AERONAUTICS AND SPACE ADMINISTRATION

NASA SP-5102

TECHNOLOGY OF FORCED FLOW AND ONCE-THROUGH BOILING

A SURVEY

By Heinz F. Poppendiek
and Cullen M. Sabin

Prepared under contract by
Geoscience Ltd.

Technology Utilization Office 1975
NATIONAL AERONAUTICS AND SPACE ADMINISTRATION
Washington, D.C.

Preface

A large amount of the recent technical information in the field of forced flow and once-through boiling heat transfer and pressure drop has resulted from the NASA-AEC Rankine cycle space power programs. This information is in the form of experimental, semi-empirical, and analytical functions. A range of working fluids including liquid metals, organics, and cryogenics in addition to water and refrigerants has been studied. As a result of this work, a number of advances have been made in forced flow boiler design. The use of boiler tube inserts to improve heat transfer performance is of particular note.

A number of new forced flow boiler applications have become important in the last several years (for example, in mobile propulsion systems, topping cycles for power plants, bottoming cycles for power plants, advanced refrigeration systems, boiling nuclear reactors, and geothermal power systems). There are also many familiar forced flow boiler applications where further design optimization may be of value (for example, in auxiliary power plants, solar evaporation systems, and process heat exchangers involving change of phase). Therefore, this monograph has been written with the thought that the newly-developed boiler technology may be of value to such boiler applications.

Experimental, semi-empirical, and analytical boiling information has been compiled in this monograph, together with boiling regime transition

criteria. These boiler design functions are then applied in example boiler designs; the illustrations give the reader sufficient information to demonstrate the value of using boiler tube inserts and developing optimum boiler designs.

The monograph contains over 100 technical references in the boiling field (many of which contain other references and compilations of other contributions which can be found in the literature). It is clear that reference omissions exist because of the breadth of the field and space limitations. The references presented are thought to be representative and useful to those who may want further details.

Solana Beach, California
December 1973

Heinz F. Poppendiek
Cullen M. Sabin

Acknowledgments

The authors want to acknowledge a number of people who contributed to this monograph.

Mr. Martin Gutstein, of NASA-Lewis Laboratory, the technical monitor, made a detailed technical review of the manuscript; his valuable suggestions were incorporated, thereby yielding a more complete document. Mr. Donald Vargo of NASA-Lewis Laboratory, the Technology Utilization monitor, made recommendations about the format in which the complex technical information was presented to make it more valuable to the range of potential readers in technology. Mr. E. R. Furman also reviewed the final manuscript.

Appreciation is extended to Ms Doña Gossett, who typed the manuscript, and to Ms Doris Malley, who prepared the figures and drew the boiling phase-distribution illustrations.

Messrs Robert English of NASA-Lewis Laboratory and R. Miner and J. Hamilton of the NASA Technology Utilization Office in Washington played important parts in initiating the program.

TABLE OF CONTENTS

Chapter	Title	
1	INTRODUCTION	1
2	PHYSICAL DESCRIPTION OF BOILING HEAT TRANSFER PROCESSES	19
3	REPRESENTATIVE EXPERIMENTAL, SEMI-EMPIRICAL AND ANALYTICAL INFORMATION ON BOILING HEAT TRANSFER AND PRESSURE DROP	51
4	FLOW REGIME TRANSITIONS	125
5	BOILER DESIGN EXAMPLES	213
6	BOILER APPLICATIONS	255
Appendix		
A	THERMAL PROPERTIES OF SOME OF THE IMPORTANT WORKING FLUIDS	259
B	EQUATION SETS FOR CHAPTER 3	267
	EQUATION SETS FOR CHAPTER 4	281
C	ILLUSTRATIVE HEAT TRANSFER AND PRESSURE DROP DERIVATIONS	297
D	COMMENTS ON SOME ASSOCIATED TOPICS	305

CHAPTER 1: INTRODUCTION

This monograph contains representative boiling heat transfer and pressure drop information obtained primarily from past NASA and AEC programs; the results presented are directly applicable to forced flow and once-through boiler systems found in many technological areas.

The primary purpose of this monograph is to present representative boiling data that describe the technology of forced flow and once-through boiling. The information given in this document is intended to be useful for both technical and non-technical readers. Chapters 1, 2, and 6 have been primarily prepared for managers and those who are not directly involved in technical activities. Chapters 3, 4, 5, and the Appendix have been prepared for technical people such as designers of power systems.

The forced convection boiler has a number of advantages that should be of particular interest to designers in modern technology. In a properly designed system, there is little possibility of flow mal-distribution such as sometimes occurs in natural circulation systems. Heat transfer characteristics are usually consistent, and conductances are predictable, so that higher heat fluxes may be employed with safety. This leads to more compact, lighter weight equipment. It should be noted, however, that in gas-fired systems particularly, the controlling heat transfer resistance may be on the hot side, so that increased fluxes would require extended surfaces. If in a power generation system the working fluid is very expensive, a forced flow boiler can be designed especially for small holdup volume. If the fluid is temperature sensitive, the boiling side wall temperatures can be "tailored" to

maintain maximum heat transfer rates without overheating the fluid. Finally, the forced flow and once-through configurations may be the only type which can satisfy a specific need (such as the automotive Rankine cycle power plant design having a very short time-response boiler).

Forced convection vaporization processes to which the material in this monograph is appropriate occur in many areas of technology; in power generation, in refrigeration machinery, in vaporization of cryogenic fluids, and many other applications. However, since the majority of the information presented here was originally obtained in Rankine cycle power system development programs, the terminology appropriate to power systems engineering has been used throughout most of the text.

BOILER TYPES

The simplest form of boiler is a pressure vessel containing a vaporizing fluid, with a heat source surrounding it. Usually, however, the heat transfer area is increased by utilizing arrays of tubing together with one or more larger pressure vessels.

There are two general classifications of boilers with tube matrices to increase heat transfer area. These are the "fire-tube" type, in which the vaporizing fluid surrounds tubes through which a heated stream flows; and the "water-tube" type, in which the heated stream flows over the outside of the tubing and the vaporizing fluid flows within. In each of these two classifications, there are also two subclassifications: the vaporizing fluid may be circulated by gravity through density difference ("natural convection") or the vaporizing liquid may be circulated by a pump ("forced convection") The distinction between the latter two categories is clear from a systems standpoint; however, the boiling mechanisms are probably little affected by the means of circulation. The once-through boiler is a specific type of forced convection "water tube" boiler.

HISTORICAL INFORMATION

It is thought appropriate to present to the reader some historical information on boilers that have been used in technology. This summary is not intended to be all-inclusive, but only illustrative of some of the contributions made in the past. The classifications into which the boilers described in the following paragraphs fall are outlined below.

A. Vaporizing Fluid Flowing Over Tubes ("Fire Tube")
   1. Natural Convection
      a. Horizontal return-tubular
      b. Vertical tube internally fired
      c. Scotch Marine
   2. Forced Convection
      Large air conditioning water chiller evaporator

B. Vaporizing Fluid Flowing Inside Tubes ("Water Tube")
   1. Natural Convection
      a. Longitudinal drum
      b. Two drum
   2. Forced Convection
      a. Recirculating types
         (1) Steam pumping (Loeffler)
         (2) Water pumping (LaMont)

b. Once through

(1) Flash boiler (Serpollet)

(2) Steam automobile (White)

(3) Mercury vapor Rankine cycle (SNAP-8)

Horizontal Return-Tubular Boiler

Figure 1-1 shows the primary elements of a horizontal return tube boiler wherein hot combustion gases flow through tubes to heat the surrounding water. In this particular boiler, the combustion chamber is external to the boiler itself. This type has been used for small, stationary steam plants.

Internally-Fired Vertical Tube Boilers

Figure 1-2 shows a typical internally-fired vertical tube boiler. In this system, the combustion chamber is directly below the vertical fire tube array. The type is referred to as internally fired because the lower portion of the water tank surrounds the furnace. It is also used for small, stationary steam plants.

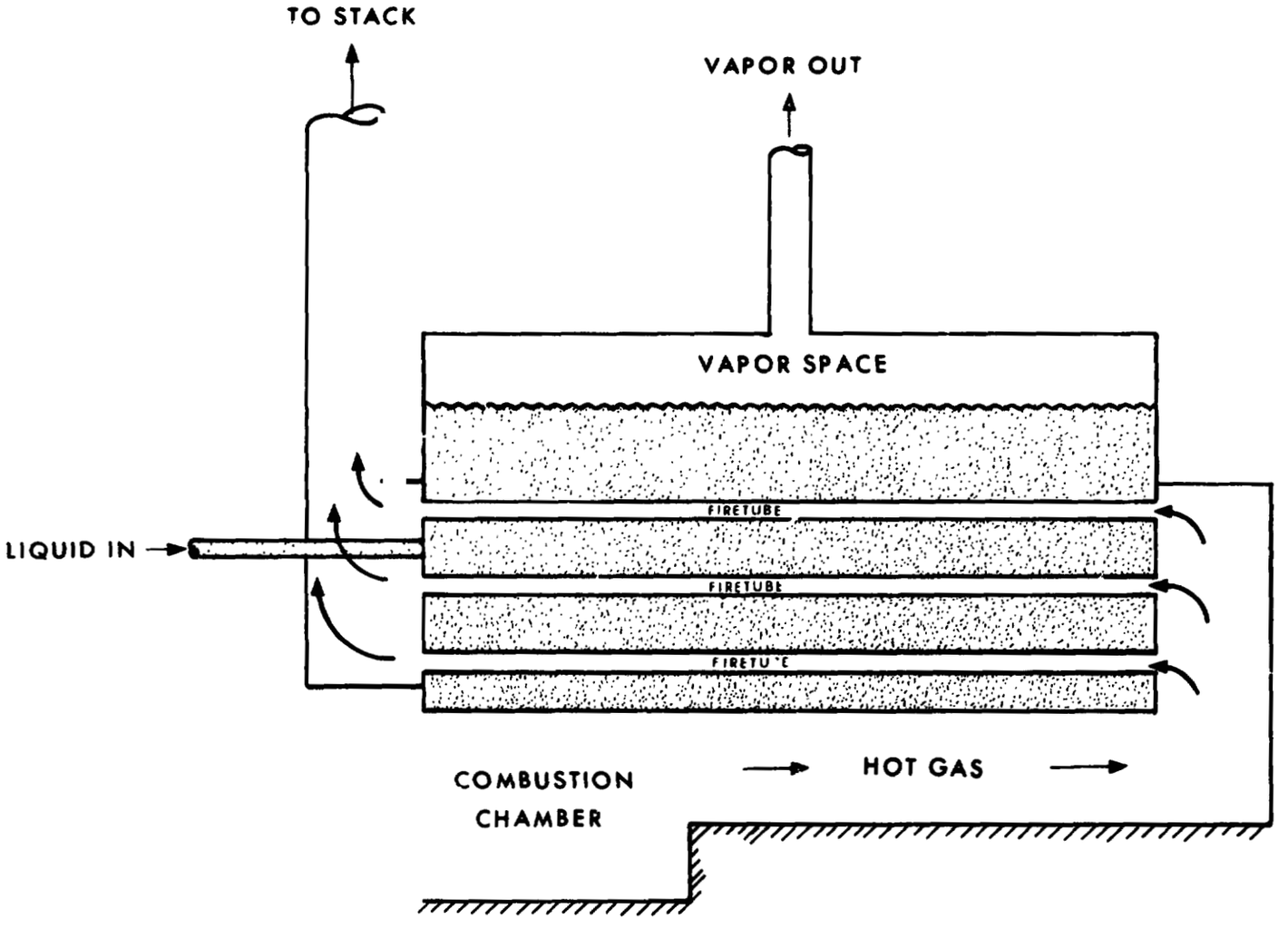

Figure 1-1. Horizontal return-tubular boiler.

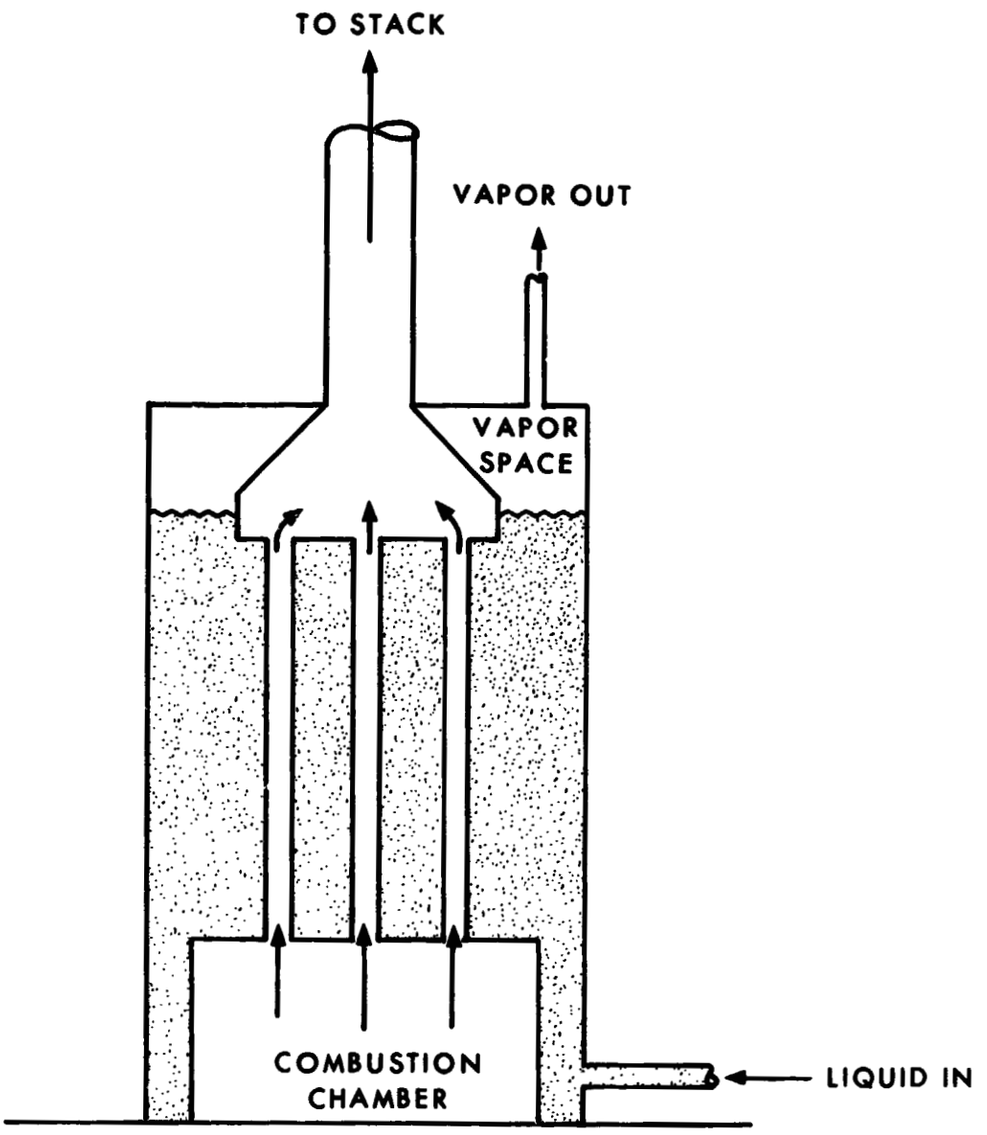

Figure 1-2. Vertical tube internally fired boiler

Scotch Marine Boiler

Geometrically, this boiler is not much different from the horizontal return-tubular type, except that it is internally fired. The combustion chamber is directly below the horizontal boiler tubes, and completely inside the boiler shell, with a hot gas passage leading to one end of the tube array. These boilers contain large quantities of water and steam and are utilized in marine service where space is of importance and there are advantages to significant energy storage in the boiler.

Water Chiller Evaporator

An example of a forced convection boiler in which the vaporizing fluid flows over the outside of the tube bank is found outside of the field of power generation. The evaporators in many mechanical refrigeration machines using cold water as an intermediate heat exchange fluid employ such an arrangement. In this case, the water to be chilled flows through horizontal tubing instead of combustion gases, and the vaporizing refrigerant is pumped into the tube bank from below. A considerable amount of recirculation due to gravity and momentum exchange from the refrigerant inlet stream is also found in a typical evaporator of this type since the inlet flow is not usually well distributed along the bank. A schematic diagram of such a boiler is shown in Figure 1-3. Not shown are the baffles which usually are included to improve flow distribution.

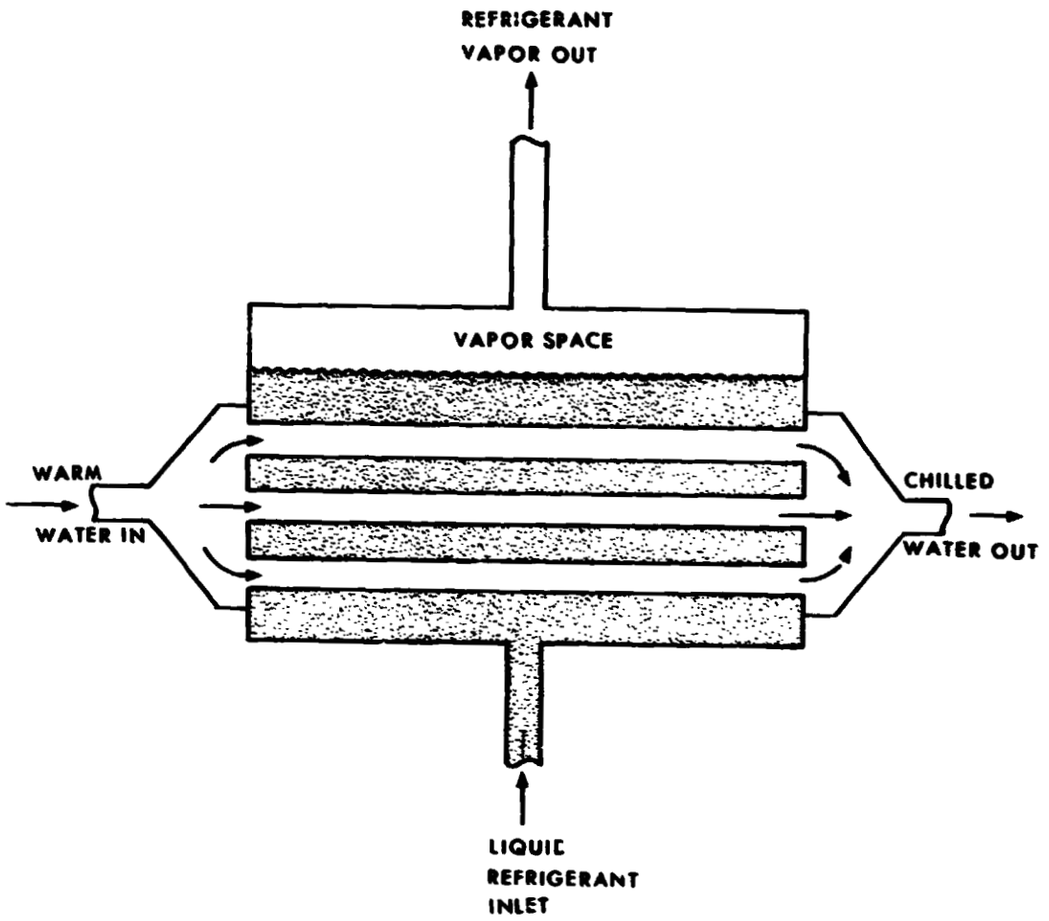

Figure 1-3. Water chiller evaporator.

Longitudinal-Drum Water Tube Boiler

Figure 1-4 shows a schematic diagram of a longitudinal-drum water tube boiler. Combustion gases are ducted across the tube bundle by means of a baffle system. Typical installations also include a superheater tube bank and a water preheater, or "economizer," which are not shown in the diagram. In this boiler, water circulation is insured by the inclined tube bank. Direction of the circulation is indicated by arrows.

Multiple Drum Water Tube Boiler

There are many arrangements for straight and bent tube, two and three (or more) drum boilers. Most of these installations include air preheaters, water preheaters (economizers) and superheaters. Usually the furnace walls are lined with water tubing in addition.

Steam Pumping Boiler

In a forced convection recirculating boiler, the designer can choose to pump either saturated steam or saturated water. In the Loeffler boiler, steam is pumped through a superheater coil, and most of the steam is recirculated to the unfired liquid reservoir to produce more steam. This system must be operated at high pressure in order to reduce the steam volume to be pumped to manageable proportions. The salient feature of this boiler is that the liquid supplied to it need not be particularly pure. Impurities are retained within the liquid reservoir. A diagram of this arrangement is shown in Figure 1-5.

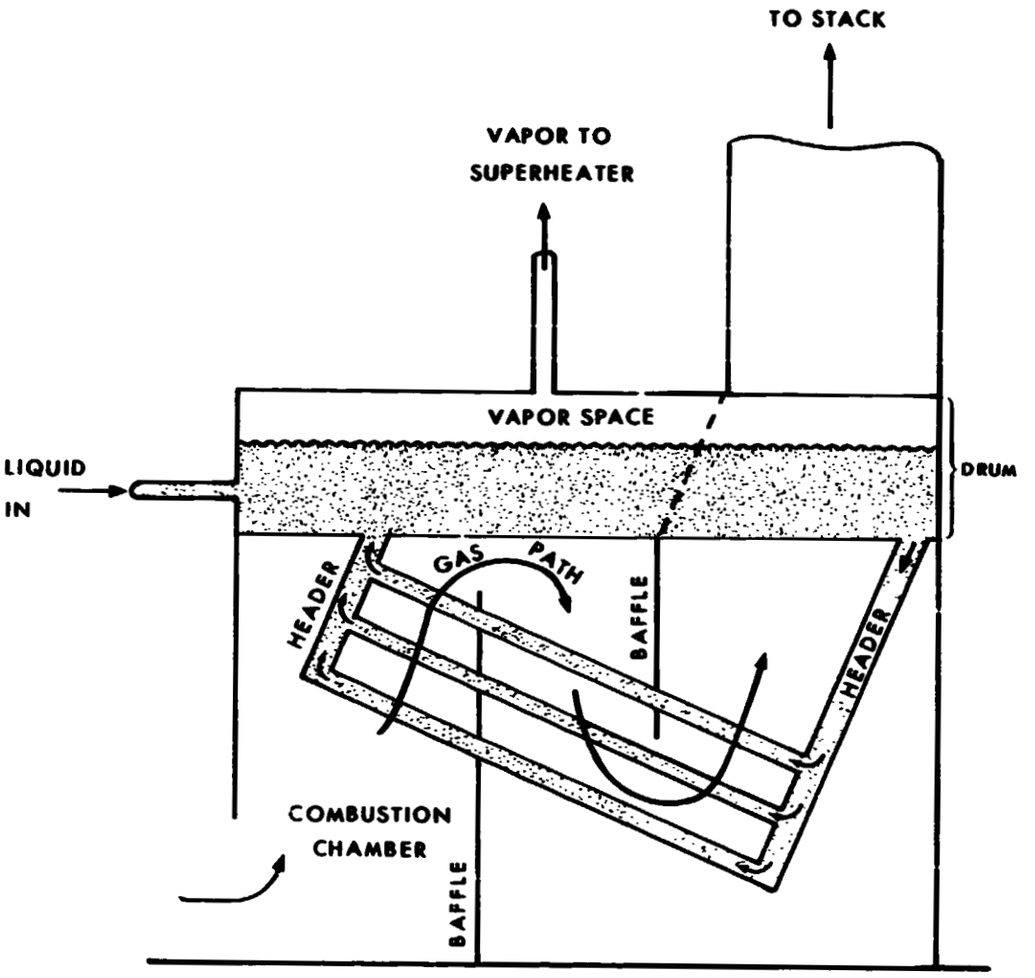

Figure 1-4. Longitudinal drum water tube boiler.

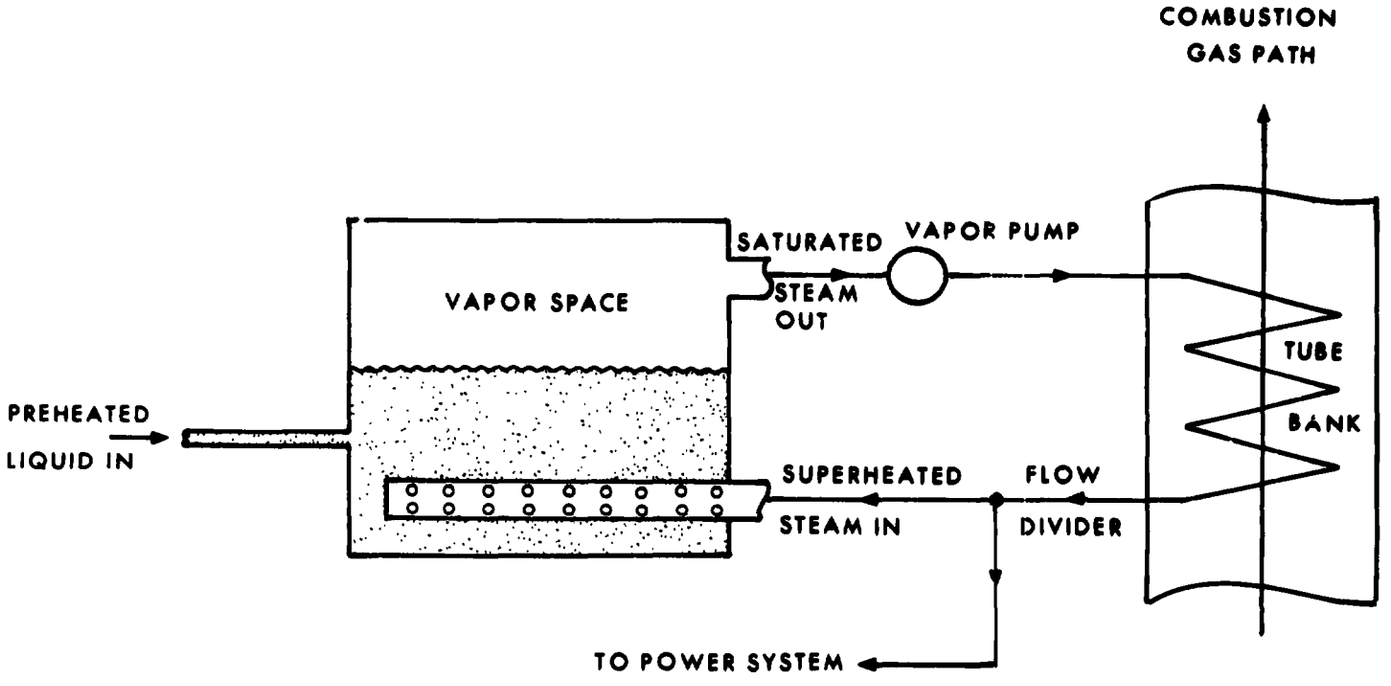

Figure 1-5 Vapor pumping boiler.

Water Pumping Boiler

In the LaMont boiler, the designer has chosen to circulate saturated water. As in the Loeffler boiler, the liquid drum is unheated, but the tube surfaces in this case have water pumped through them at several times the rate required to provide the necessary steam flow. Steam separation is accomplished in the drum, and the steam produced is routed to a superheater.

Flash Boiler

A type of once through boiler is the so-called flash boiler, in which the preheated vaporizing fluid is sprayed into the hot tubing, partially vaporizing in the nozzle. The liquid droplets film boil under normal circumstances, since without elaborate temperature control, the tube wall temperature will always be above the transition temperature. Some modern work associated with space auxiliary power programs has come very near to this design concept.

Steam Automobile Boiler

Most steam automobile boilers have been of the once through, single coiled tube design. An example of this type is the White Automobile, developed in 1907, shown schematically in Figure 1-6. This unit is quite similar to some of the boilers being used in steam car developments today. One notable difference is that in the White boiler the liquid flow was downward through the coil and vertical tubing interconnections were required to prevent water from flowing through the coil unvaporized.

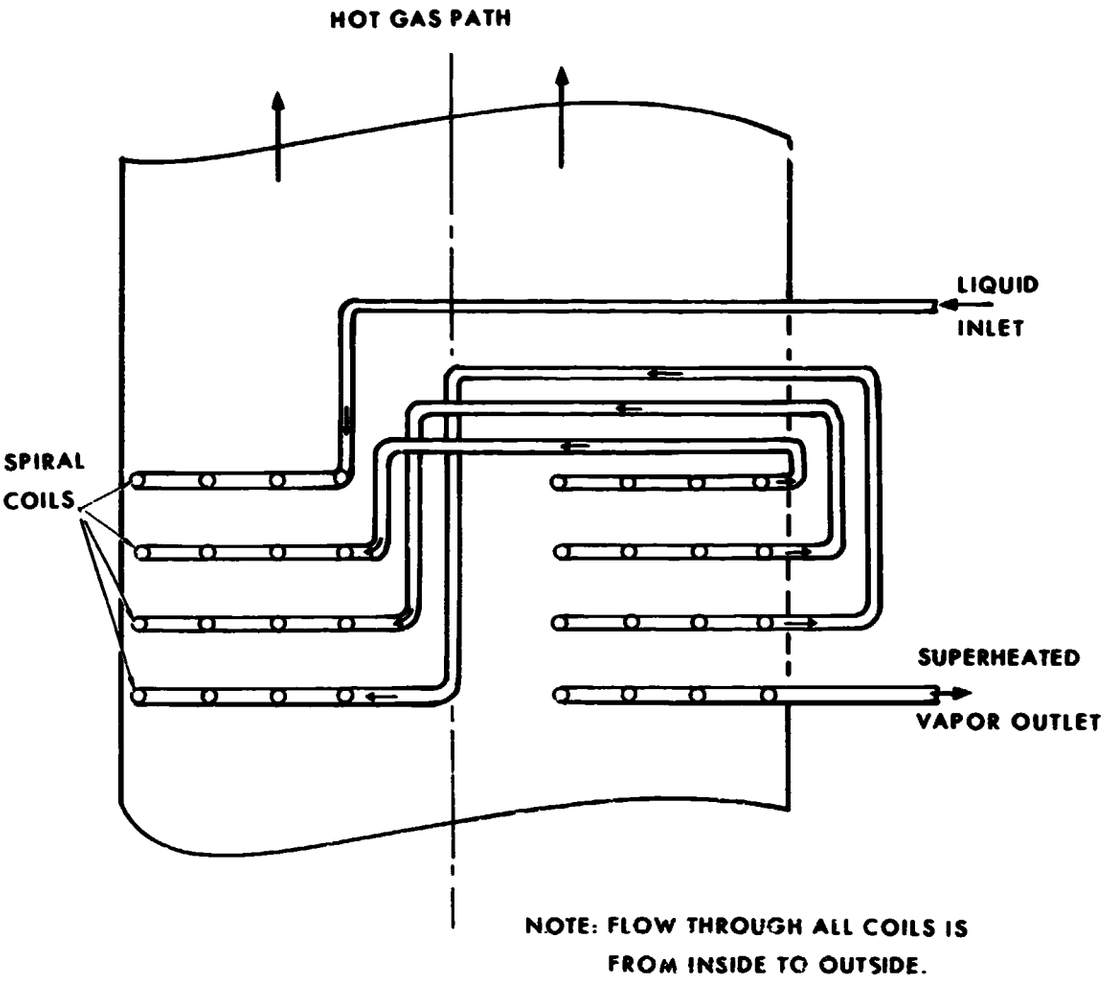

Figure 1-6. Section through a portion of the White automobile boiler.

In most of the present day automobile boilers, the first few rows of tubes next to the combustor are usually vaporizers, and rows farthest from the combustor are devoted to liquid preheating, with superheater rows between.

Mercury Boiler

An example of a liquid heated boiler is the Space Nuclear Auxiliary Power (SNAP-8) mercury system, which utilizes NaK as the heat source. The arrangement is pure counterflow, with the vaporization taking place in seven identical parallel passages. A schematic drawing of this system is shown in Figure 1-7. A complete description of this unit is given in Chapter 5.

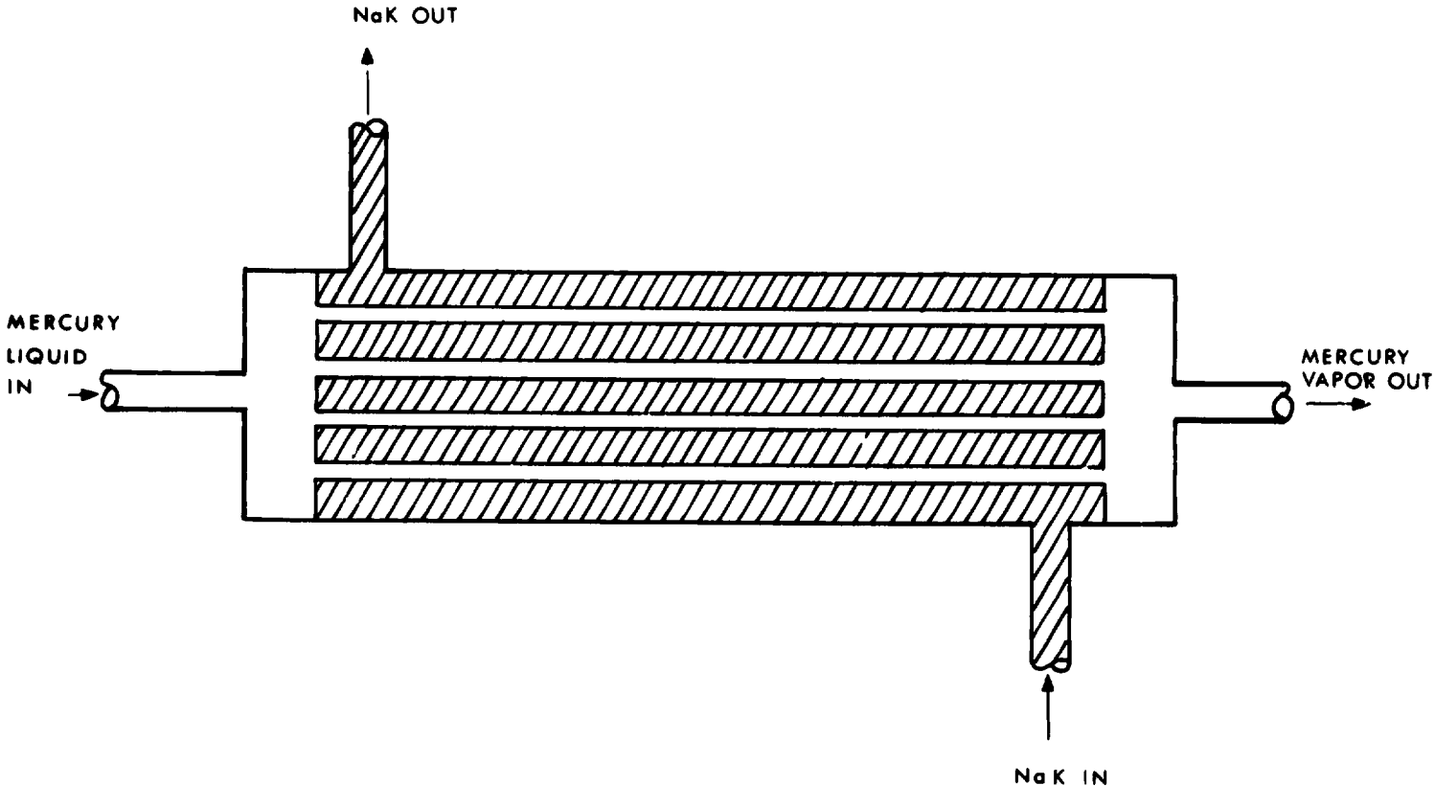

Figure 1-7. NASA SNAP-8 boiler arrangement.

WORKING FLUID TYPES

There are a number of working fluids that are used in boiler systems; the specific application involved usually defines the fluid type to be considered. Liquid metals are normally used in compact, high-power density systems because these fluids have excellent heat transfer properties and are characterized by relatively low vapor pressure. The latter feature means that heavy pressure vessels are not required. Organics are also used in power generation systems where low vapor pressures are desired in contrast to the high pressure water systems; however, the heat transfer characteristics are not as good as water or the liquid metals. Freons are used in refrigeration and airconditioning systems (the evaporators in these systems are special cases of boilers). Cryogenic fluids are normally used in aerospace systems where auxiliary power systems are driven by cryogenic vapor bleedoff.

In Appendix A there are presented in graph form the thermal conductivity, specific heat, viscosity, and density of the liquid and vapor phases of some of the more practical working fluids found in technology. Vapor pressure and surface tension information is also given.

CHAPTER 2

PHYSICAL DESCRIPTION OF BOILING HEAT TRANSFER PROCESSES

When compared to single phase heat transfer and pressure drop in forced flow heat exchange systems, two phase or boiling heat transfer and pressure drop are more complex. In boiling flow, the presence of the two phases complicates the flow type because the relative location of the two phases in a flow tube both in radial and transverse positions is variable. This relative location depends on whether the composite flow is linear or helical in character, and on the vapor quality and mass flow rate. In this chapter, physical descriptions are given of the more important distributions of the liquid and vapor phases that can exist in forced flow boiling. These descriptions are presented as an introductory basis for the experimental, semi-empirical and analytical boiling functions given in Chapters 3 and 4.

The phase distribution descriptions which follow are arranged approximately in the order in which they occur along a boiler tube. Figure 2-1 shows the general locations of the various phase distributions in a boiler tube in relation to the vapor quality (fraction of vapor) and bulk fluid temperature profiles. It is pointed out, however, that not all regimes exist in a given boiler tube. The criteria that will assist the designer in defining the phase distributions in operation are discussed in Chapter 4. It is also reemphasized that because flow conditions change continually along a boiler tube, the processes involved are developing rather than steady state. In addition, two phase flow has much larger changes in mass flow rates and velocities than are found in single phase flow.

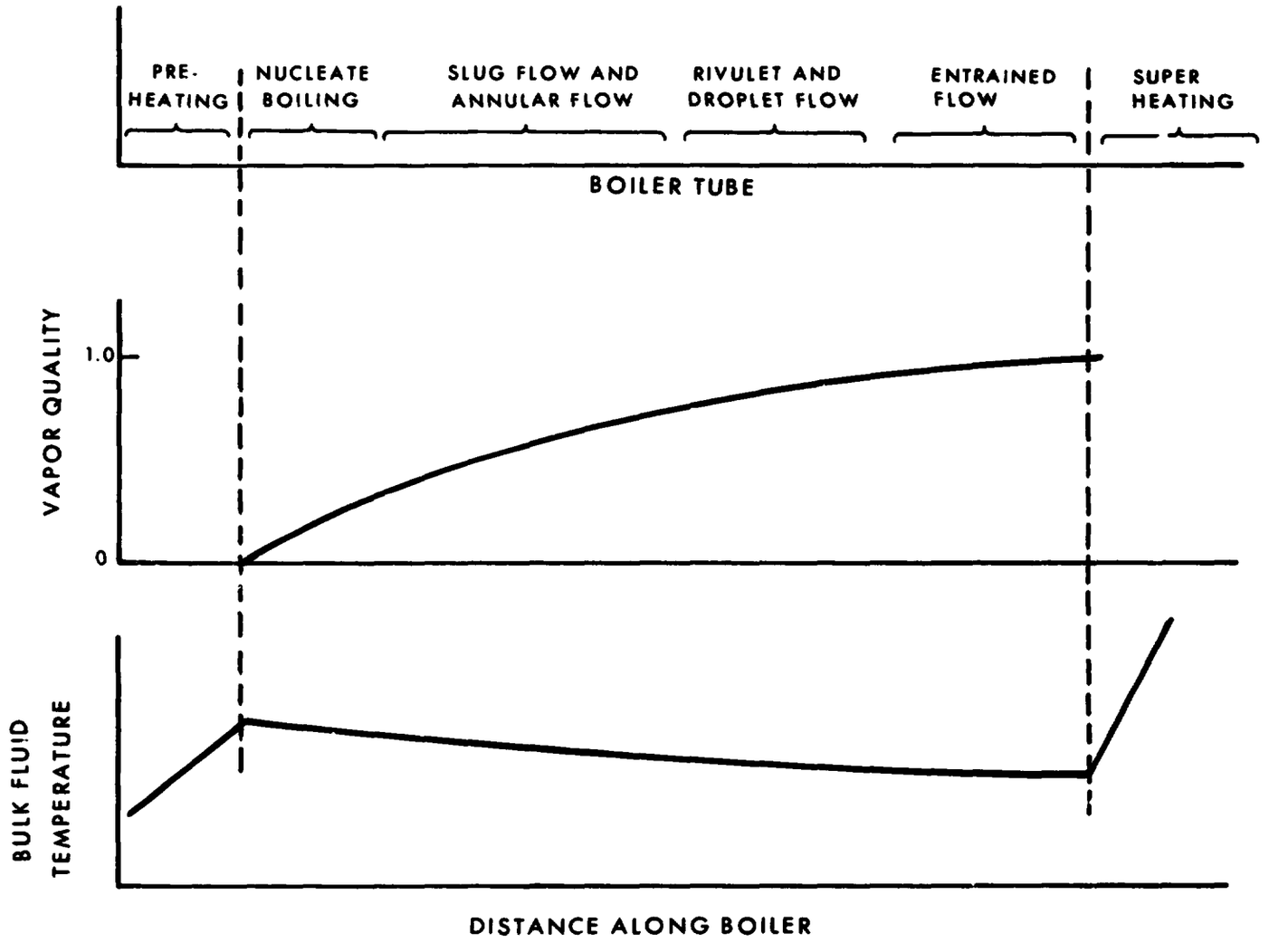

Figure 2-1. Typical flow regimes in a boiler tube.

DESCRIPTION OF THE MAJOR BOILING REGIMES

1. Nucleate Boiling or Boiling Inception At A Surface

As a working fluid flows through a boiler, it first encounters a zone or component called the preheater wherein the bulk liquid temperature is raised to the boiling point. Near the preheater exit the temperatures at the tube wall are somewnat greater than the saturation temperature (thermodynamic equilibrium boiling temperature). When the liquid superheat temperature at the wall reaches a certain critical value (depending upon the type of tube material, the number of nuclei at the surface, the amount of dissolved gases present and many other parameters), ebullition or boiling begins at the tube surface. Bubbles are born, grow, and collapse at nucleation sites covering various parts of the surface. This process, which repeats itself over and over again, is illustrated by an artist's drawing in Figure 2-2. In nucleate boiling, heat transfer is improved significantly over forced convection where no phase change occurs. The improvement is related primarily to two mechanisms: namely, turbulent agitation of the boundary layer by bubble growth and collapse,[1] and the added evaporative heat transfer within the bubble.[2,3]

The amount of liquid superheat observed can range up to several hundred degrees Fahrenheit, although in most forced flow systems it is usually small. Usually bubble generation starts in the region where the bulk is still subcooled. Even beyond this point, net vapor generation does not necessarily coincide with the location at which

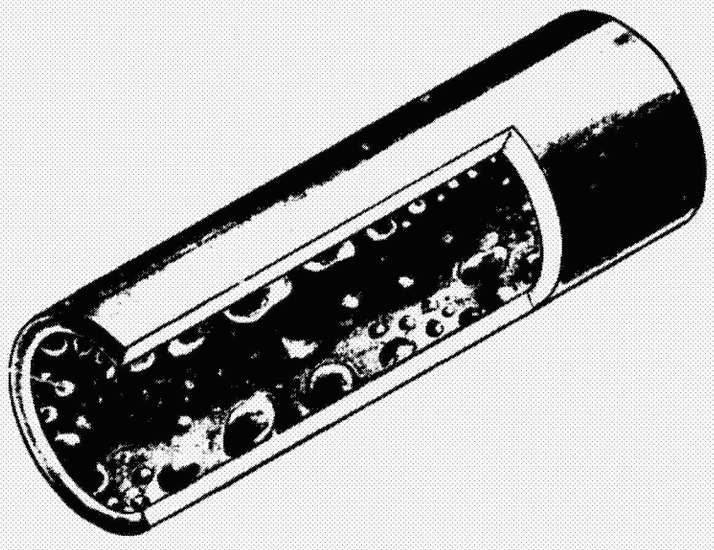

Figure 2-2. Nucleate boiling.

the bulk mixed mean fluid temperature is at the saturation temperature. The fluid in the center of the tube can still be subcooled while a stable layer of bubbles is carried along in the wall layers. There is frequently a significant void fraction in the flow by the time the equilibrium saturation temperature is reached.

B. Slug Flow

As one proceeds down the boiler tube beyond the nucleate boiling region (in the preheating zone), a net quantity of vapor is generated because the bulk of the liquid is now saturated and bubble collapse no longer occurs. Consequently, slugs of vapor and liquid exist in that part of the boiler tube, each phase moving through the tube at about the same velocity. Depending upon the surface tension and wetting characteristics of the liquid and the tube wall surface conditions, the liquid slugs can wet or not wet the tube wall. In the former case, large vapor bubbles flow through that part of the tube. In the latter case, the flow is characterized by large drops flowing through that region of the tube. These features are shown in Figure 2-3.

C. Annular Flow

There is another phase distribution type that can occur in the low vapor quality region and it is called annular flow. Usually, a low velocity liquid annulus exists contiguous to the boiler tube wall with a higher velocity vapor core. The opposite arrangement can also exist under some circumstances; namely, a vapor annulus at the wall with a liquid core.

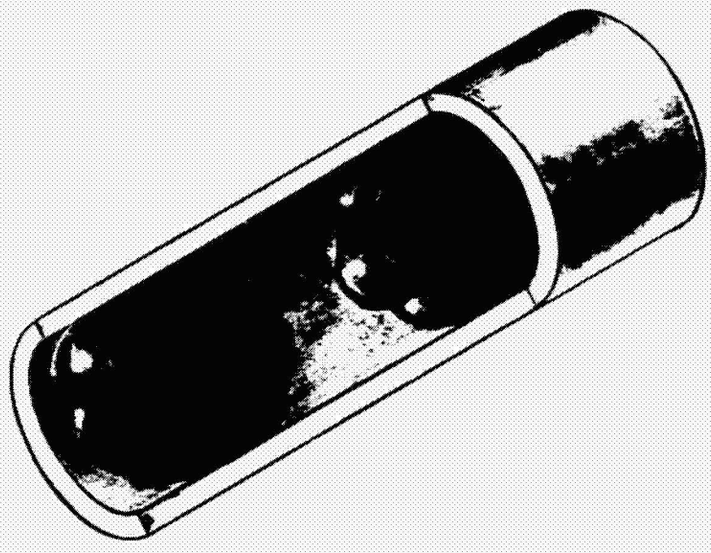

nonwetting

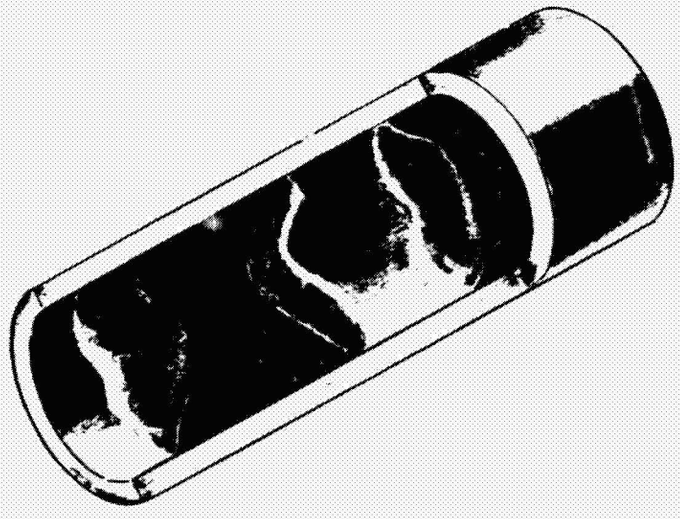

wetting

Figure 2-3. Slug flow.

These two different versions of annular flow (shown in Figure 2-4) are controlled by the liquid wetting characteristics, the wall-fluid temperature difference and whether vaporization is in operation at the solid-liquid interface or the liquid-vapor interface. The fluid flow fields in the two phases are related by the common velocities and shear stresses at the vapor-liquid interface.

D. Rivulet and Droplet Flow

In the intermediate vapor quality region, slug and annular flow distributions can change to rivulet and droplet flow. When the liquid phase mass fraction becomes small, the large drops (which used to fill the total tube cross section in slug flow) are converted to droplets and rivulets that flow along the boiler tube wall; likewise, the liquid film (which used to completely cover the tube wall in annular flow) is ruptured and converted to rivulet and droplet flow. The surface tension characteristics of the system can cause good contact (wetting) between the droplets and rivulets with the tube wall or, alternatively, vapor film insulation (nonwetting) can exist. These features are shown in Figure 2-5.

E. Entrained Flow

In all practical boilers, the mixed mean vapor quality at that point down the boiler tube where the wall is no longer wet is significantly less that 100 percent. The remaining liquid must, therefore, be entrained in the vapor flow. The quality at which the annular flow

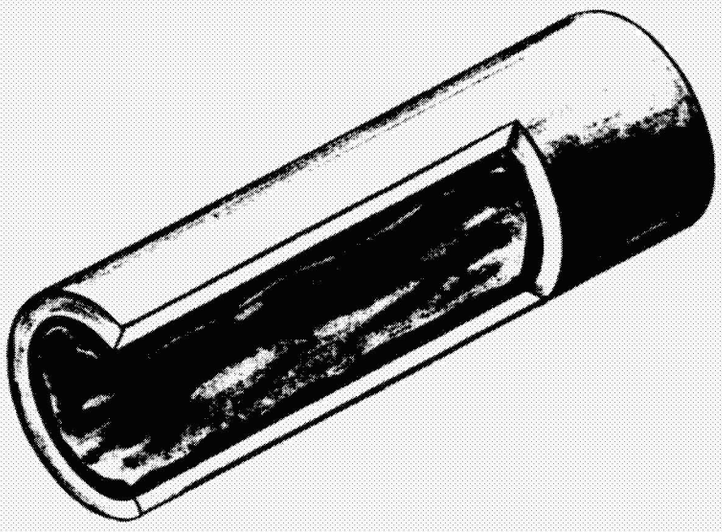

wetting

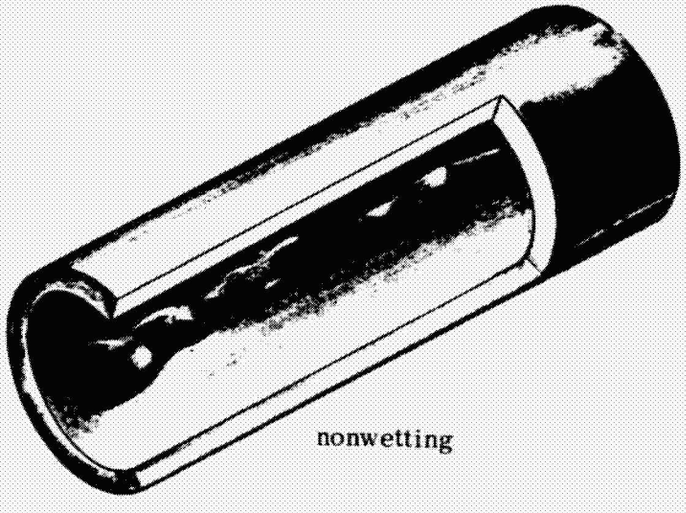

nonwetting

Figure 2-4. Annular flow.

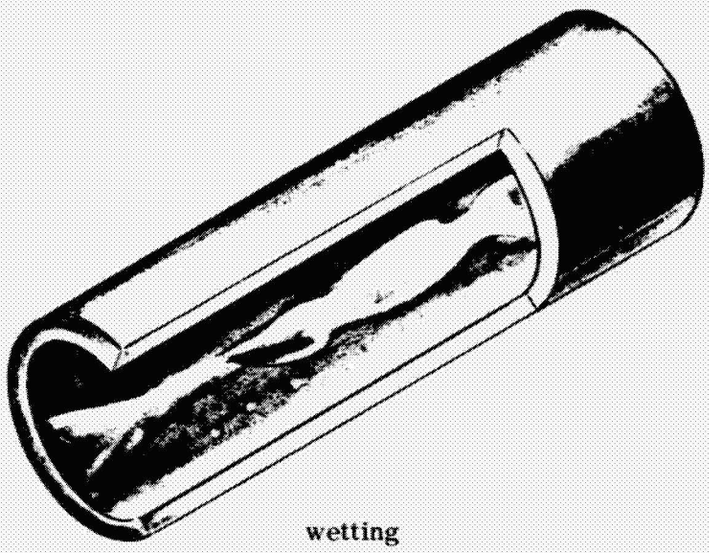

wetting

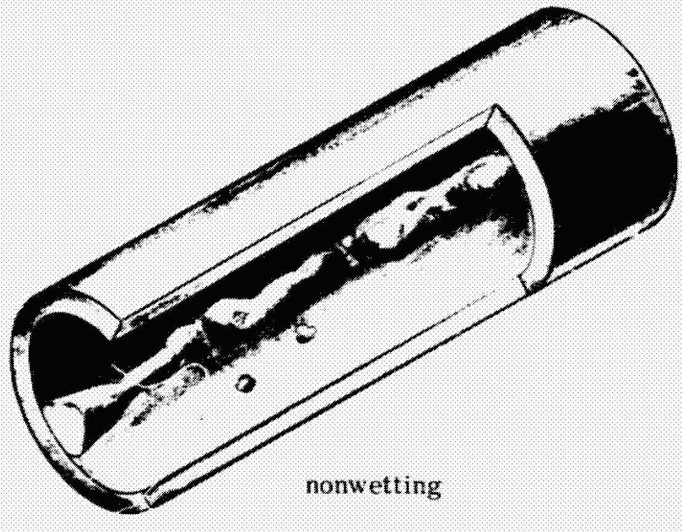

nonwetting

Figure 2-5. Rivulet and droplet flow.

ends can vary for over a wide range, with typical values for good designs with wetting fluids ranging from 60 to 80 percent. Under extreme conditions with wetting fluids however, the loss of the liquid layer on the wall has been shown to occur at qualities as low as ten percent.

Some of the major entrainment mechanisms are related to non-wetting of the liquid at the boiler tube wall, roll wave action at the surface of liquid annuli, spray from bubble generation in thin liquid annuli, and vapor generation under a liquid layer at the wall under high temperature difference (film boiling) conditions. Fog flow is a special case of entrained flow in which the droplets are very small. This case occurs in the high quality region. When the temperature difference between the wall and saturation values becomes sufficiently large in forced flow boiling, rivulet and droplet flow becomes unstable in that tiny droplets of the liquid are spalled or shed from the rivulet or droplet (see Figure 2-6). When the drops get small enough they can even bounce back and forth between opposite sides of a boiler tube wall (see Figure 2-7). This disintegration mechanism plays an important role in creating fog droplets which comprise fog flow (see Figure 2-8), wherein tiny entrained fog droplets are distributed across the diameter of a boiler tube with probably the greatest density in the central region because evaporation processes are taking place near the wall. Small droplets can also be formed by fragmentation from large entrained droplets by shear forces. This flow

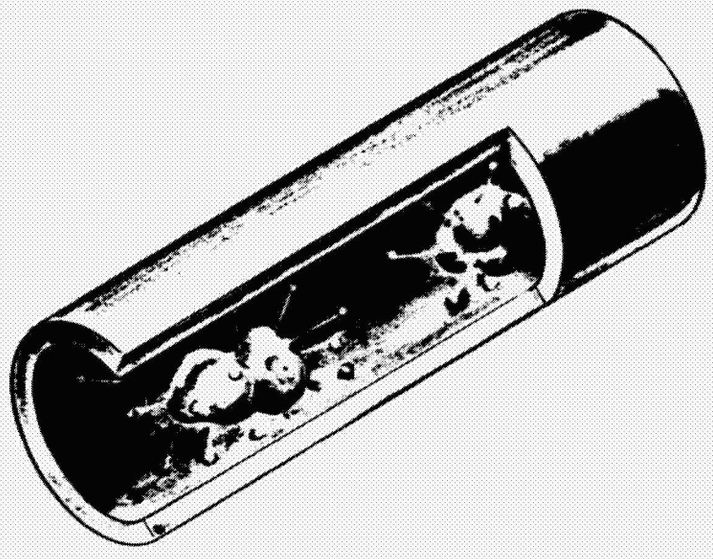

Figure 2-6. Spalling drops.

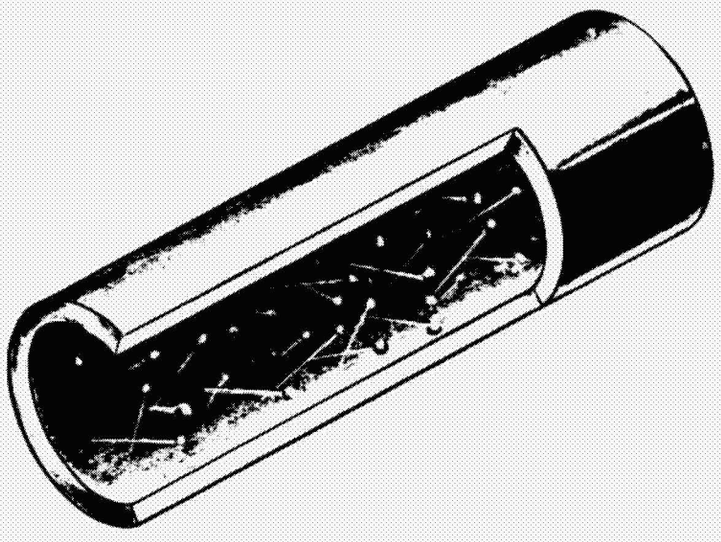

Figure 2-7. Bouncing droplets.

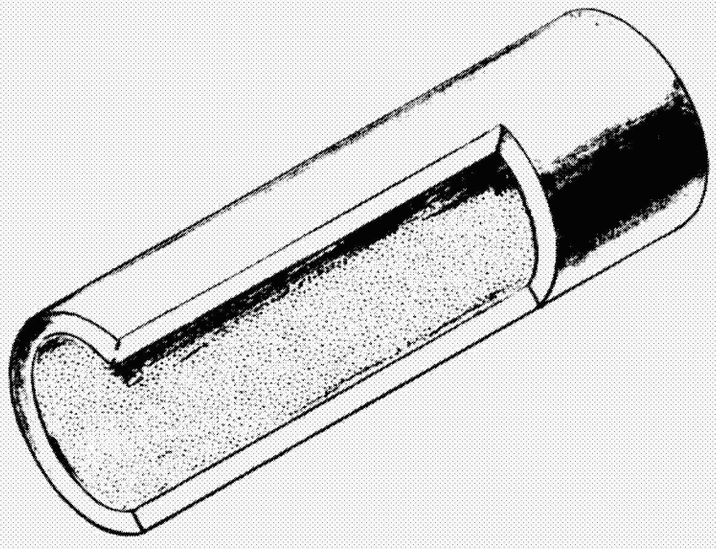

Figure 2-8. Fog flow.

distribution type occurs in the high vapor quality region as well as in the initial part of the superheated region.

F. Superheated Vapor Flow

Superheating of the vapor can occur beyond the boiling region prior to delivery of the working fluid to the turbine or expander. Sometimes a separate component called the superheater is used in the system to achieve this step. As indicated previously, small liquid fog droplets can, at times, exist in the core of the superheated vapor flow in a nonequilibrium state.

G. Flow Region Control by Tube Inserts

In traditional vapor generators, boilers, or evaporators, phase separation has been accomplished by gravity. A few arrangements have included centrifugal separators to remove last traces of liquid from the vapor flow. Liquid entrainment has usually been minimized by employing very long superheater tubing with complex flow paths. With the development of space power systems, however, neither gravity nor a long, complex flow path could be employed to prevent liquid carry-over into the expander, and boiler inserts began to be employed. Early boiler tube inserts were simply turbulence enhancing devices, although these have been replaced almost universally with flow rotating inserts; some of the pioneering work was done at the Oak Ridge National Laboratory in 1957.[4,5] The purpose of the flow

rotator is to centrifuge the more dense liquid droplets onto the heat transfer surface.

There are four principal tube inserts which provide fluid rotation which have been used in space power plant vapor generators. They are described below:

1. The helically grooved plug

   This device is a rod that has a number of spiral grooves around the outside, which fits inside the boiler tube tightly. When this device is inserted into the boiler tube, the spiral grooves form a number of parallel, small channels lying against the heat transfer area where the grooved plug is installed, usually in the preheat and low quality end of the boiler.[6] An illustration of the flow pattern type is shown in Figure 2-9.

2. The twisted tape divider

   This device is formed from a ribbon which is twisted around its long axis. When inserted into the boiler tube, it divides the tube across the diameter into two channels which spiral around the axis. Because of properties of usual boiler materials, the pitch-to-diameter ratio of these dividers is limited to about four, unless relatively thick ribbons are used.[7] An illustration of the flow pattern type is shown in Figure 2-10.

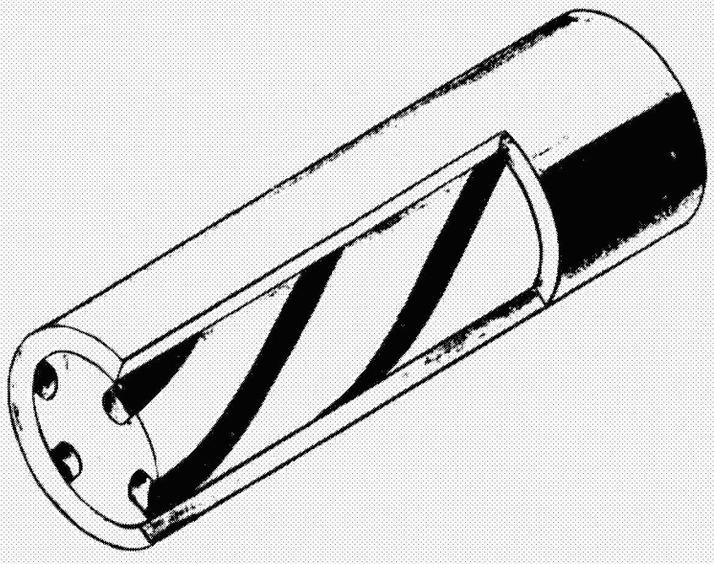

Figure 2-9. Helical flow: plug.

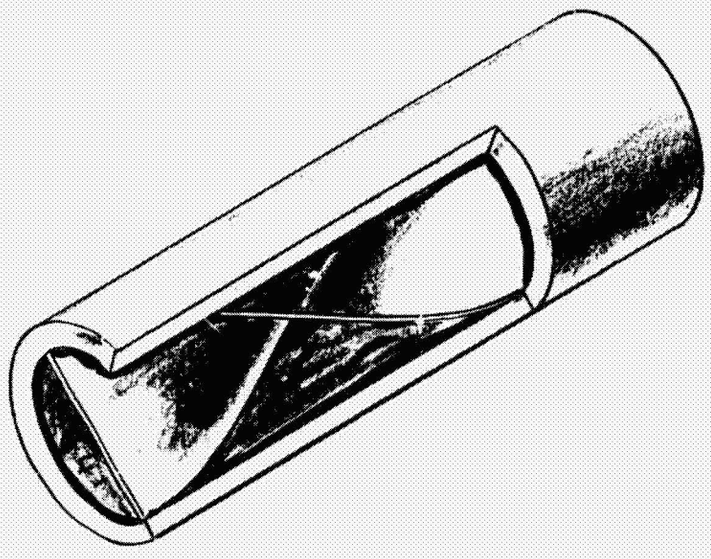

Figure 2-10. Twisted divider insert.

3. The helical vane

This device is a single screw thread of rectangular cross section which may extend all the way from the wall to the tube centerline. This geometry can be formed by wrapping rectangular stock around a mandrel, or by splitting washers along a diameter, welding them edge to edge, and then stretching the resultant helix to the proper pitch. In contrast to the twisted divider, the helical vane can be made in any pitch. Frequently, the vane is attached to a rod or tube called a centerbody, which lies along the axis of the boiler tube. This element serves to support the vane and can carry instrumentation as well.[8] Figure 2-11 illustrates the flow pattern for this insert.

4. The wire coil

This device is a helical wire coil which lies against the wall of the boiler tube.[9] Although it is usually made of round wire, it can be made of square wire as well, and in that form it is identical to a helical vane of square cross section. It can be made in any pitch. The resulting flow patterns are shown in Figure 2-12.

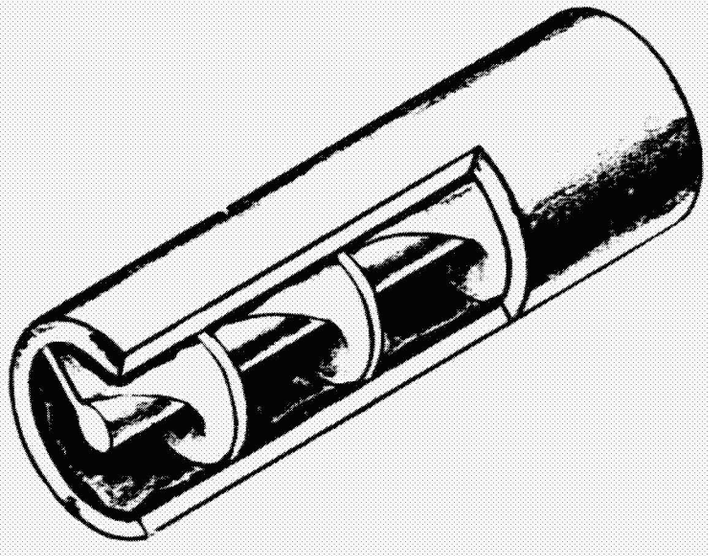

Figure 2-11. Helical vane.

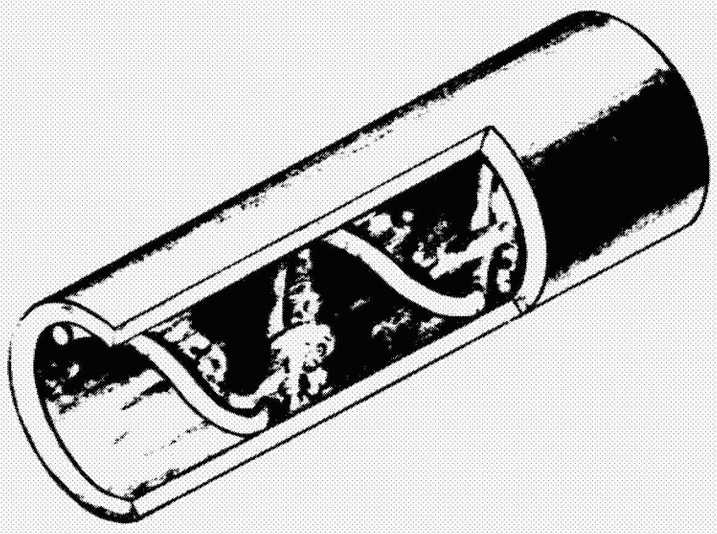

Figure 2-12. Helical flow: wire coil.

PHOTOGRAPHS OF SOME OF THE BOILING REGIMES

A number of photographs have been compiled which illustrate some of the phase distributions that have been discussed above; they are shown in Figures 2-13 to 2-18. In some cases, simulated forced flow boiling is depicted using water-air mixtures in glass pipes. In other cases, transparent heating films and optical ports have been used so that actual forced flow boiling phase distributions can be seen.

In the previous discussion of slug, annular, rivulet and droplet flows, it was noted that the effect of wetting on the phase distributions must be considered. The degree of wetting of a liquid on a heat transfer surface, defined in terms of a contact angle, can vary significantly with temperature level.[10] See Figure 2-19, for example, where the contact angle of a mercury drop on a clean tantalum surface in a mercury vapor environment is shown to change markedly with temperature beyond 700°F. Actual photographs showing two illustrative contact angles measured are shown in Figures 2-20 and 2-21.

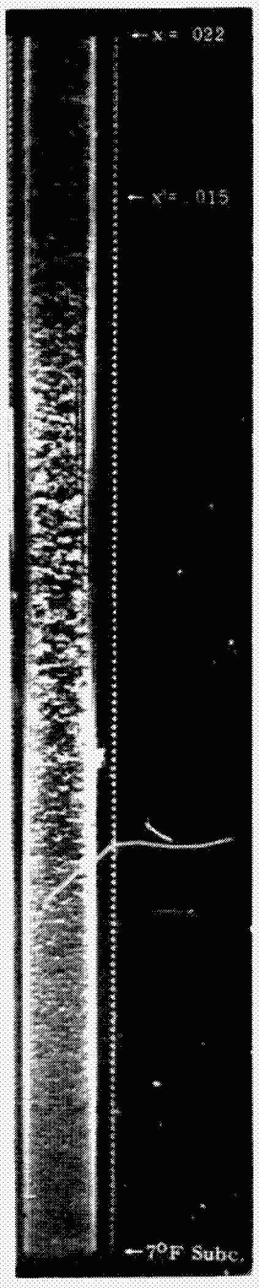

Figure 2-13. Linear, forced flow nucleate boiling (Freon at a low vapor quality). Courtesy of General Electric Company, Schenectady, New York.

Figure 2-11. Helical forced flow nucleate boiling using a vane (water-air simulation at a low vapor quality).
Geoscience Ltd photograph.

Figure 2-15. Linear, wetted-wall slug flow (Freon at low vapor quality). Courtesy of General Electric Company, Schenectady, New York.

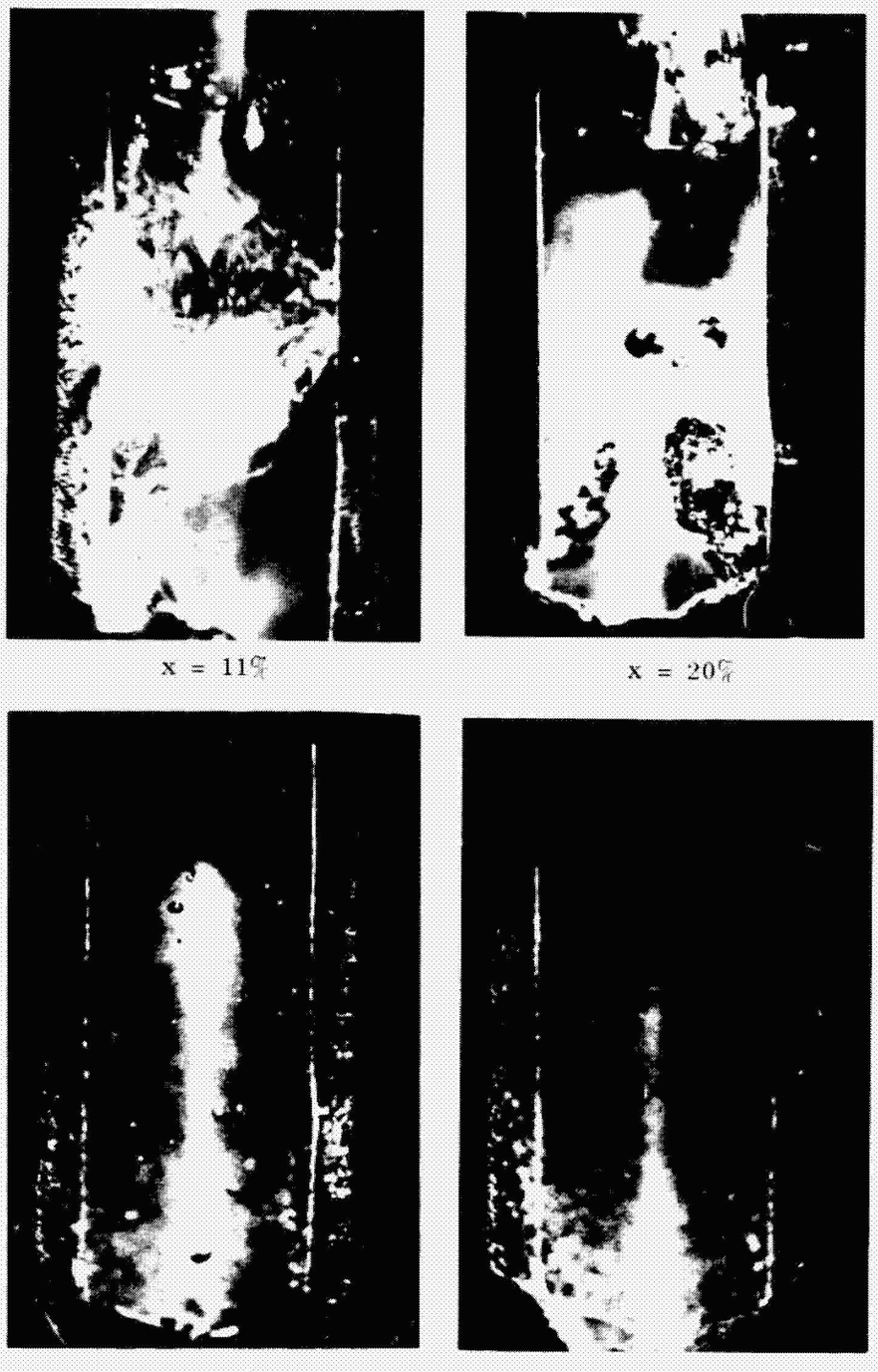

Figure 2-16. Serial views of linear forced flow boiling (mercury at various vapor qualities).
Geoscience Ltd photographs.

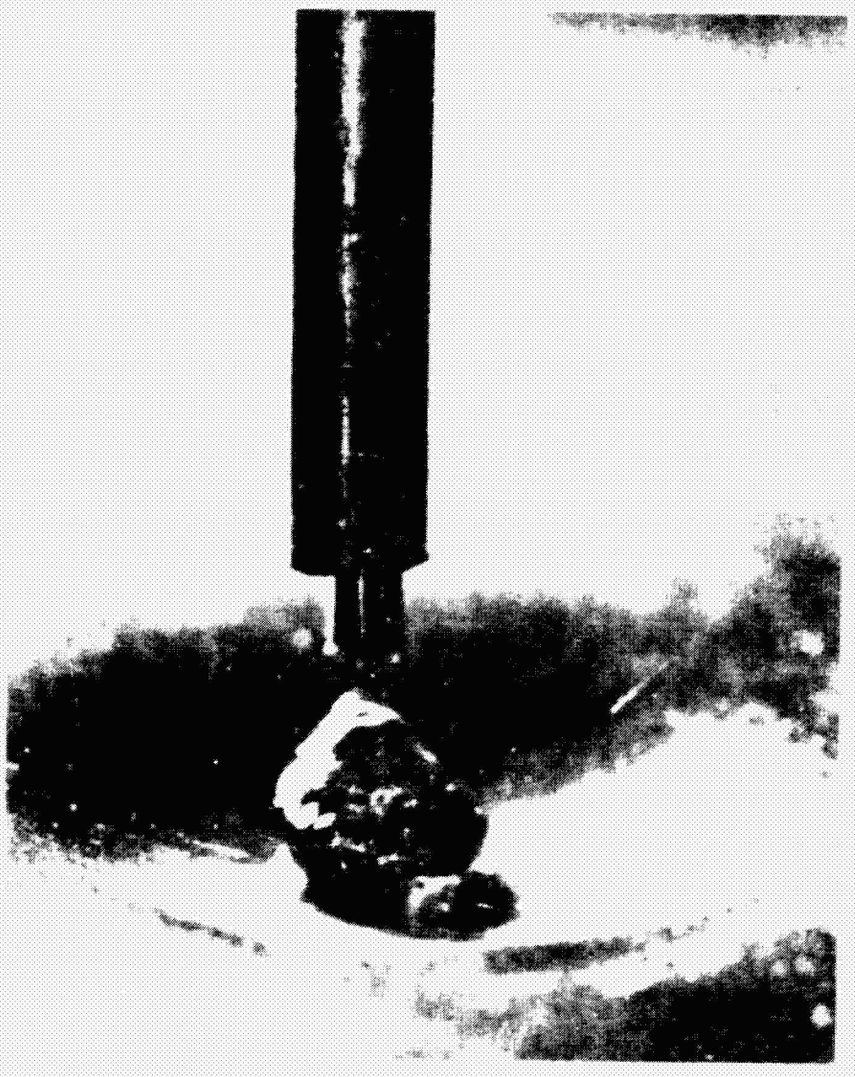

Figure 2-17. Spalling mercury droplet on a heated plate. Geoscience Ltd photograph.

Figure 2-18. Helical forced flow boiling using a wire coil insert (water-air simulation).
Courtesy General Electric Company, Cincinnati, Ohio

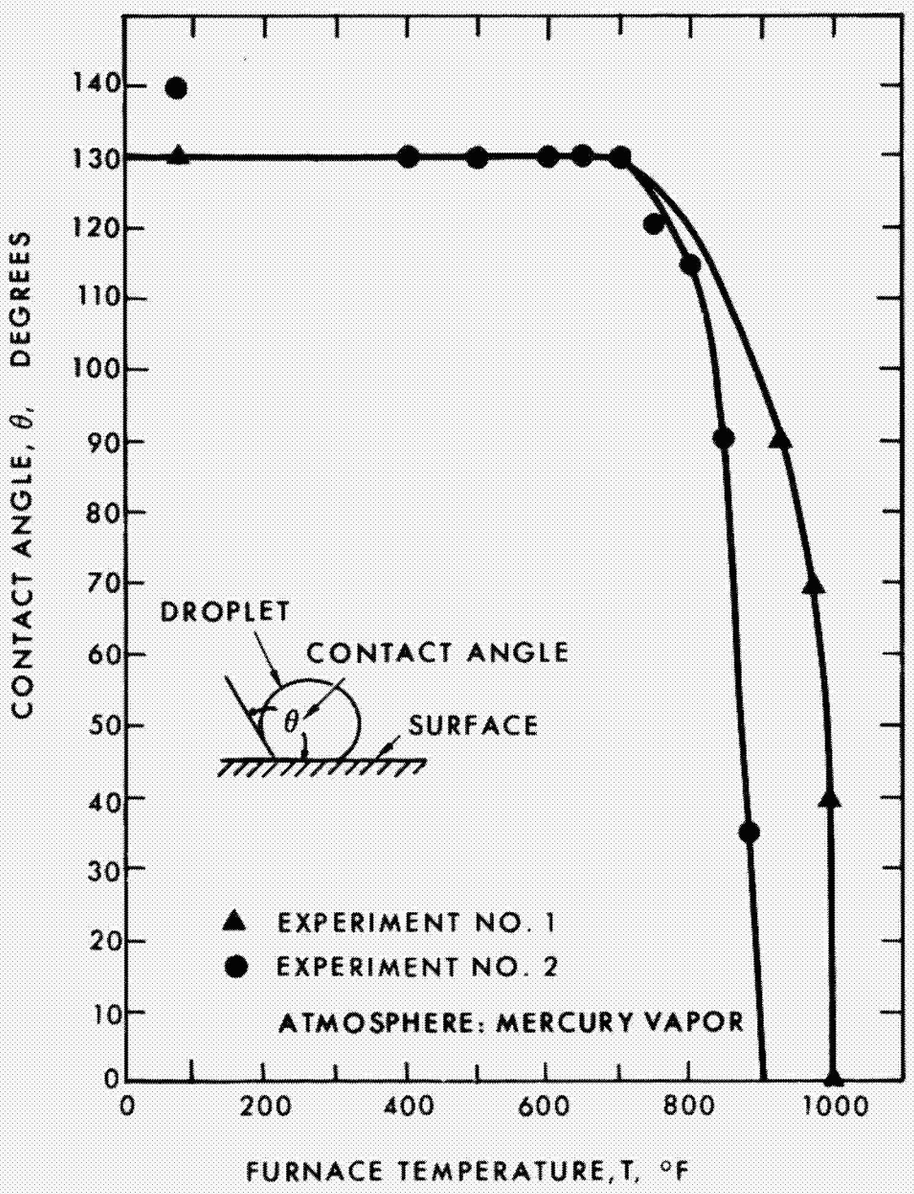

Figure 2-19. Contact angle formed between a mercury droplet and a chemically etched tantalum surface versus furnace temperature.

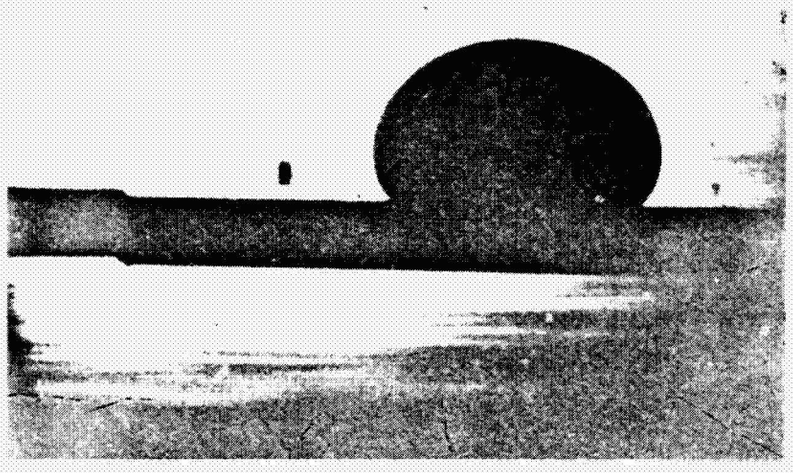

Figure 2-20. Non-wetting mercury drop on tantalum (low temperature).

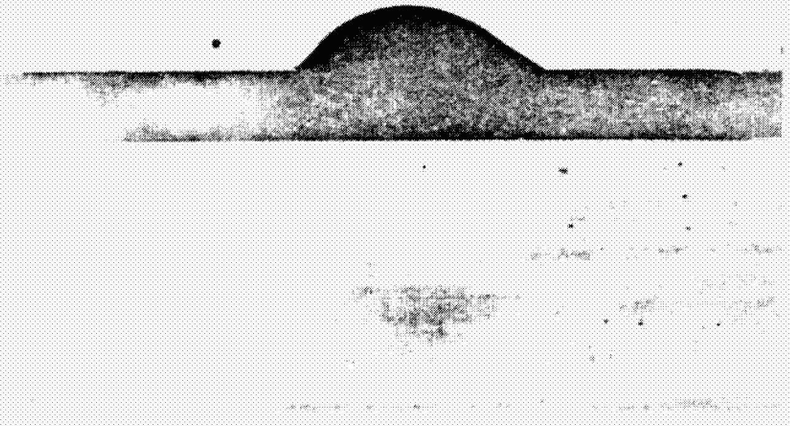

Figure 2-21. Wetting mercury drop on tantalum (high temperature).

DISCUSSION

The material presented in this chapter gives a physical description of the various ways in which the liquid and vapor phases could be distributed in a boiler tube. When compared to single phase heat transfer and pressure drop in forced flow heat exchanger systems, two phase, or boiling heat transfer, is more complex. One immediate complication of two phase flow is that the relative location of the phases in a flow tube is a variable. The phase location depends on whether the composite flow is linear or helical in character and on the vapor quality and mass flow rate of the fluid. Quantitative experimental and analytical descriptions of these boiling heat transfer regimes are presented in Chapters 3 and 4

REFERENCES

1. Gunther, F. C.; "Photographic Study of Surface-Boiling Heat Transfer to Water with Forced Convection," ASME Trans, 73 115-23 1951.

2. Poppendiek, H. F.; "Preliminary Concepts Concerning the Mechanism of Heat Transfer in Forced Convection Local Boiling," Chap 8, UCLA Eng Research Prog Rep No. 1 on Boiling Studies, AEC Contract AT-11-1-Gen-9, Aug 1949.

3. Snyder, N. W.; Robin, T. T.; "Mass Transfer Model in Subcooled Nucleate Boiling," ASME Trans, pp 404-412, Aug 1969

4. Poppendiek, H. F.; Greene, N. D.; Palmer, L. D.; ANP Quarterly Progress Report, Chap 4.1, Heat Transfer in Reflector-Moderator Cores, ORNL-2221, Dec 1956.

5. Gambill, W. R.; Greene, N. D.; "Boiling Burnout with Water in Vortex Flow," Chem Engr Progress, pp 68-76, Oct 1958.

6. Sellers, A. J.; "Topical Report on Thermal Design of SNAP-8 Tantalum-Stainless Steel Boiler," Aerojet General, NASA CR 72760.

7. Poppendiek, H. F.; Greene, N. D.; MacDonald, F. R.; Wright, H. R.; Sabin, C. M.; Thompson, A. S.; "Annual Technical Report on High Acceleration Field Heat Transfer for Auxiliary Space Nuclear Power Systems," Aec Contract AT(04-3)-409, Sept 1, 1961 - Aug 31, 1962.

8. Peterson, J. R.; "High Performance "Once-Through" Boiling of Potassium in Single Tubes at Saturation Temperatures of 1500° to 1750°F," NASA CR-842.

9. Gido, R. G.; Koestel, A.; Haller, H. C.; Huber, D. D.; Deibel, D. L.; "The SNAP-2 Power Conversion System Topical Report No. 12, Boiler Development," TRW ER-4521, July 17, 1961.

10. Poppendiek, H. F.; Feigenbutz, L. V.; Petrovits, Z. J.; Sabin, C. M.; Goddard, W. B.: "An Investigation of the Boiler Conditioning Characteristics in a Mercury-Tantalum System," Aerojet Contract OP 119224, July 1968.

CHAPTER 3: REPRESENTATIVE EXPERIMENTAL, SEMI-EMPIRICAL AND ANALYTICAL INFORMATION ON BOILING HEAT TRANSFER AND PRESSURE DROP

In Chapter 2, physical descriptions of the major phase distributions for boiling heat transfer that are known to exist in forced flow were presented. The present chapter outlines representative experimental, semi-empirical, and analytical information on the frictional pressure drop* and heat transfer in tubes with circular cross sections for these different phase distributions or flow regimes. In most cases, not all three types of information are available for a given regime. Whenever possible, however, comparisons between the experimental, empirical, and analytical functions are made. These three types of information have a range of applicability. The design engineer must consider each information set and, on the basis of the limitations given, determine how he can use it in design. The material on transition phenomena in Chapter 4 will also assist him in establishing where and when these various boiling regimes are in operation.

Sufficient information is presented in Chapters 3 and 4 so that reasonable boiler designs can be carried out. Examples of such designs and their comparison to actual performance are presented in Chapter 5.

---

*The total pressure drop is the sum of the frictional and momentum change terms. The latter quantity is defined in terms of differences between boiling fluid outlet and inlet momentum rates for the cases of separated and mixed flows.

FORCED FLOW BOILING HEAT TRANSFER AND PRESSURE DROP INFORMATION

The major forced flow boiling regimes found in a practical boiler system as outlined in Chapter 2 are presented in this section.

A. Liquid Preheating*

Experimental Information

Classical information on single phase pressure drop and heat transfer in terms of friction factors and Nusselt moduli are well-described in the literature. The experimental viscous and turbulent flow friction factors are shown in Figure 3-1 for tubes with circular cross sections.[1] The experimental Nusselt/Prandtl modulus versus Reynolds modulus function for turbulent flow in tubes with circular cross sections is shown in Figure 3-2 for ordinary fluids[2] (Prandtl number greater than about 0.5) and in Figure 3-3 for liquid metals[3] (Prandtl number less than about 0.05).

Semi-Empirical Information

Also shown in Figure 3-2 is the classical semi-empirical

---

* Liquid preheating has been added to the beginning of the boiling regimes and vapor superheating added at the end to complete the overall forced flow boiling process description.

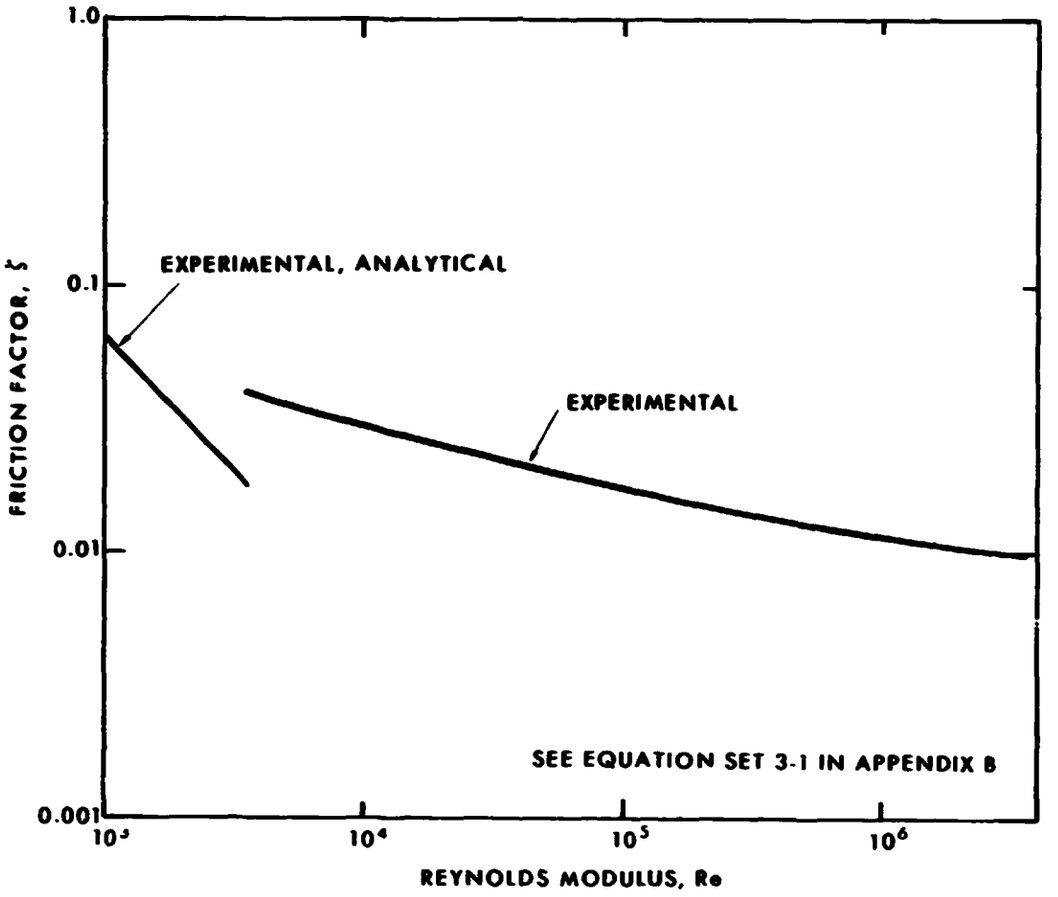

Figure 3-1. Friction factors for fully-established. laminar and turbulent single phase flow (circular cross section).

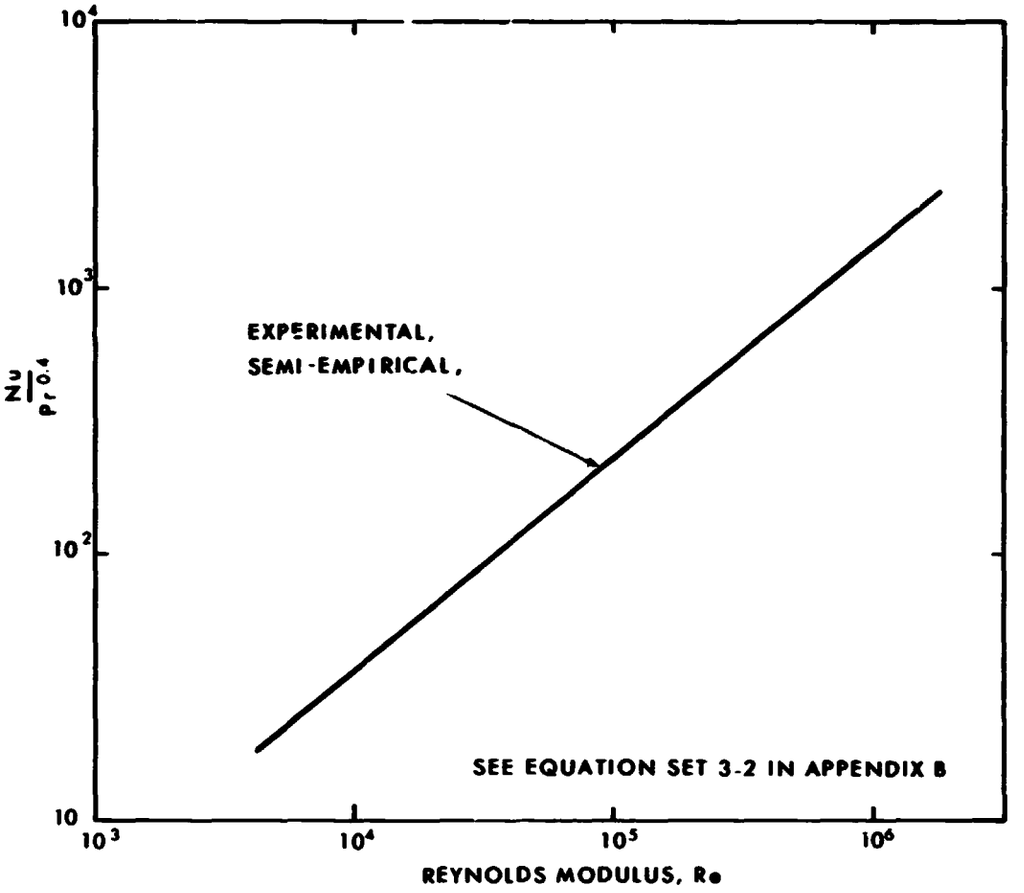

Figure 3-2. Nusselt modulus for fully-established, turbulent single phase flow of ordinary fluids (circular cross section).

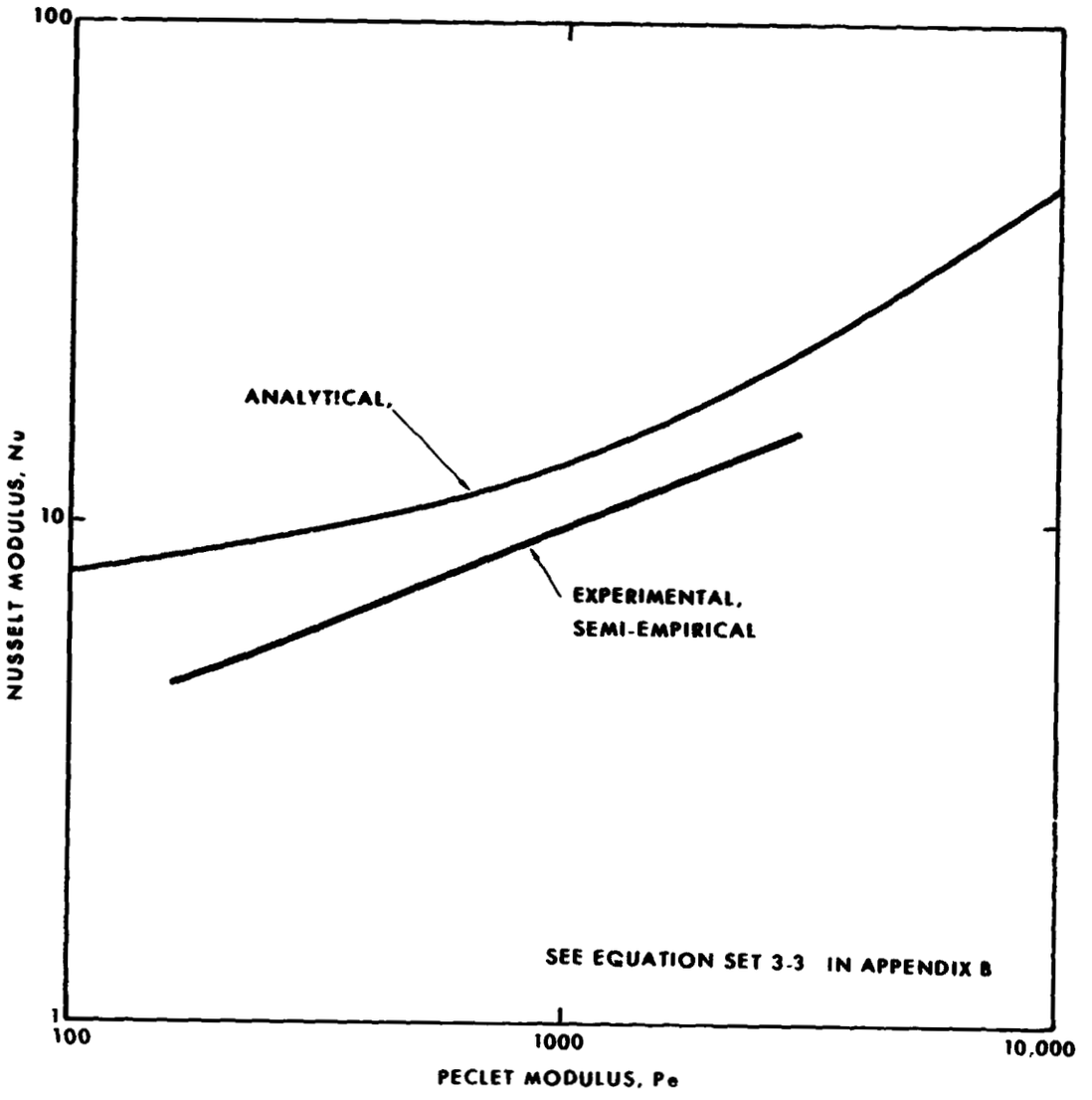

Figure 3-3. Nusselt modulus for fully-established, turbulent single phase liquid metals (circular cross section).

convective heat transfer function which coincides with the mean experimental function. A specific semi-empirical correlation for liquid metal convective heat transfer was developed for turbulent flow in tubes with circular cross section.[4] It is shown in Figure 3-3.

Analytical Information

The classical viscous flow friction factor for circular cross section tubes[1] is also shown in Figure 3-1; agreement with experimental data is excellent.

A number of analytical expressions for forced flow convective transfer have been developed in the literature. Nusselt modulus functions for viscous flow in tubes with circular cross sections range from 3.65 for uniform wall temperatures to 4.36 for uniform wall heat fluxes.[5] The most well-known turbulent flow Nusselt modulus function for all Prandtl moduli is based on the analogy between heat and momentum transfer and the existence of the classical generalized velocity profile defined by a laminar sublayer, buffer layer, and a turbulent core.[6] The results of this work can be seen in Figure 3-4. An analogy solution for liquid metals in circular cross section tubes[7] is also shown in Figure 3-3.

B. Martinelli Representations for Two Phase Flow

A simplified description of forced flow boiling in extensive use

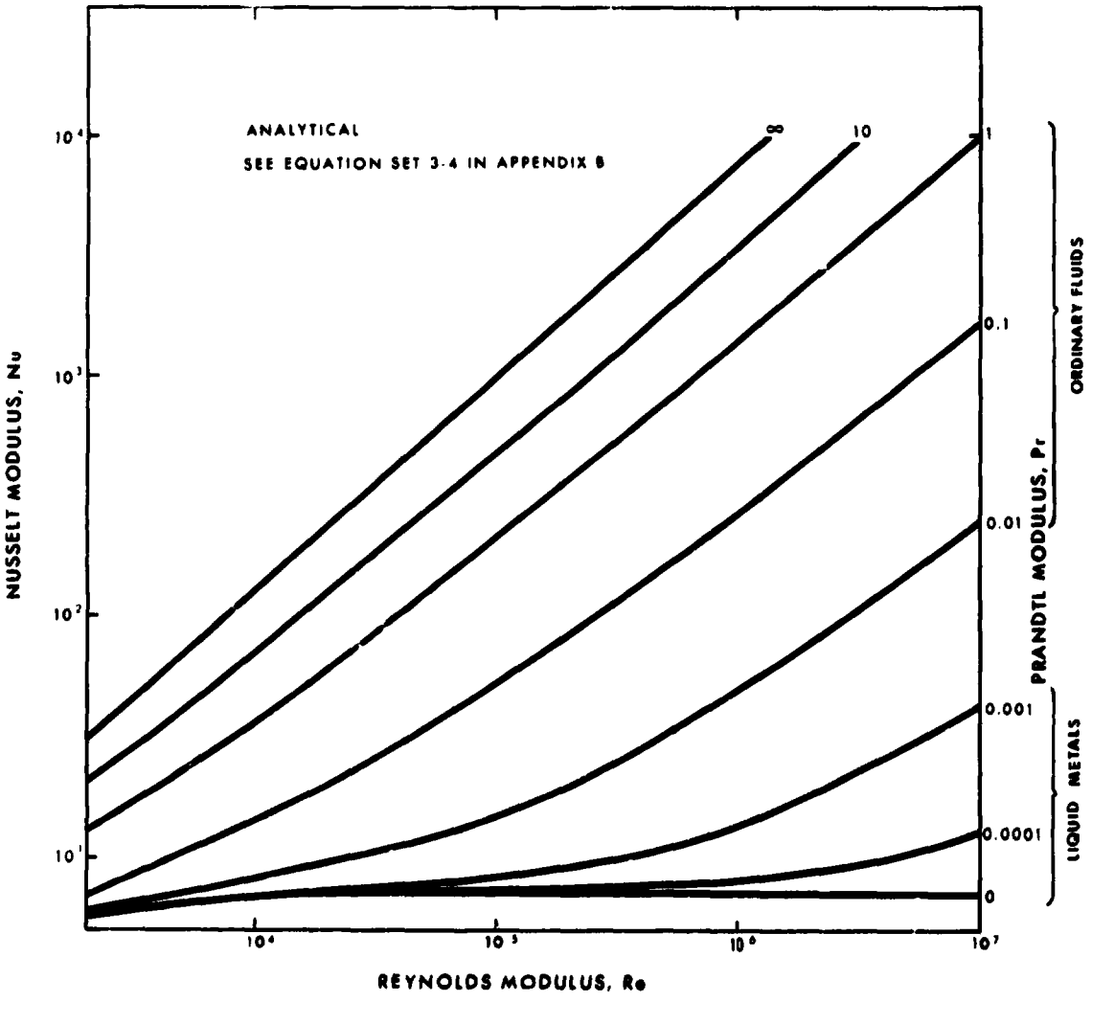

Figure 3-4. Heat-momentum transfer analogy for a smooth tube (applicable to both ordinary fluids and liquid metals).

was originally developed by Martinelli. Although both fluids are postulated to be in the turbulent state, their distribution in the tube is undefined. This gross, nondetailed representation of two phase flow has been used successfully to estimate pressure drop in boiling systems. Experimental water-air pressure drop data were generalized by analysis and the results extended to forced flow water boiling.[8] Information on the ratio of two phase pressure gradients to the pressure gradients for all-liquid flowing alone is shown in Figure 3-5. The local pressure drops are integrated along the boiler tube to obtain the total frictional pressure loss. Similar procedures have been carried out for estimating the pressure losses in forced flow sodium boiling[9] and potassium boiling.[10]

C. Slug Flow

Experimental Information

Figure 3-6 shows a graph of some experimental boiling mercury pressure drop data as a function of vapor quality under non-wetting, linear slug flow conditions.[11] The data shown have been corrected for the acceleration terms so that only frictional pressure drop is involved. The corresponding heat transfer data are shown in Figure 3-7. These data were obtained in an electrically-heated tube system (defined by a nearly uniform wall heat flux condition).

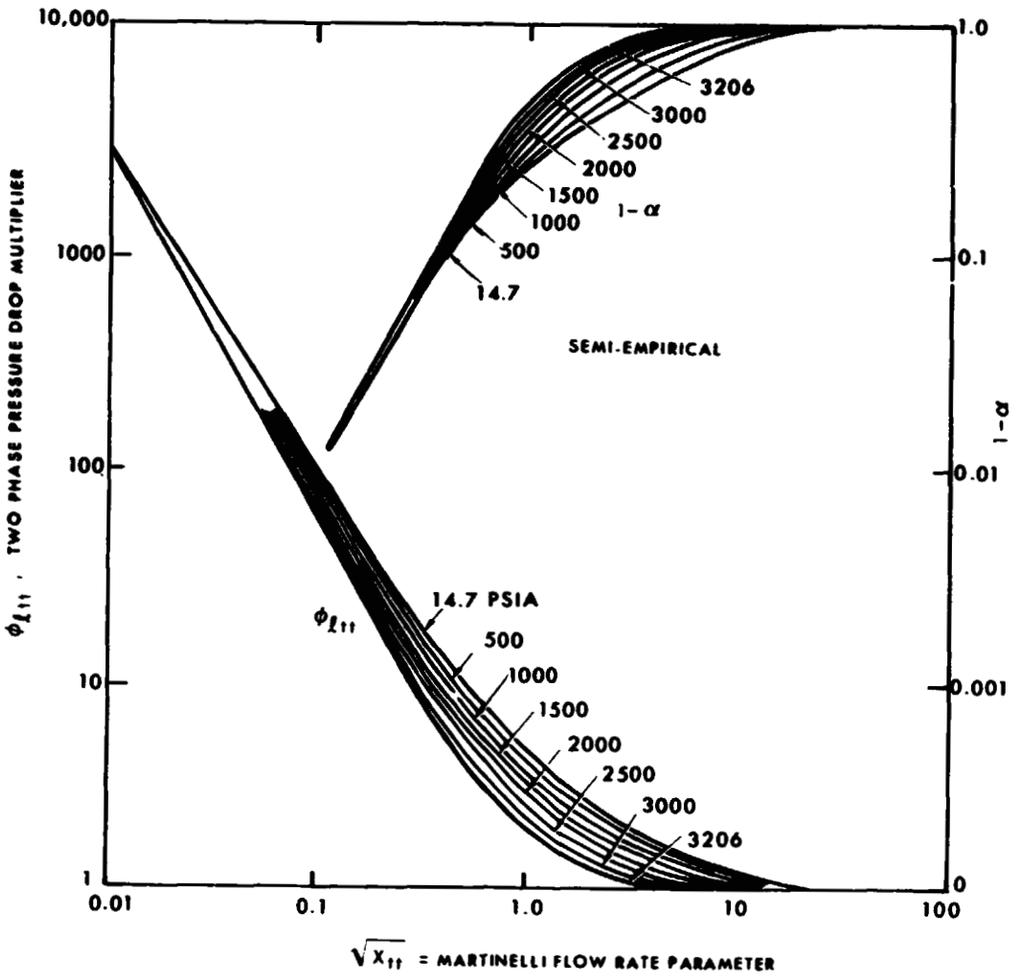

Figure 3-5. Two-pnase flow pressure drop multiplier and void fraction for water boiling in a round tube.

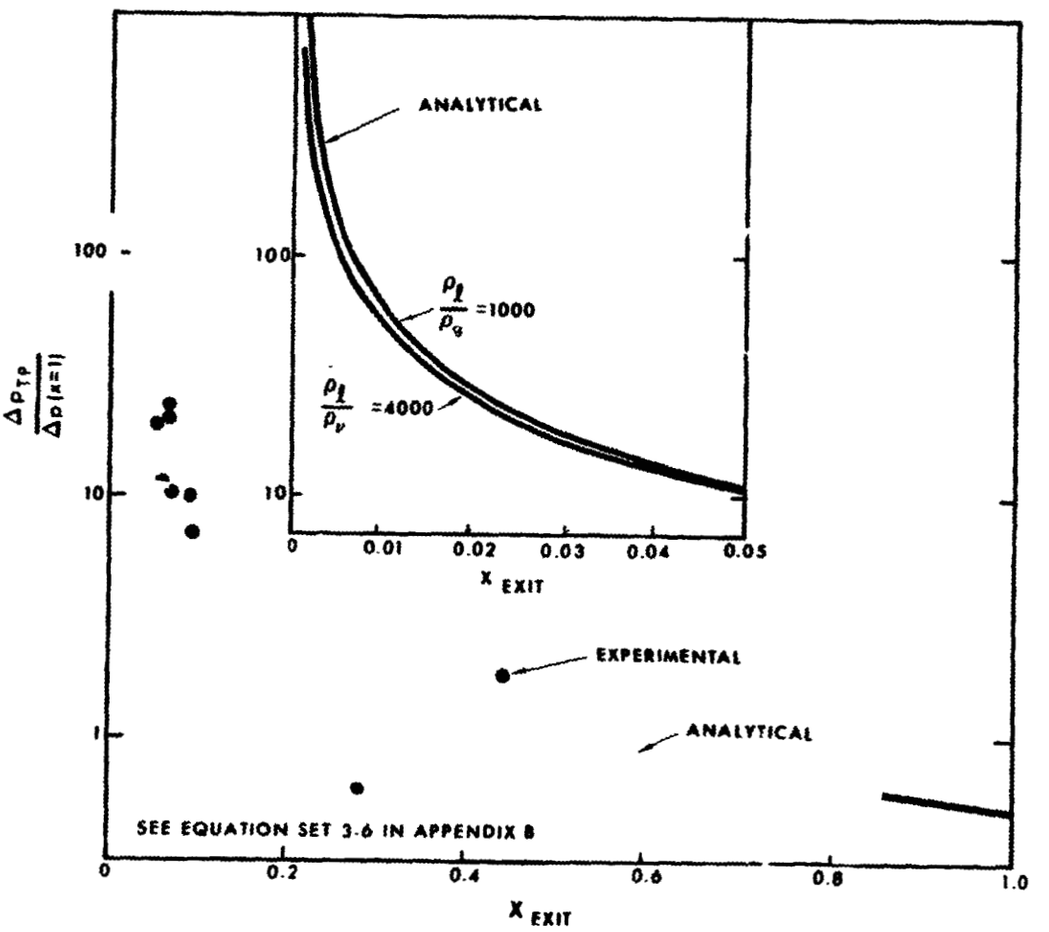

Figure 3-6. Integrated frictional pressure drop versus exit quality for the nonwetting slug flow model.

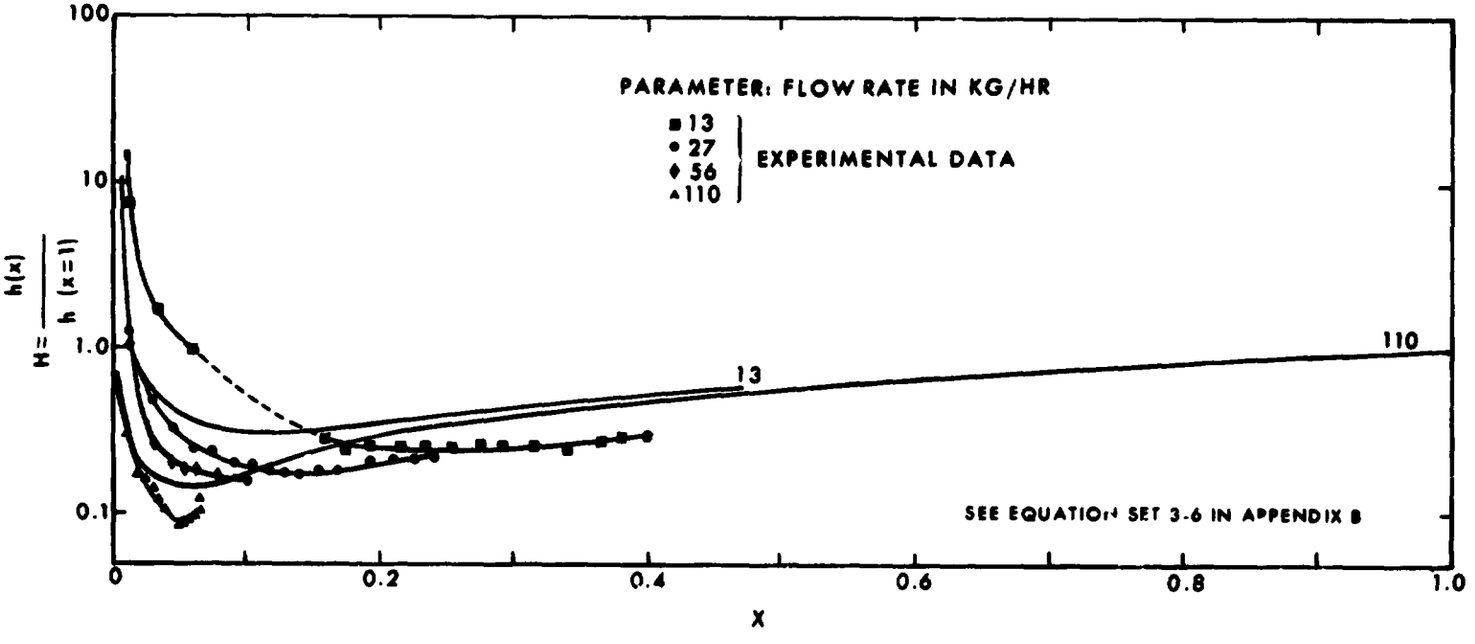

Figure 3-7. Comparison of experimental and predicted boiling mercury conductances for nonwetting slug flow.

Analytical Information

A two phase flow model consisting of alternate nonwetting slugs of liquid and vapor, each of which fills the cross section of the tube, has been proposed. Although the instantaneous flow at a cross section is unsteady, the time average mass flow rates of the liquid and vapor phases may be used to define a time average vapor quality. This model has been analyzed to determine the average frictional pressure drop of the flow.[11] The model was evaluated for the case where physical fluid properties are invariant, the slug friction factors are equal and invariant, and the vapor quality varies linearly with axial distance (uniform wall heat addition); the total frictional pressure drop function along a boiler tube was determined and is shown in Figure 3-6. A corresponding heat transfer analysis[11] (which is outlined in Appendix C where the method is illustrated), gives a normalized heat transfer conductance versus vapor quality along the boiler tube (see Figure 3-8).

An analytical prediction of void fraction in wetted wall slug flow has been presented.[12] This expression, which helps to define the flow state, gives fairly good agreement for adiabatic systems of dissimilar fluids such as air and water. It is shown compared to some data[13] for steam and water in Figure 3-9. Some of the discrepancy between theory and experiment is probably attributable to the fact that the experimental system was an annular test section. The inner cylinder of the annulus is one plate of a capacitance probe

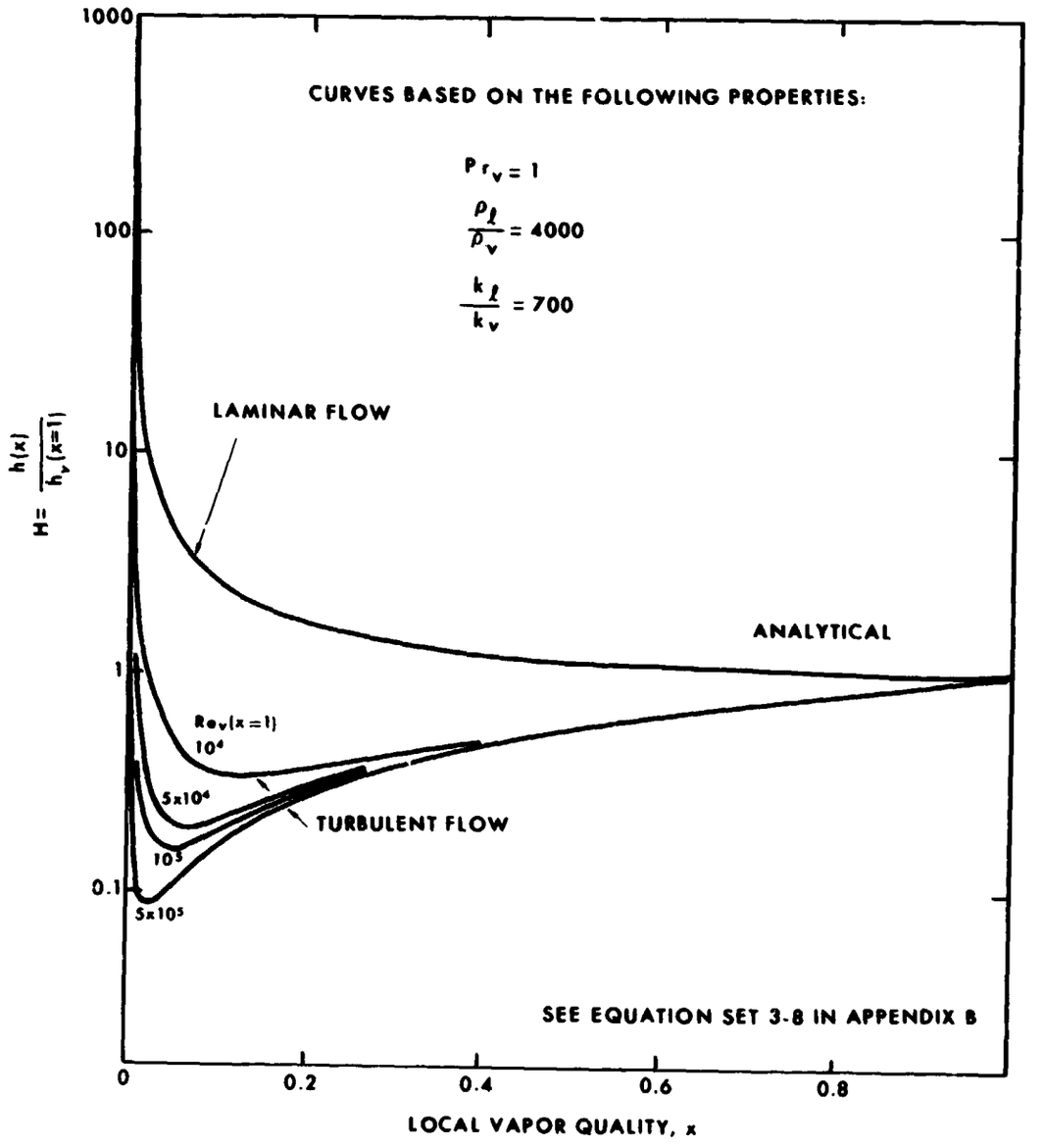

Figure 3-8. Dimensionless boiling heat transfer conductances for the nonwetting laminar and turbulent slug flow models.

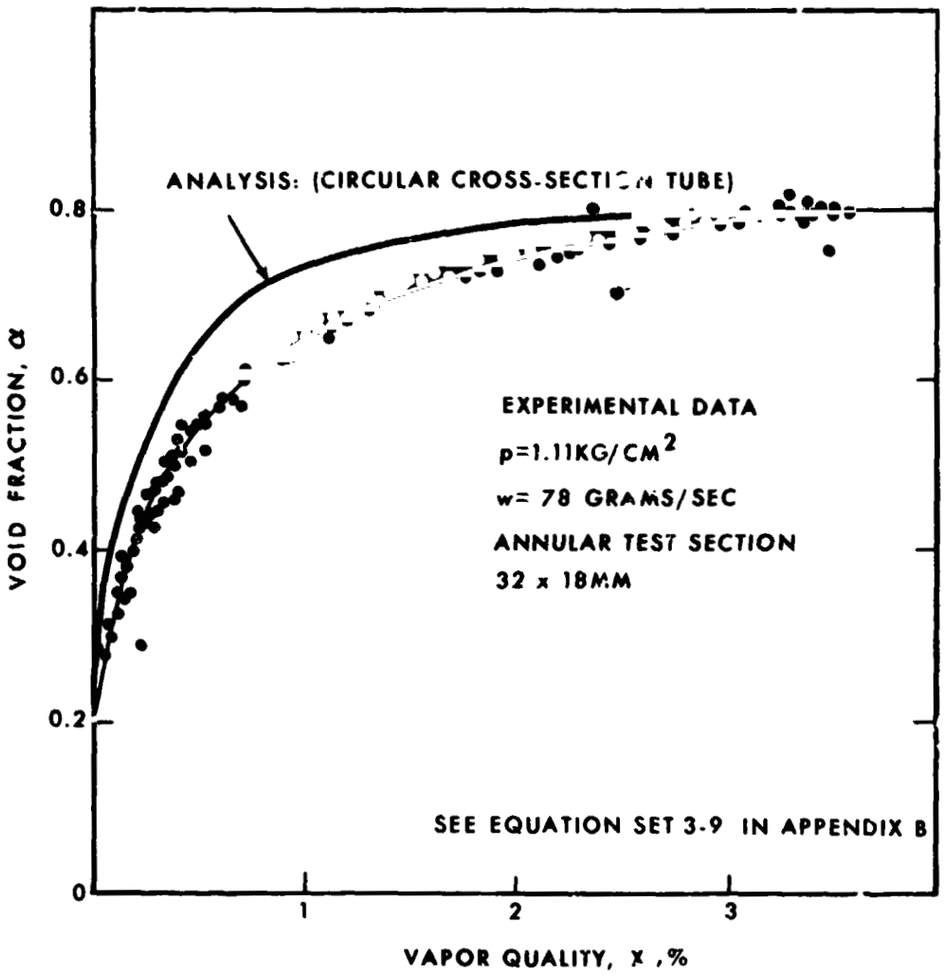

Figure 3-9. Void fraction versus steam quality for upward wetting slug flow.

from which the void fraction was determined. In a system with heat transfer, the void fraction is not zero at zero vapor quality, because the void fraction in subcooled boiling (a departure from thermodynamic equilibrium) is in typical systems as much as 0.5 (see, for example, Reference 14).

D. Annular Flow

Experimental Information

A number of experimenters have studied pressure drop and heat transfer in forced flow boiling systems wherein the two phases distribute themselves in an annular arrangement (usually the liquid phase is at the wall and the vapor in the core). Some examples of such data are shown in Figures 3-10, 3-11, and 3-12.[15,16,17,18] The relatively large amount of scatter in Figure 3-11 suggests that for the high points, both phases were probably in the turbulent state or large surface roughnesses existed at the liquid layer surface.

Semi-Empirical Information

Algebraic correlations for turbulent-turbulent annular upward flow of air and water based on some theoretical models have been established.[19] The correlations include both void fraction and two phase frictional pressure drop. These expressions agree well with Martinelli's data, which are based on horizontal flow of a number of fluid combinations. Therefore, it is plausible that the correlations have application to fluids other than air

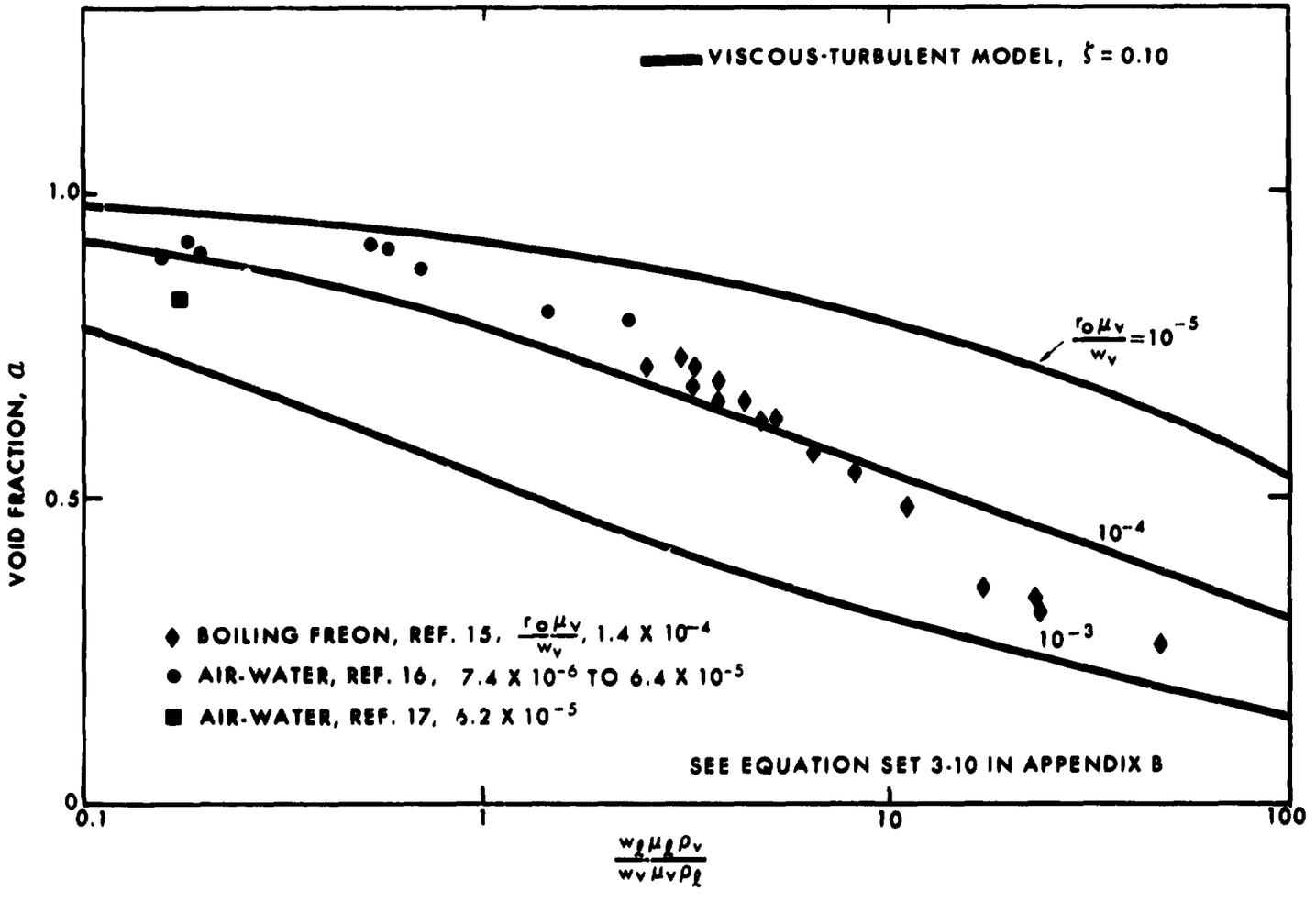

Figure 3-10. Experimental void fraction in upward annular flow--analytical predictions also shown.

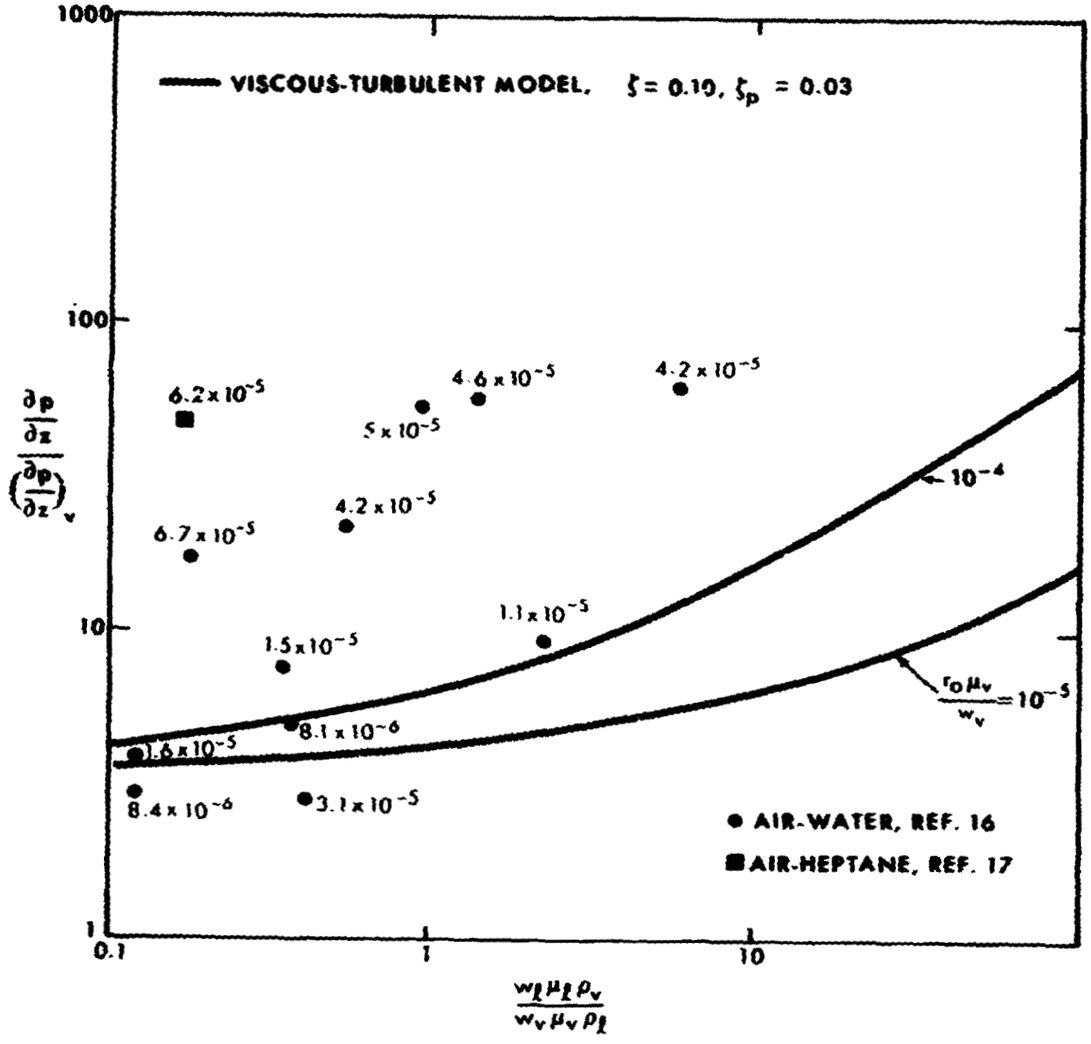

Figure 3-11. Experimental two-phase pressure drop in upward annular flow--analytical predictions also shown.

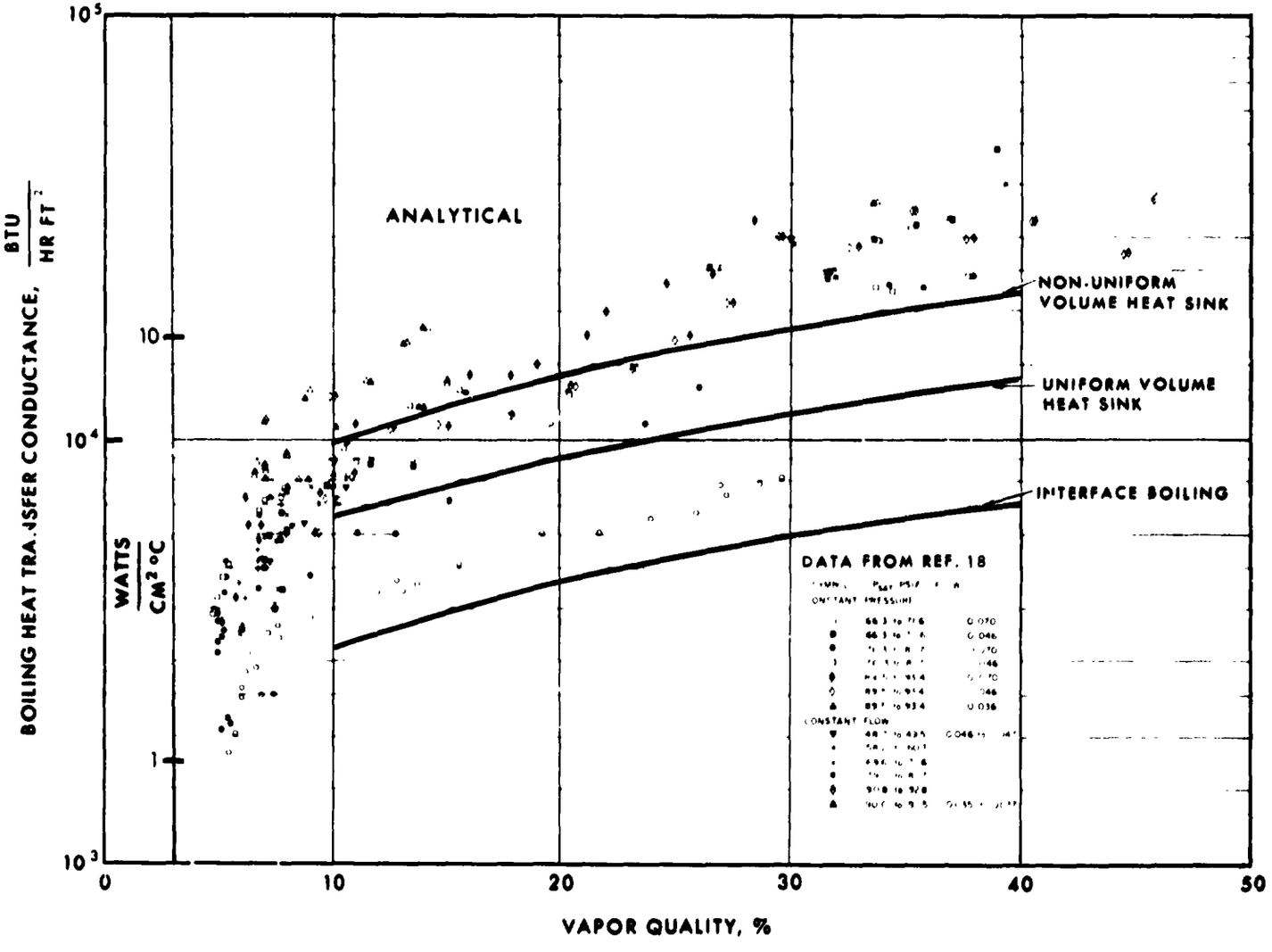

Figure 3-12. Comparison of superheated annular liquid film model with boiling potassium data.

and water. The pressure drop correlation (shown in Figure 3-13) is specifically restricted to cases in which the liquid entrained in the gas phase is less than 20 percent of the total local liquid flow, and in which viscous forces in the liquid film are negligible.

Analytical Information

A number of annular flow pressure drop analyses for different flow regimes in the annulus and core regions have been performed;[20] typical results for viscous-turbulent flow are shown in Figure 3-14. An outline of this solution is presented in Appendix C. These results are also compared to experimental data in Figures 3-10 and 3-11.

The heat transfer in an annulus system can be defined by the temperature drop across the liquid or vapor annulus contiguous to the heat transfer wall. In the former case, heat conduction through the liquid film supplies heat to the liquid-vapor interface where boiling takes place at the saturation temperature. In the latter case, convection and radiation through the vapor film control the heat of vaporization at the liquid-vapor interface. Examples of three analytical representations are shown in Figure 3-12, where predictions are compared with experimental liquid boiling information. These models are based on idealized, annular, liquid layers contiguous to a wall. The first model consists of a superheated liquid layer that is heated from the tube wall and loses heat from the liquid-vapor interface by

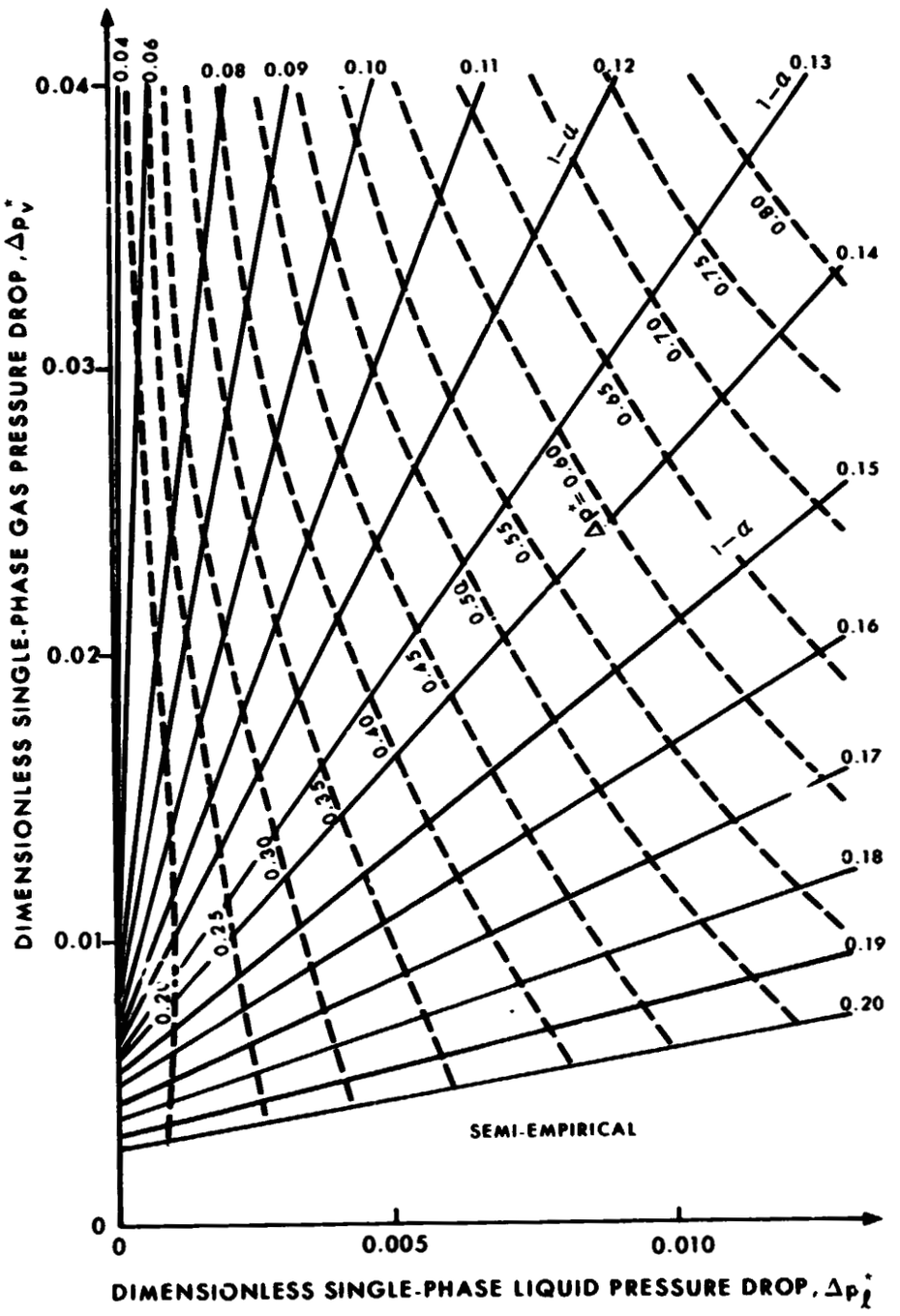

Figure 3-13. Correlation for two-phase pressure drop in annular flow.

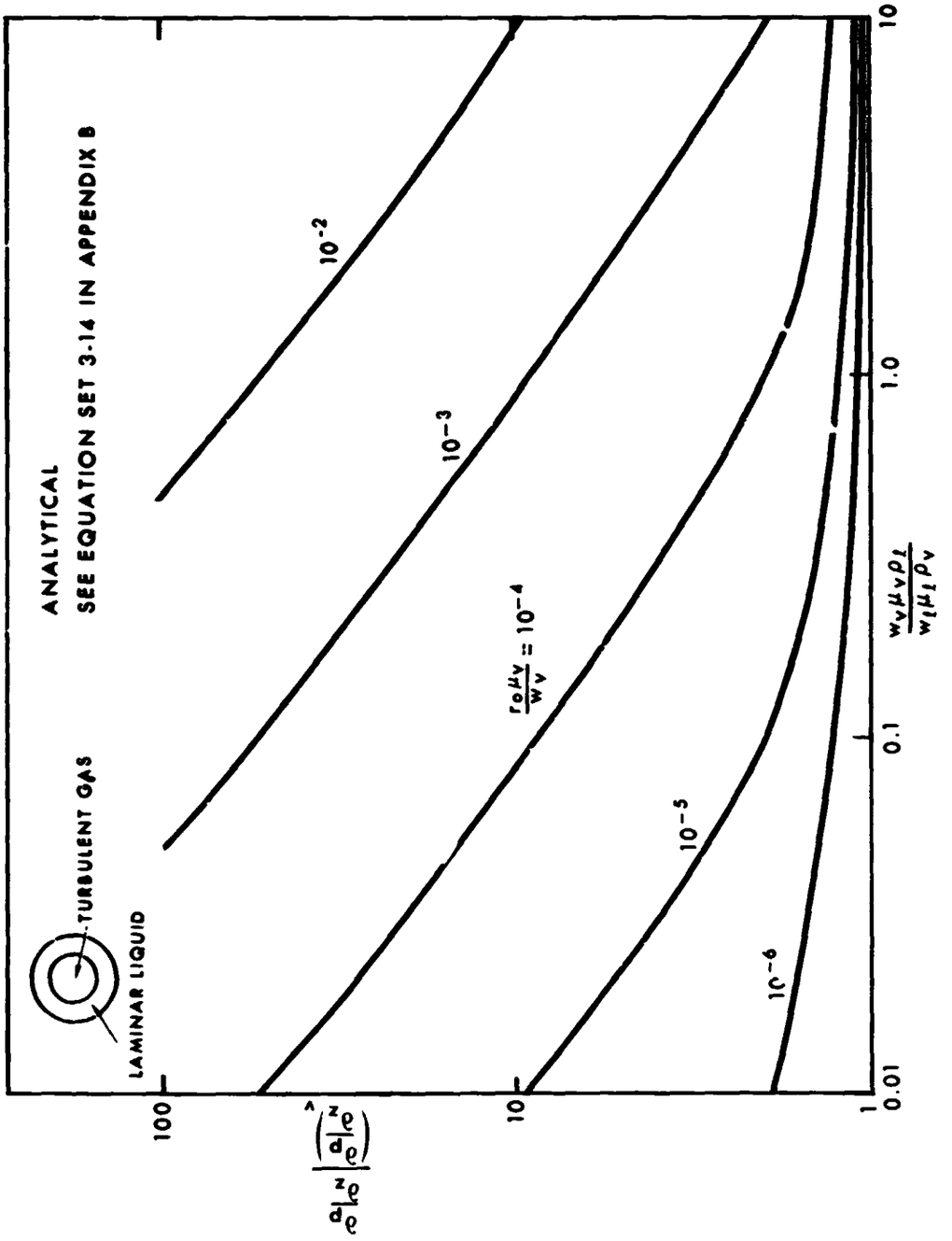

Figure 3-14. Viscous-turbulent annular flow with smooth interface ($\zeta \quad \zeta_p = 0.03$).

evaporative heat transfer; heat transmission through the layer consists of conduction only. The second model is defined by a superheated liquid layer with wall heat addition and a uniform heat sink representing volume boiling. The third model is defined by a superheated liquid layer with wall heat addition and a volume heat sink that varies linearly from a maximum value at the wall to zero at the liquid-vapor interface. The resulting analytical Nusselt moduli for these cases can be shown to be D/δ , $2D/\delta$, and $3D/\delta$, respectively.[21] The liquid film thickness δ is obtained from Equation Set 3-14 in Appendix B.

A closed form algebraic relationship between the void fraction and two phase pressure drop has been derived for turbulent-turbulent flow.[19] The model on which the analysis is based utilizes a one-seventh power velocity profile in the liquid phase. It is not necessary to define the properties of the core flow, or the nature of the interaction between the core flow and the annulus to obtain this relationship. A comparison of the analytical result and the experimentally-established relationship from Martinelli's[23] data is shown in Figure 3-15.

Prediction of void fraction from the properties of the two streams and an interaction model to be applied at the interface has been attempted by several authors. This is a difficult task, since the models must represent by time invariant functions some processes which vary rapidly with time in an apparently random manner.

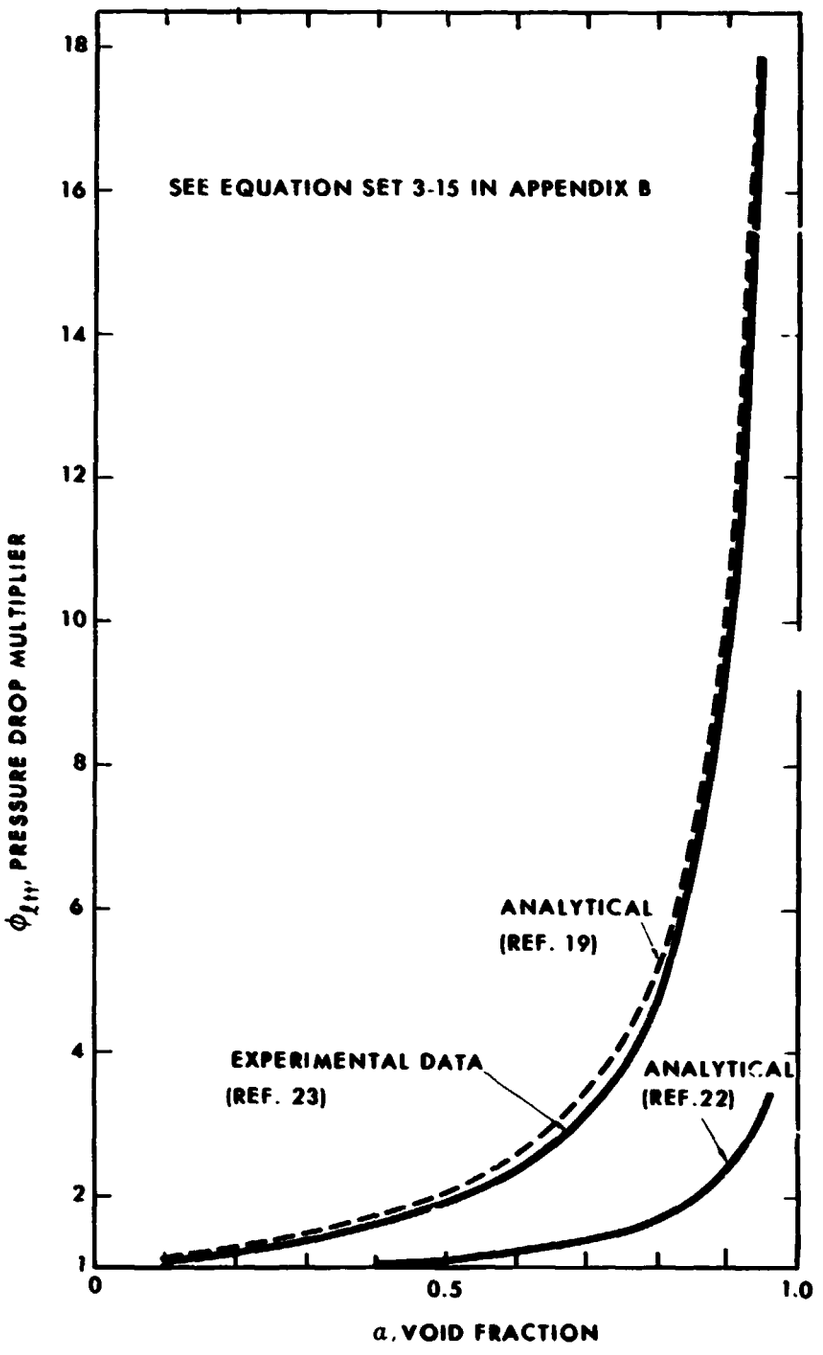

Figure 3-15. Relationship between void fraction and two-phase pressure drop for turbulent-turbulent annular flow.

The apparent liquid-vapor interface, which one may compute from void fraction data, is irregular, wavy, and unsteady in time. For these reasons, predictions of void fraction from physical models have not been very successful. An example of predicted void fraction and pressure drop,[22] utilizing a flow model in which both streams are characterized by one-seventh power velocity profiles, is shown in Figure 3-15.

The annular flow heat transfer model based on conduction through the liquid film gives good results for laminar liquid layers or for liquid metals, where the thermal conductivity is large compared to turbulent transfer. However, for thick liquid layers of ordinary fluids, the heat flow through the film would be expected to be controlled by turbulent convection. This case may be treated by replacing the thermal conductivity in the previous conduction heat transfer model by a mean effective thermal conductivity constructed with the aid of an appropriate turbulence model. One such mean turbulent conductivity,[24] based on the idealizations that the velocity profile in the liquid layer is identical to the one-seventh power velocity profile measured for a tube running full of liquid and that the turbulent Prandtl modulus is unity, is shown in Figure 3-16. The liquid-vapor interface radius, r_i, in Figure 3-16, is obtained from the corresponding pressure drop analysis.

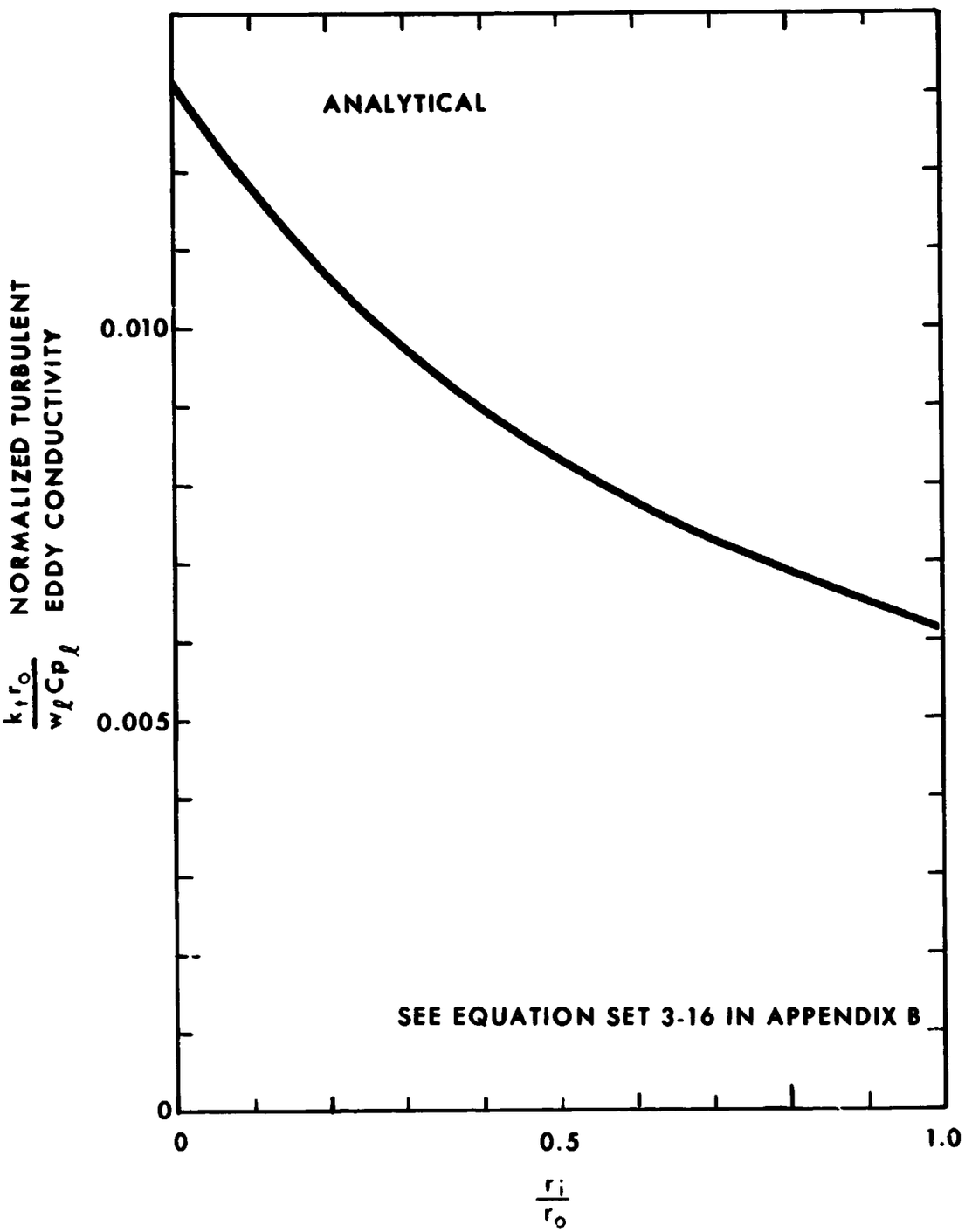

Figure 3-16. Mean effective thermal conductivity of a turbulent annular liquid layer of an ordinary fluid as a function of interface radius.

E. Rivulet Flow-Wetting

When a liquid film, which is clinging to the wall of a boiler tube, ruptures because of some hydrodynamic disturbance, a wetting rivulet results that maintains direct contact with the wall.

Analytical Information

An analysis for this phase distribution has been made;[25] it accounts for vaporization at the liquid-vapor interface of the rivulet and convective heat transfer from the bare portion of the tube wall. The resulting normalized boiling conductance function is shown in Figure 3-17. The contact fraction, F, for the rivulet is defined by the contact angle* and the vapor quality. This conductance function predicts the heat transfer in a boiler tube from the point where a complete liquid annulus exists (with only surface vaporization operating) to the point where the liquid rivulet on the wall is all gone (with only vapor convection remaining). The change in heat transfer between these two end points is normally equal to several orders of magnitude.

F. Entrained Flow

Experimental Information

Considerable experimental data are available on annular flows

---

*Contact angles are generally determined experimentally for the particular surface, liquid and vapor present.

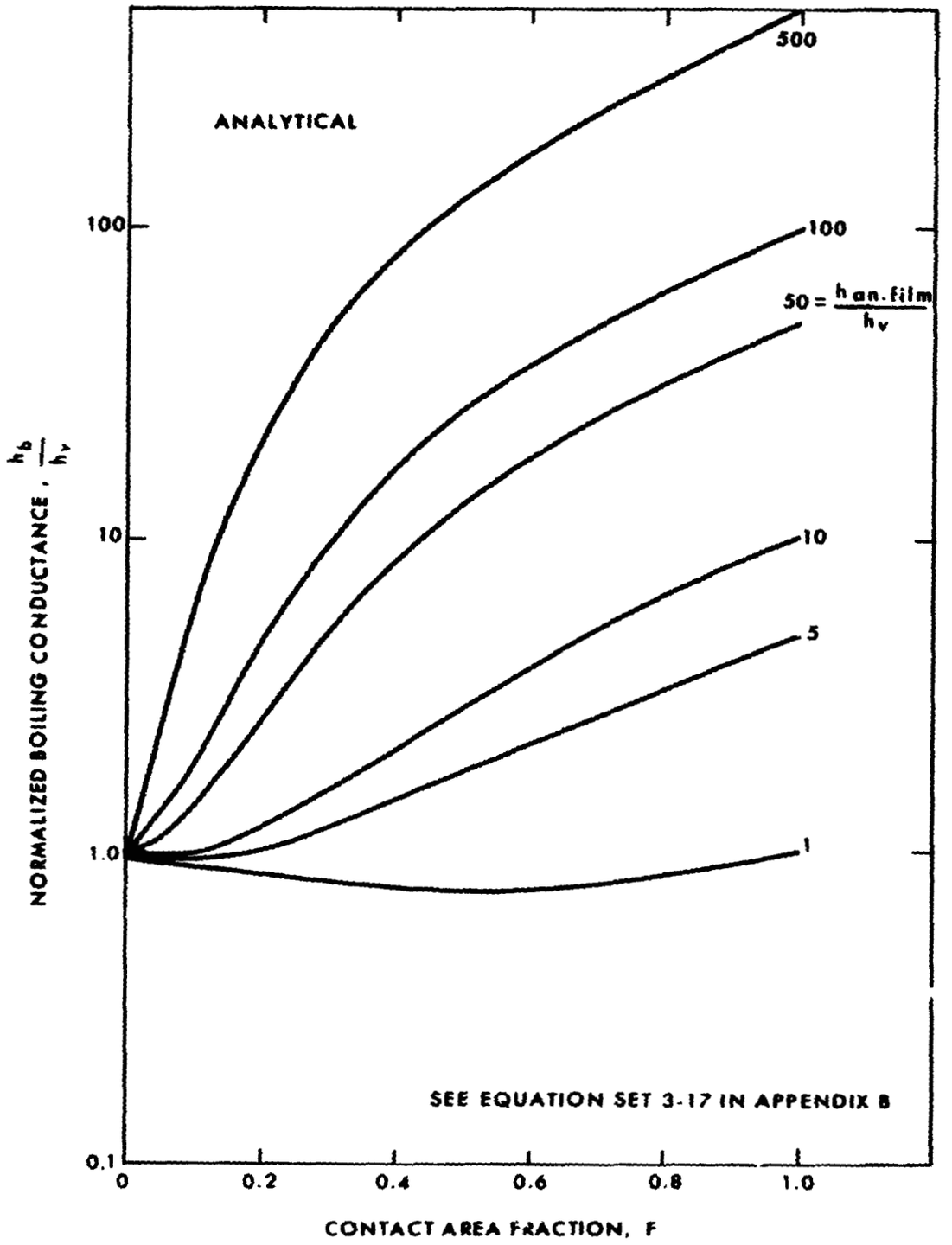

Figure 3-17. Boiling conductance for wetted rivulet flow.

with liquid entrainment in the core, for specific systems. A flow regime map showing the nature of the boundary for entrainment, taken from Reference 19, is shown in Figure 3-18. Although this figure is for air-water simulated boiling and cannot be used to predict entrainment in a general case, the regime dependence on velocities of the phases may be expected to be qualitatively the same for most ordinary boiling fluids (excepting liquid metals). Additional data on entrained flows in simulated boiling may be found in References 26 and 27. The number of physical parameters which can potentially influence the pressure drop and phase distribution in an entrained flow is large. For this reason, some theoretical or semi-empirical treatment is necessary to make useful predictions of conditions in a boiler. The following sections outline some useful procedures.

Semi-Empirical Information

Pressure drop in the so-called annular-dispersed flows, which are flows with a continuous liquid film on the wall and a significant portion of the total local liquid flow entrained as fine droplets in the vapor stream has been treated successfully by a model representing the flow as a homogeneous mixture of the two fluids moving at a single velocity.

In Reference 28 it is shown that such a model, used with a constant friction factor of 0.02, gives an acceptable fit to adiabatic pressure drop data for a wide range of fluids. The fluid combinations include air-water, air-Heptane, Argon-Ethyl Alcohol, and steam-water at

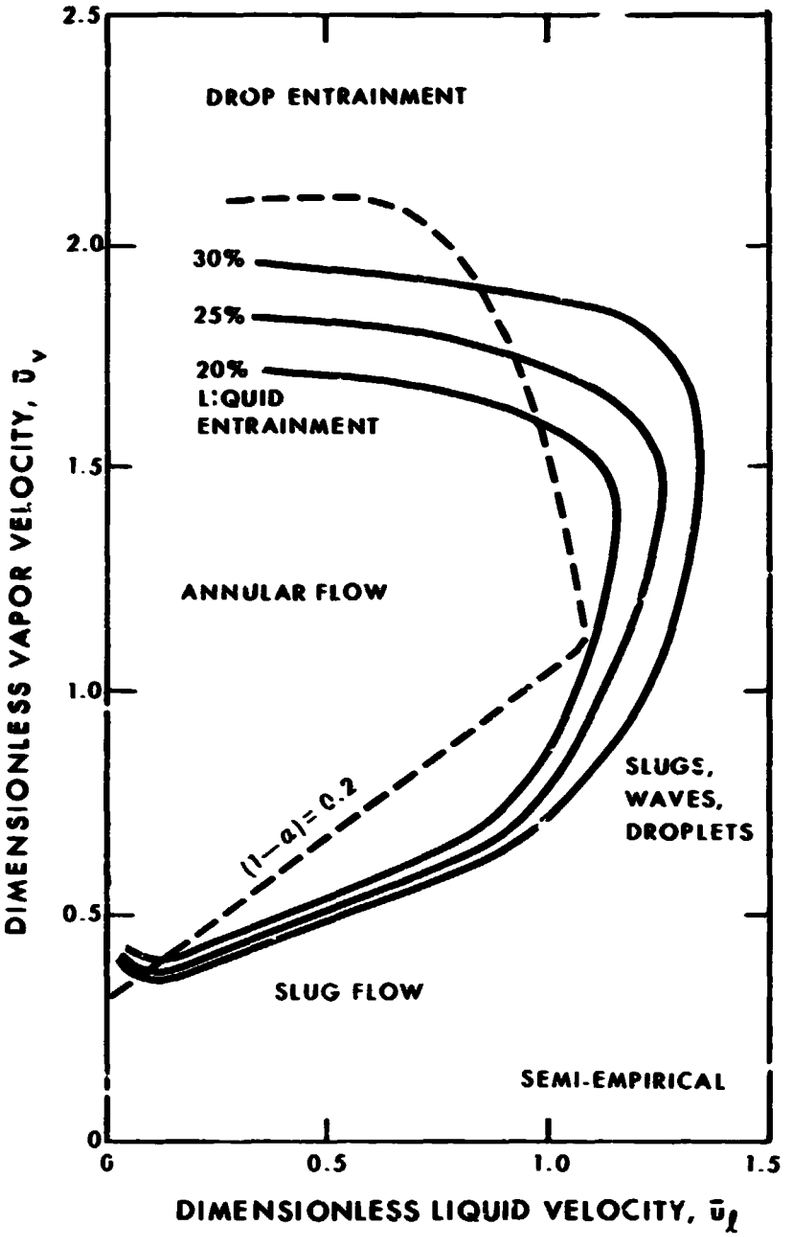

Figure 3-18. Boundaries of the annular flow regime for upward flow of water and air (from Reference 19).

a wide range of pressures. This approximation is applicable at entrained flows above 20 percent of the local total liquid flow.

There is a significant pressure drop associated with the entrainment process, since the liquid droplets must be accelerated to a velocity approaching that of the vapor. In Reference 29, it is shown that a good estimate of the acceleration pressure gradient is obtained by the difference of product of the local entrained liquid mass flow and the superficial vapor velocity at two stations, divided by the distance between the two stations. The superficial vapor velocity is the local vapor volume flow divided by the tube cross sectional area. This approximation was originally proposed in Reference 30.

Theoretical Information

An analytical treatment of annular flow with large entrainment is presented in Reference 31. This analysis considers the momentum and mass transfer components of the shear at the liquid-vapor interface. It is shown that the momentum term controls in the liquid film, and the mass transfer term controls in the vapor core. The vapor core is idealized to be a homogeneous mixture, and the liquid layer is defined by the universal velocity profile. In both regions, the mixing length is postulated to be proportional to the distance from the channel wall. A semi-empirical correction is employed to account for slip in the core. A second semi-empirical correction is also employed to account for wave height, and empirical data are used to evaluate a universal function for the normalized interface radius. This function, which was evaluated using data for water-argon and alcohol-argon, is shown in Figure 3-19.

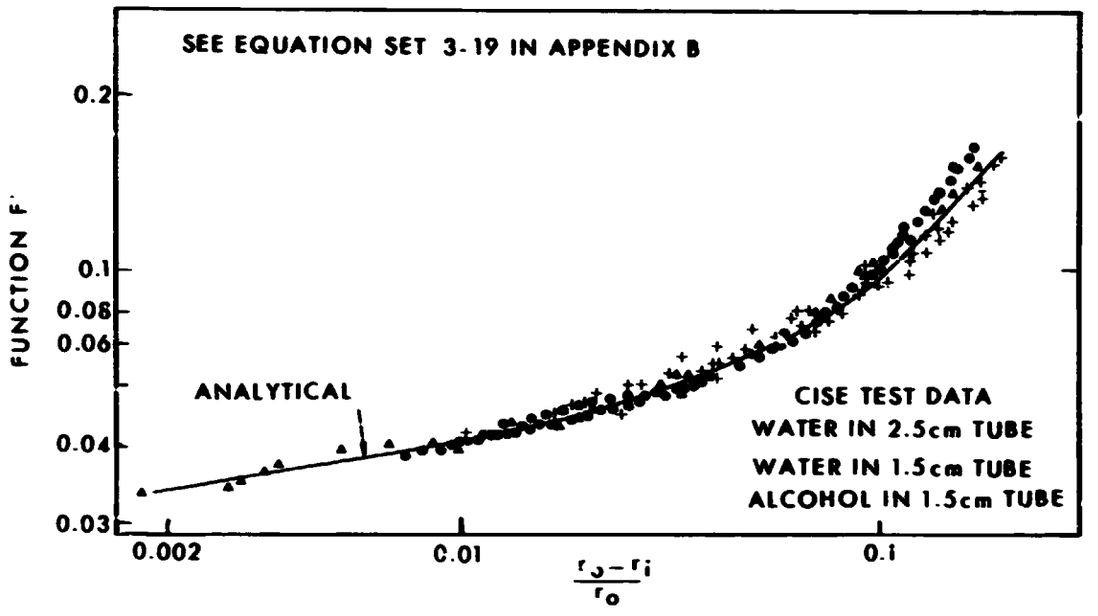

Figure 3-19. Relationship between pressure gradient and liquid film thickness for annular flow with entrainment (from Reference 31).

A prediction system relating the film thickness and pressure drop was developed in the same reference for the additional restrictions that the gas density is much smaller than the liquid density and the liquid velocity is much smaller than the vapor velocity. The prediction procedure is as follows:

1. Compute pressure drop from any method or correlation.
2. Obtain liquid film thickness from Figure 3-19 and Equations (1) and (2) in Equation Set 3-19.
3. Compute liquid film flow rate using Equations (3), (4), and (5) in Equation Set 3-19.
4. Compute liquid entrainment from total liquid flow and film flow rates.

A comparison of some experimental data with this prediction method is shown in Figure 3-20.

G. Superheated Vapor Flow

Semi-Empirical Information

Superheated vapor flow is identical to ordinary gaseous convection. However, since superheater lengths are frequently hydrodynamically short and the flow in the boiler is a developing one, so that fully-established flow may not be obtained in the superheat region, some judgment is required in choosing the proper heat transfer relationship.

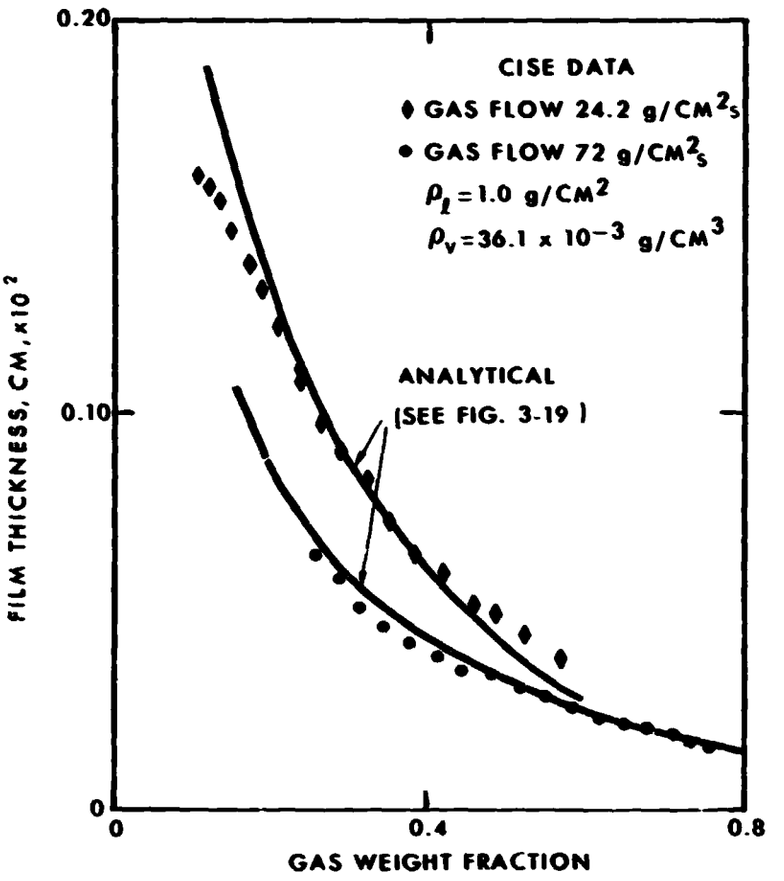

Figure 3-20. Comparison of predicted film thickness with experimental data for annular flow with entrainment (from Reference 31).

However, since the vapor flow is almost invariably in the Reynolds modulus range associated with the turbulent flow regime, the superheater conductance may be expected to tend toward that given by relationships for fully-established turbulent flow. The fully-established correlation can then be modified by a term dependent upon normalized tube length.

Under some circumstances, particularly in uniform heat flux systems or where cryogenic fluids are being vaporized, the wall-to-bulk temperature differences can be large compared to the absolute temperature, so that the thermal properties of the fluid may vary significantly through the wall boundary layer. A number of authors have proposed methods of compensating for variable fluid properties. Usually the correction procedures involve the use of fluid properties based on the bulk temperature, the wall temperature, a mean "film" temperature, or a combination of these properties. By use of some relationships for ideal gases, it is possible to reduce these various correlations to expressions based on bulk fluid properties and a correction term. Eight correlations (References 32 through 39), based on data for air, hydrogen, carbon dioxide, and helium, have been reduced to a common form, and the correction terms compared. The correction terms for tube length are shown in Figure 3-21; the correction terms for temperature are shown in

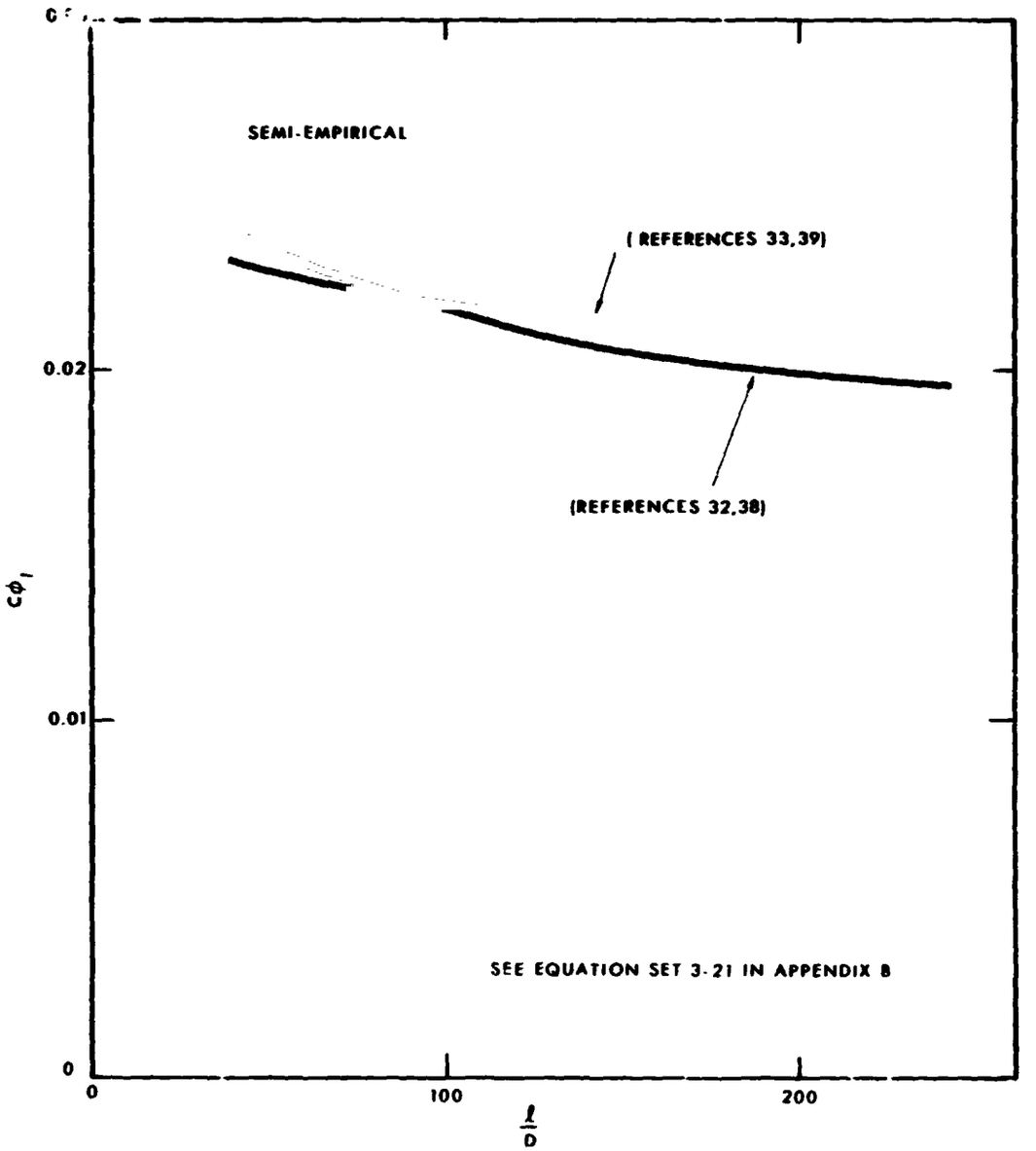

Figure 3-21. Change in Nusselt modulus with tube length according to several correlations.

Figure 3-22. Also shown for comparison is the well-known correlation given by McAdams.[2]

The friction factor is also affected by temperature dependent fluid properties and developing flow. The adiabatic fully-established friction factor can be modified by multiplicative correction terms in the same manner as the Nusselt modulus relationship. The temperature variation of a typical friction factor relationship* reduced to this multiplicative form, is compared to experimental data in Figure 3-23. Another such friction factor correlation with a multiplicative wall-to-bulk temperature ratio correction is given in Reference 36. This latter correlation is, however, based on the Reynolds modulus constructed with properties evaluated at the wall temperature. Typical tube length functions are similar to the ones used in heat transfer relationships; their variation can be found in fluid dynamics texts.

---

* The relationship shown in Figure 3-23 was derived from an expression taken from Reference 35 by use of a Sutherland model for the vapor viscosity.

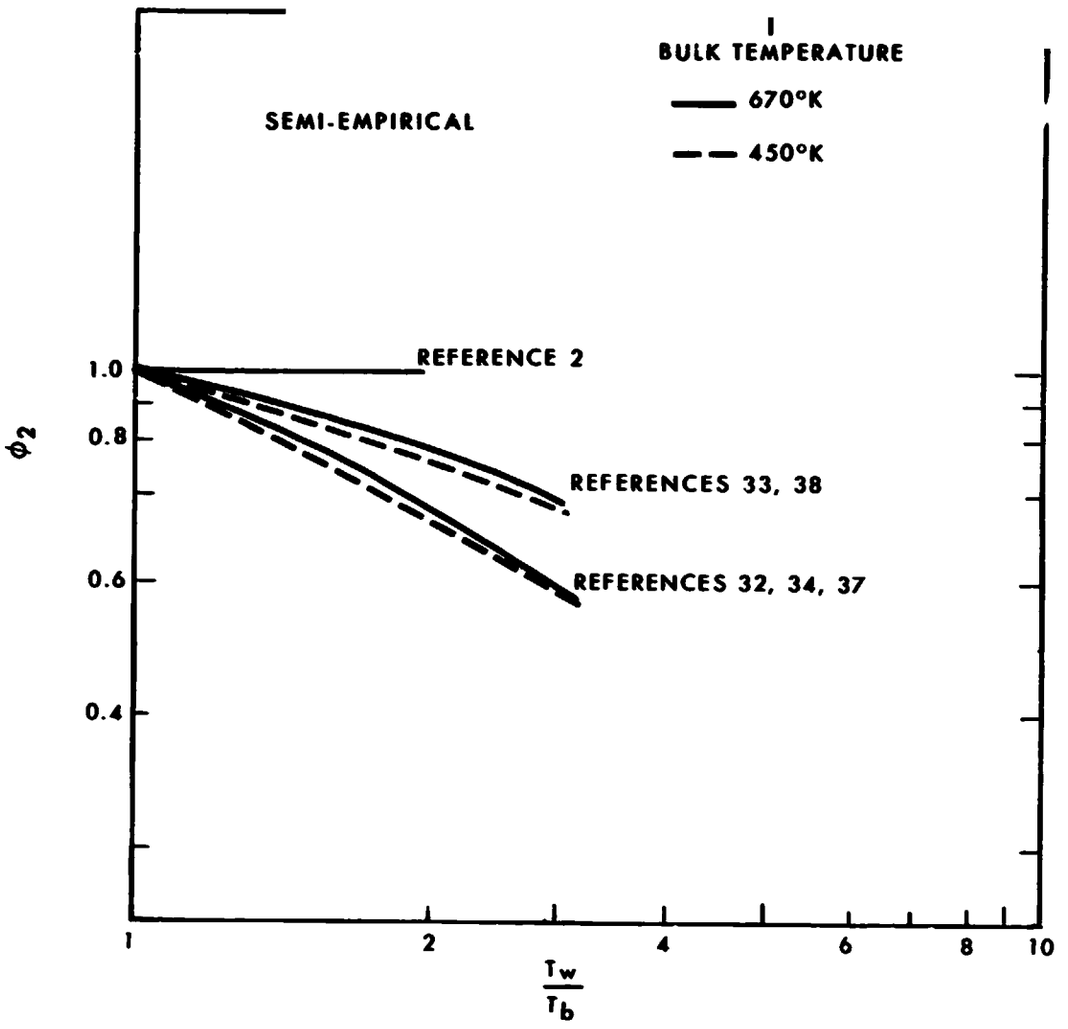

Figure 3-22. Effect of wall to bulk temperature ratio on Nusselt modulus according to several correlations.

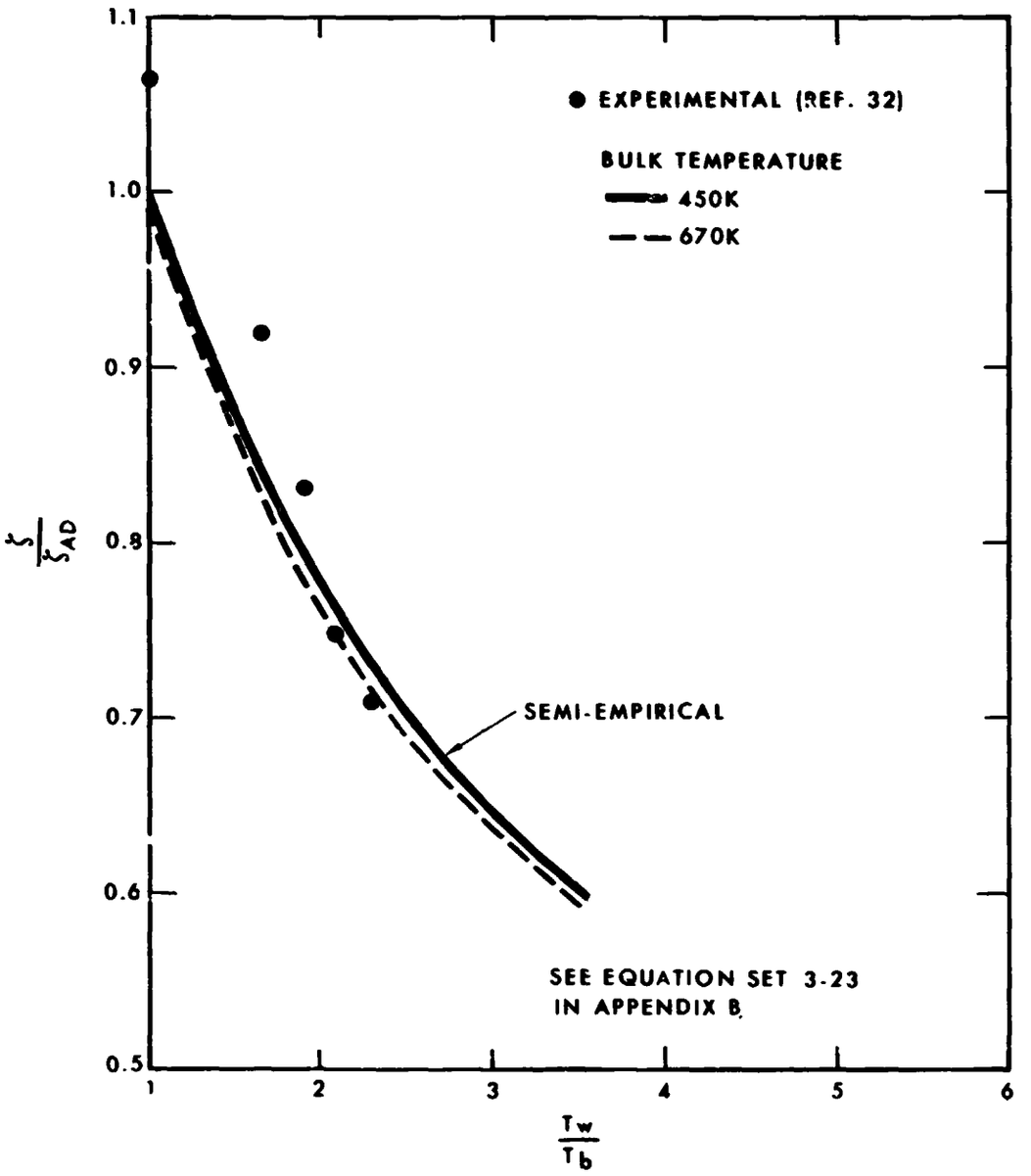

Figure 3-23. Temperature variation of friction factor for single phase vapor flow.

H. Flow Through Tubes with Inserts

The material on flow through tubes with inserts is divided into two parts, namely, (1) a general description of helical flow, and (2) a discussion of flow in specific insert systems currently in use.

General Characteristics of Helical Flow.

1. Single Phase Flow

Experimental Information

Available single phase helical flow friction factor data in the literature (primarily measured under adiabatic conditions) have been converted to a common basis.[40] The mean experimental curves presented in terms of helical to linear friction factor ratios as a function of pitch to diameter ratio for $10^4 < Re_\ell < 10^5$ are shown in Figure 3-24. Helical-flow forced convection data available in the literature obtained for heating water, air, and ethylene glycol were also correlated.[40]

Mean experimental helical to linear Nusselt modulus ratios as a function of pitch to diameter ratio for $10^4 < Rc_\ell < 10^5$ are shown in Figure 3-25.

Analytical Information

The increased heat transfer in single-phase helical-flow systems results primarily from increased fluid turbulence and free

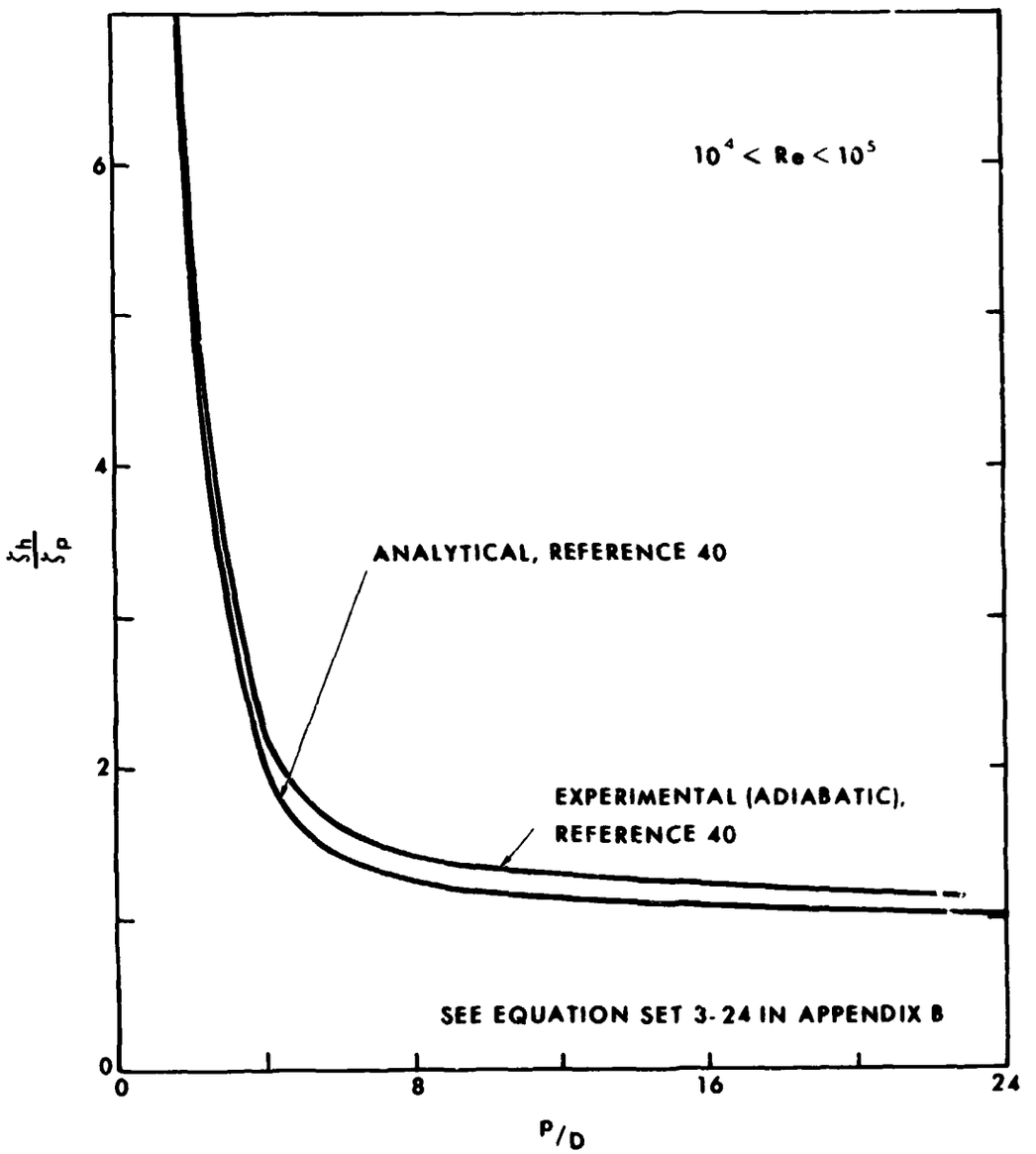

Figure 3-24. Ratio of helical to linear friction factor versus pitch-to-diameter ratio.

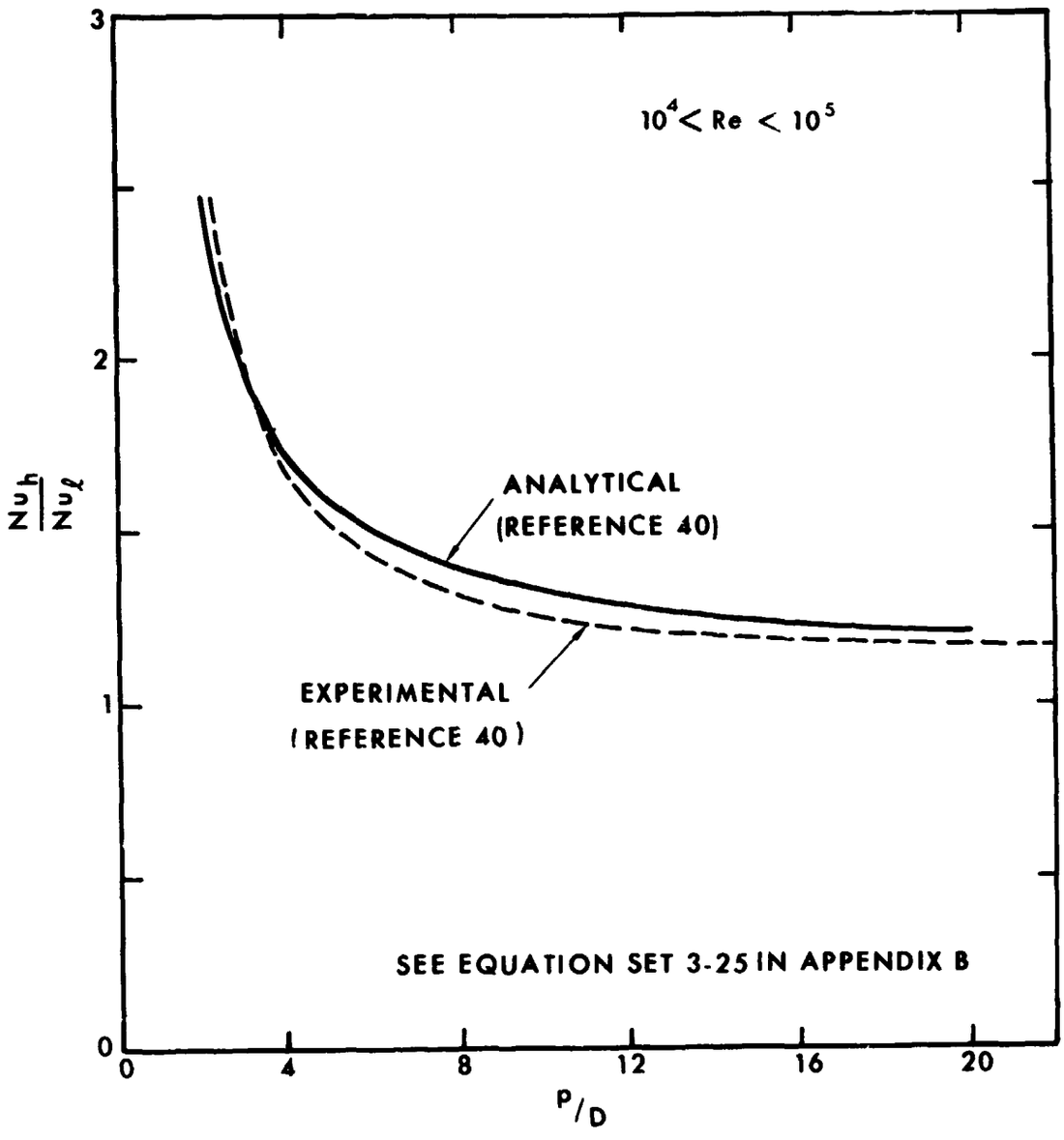

Figure 3-25. Ratio of helical to linear flow Nusselt modulus versus pitch-to-diameter ratio.

convection (under conditions of wall heat addition). Exact analytical descriptions of the heat and momentum transfer in helical flow systems are difficult to obtain because of the complex geometries and fluid flow patterns involved. Flow instability in curvilinear flow systems and superposed natural convection processes further complicate the transport processes in helical flow. It is possible, however, to examine the relative importance of some of the transport models which can be used to characterize single-phase helical flow systems.

A number of fluid dynamics analyses applicable to helical or rotational flow can be found in the literature. An interesting study has been reported[41] for single-phase flow in a tube with a twisted divider. An approximate pressure drop expression is derived which accounts for axial and tangential flow and vortex mixing. The predicted results are in good agreement with several sets of experimental data.

A simplified expression for the isothermal friction factor in the turbulent flow regime can be derived by considering only gross flow features.[40] A large fraction of a fluid flowing in a tube exists in an annular region near the wall. If the fluid flows helically through the tube, the effective flow length has been increased by the ratio of the helical path at the tube wall per unit of axial distance, $\left|1 + (\pi D/p)^2\right|^{1/2}$. Similarly, the resultant fluid velocity in the annular region near the wall has increased approximately by the same ratio. If these

quantities are substituted into the pressure drop equation, a group of terms results which is defined as the friction factor for helical flow; this function is shown in Figure 3-24.

Several heat transfer analyses applicable to helical or rotational flow can be found in the literature. One involves heat transfer conductances in curved channels.[42] An expression for convective heat transfer in a tube with a twisted divider was also described.[41] The effect of free convection on the overall heat transfer was not included.

An expression for the turbulent Nusselt modulus for helical flow (excluding free convection) has been derived on the same basis given for the simple friction factor described above.[40] Free convection heat transfer expressions for idealized natural convection cells in a horizontal fluid layer under unstable temperature gradient conditions have also been developed. Typical power law Grashof-Prandtl modulus equations result that are similar to the experimental expressions for turbulent free convection from horizontal cylinders. The sum of such analytical normalized forced and free convection conductances in terms of Nusselt moduli can be used to estimate single phase helical flow; a comparison with experimental information is shown in Figure 3-25.

2. Helical Vapor and Droplet Flow (Nonwetting)

Consider the case where droplets and vapor are flowing helically through a boiler tube wherein the droplets flow along the wall but do not wet it. The heat transfer from the tube wall consists of both gaseous convection and droplet vaporization. Because these two mechanisms are operating in parallel, the boiling conductance for the tube is equal to the sum of the gaseous convection and droplet vaporization conductances.

Analytical Information

An analysis for the droplet vaporization conductance has been made[25] and the results in the form of a normalized conductance as a function of vapor quality are shown in Figure 3-26. This model describes film boiling vaporization from beneath a droplet contiguous to a heat transfer surface; heat conduction through the vapor film under the drop causes drop evaporation. The centrifugal force field on the drop is balanced by the pressure field under the drop. The vapor conductance (which is the remaining part of the boiling conductance) for helical vapor flow was described previously in this chapter.

A comparison of predicted and experimental potassium boiling conductances for this type of phase distribution can be seen in Figure 3-27.

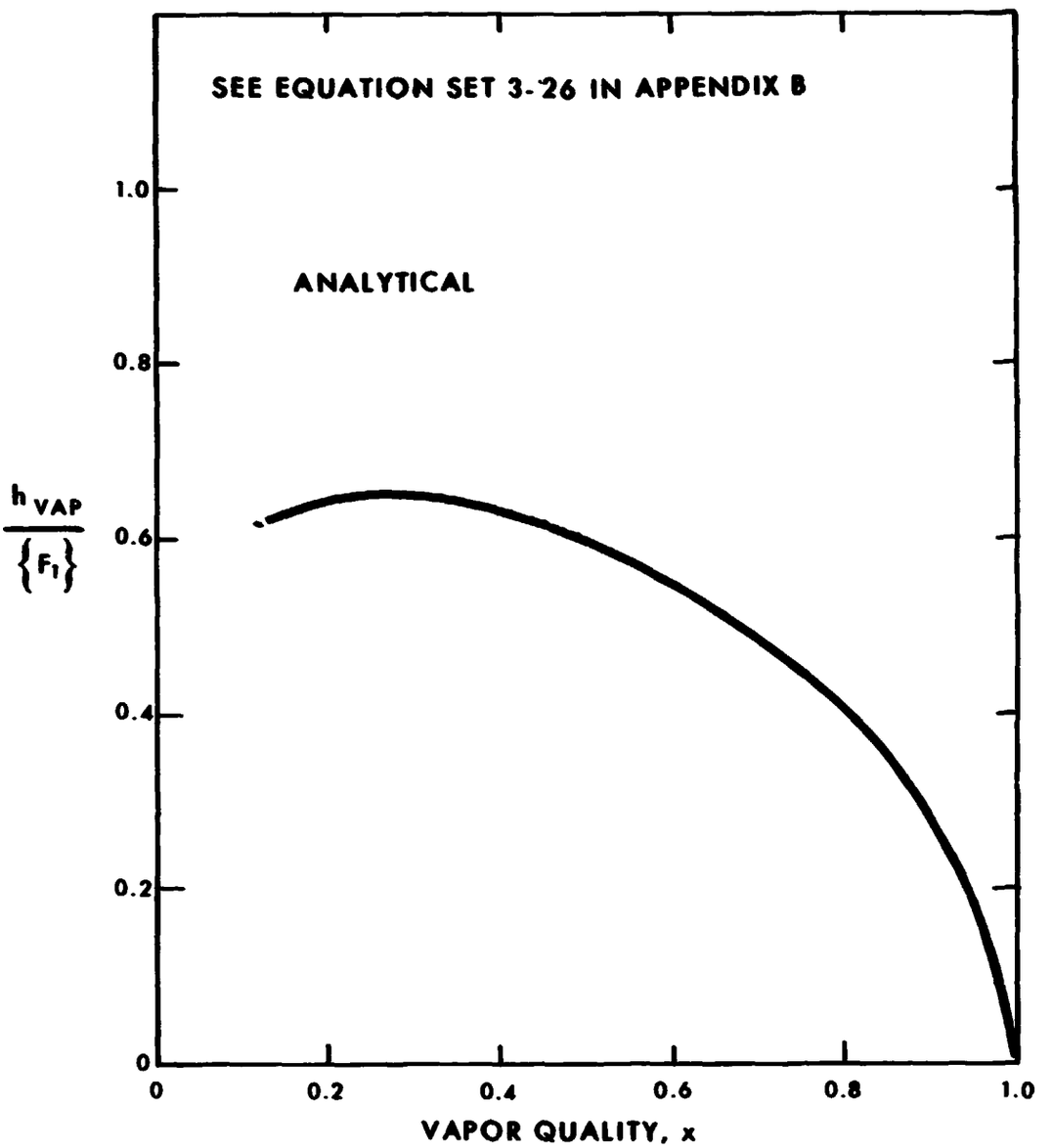

Figure 3-26. Normalized evaporative conductance as a function of vapor quality for nonwetting rivulet flow with helical insert.

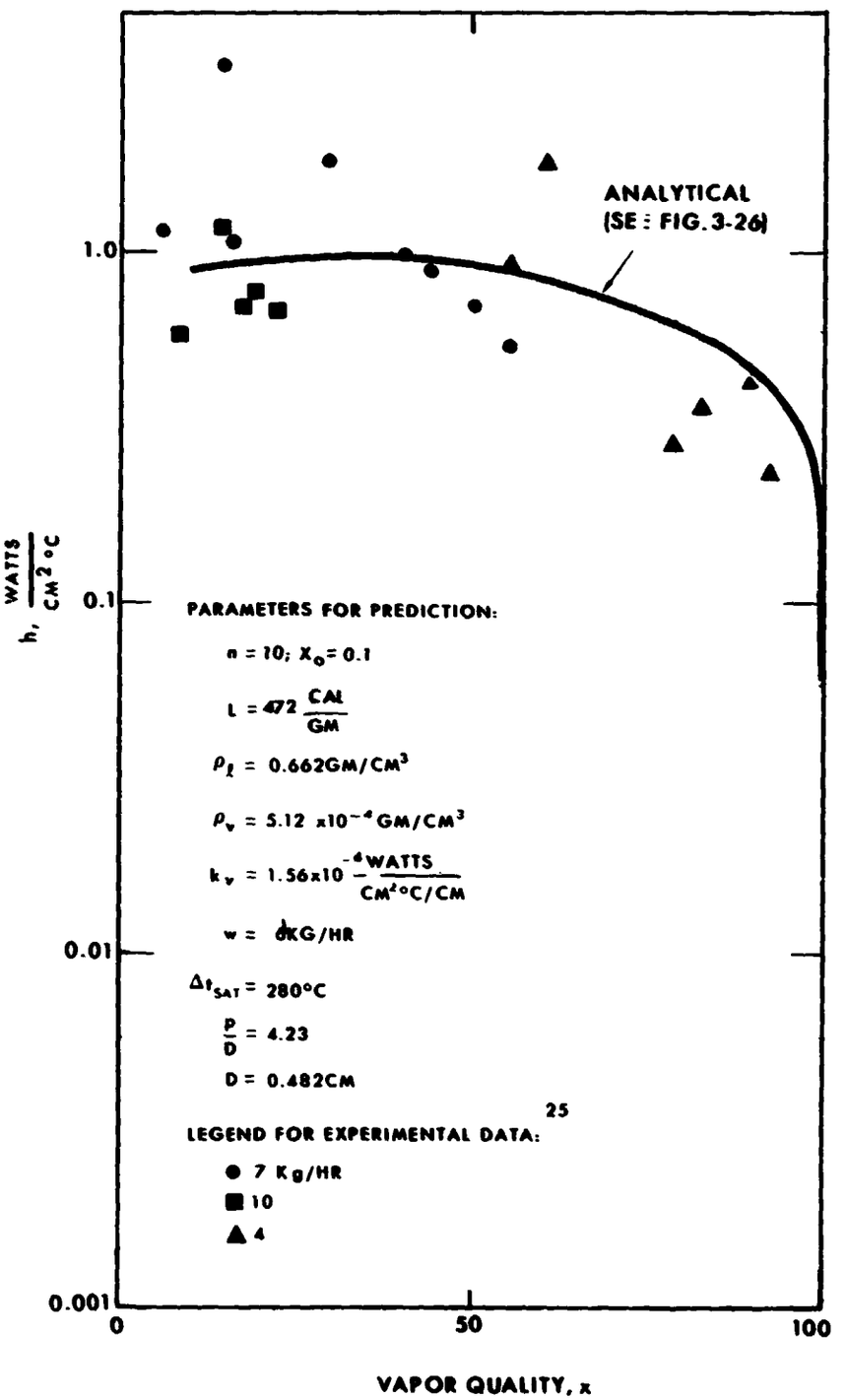

Figure 3-27. Predicted and experimental helical flow boiling potassium results.

Flow Through Specific Inserts.

(1) Helical Grooves in a Rod

If helical grooves are machined in the periphery of a rod that is inserted in a boiler tube, boiling heat transfer takes place in an efficient manner. The two phases are readily separated by the centrifugal force field with a thin liquid layer located at the boiler tube wall in the grooves. An analysis of this flow system has been made[43] and the details are found in the Appendix.

(2) Twisted Tape Insert

When the fluid flowing through a straight tube is brought into rotation by a twisted divider across its diameter, the flow is forced into a path and configuration that has an equivalent diameter, cross sectional area, and velocity different from those in the original tube. A mathematical relationship[44] for the equivalent diameter of this insert geometry is shown in Figure 3-28.

(3) Helical Vane

If the twisted divider discussed in the previous paragraph only extends halfway across the tube diameter, a helical vane system results. The corresponding equivalent diameter expression[44] for this geometry is also shown in Figure 3-28.

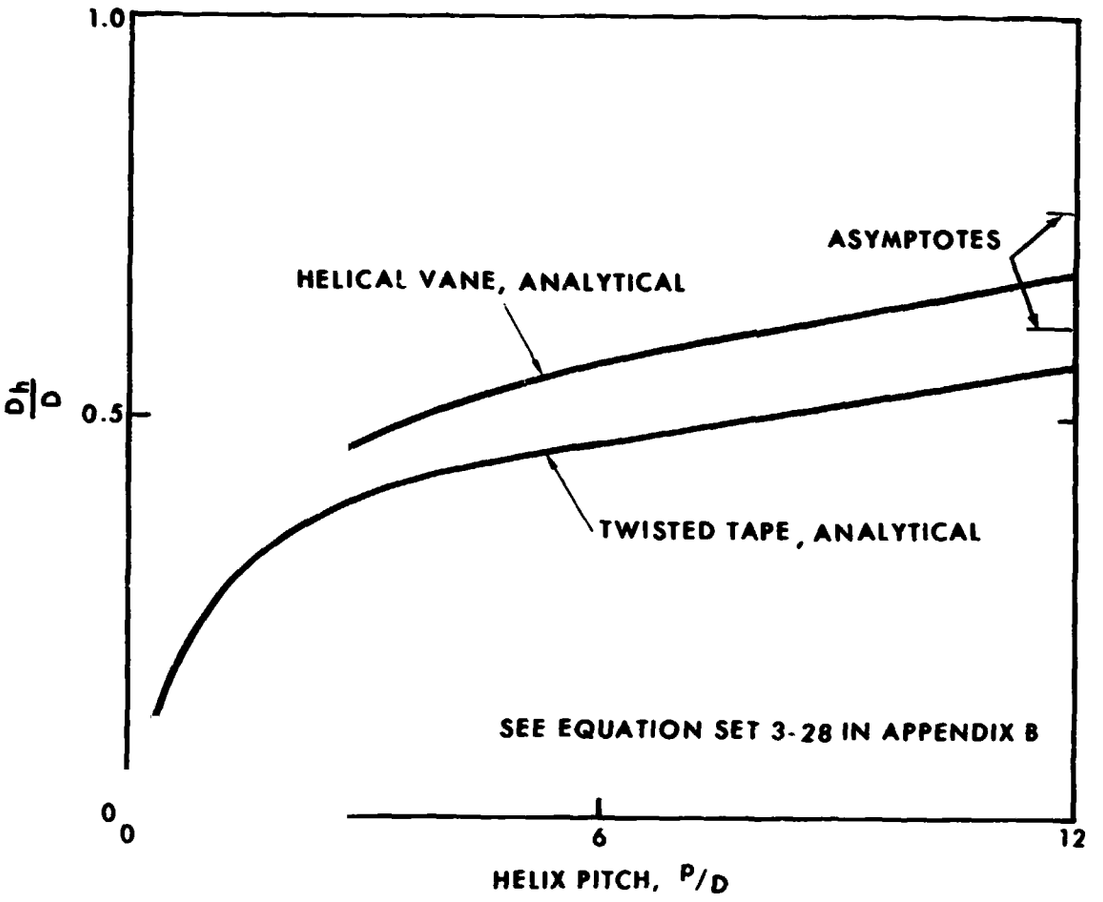

Figure 3-28. Equivalent diameters for tubes with helical inserts (from Reference 44).

Helical Wire Coils.

The preceding sections contain a discussion of heat transfer and pressure drop in tubes in which the flow follows a helical path. In tubes containing twisted dividers, grooved plugs, or helical vanes which extend nearly to the tube centerline, the helical path is well defined. This is not necessarily the case for helical wire coils. There is, of course, no substantial difference between a coil made up of wire equal to the tube radius and a helical vane the height of which is equal to the tube radius. However, in a number of cases wire coil inserts have been used in which the wire diameter is small compared to the tube radius, so that the bulk of the fluid can slip with respect to the wire. The helical path of the fluid can, therefore, be significantly different from the path defined by the wire helix.

Wire coils can be made up from wire of any cross section. However, in the following sections, the data and analyses pertain specifically to coils made from round wire.

Experimental Information

Experimental programs to determine the heat transfer and pressure drop characteristics of single phase flow through tubes containing wire coil inserts are reported in References 37 and 45. Results of those investigations are shown in Figures 3-29 and 3-30.

Semi-Empirical Information

For very short pitch helical wire inserts, the slip of the flow with

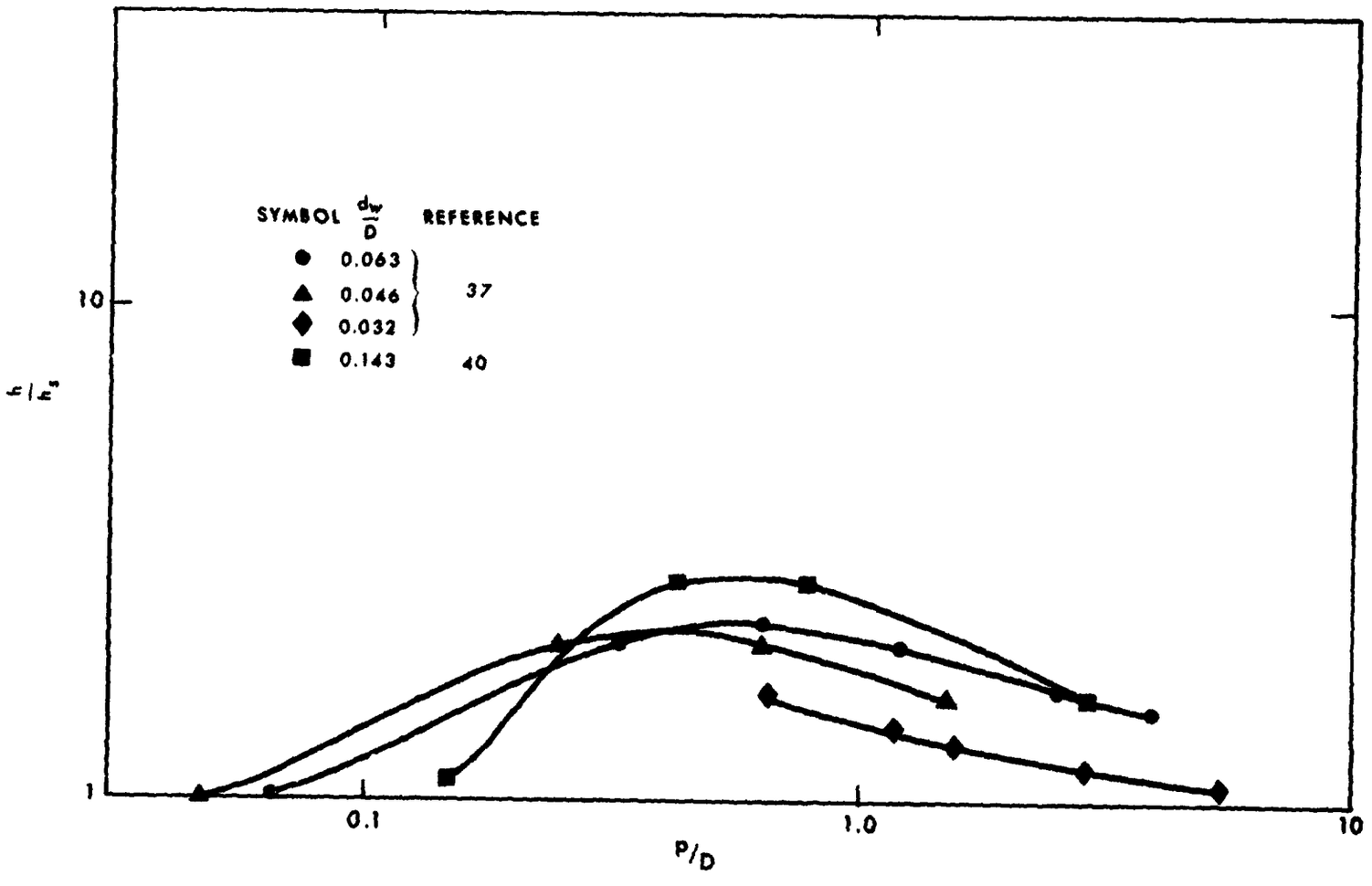

Figure 3-29. Ratio of measured heat transfer conductance for wire coils to that calculated for axial flow in a smooth tube (adapted from Reference 45)

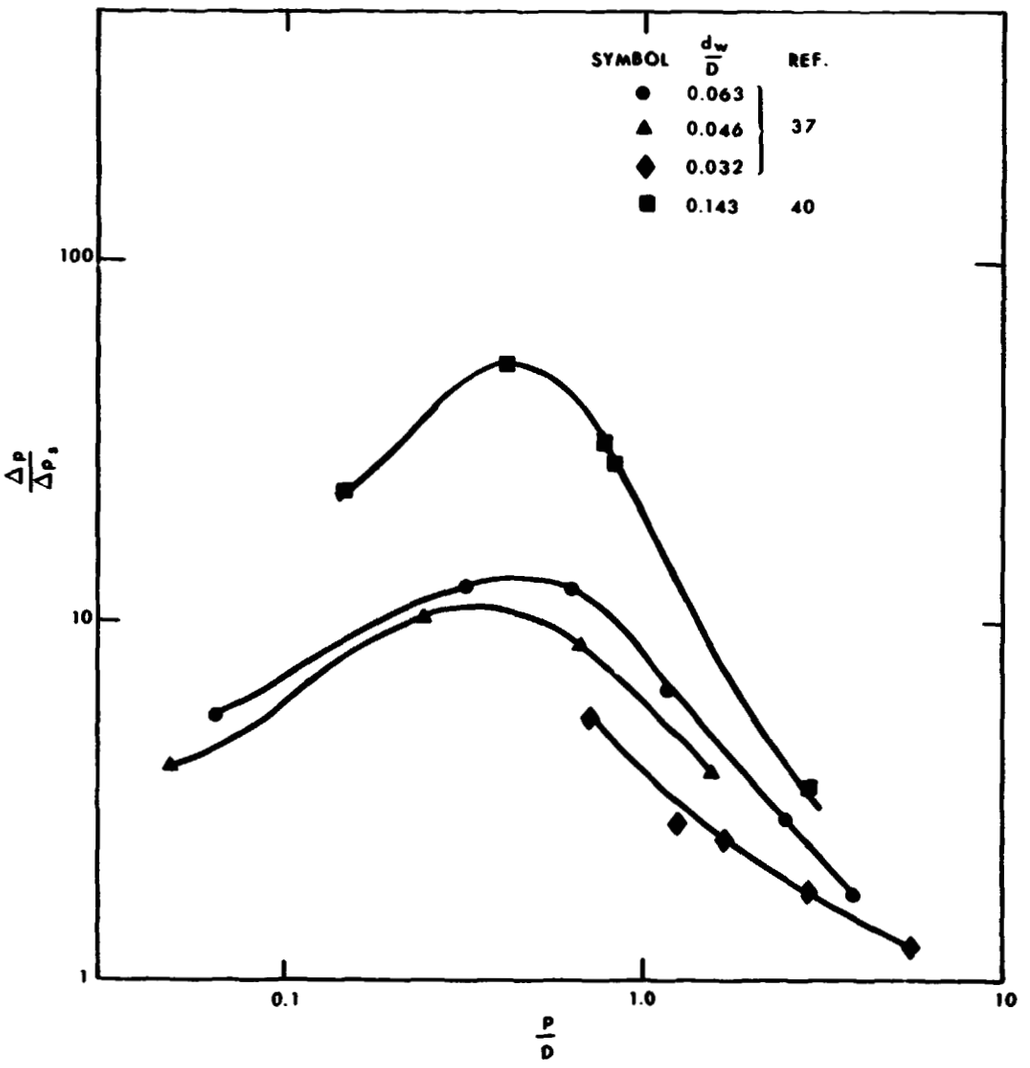

Figure 3-30. Ratio of measured pressure drop for wire coils to that calculated for axial flow in a smooth tube (adapted from Reference 45).

respect to the wire rotation would be expected to be large, so that the flow is similar to that in a tube containing annular rings, or corrugations. The limiting minimum pitch for a helical wire coil is that pitch at which adjacent coils touch each other. At this condition the interior wall of the flow passage appears as a corrugated wall tube whose minimum diameter is the inner diameter of the wire coil.

In Figure 3-30 it was seen that the friction factor passes through a maximum. This maximum apparently occurs at the pitch at which flow reattachment just occurs between the wires. Very little flow rotation would be expected under these conditions. A semi-empirical correlation of the pressure drop characteristics of short pitch helical wire inserts is presented in Reference 25. The results of this work are compared to experimental data for both helical wire coil inserts and corrugated tubes in Figure 3-31.

In the analysis of Reference 25, it is shown that for short pitch wire coils in which the flow reattaches between coil turns, the dominant term in the pressure drop equation is the drag of the wire coils so that the friction factor should vary inversely as the wire coil pitch; i.e., the friction is directly proportional to the number of drag elements per unit of length. That this is the case may be seen in the figure.

Analytical Information

An analysis of the friction and flow rotating characteristics of long pitch ($p/D > 1$), wire coils in fully-established single phase flow is

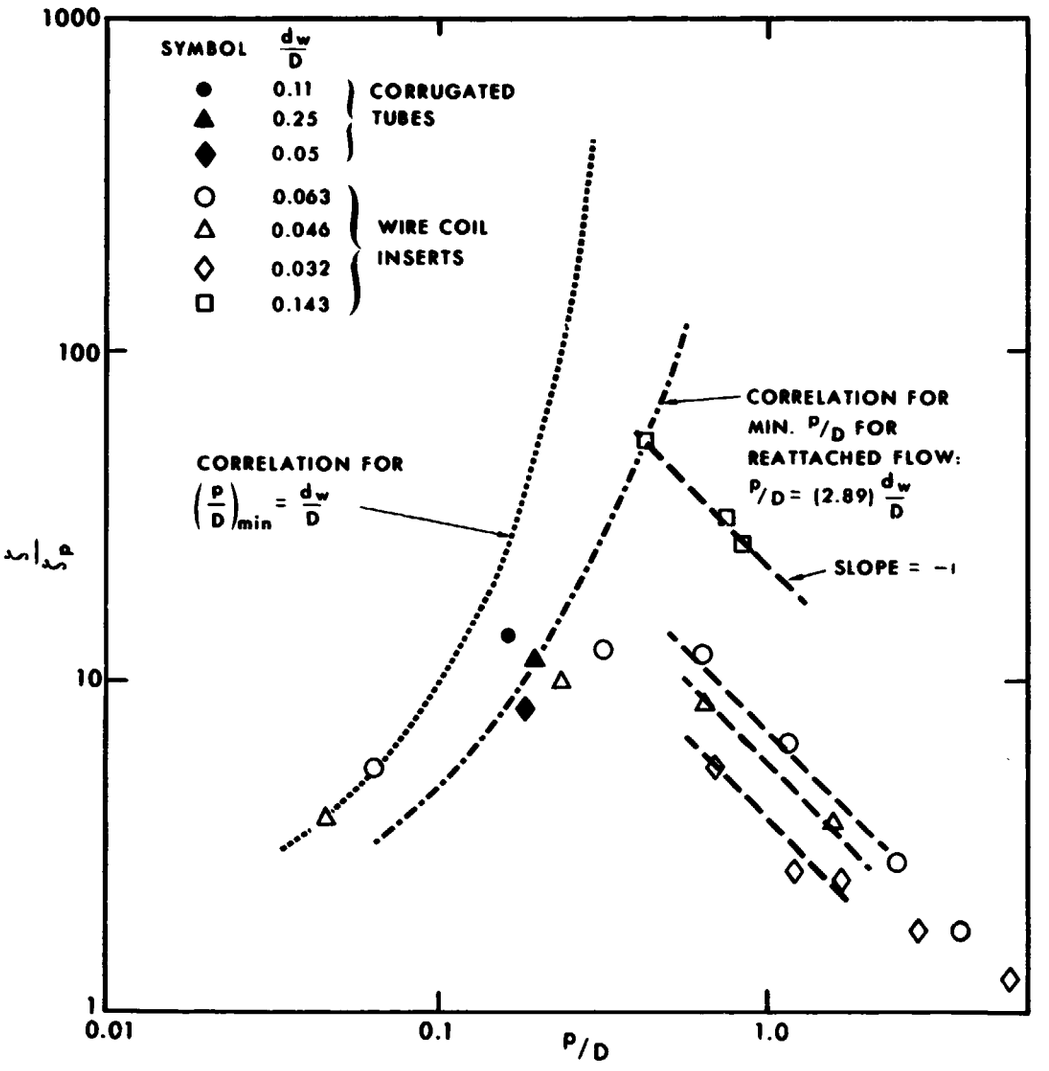

Figure 3-31. Helical wire coil friction factors as functions of flow regime (Reference 25)

presented in Reference 25. The mathematical model is based upon solid body rotation for the fluid, a one-seventh power velocity profile, and wire drag and wall friction coefficients which are independent of the Reynolds modulus. The pressure drop results of this analysis are compared to experimental data in Figure 3-32. The predicted rotation of the flow is shown in Figure 3-33. In this same reference, the tube length required for the flow to attain equilibrium rotation is also considered. This length is such that for practical boilers and wire coil pitches fully-established flow will probably not be attained. This topic is considered in more detail in Chapter 4, which takes up flow transitions.

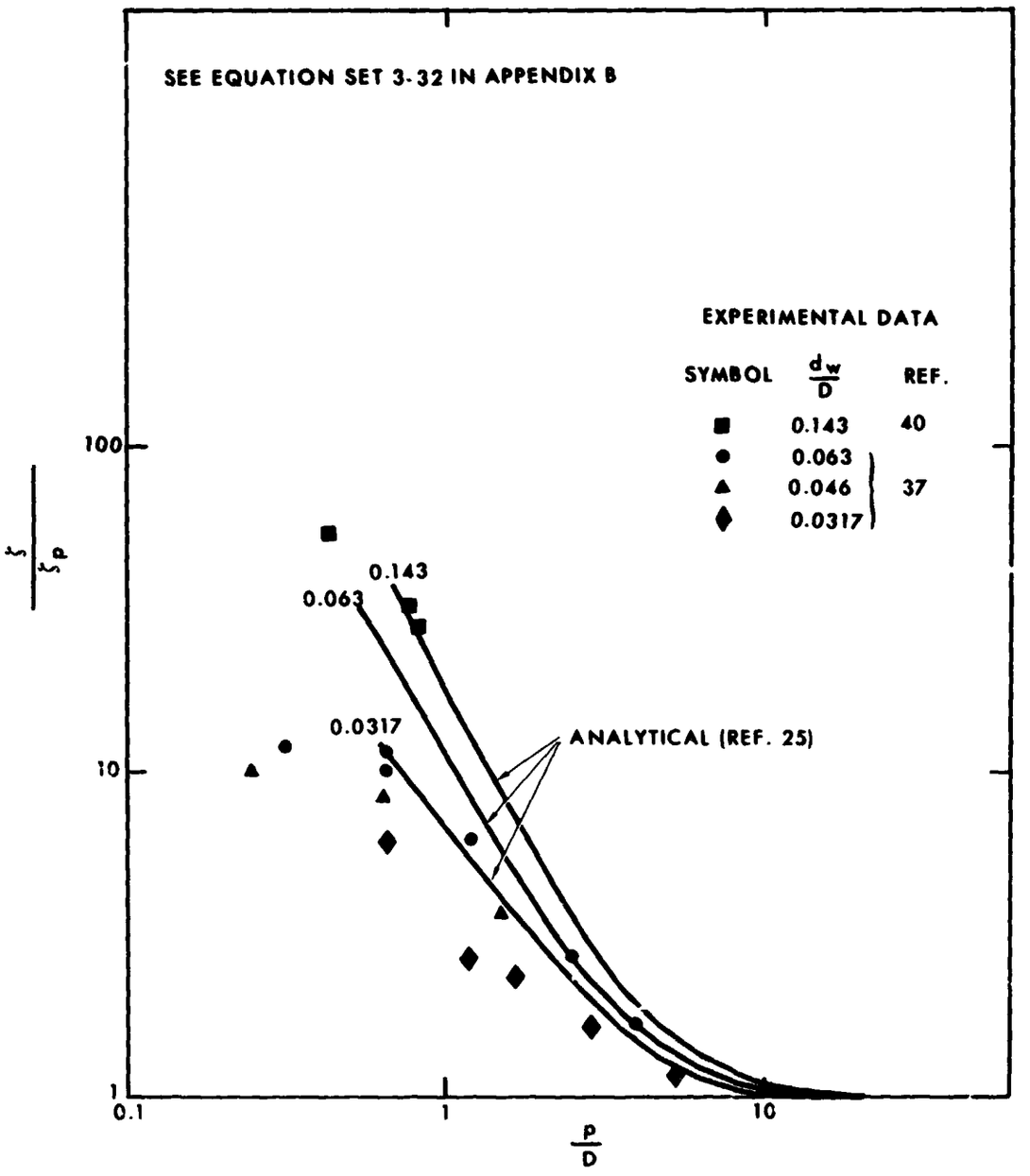

Figure 3-32. Comparison of helical wire pressure drop data with analysis.

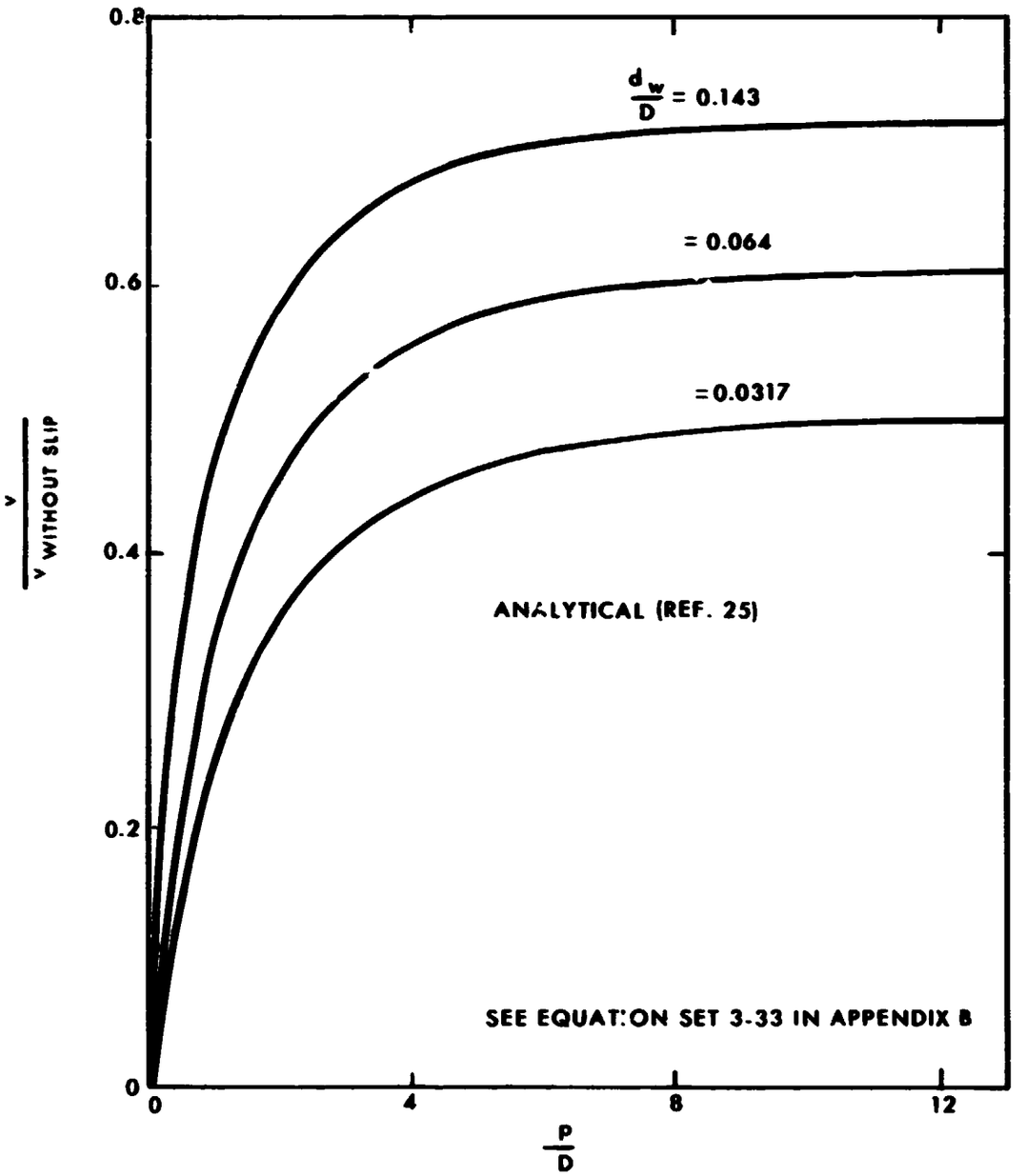

Figure 3-33. Rotating component of velocity as a function of wire coil pitch and wire diameter.

DISCUSSION

This chapter has presented representative quantitative information on the important phase distributions that define forced flow boiling heat transfer and frictional pressure drop. The parameters vapor quality, liquid wetting, fluid flow rate and insert type, among others, control the phase distributions. The qualitative boiling conductance functions as a function of vapor quality are shown in a schematic graph in Figure 3-34. The wetted wall annular flow conductances are the greatest (because of the existence of very thin vaporizing liquid film at the wall) and the nonwetting slug flow conductances are the smallest (because of the controlling, poor vapor convection). The conductances for these two flow regimes can, at times, differ by three or four orders of magnitude.

In the higher vapor quality regions, linear flow yields low boiling conductances defined by slug flow or entrained droplet flow (with poor contact between drops and the boiler tube wall). To improve the conductances by a factor of a hundred or a thousand, rotational flow is generated by tube inserts to provide annular flow or high radial acceleration droplet flow.

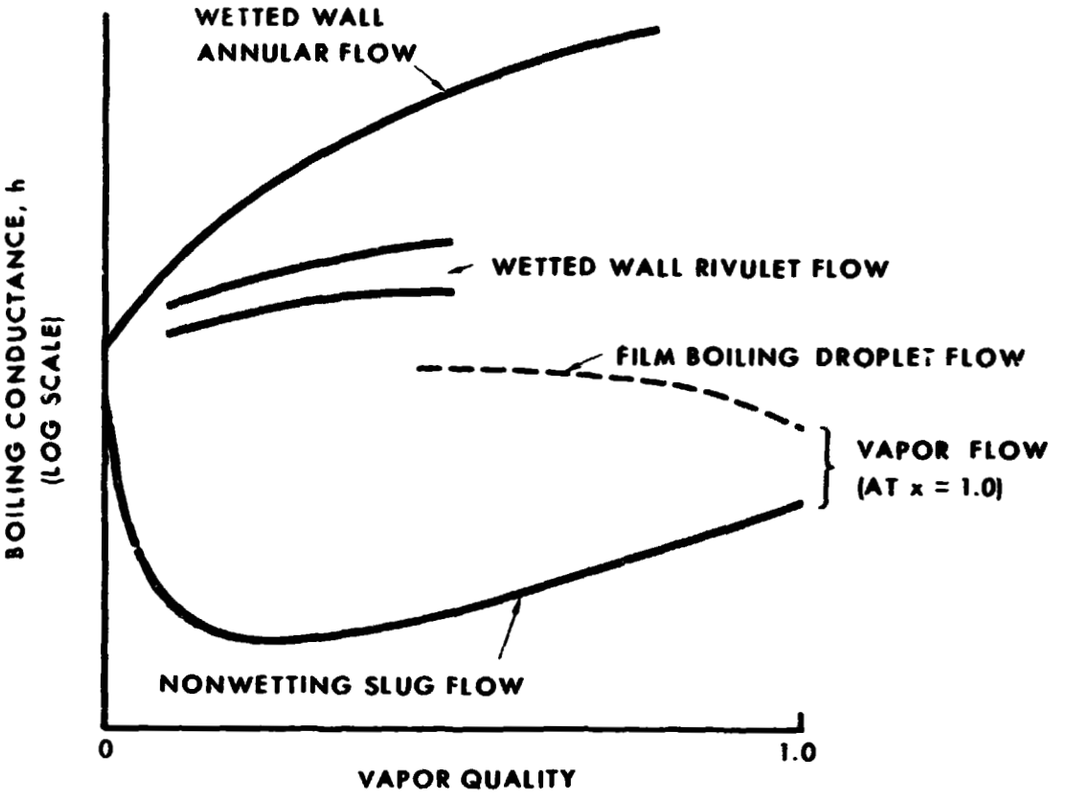

Figure 3-34. Schematic representation of the limits of forced flow boiling conductance functions.

NOMENCLATURE

A = tube cross sectional area

C = a numerical constant

c_{p_ℓ} = liquid specific heat at constant pressure

D = tube inner diameter

D_h = tube equivalent diameter with helical insert

d_w = diameter of wire for wire coil insert

F = a function (see Figure 3-17)

F' = a function (see Figure 3-19)

F_1 = a parameter (see Figure 3-26)

g = acceleration of gravity

H = normalized conductance, $\frac{h(x)}{h_v(x = 1)}$

h = convective heat transfer conductance

$h_{an.film}$ = conductance for an unbroken annular film

h_b = boiling heat transfer conductance

h_h = helical flow heat transfer conductance

h_ℓ = linear flow heat transfer conductance

h_s = heat transfer conductance for a smooth tube

h_v = conductance for dry areas

$h_v(x = 1)$ = conductance for flow at 100 percent vapor quality

h_{vap} = conductance due to vaporizing droplets

k_ℓ = liquid thermal conductivity

k_t = apparent thermal conductivity of turbulent liquid film

k_v = vapor thermal conductivity

L = latent heat of vaporization

ℓ = tube length

Nu = Nusselt modulus

Nu_h = Nusselt modulus in helical flow

Nu_ℓ = Nusselt modulus for linear flow

n = number of droplets in tube length of one diameter entrained in vapor at reference quality x_o

Pe = Peclet modulus

Pr = Prandtl modulus

Pr_v = Prandtl modulus of vapor

p = absolute pressure, pitch of helical insert

Re = Reynolds modulus

Re_ℓ = Reynolds modulus based on axial flow in the tube

Re_v = Reynolds modulus evaluated with vapor properties

r_i = radius of gas-liquid interface in annular flow

r_o = tube inside radius

T_b = fluid mixed mean absolute temperature

T_w = tube wall absolute temperature

u_ℓ = superficial liquid velocity, $\frac{w_\ell}{\rho_\ell A}$

$\bar{u}_\ell$ = normalized superficial liquid velocity, $u_\ell \left[g D(\rho_\ell - \rho_v)\right]^{-\frac{1}{2}}$

u_v = superficial vapor velocity, $\frac{w_v}{\rho_v A}$

$\bar{u}_v$ = normalized superficial vapor velocity, $u_v \left[g D(\rho_\ell - \rho_v)\right]^{-\frac{1}{2}}$

v = rotating component of velocity at wall (Figure 3-37)

w = mass flow rate

w_ℓ = liquid mass flow rate

w_v = vapor mass flow rate

x = vapor quality

x_{exit} = vapor quality at tube exit

x_o = a reference vapor quality

X_{tt} = Martinelli parameter, Figure 3-5, $X_{tt} = \left(\frac{\rho_v}{\rho_\ell}\right)^{0.571} \left(\frac{\mu_\ell}{\mu_v}\right)^{0.143} \left(\frac{1}{x} - 1\right)$

GREEK SYMBOLS

α = void fraction, contact angle of liquid on wall

Δp = pressure drop

Δp^* = dimensionless two-phase pressure drop, $\dfrac{-\left(\frac{\partial p}{\partial z}\right) - \rho_v g}{g D (\rho_\ell - \rho_v)}$

Δp_ℓ^* = dimensionless single phase liquid pressure drop, $\dfrac{-\left(\frac{\partial p}{\partial z}\right)_\ell}{g D (\rho_\ell - \rho_v)}$

Δp_s = pressure drop in a smooth round tube

Δp_{tp} = two phase flow pressure drop

Δp_v^* = dimensionless single phase vapor pressure drop, $\dfrac{-\left(\frac{\partial p}{\partial z}\right)_v}{g D (\rho_\ell - \rho_v)}$

$\Delta p(x = 1)$ = single phase flow pressure drop for 100 percent vapor quality

ΔT_{sat} = wall to saturation temperature difference

δ = annular liquid film thickness

ϵ = root mean square surface roughness

ζ = Weisbach friction factor

ζ_{ad} = adiabatic friction factor

ζ_h = friction factor for helical flow

ζ_p = friction factor for a smooth pipe

μ_ℓ = absolute liquid viscosity

μ_v = absolute vapor viscosity

π = 3.14159...

ρ_ℓ = liquid density

ρ_v = vapor density

ϕ_1 = a function of tube length to diameter ratio (Figure 3-21)

ϕ_2 = a function of wall to bulk absolute temperature ratio (Figure 3-22)

$\phi_{\ell\,tt}$ = Martinelli two-phase pressure drop multiplier, $\frac{(\frac{\partial p}{\partial z})}{(\frac{\partial p}{\partial z})_\ell}$

DERIVATIVES

$\frac{\partial p}{\partial z}$ = axial pressure gradient for two phase flow

$(\frac{\partial p}{\partial z})_\ell$ = axial pressure gradient for liquid flowing alone in tube

$(\frac{\partial p}{\partial z})_v$ = axial pressure gradient for vapor flowing alone in tube

REFERENCES

1. Schlichting, H.; "Boundary Layer Theory," Fourth Edition, McGraw-Hill Book Company, 1960.

2. McAdams, W. H.: "Heat Transmission," Third Edition, McGraw-Hill Book Company, 1954.

3. Lyon (editor); "Liquid Metals Handbook," Second Edition, Atomic Energy Commission, June 1952.

4. Lubarsky, B.; Kaufman, Samuel J.; "Review of Experimental Investigations of Liquid-Metal Heat Transfer," NACA Rep 3336, March 1955.

5. Norris, R. H.; Streid, D. D.; "Laminar-Flow Heat-Transfer Coefficients for Ducts," ASME Trans 62:525-33, 1940.

6. Martinelli, R. C.; "Heat Transfer to Molten Metals," ASME Trans 69:947-59, 1947.

7. Lyon, R. N.; "Liquid Metal Heat-Transfer Coefficients," Chem Engrg Prog, 47 75-79, 1951.

8. Martinelli, R. C.; Nelson, D. B.; "Prediction of Pressure Drop During Forced Circulation Boiling of Water," ASME Trans 70:695-702, 1948.

9. Goldmann, K.; "Selected Parameters for Two-Phase Flow of Sodium," Proc of 1963 High Temp Liq Metal Heat Transfer Tech Meeting, ORNL-3605, Vol 2.

10. Peterson, J.: "High Performance 'Once-Through' Boiling of Potassium in Single Tubes at Saturation Temperatures of 1500° to 1750°F," NASA CR-842, Aug 1967.

11. Poppendiek, H. F.: Greene, N. D.; Sabin, C. M.; Livett, R. K.; MacDonald, F. R.; Feigenbutz, L. F.; "Annual Technical Report on High Acceleration Field Heat Transfer for Auxiliary Space Nuclear Power Systems," Geoscience Ltd GLR-27, June 30 to Aug 31, 1964.

12. Nicklin, D. J.; Wilkes, J. O.; Davidson, J. F.; "Two-Phase Flow in Vertical Tubes," Trans Inst Chem Eng, Vol 40, p 61, 1962.

13. Cimorelli, L.; Evangelisti, R.; "Experimental Determination of the "Slip Ratio" in a Vertical Boiling Channel Under Adiabatic Conditions at Atmospheric Pressure," Int J Heat Mass Transfer, Vol 12, No. 6, June 1969.

14. Evangelisti, R.; Lupoli, P.; "The Void Fraction in an Annular Channel at Atmospheric Pressure," ibid.

15. Staub, F. W.; Zuber, N.; "A Program of Two-Phase Flow Investigation," Sixth Quarterly Rep GEAP-4733, General Electric, Schenectady, N. Y., Oct 1964.

16. Wallis, G. B.; Meyer, P. E.; Turner, J. M.; "Two-Phase Flow and Boiling Heat Transfer," Quarterly Prog Rep NYO-3114-11, Dartmouth College, Oct 1965.

17. Wallis, G. B.; "An Analysis of the Liquid Film in Annular Flow," Interim Rep NYO-3114-13, Dartmouth College, Dec 1965.

18. Longo, J., Jr. (editor); "Alkali Metals Boiling and Condensing Investigations," Quarterly Prog Rep No. 4, NASA Contract NAS 3-2528, General Electric, Cincinnati, July 1963.

19. Wallis, G. B.; "Two Phase Flow and Boiling Heat Transfer Final Report," NYO 3114-14, Dartmouth College, Feb 1966.

20. Poppendiek, H. F.; Greene, N. D.; MacDonald, F. P.; Wright, H. R.; Sabin, C. M.; Thompson, A. S.; "Annual Technical Report on High Acceleration Field Heat Transfer for Auxiliary Space Nuclear Power Systems," AEC Contract No. AT(04-3)-409, Geoscience Ltd GLR-10, Sep 1, 1961 - Aug 31, 1962.

21. Poppendiek, H. F.; Greene, N. D.; Sabin, C. M.; Feigenbutz, L. V.; Mouritzen, G.; Schwartz, P. E.; Connelly, D. J.; Morton, W. A.. "Annual Technical Report on High Acceleration Field Heat Transfer for Auxiliary Space Nuclear Power Systems," AEC Contract No. AT(04-3)-409, Geoscience Ltd GLR-41-SAN-409-28, Sep 1, 1964 - Aug 31, 1965.

22. Levy, S.: "Theory of Pressure Drop and Heat Transfer for Annular Steady State Two-Phase Two-Component Flow in Pipes," Proc Second Midwestern Conference on Fluid Mechanics, 1952.

23. Lockhart, R. W.: Martinelli, R. C.: "Proposed Correlation of Data for Isothermal Two-Phase, Two Component Flow in Pipes," Chem Eng Prog 45, 1944.

24. Sabin, C. M.; Greene, N. D.; Poppendiek, H. F.; Connelly, D. J.; "Steady State and Transient Performance of the Rocketdyne Organic Preheater-Boiler Unit," Geoscience Ltd GLM-15, Oct 1966.

25. Sabin, C. M.; Poppendiek, H. F.; "Heat and Momentum Transfer Model Studies Applicable to Once-Through, Forced Convection Potassium Boiling," NASA CR-1896, Geoscience Ltd GLR-71, Sept 1971.

26. Adorni, N.; Casagrande, I.; Cravarolo, L.; Hassid, A.; Pedrocchi, E. Silvestri, M.; "Further Investigations in Adiabatic Dispersed Two-Phase Flow: Pressure Drop and Film Thickness Measurements with Different Channel Geometries - Analysis of the Influence of Geometrical and Physical Parameters," CISE Rep R-53, 1963.

27. Casagrande, I.; Cravarolo, L.; Hassid, A.; Pedrocchi, E.; "Adiabatic Dispersed Two-Phase Flow: Further Results on the Influence of Physical Properties on Pressure Drop and Film Thickness," CISE Rep R-73, 1963.

28. Meyer, P. E.; Wallis, G. B.; "Cocurrent Upwards Annular - Mist Flow," Rep NYO 3114-10, Dartmouth College, Sept 1965.

29. Gravarolo, L.: Hassid, A.; Pedrocchi, E.: "Further Investigation on Two-Phase Adiabatic Annular Dispersed Flow: Effect of Length and of Some Inlet Conditions on Flow Parameters," CISE Rep R-93, Sept 1964.

30. Magiras, P. G.; Dukler, A. E.; "Entrainment Pressure Drop in Gas-Liquid Flow," Developments in Mechanics, Vol I, p 532, North Holland Publishing Co., Amsterdam, 1961.

31. Levy, S.: "Prediction of Two-Phase Annular Flow with Liquid Entrainment," Int J Heat Mass Transfer, Vol 9, No. 3, Mar 1966.

32. Humble, L. V.; Loudermilk, W. A.; Desmon, L. G.; "Measurements of Average Heat Transfer and Friction Coefficients for Subsonic Flow of Air in Smooth Tubes at High Surface and Fluid Temperatures," NACA Rep 1020.

33. Taylor, M. F.; Kirchgessner, T. A.; "Measurements of Heat Transfer and Friction Coefficients for Helium Flowing in A Tube at Surface Temperatures Up to 5900°R," ARS Semi-annual Meeting, June 8-11, 1959.

34. McEligot, Magee, "Aerothermodynamic Studies at High Temperature," Stanford University Mechanical Engineering Dept Nuclear Engineering Laboratory Rep SU-TR-326-1, June 30, 1962.

35. Private communication to the authors from Mr. William Roberts, Marquardt Corporation, 1963.

36. Taylor, M. F.; "A Method of Correlating Local and Average Friction Coefficients for Both Laminar and Turbulent Flow of Gases Through a Smooth Tube with Surface to Fluid Bulk Temperature Ratios from 0.35 to 7.35," Int J Heat Mass Transfer, Vol 10, No. 8, p 1123, Aug 1967.

37. Sams, E. W.; "Heat Transfer and Pressure Drop Characteristics of Wire Coil Type Turbulence Promoters," Reactor Heat Transfer Conference, USAEC, New York, Nov 1956.

38. Durham, F. P.; Neal, R. C.; Newman, H. J.; "High Temperature Heat Transfer to a Gas Flowing in Heat Generating Tubes with High Heat Flux," ibid.

39. Davenport, M. E.; Magee, P. M.; "Heat Transfer and Pressure Drop for a Gas at High Temperature," Stanford University, Dept Mech Eng, Nuclear Technology Laboratory, TR 247-2, May 1961.

40. Poppendiek, H. F.; Geoscience Ltd: Gambill, W. R.; Oak Ridge National Laboratory. Greene, N. D.; Geoscience Ltd, "Helical, Forced Flow Heat Transfer and Fluid Dynamics in Single and Two-Phase Systems," Third United Nations International Conference on The Peaceful Uses of Atomic Energy, May 1964.

41. Smithberg, E.; Landis, F.; "Friction and Force Convection Heat Transfer Characteristics in Tubes with Twisted Tape Swirl Generators," ASME, J Heat Transfer, Vol 86, pp 39-49, Feb 1964.

42. Kreith, Frank; "Heat Transfer in Curved Flow Channels," Heat Trans. and Fluid Mech. Inst., pp 111-122, Stanford Univ. Press, 1953.

43. Poppendiek, H. F,; "SNAP-δ Boiler Performance Degradation and Two-Phase Flow Heat and Momentum Transfer Models," NASA CR-72759, Geoscience Ltd GLR-84, Aug 1970.

44. Mouritzen, G.; "Forced Rotation of Flow in Pipes," Geoscience Ltd GLM-36, July 1965.

45. Converse, G. L.; "Air Heating Experiments," GE Missile and Space Div Memorandum HTC-12, Cincinnati, April 1969.

Bibliography

1. Gido, R. G.; Koestel, A.; "The SNAP-II Power Conversion System. Topical Report 17. Mercury Boiling Research," NAA-SR-6309, TRW Rep ER-4833, Oct 1962.

2. Goldmann, K.: Firstenberg, H.; Lombardi, C.; "Burnout in Turbulent Flow - A Droplet Diffusion Model," Trans ASME, J Heat Trans, Vol 83, Series C. No. 2, pp 158 - 162.

3. Stein, R. P.; Crane, M.; Firstenberg, H.; Hankel, R.; Israel, S.; "Investigation of Wet Steam as a Reactor Coolant (CAN-2)," United Nuclear Corp., Rep UNC 5008-I, NYO-9844-I, 1962.

4. Hendricks, R. C.; Graham, R. W.; Hsu, Y. Y.; Friedman, R.; "Experimental Heat Transfer and Pressure Drop of Liquid Hydrogen Flowing Through a Heated Tube," NASA TN D-765, May 1961.

5. Hendricks, R. C.; Graham, R. W.; Hsu, Y. Y.; Friedman, R.: "Experimental Heat-Transfer Results for Cryogenic Hydrogen Flowing in Tubes At Subcritical and Supercritical Pressures to 800 PSIA," NASA TN D-3095.

6. Bond, J. A.: Converse, G. L.: "Vaporization of High-Temperature Potassium in Forced Convection at Temperatures of 1800°F to 2100°F," NASA CR-843, July 1967.

7. Hsia, E. S.; "Topical Report No. 7 - SNAP-8 Refractory Boiler Development Program - Analysis and Testing of a Single Tube Mercury Boiler," NASA CR-72897, Sept 1971.

8. Tong, L. S.: "Boiling Heat Transfer and Two-Phase Flow," John Wiley & Sons, Inc., New York, 1965.

9. Bergles, A. E.: Rohsenow, W. M.; "The Determination of Forced Convection Surface Boiling," ASME Paper 63-HT-22.

10. Gido, R. G.; Koestel, A.; Haller, H. C.; Huber, D. D.: Deibel, D. L.: "The SNAP-II Power Conversion System Topical Report N 12 Boiler Development," TRW Rep ER-4521, 1961.

11. Koestel, A.: Gutstein, M.: Wainwright, R.: "Fog-Flow Mercury Condensing Pressure Drop Correlation," Proc 1963 High-Temperature

Liquid-Metal Heat Transfer Technology Meeting, ORNL-3605, Vol 2, UC-33, Propulsion Systems and Energy Conversion, TID-4500, 34th ed. p 198, Dec 1964.

12. Berenson, P. J.; Killackey, J. J.; "An Experimental Investigation of Forced-Convection Vaporization of Potassium," ibid, p 1.

13. Peterson, J. R.; Weltmann, R. N.; Gutstein, M. U.; "Thermal Design Procedures for Space Rankine Cycle System Boilers," GESP-67, presented at the Intersociety Energy Conversion Engineering Conference, Aug 13-16, 1968.

14. Stevens, W. D.; Daman, E. L.; Zebroski, E. L.; Tippets, F. E.; "Steam Generator Development for a Proposed 350 MWe Liquid Metal Fast Breeder Reactor Demonstration Plant," ASME 71-WA/NE-6, 1971.

15. Gutstein, M. U.; Converse, G. L.; Peterson, J. R.; "Theoretical Analysis and Measurement of Single-Phase Pressure Losses and Heat Transfer for Helical Flow in a Tube," NASA TN D-6097, Nov 1970.

16. Schuster, J. R.; Berenson, P. J.; "Final Report, Simulated Potassium Boiler Experiments, Insert Evaluation Tests Using Freon-113," AiResearch Rep 69-4568, NASA Contract NAS 3-10929, Feb 1969.

17. Peterson, J. R.; Converse, G. L.; Gutstein, M. U.; "An Experimental Study of Pressure Loss and Phase Distribution for Air-Water Flow in A Tube Containing Swirl Generators," presented at the Fifth Intersociety Energy Conversion Engineering Conference, GESP-449, Sept 21-25, 1970.

18. Bernstein, E.; Petrek, J. P.; Rose, G. J.; Horan, J. J.; "Experimental Results of Forced Convection Boiling Potassium Heat Transfer and Pressure Drop Tests," Pratt & Whitney Rep PWAC-429, for AEC Contract AT(30-1)-2789, July 1964.

19. Hess, H. L.; Hooper, J. R.; Organ, S. E.; "Analytical and Experimental Study of the Dynamics of a Single-Tube Counterflow Boiler, NASA CR-1230, Feb 1969.

20. Hoffman, H. W.; "Recent Experimental Results in ORNL Studies with Boiling Potassium," Proc 1963 High-Temperature Liquid-Metal Heat Transfer Technology Meeting' ORNL-3605, Vol 1, TID-4500, 34th ed., p 334, Nov 1964.

21. Balzhiser, R. E.; "Boiling Studies with Potassium," ibid, p 351.

22. Noyes, R. C.; "Summary of Recent Results of Sodium Boiling Studies," ibid, Vol 2, p 24.

23. Chen, J. C.; "A Proposed Mechanism and Method of Correlation for Convective Boiling Heat Transfer with Liquid Metals," ibid, p 47.

24. Fisher, C. R.; "Heat Transfer and Pressure Drop Characteristics for Boiling Rubidium in Forced Convection," ibid, p 64.

25. Peterson, J. R.; "The Effect of Swirl Flow Upon the Performance of Monotube Steam Generators," presented at the 1970 SAE Automotive Engineering Congress and Exposition, Jan 1970.

26. Vohr, J. H.; "Evaporative Processes in Superheated Forced Convective Boiling," Mechanical Technology, Inc., Rep MTI-70TR15, Dec 1970.

27. Vohr, J. H.; Chiang, T.; "A Review of Criteria for Predicting Incipient Nucleation in Liquid Metals and Ordinary Fluids," Mechanical Technology Inc., Rep MTI-69TR45, Nov 1969.

28. Chisholm, D.: "A Theoretical Basis for the Lockhart-Martinelli Correlation for Two-Phase Flow," Int J Heat Mass Transfer, Vol 10, pp 1767-1778, Dec 1967.

29. Tippets, Frank E.; "Critical Heat Flux and Flow Pattern Characteristics of High Pressure Boiling Water in Forced Convection," General Electric Rep GEAP-3766, Apr 1962.

30. Dougall, Richard S.; Rohsenow, Warren M.; "Film Boiling on the Inside of Vertical Tubes with Upward Flow of the Fluid at Low Qualities," Massachusetts Institute of Technology Rep MIT-TR-9079-26, Sept 1963.

31. Laverty, William F.; Rohsenow, Warren M.; "Film Boiling of Saturated Liquid Flowing Upward Through a Heated Tube: High Vapor Quality Range," Massachusetts Institute of Technology Rep MIT-TR-9857-32, Sept 1964.

32. Bankoff, S. G.: "A Variable Density Single-Fluid Model for Two-Phase Flow with Particular Reference to Steam-Water Flow," J Heat Transfer, Vol 82, No. 4, pp 265-272, Nov 1970.

33. Topper, L.; "A Diffusion Theory Analysis of Boiling Burnout in the Fog Flow Regime," J Heat Transfer, Vol 85, No. 3, pp 284-285, Aug 1963.

34. Deissler, Robert G.; "Analysis of Turbulent Heat Transfer, Mass Transfer and Friction in Smooth Tubes at High Prandtl and Schmidt Numbers," NACA TR-1210, 1955.

35. Silvestri, Mario; "Fluid Mechanics and Heat Transfer of Two-Phase Annular-Dispersed Flow," Advances in Heat Transfer, Vol 1, pp 355-446, Academic Press, 1964.

36. Hsia, E. S.; "Forced Convective Annular-Flow Boiling with Liquid Mercury Under Wetted and Swirl Flow Conditions," presented at the Winter Annual Meeting of ASME, Heat Transfer Division, Liquid-Metal Heat Transfer and Fluid Dynamics, p 76, Nov 1970.

37. Schultheiss, G. F.; "Experimental Investigation of Incipient Boiling Superheat in Wall Cavities," ibid, p 100.

38. Kottowski, H.; Grass, G.: "Influence of Superheating by Suppression of Nucleation Cavities and Effect of Surface Microstructure on Nucleation Sites," ibid, p 108.

39. Chen, J. C.; "An Experimental Investigation of Incipient Vaporization of Potassium in Convective Flow," ibid, p 129.

40. Fauske, H. K.; Grolmes, M. A.: "Pressure Drop for Forced Convection Flashing Sodium," ibid, p 135.

41. Singer, R. M.; Holtz, R. E.: "Bubble Growth Measurements in Non-Uniformly Superheated Sodium," ibid, p 144.

42. Daniel, J. Harrison, Jr.: "Acceptance Tests of 3.0-KW, 60-Hz, Organic, Rankine-Cycle Power Plant," USAMERDC Rep 2049, Jan 1973.

43. Teagan, W. P.; Morgan, D. T.: "3 KW Closed Rankine-Cycle Powerplant," USAMERDC Rep TE5092-99-72, prepared by Thermo Electron Corp., June 1973.

44. Doyle, E. F.; Raymond, R. J.; et al; "Detailed Design, Rankine-Cycle Power System with Organic-Based Working Fluid and Reciprocating Expander for Automobile Propulsion," EPA Rep 4134-71-72, Vol 1, prepared by Thermo Electron Corp., May 1972.

45. Robin, Theodore, T., Jr.: Snyder, Nathan W.; "Bubble Dynamics in Subcooled Nucleate Boiling Based on the Mass Transfer Mechanism," Int J Heat Mass Transfer, Vol 13, pp 305-318, 1970.

46. Gutierrez, Orlando, A.; Fenn, David B.; "Experimental Cavitation and Flashing of Potassium Flowing Adiabatically Through a Venturi Sized as a Boiler Inlet," NASA TN D-5738, Lewis Research Center, April 1970.

47. Bikerman, J. J.; "Surface Roughness and Contact Angle," J of Physical Chemistry, Vol 54, 1950.

48. Kottowski, H.: Grass, G.: "Influence of Superheating by Suppression of Nucleation Cavities and Effect of Surface Microstructure on Nucleation Sites," Liquid Metal Heat Transfer and Fluid Dynamics, Winter Annual Meeting of the ASME, Library of Contress No. 76-141516, Nov 30, 1970.

49. Dean, C. W.: Rohsenow, W. M.; "Mechanism of Nucleate Boiling Heat Transfer to Alkali Liquid Metals, ibid.

50. Sutherland, W. A.: "Heat Transfer to Superheated Steam," General Electric Co., GEAP-4258, May 1963.

51. Hoffman, E. E.: "Boiling Potassium Stability Studies," Metals and Ceramics Division Annual Progress Report for Period Ending May 31, 1963, ORNL-3470, pp 114-118, Nov 11, 1963.

52. Bond, J. A.: "The Design of Components for an Advanced Rankine Cycle Test Facility," General Electric Co., GESP-451, presented at the Intersociety Energy Conversion Engineering Conference Energy 70, Vol 1, Paper 709105, p 7-66.

53. Harrison, R. W.; Hoffman, E. E.; General Electric; Davies, R. L.; NASA-Lewis, "Recent Materials Compatibility Studies in Refractory Metal-Alkali Metal Systems for Space Power Applications," GESP-452, ibid, Paper 709133, p 11-12.

54. Morgan, D.; Raymond, R.; Thermo Electron Corp., Machacek, R.; Dawson, D.; National Air Pollution Control Administration, HEW, "Rankine-Cycle Power System with Organic Fluid and Reciprocating Engine for Low-Emission Automotive Propulsion," ibid, Paper 709139, p 11-45.

55. Morgan, D. T.; Doyle, E. F.; Kitrilakis, S. S.; "Organic Rankine Cycle with Reciprocating Engine," presented at the Fourth Intersociety Energy Conversion Engineering Conference, Washington, D. C., Paper 69901, Sept 22-26, 1969.

56. Niggeman, R. E.; Bland, T. J.; Wigmore, D. B., "A 6 KWe Organic Rankine Power Conversion System for Space Applications," ibid, p 11-56.

57. Furman, Edward R.; Brooks, R. D.; Harrison, R. W.; "Experimental Evaluation of Tantalum/Stainless Steel Mercury Boilers for the SNAP-8 System," ibid, Paper 709144, p 11-74.

58. Fraas, A. P.; "A Potassium-Steam Binary Vapor Cycle for Better Fuel Economy and Reduced Thermal Pollution," Trans ASME J of Engineering for Power, p 53, Jan 1973.

59. Wilson, A. J.; "Space Power Spinoff Can Add 10 + Points of Efficiency to Fossil-Fuel Power Plants," presented at the Seventh Intersociety Energy Conversion Engineering Conference, San Diego, California, p 260, 1972.

60. Dukler, A. E.; Wicks III, Moye: Cleveland, R. G.; "Frictional Pressure Drop in Two-Phase Flow: A Comparison of Existing Correlations for Pressure Loss and Holdup," AICHE J, Vol 10, No. 1, p 38, Jan 1964.

61. Dukler, A. E.; Wicks III, Moye: Cleveland, R. G.; "Frictional Pressure Drop in Two-Phase Flow: An Approach Through Similarity Analysis," ibid, p 44.

CHAPTER 4: FLOW REGIME TRANSITIONS

In Chapter 3, information was provided for defining quantitatively the heat transfer and frictional pressure drop of two phase flow in boilers, provided that the phase distributions were known. These experimental, semi-empirical and analytical data were usually presented in terms of single phase functions (for one or both phases). The functions contain single phase relationships modified by terms dependent upon vapor quality, geometry, flow rate, and other parameters. These results demonstrated that the apparently complicated two-phase processes can be related to familiar single phase processes.

In the present chapter, information is provided that will assist the designer in determining what phase distributions exist along the length of the boiler tube. The phase distribution transitions of principal interest to the boiler designer are listed below under five categories, namely, (1) fluids which wet the tube wall, (2) fluids which do not wet the tube wall, (3) boiler tube inserts, (4) boiler tube thermal conductivity and wall thickness, and (5) boiler tube wall surface chemistry and physics. The contents of these categories (as they appear in the chapter) are outlined below.

A. Fluids Which Wet the Tube Walls

1. Superheating of the liquid without phase change
2. Onset of subcooled boiling

3. Transition from bubbly flow to wetted-wall slug flow
4. Transition from wetted-wall slug flow to annular flow
5. Onset of entrainment from waves on the annular film
6. Onset of nucleate boiling in an annular film
7. "Burnout," "Boiling Crisis," and "Critical Heat Flux"
8. Termination of the annular film

B. Fluids Which Do Not Wet the Tube Walls

1. Onset of nonwetting slug flow
2. Onset of transition from slug flow to helical rivulet flow

C. Boiler Tube Inserts

1. Some aspects of two-phase flow in insert transitions
2. Transition from a helical plug to a helical wire coil
3. Interrupted inserts

D. Boiler Tube Thermal Conductivity and Wall Thickness

E. Boiler Tube Surface Chemistry and Physics

1. Nucleation sites
2. Droplet vaporization

PHASE DISTRIBUTIONS TRANSITIONS

A. Fluids Which Wet the Tube Walls

1. Superheating of the liquid without phase change

The phenomenon of nucleate boiling in conventional pool boiling systems is attributed to minute cavities with residual gas trapped inside. These cavities form the visible nucleation sites which are the source of vapor bubbles. Water usually boils in metal containers with only a degree or two of superheat at the wall. However, it has the ability to superheat in the liquid phase to almost 150°F above the saturation temperature if carefully degassed and heated in a system which has been evacuated to remove the trapped gas from the cavities in the heated surface. In contrast to metal, glass usually has few cavities in the surface which can act as nucleation sites. Boiling chips, which contain many microscopic cavities, are frequently added to water boiling systems made of glassware to reduce liquid superheating with its accompanying violent change of phase.

Many boiling systems must be carefully cleaned and evacuated before they are charged with the working fluid. This procedure is common in alkali liquid metal systems, for example, and also in systems which use oxidation-sensitive organic fluids. The removal of inert or noncondensible gases

from the system by evacuation may destroy the effectiveness of nucleation sites.

It is possible to estimate the amount of superheat required to bring on the formation of vapor cavities in the liquid in the complete absence of nucleation sites. An analysis of a model based on the thermodynamic properties of the fluid has been made, and predictions presented for water, potassium, and sodium in Reference 31. The analysis examines the conditions for existence of a vapor bubble in a superheated liquid, with temperature equilibrium between the vapor and the liquid in contact with it. The pressure within the bubble is determined by the liquid surface tension and the container pressure. Similarity between the well-established behavior of water and the behavior of the liquid metals is assumed in order to predict the behavior of potassium and sodium. These results, which represent maximum theoretical values, are reproduced in Figure 4-1.

Many experiments have been performed to determine the amount of superheat required to bring on boiling in forced convection systems. These have usually been performed with liquid metals. Measured superheats are generally lower than those predicted by the analysis (probably at least partly because system purity is not perfect), but superheats of hundreds of degrees are still common. Experiments performed with

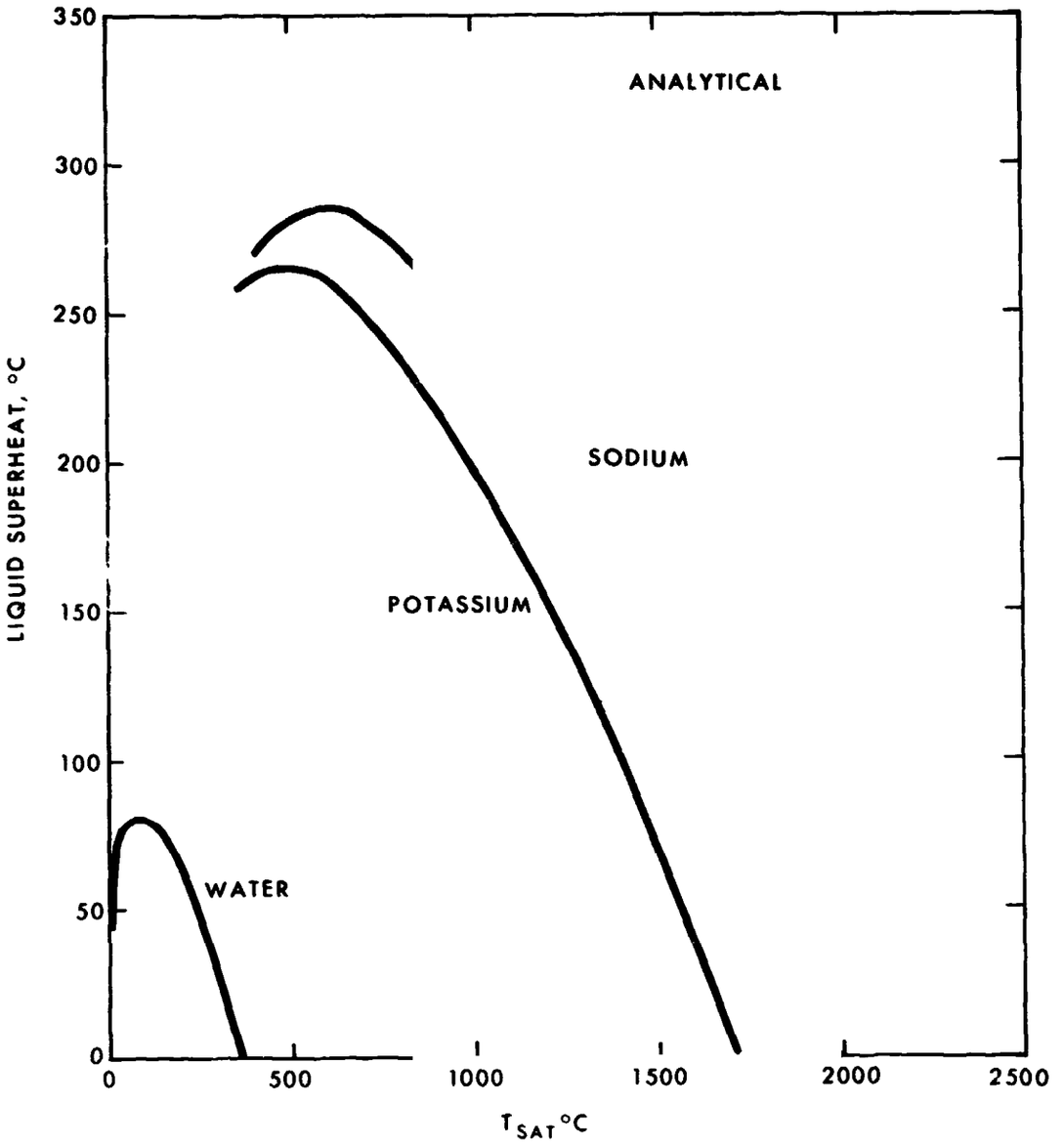

Figure 4-1. Liquid superheat predictions from Reference 31.

potassium (Reference 1) indicate that the amount of superheat required to initiate phase change decreases with increasing saturation temperature, which agrees with the analytical result.

Apparently a high flow turbulence intensity also inhibits superheating, because these same experiments indicate decreased superheat with increasing flow Reynolds number. These same trends have been observed in systems containing sodium (Reference 2).

2. The onset of subcooled boiling

Since the wall in the preheater is hotter than the bulk mixed mean temperature of the fluid, boiling begins at the heated surface before the bulk fluid reaches the saturation temperature. For ordinary fluids, the mixed mean fluid temperature can be significantly subcooled. Initially the vapor is confined to a bubble layer adhering to the surface, because bubbles separated from the wall immediately collapse as a result of condensation in subcooled liquid. As the bulk temperature increases along the tube, there comes a point where bubbles separated from the wall do not collapse. Downstream of this point the void fraction rises rapidly. A diagram illustrating this feature is shown in Figure 4-2. In Reference 3, an analysis is presented for the liquid bulk subcooling at the onset of net vapor generation. The analysis, which is derived for

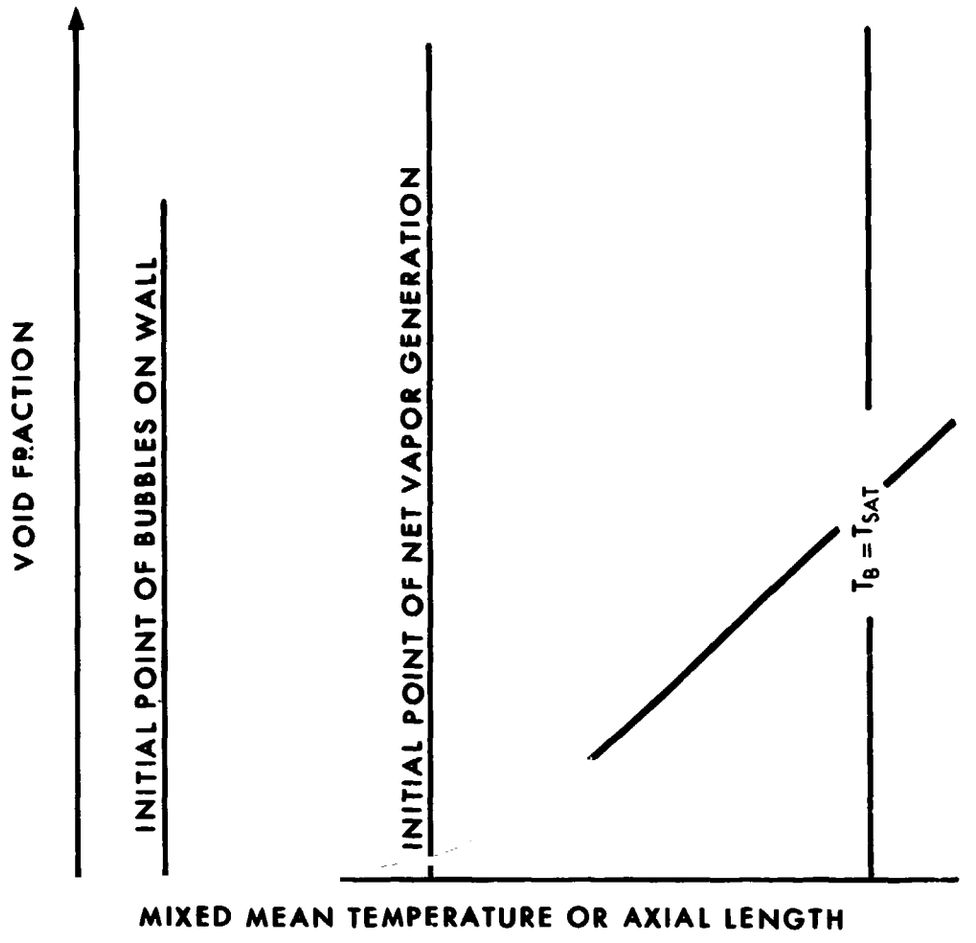

Figure 4-2. Void fraction variation in subcooled boiling.

vertical upward flow, is based upon a balance between the forces tending to hold the bubble to the wall and the forces tending to remove the bubble from the wall. A contact angle function, which describes the surface tension restraining force, is evaluated experimentally. Major idealizations include: the friction factor of the flow on the bubble layer can be obtained from classical single phase flow experiments for turbulent flow with rough walls, using the bubble radius as a roughness element size; Martinelli's analogy solution for single phase velocity and temperature profiles holds for the bulk liquid flow; and the liquid in contact with the bubbles is at the local saturation temperature.

Comparisons of the results of the analysis with experimental data for water and Freon 22 are shown in Figures 4-3 and 4-4. It may be seen that the comparison is favorable.

There are several qualifications on the use of this analysis. The foremost is that the solution is not appropriate for fluids which have very high levels of dissolved gas in them, nor for highly degassed systems, since both of those will exhibit abnormal nucleation behavior. Another qualification is that the boiling surface must have a wide size range of active nucleation sites available.

In Reference 4, relationships are derived for the vapor void fraction in subcooled boiling of ordinary fluids, utilizing an

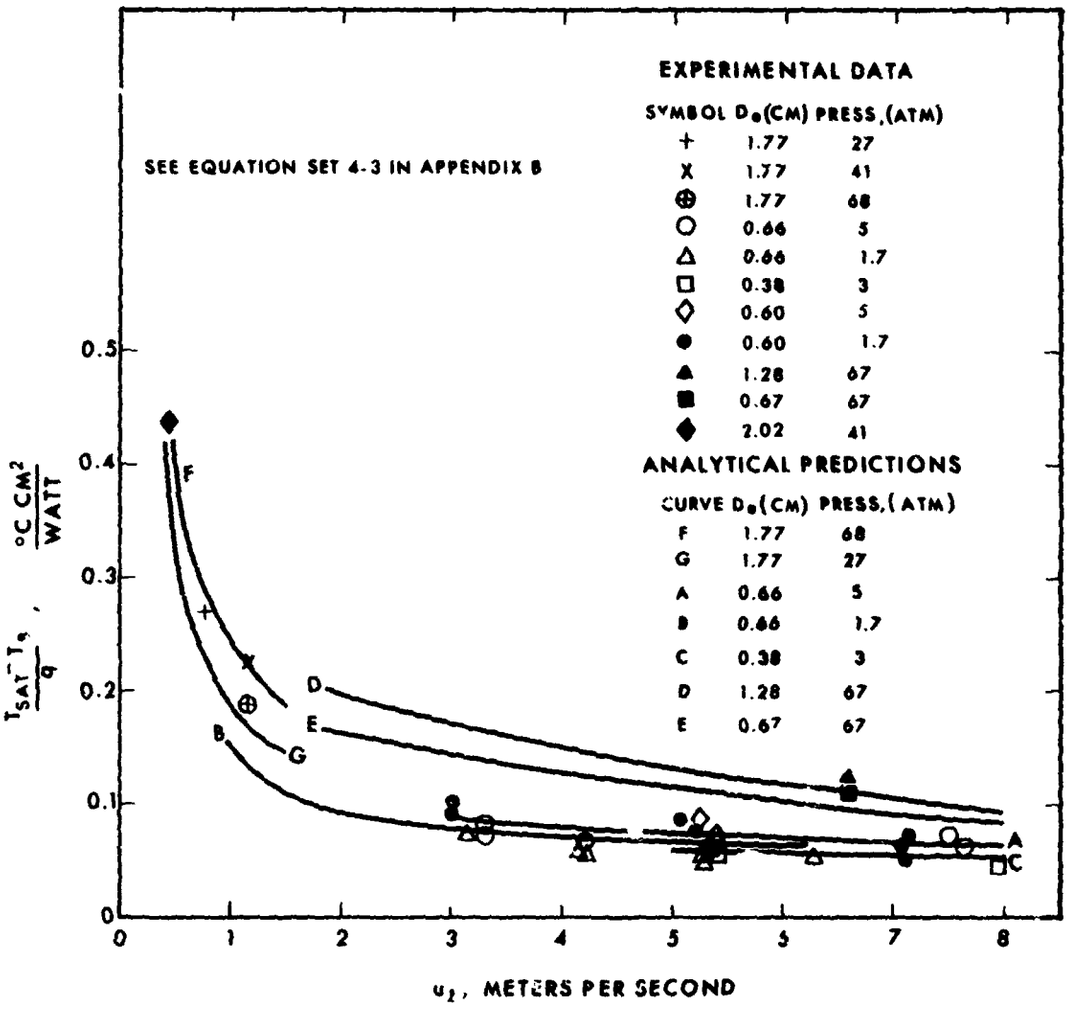

Figure 4-3. Comparison of subcooled boiling water data with analytical predictions (adapted from reference 3).

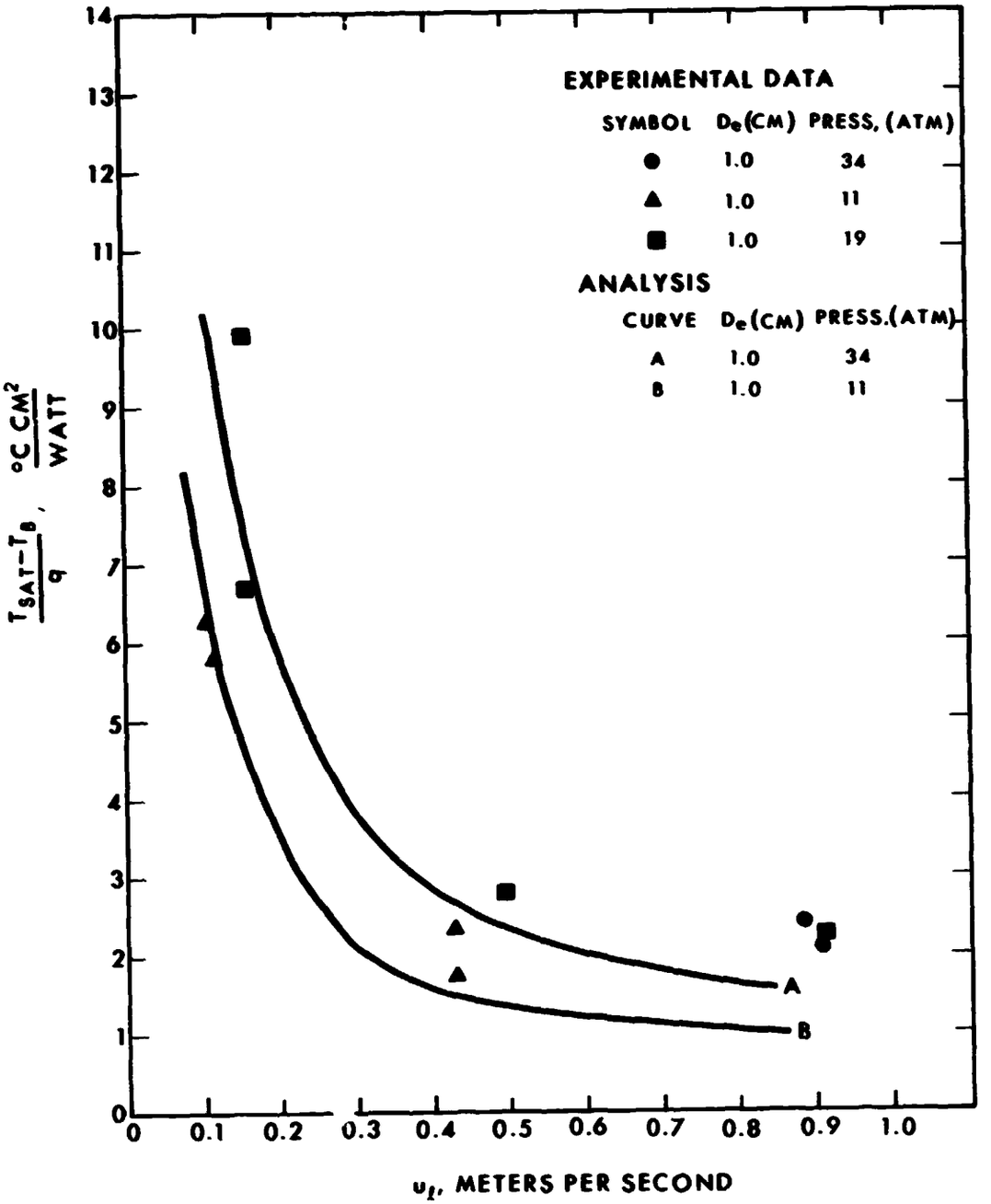

Figure 4-4. Comparison of subcooled boiling Freon 22 data with analytical predictions (adapted from Reference 3).

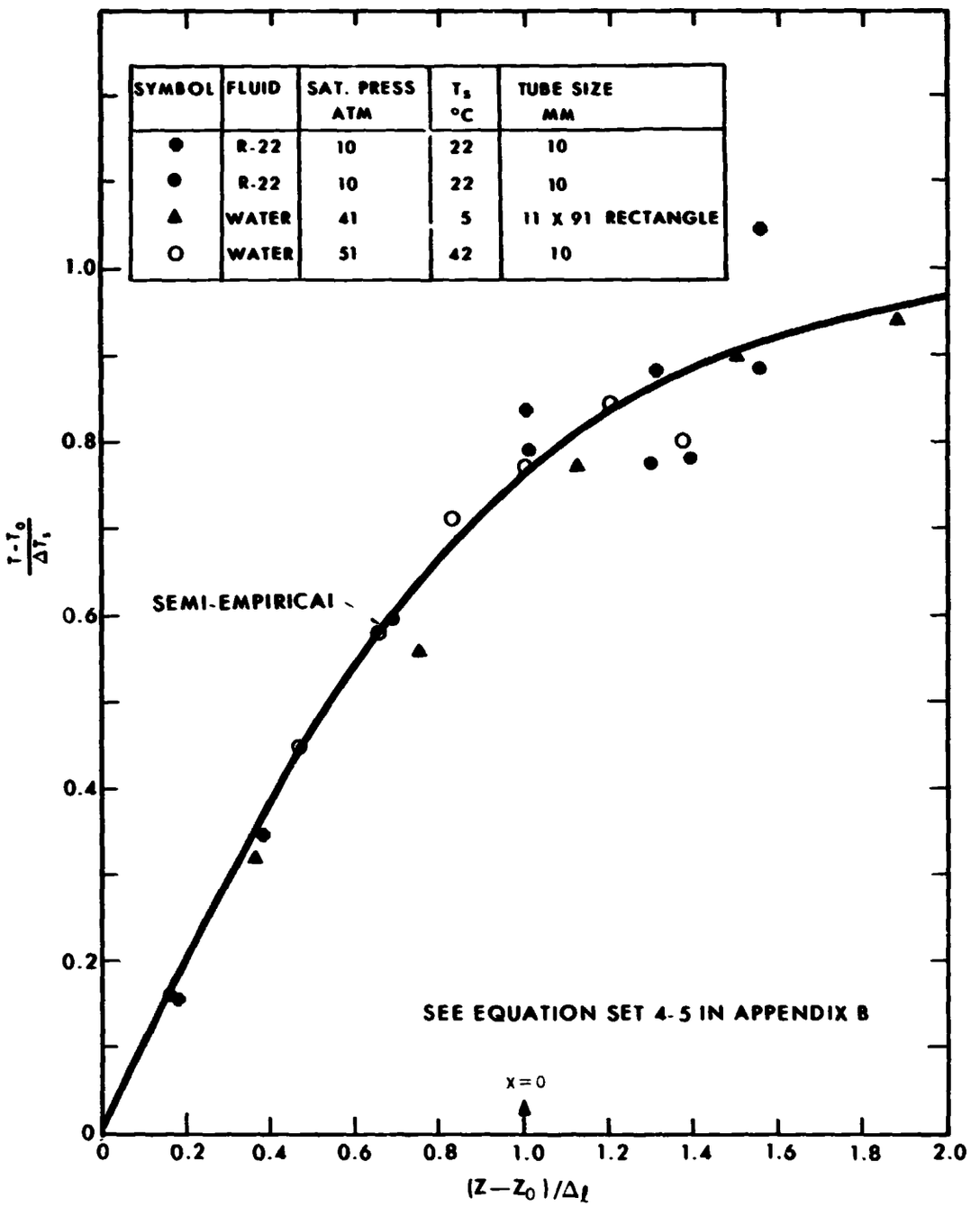

Figure 4-5. Mixed mean temperature variation in subcooled boiling (from reference 2), C_o = 1.13

analytical fit to experimental data for the mixed mean temperature distribution. The temperature distribution function is shown in Figure 4-5. With this temperature distribution and the known heat flux, the void fraction is obtained from an energy equation and the initial point of net vapor formation. The relationship for void fraction is compared to experimental data, both for negligible subcooling conditions, where there are many sets of data, and for cases with significant subcooling as well. A typical comparison is shown in Figure 4-6. It may be seen that the analysis agrees quite well with the data. The quantity C_o, given in the figure, is an experimentally determined phase distribution parameter.

3. Transition from bubbly flow to wetted-wall slug flow

Bubbly flow, a two-phase mixture of many discrete small bubbles in a primarily liquid flow, is easily produced in adiabatic systems. As the void fraction increases, this phase distribution gives way to one in which many of the bubbles coalesce to form vapor slugs separated by bubbly-liquid bridges.

A number of investigators have produced maps of flow regimes in adiabatic systems which include this transition. However, in actual boiling systems utilizing ordinary fluids, the bubbly phase distribution apparently exists only in the subcooled boiling regime (Reference 6). At inception of vapor quality, the bubbly flow is interspersed with vapor slugs, so that in the phase distribution descriptions used in this report, it would be referred to as a wetted-wall slug flow.

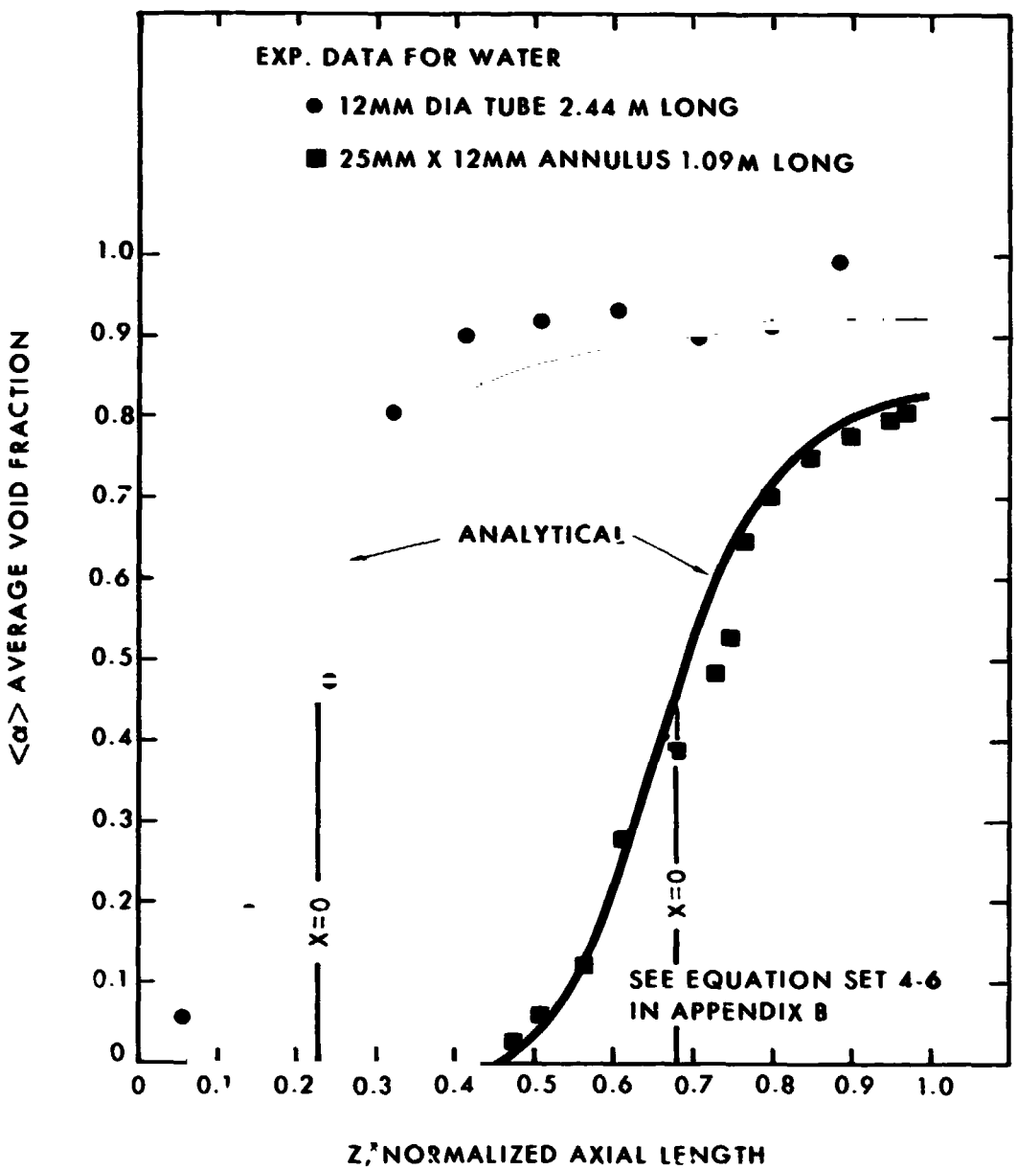

Figure 4-6. Comparison of experimental and predicted void fraction for subcooled water boiling, C_o 1.13.

In Reference 7, the authors conclude, on the basis of a literature survey and their own experiments, that for adiabatic flow there is no simple criterion which can be used to characterize this transition, but that wetted-wall slug flow always occurs at void fractions above 35 percent. In many boiling systems utilizing ordinary fluids, a void fraction this high occurs well before saturated boiling starts (see, for example, Reference 4). It appears that the vapor generator designer may assume that this transition occurs near onset of saturated boiling without serious error in either pressure drop or heat transfer conductance calculations.

4. Transition from wetted-wall slug flow to annular flow

This transition, which occurs at low vapor quality, has been studied analytically and experimentally by a number of laboratories, usually utilizing adiabatic systems.[8,9,10,11] The transition is not a particularly sharp one, and several sources describe other phase distributions in between.

A flow regime between slug and annular flow frequently described is "churn" or "semi-annular" flow, which is a very unsteady oscillation between annular flow and slug flow in adiabatic systems. However, since at the higher quality end of wetted slug flow the slugs become longer and longer so that the major portion of the flow is indistinguishable from annular flow from a heat transfer point of view, relationships which describe this transition only approximately are probably adequate.

The analysis of the transition from slug to annular flow has been undertaken by several authors, using the approach of finding the intersection of analytical expressions for void fraction of both the slug flow and annular flow regimes. Because of the difficulty in representing either of these regions analytically, and because the void fraction at the onset of annular flow is very little effected by fluid properties and flow rates (α is close to 0.80 for onset of annular flow for most ordinary fluids), these attempts at a theoretical approach have not been particularly successful.

A large body of adiabatic data was accumulated and presented in Reference 8. These data were obtained from systems with a variety of fluids and tube diameters, using as a criterion for the transition the presence or absence of liquid bridges in the flow.

On the basis of these data, two correlations for the slug-annular transition are presented in Reference 8. These correlations are shown in Figure 4-7. The sharp break in slope is attributed to the onset of spray entrainment in the vapor flow. Also reported in Reference 8 are data on void fraction and pressure gradient at transition for some specific systems (Figure 4-8). The pressure gradient goes through a rather indistinct minimum in the region of this transition.

In Reference 11, data for upward adiabatic flow of steam-water mixtures are reported. These data have been used to construct a graph of the slug-annular transition specifically for water-steam mixtures as a function of saturation pressure. This graph is shown in Figure 4-9.

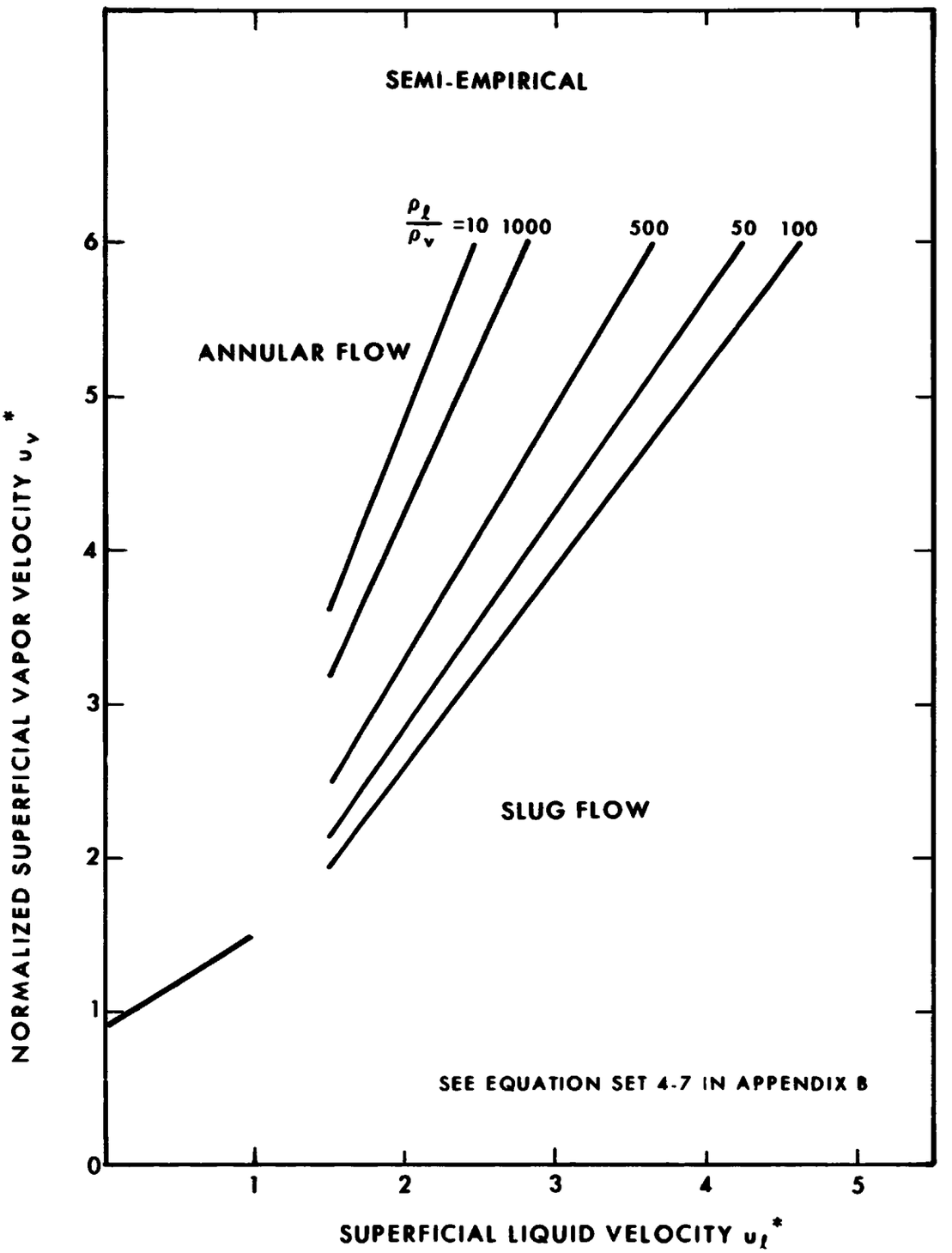

Figure 4-7. Correlation for transition from slug to annular flow.

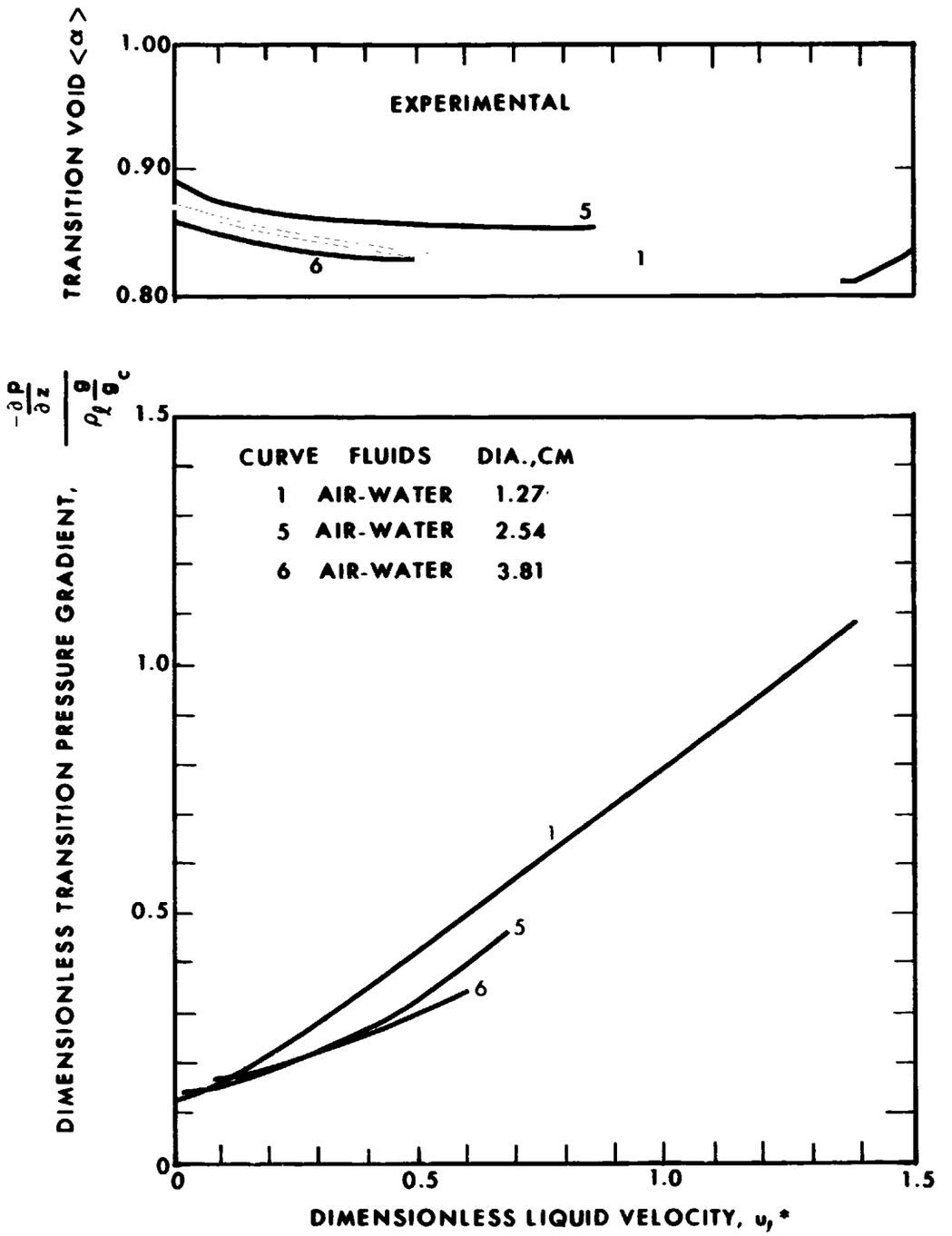

Figure 4-8. Void fraction and pressure drop at transition from slug to annular flow.

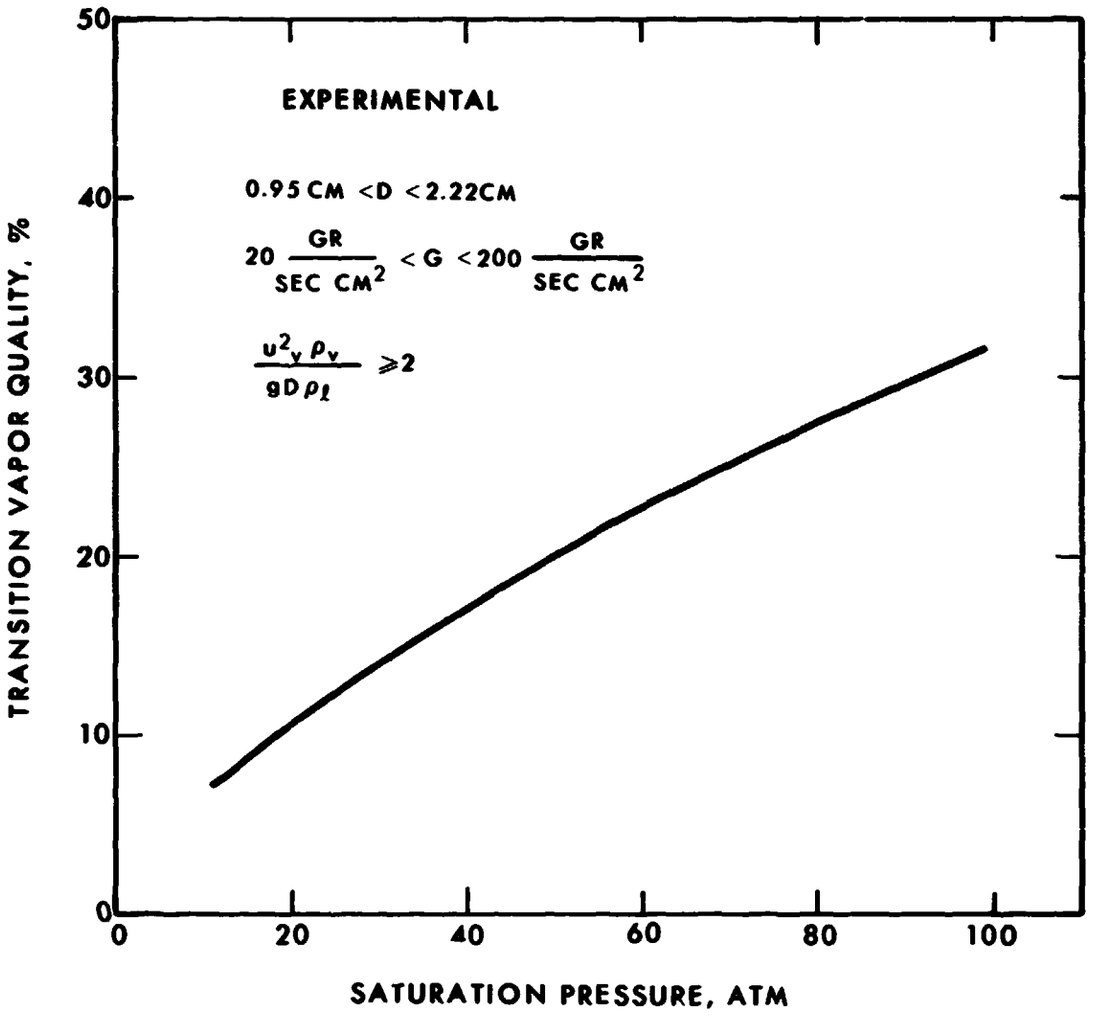

Figure 4-9. The slug-annular flow transition for steam water mixtures in upward flow.

5. Onset of entrainment from waves on the annular film

One of the important mechanisms causing the entrainment of liquid into the vapor phase from the liquid layer in annular flow boiling is vapor shear. It appears that most of the shear entrainment is from the peaks of large "breaking" waves, which have a height above the average liquid layer thickness of the same order as the layer thickness itself.[12] There is no agreement as to the conditions upon which the onset of roll waves occurs. However, there has been a correlation published for the onset of spray entrainment from these waves for adiabatic air-water systems.

A simple analysis, presented in Reference 3, allows the prediction of shear entrainment from other fluid systems, and agrees quite well with the correlation referred to above for air-water. It is based on the following model.

Presume that the waves already exist on the liquid surface, and that the flow is upward. The removal of a droplet is supposed to be due to the drag of the vapor upon the tip of an irregularity in the wave and the restraining forces considered are surface tension and gravity. A schematic drawing of this model is shown in Figure 4-10a. The force system acting upon the wave tip is indicated in Figure 4-10b. Clearly the restraining force on the wave tip decreases and the drag force increases rapidly after a "neck" appears, and a droplet is almost certain to be pulled off.

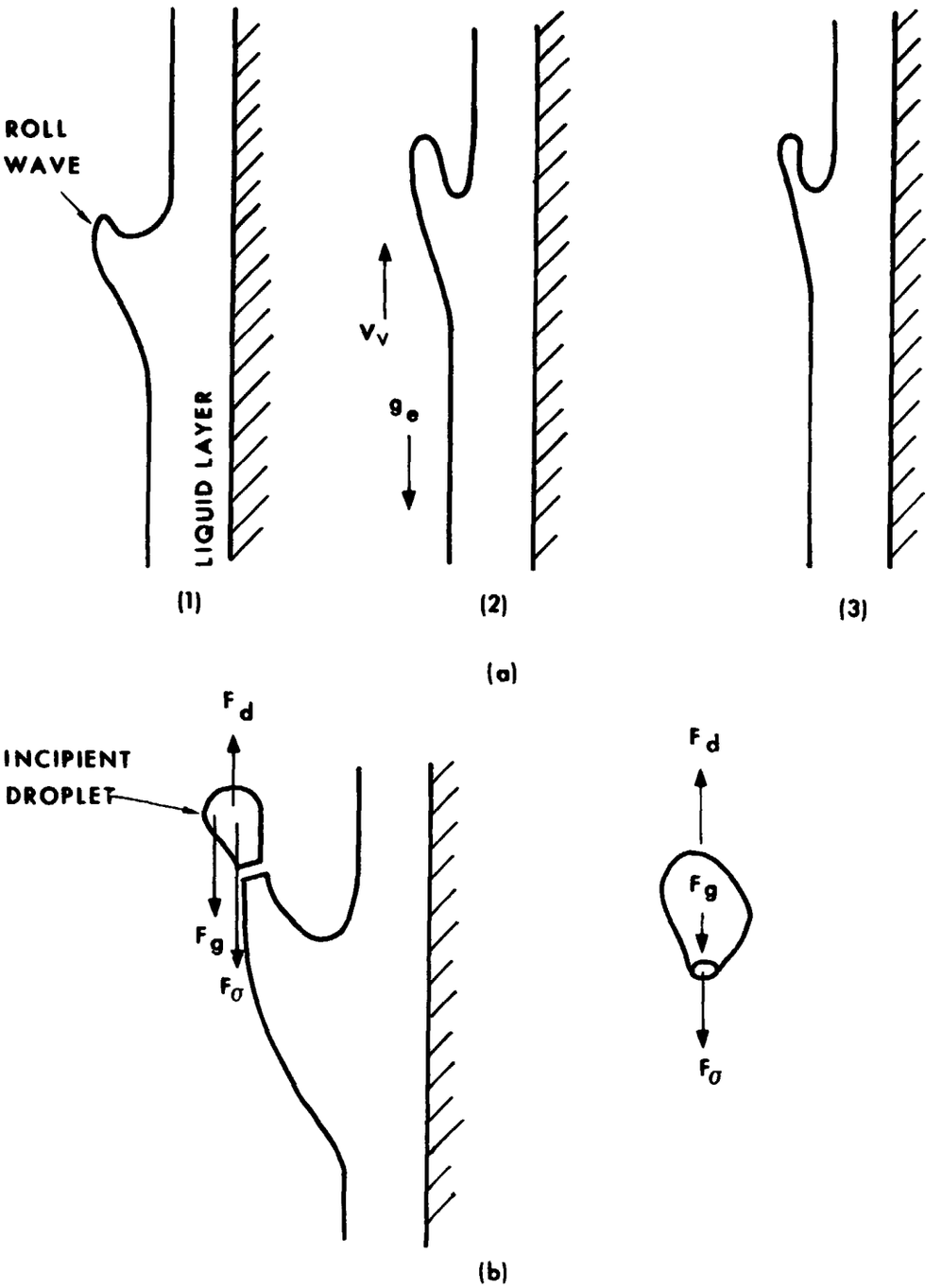

Figure 4-10. Shear entrainment model for liquid and vapor in upward flow.

Evaluation of a force balance at the point in time that the neck is beginning to form, utilizing the simplifications that the liquid velocity is negligible compared to the vapor velocity, that the resulting droplet diameter is equal to the mean liquid layer thickness, and that the drag coefficient for the downstream end of a rounded end cylindrical object is a constant, leads to a closed form relationship for the critical vapor velocity. This relationship is given in Figure 4-11.

By combining this shear entrainment criterion with the annular flow liquid film thickness predictions from Chapter 3, a map of conditions under which shear entrainment would be expected results. Two such maps are presented in Figures 4-11 and 4-12.

As an example of the interpretation of these figures, consider the graph for Freon 12 flowing in a 11.5 mm tube, Figure 4-11. By hypothesis, the film thickness must be at least equal to the droplet diameter (or wave height) for entrainment to occur. Therefore, a given size droplet will only be entrained into the vapor at qualities for which the film thickness is greater than that drop size. However, the vapor velocity must be high enough to entrain droplets of that size so the entrainment region lies above the line representing the entrainment criterion. Conditions for entrainment of 1.3 mm Freon droplets exist above the line of the shear entrainment criterion, and below the 1.3 mm film thickness line, in the

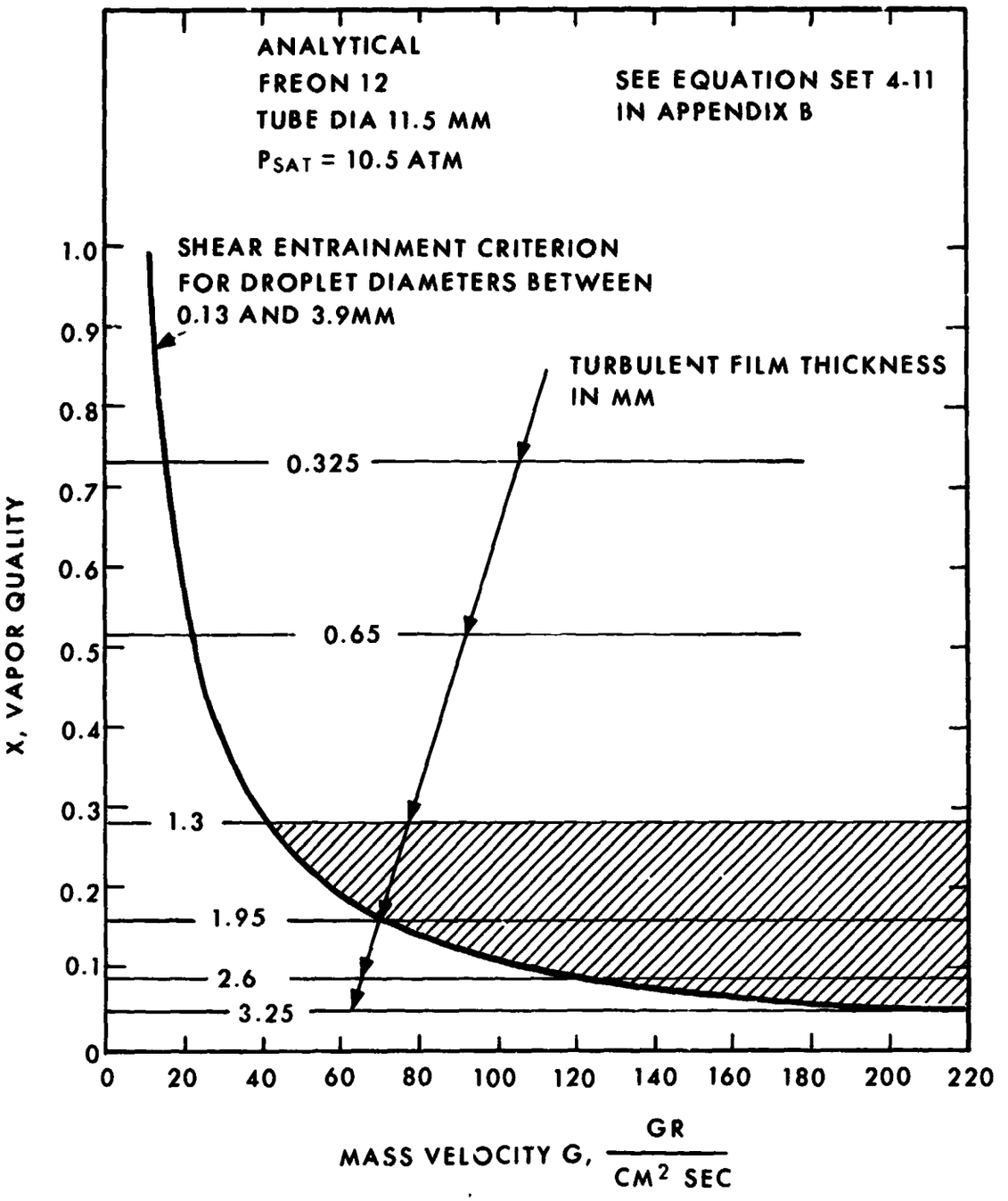

Figure 4-11. Boundaries for onset of entrainment due to shear.

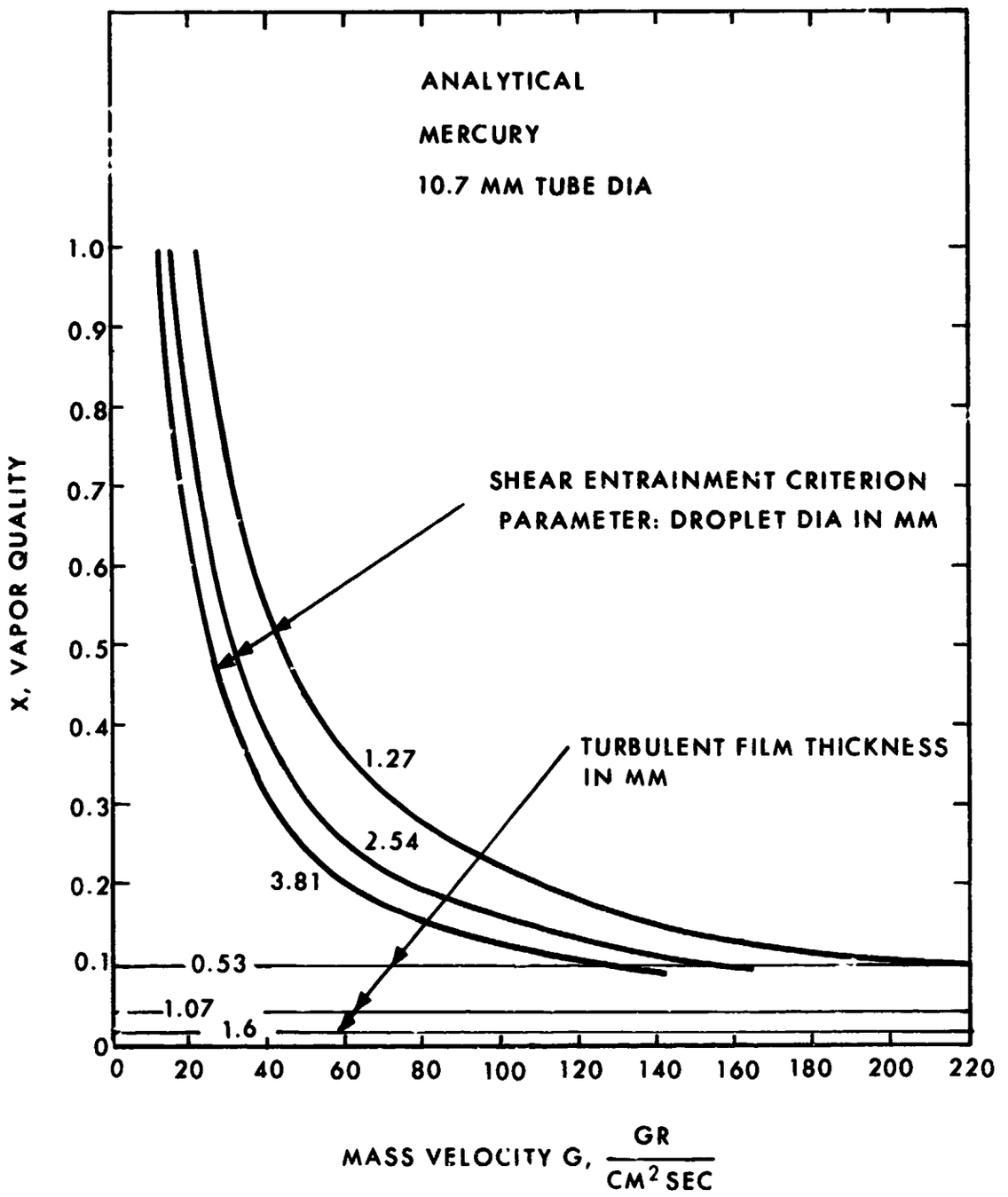

Figure 4-12. Boundaries for onset of entrainment due to shear.

cross-hatched area. Figure 4-12, which is constructed for wetting flow mercury, indicates that shear entrainment is extremely unlikely under conditions of practical importance.

6. Onset of nucleate boiling in an annular film

This transition is important for several reasons. One of these reasons is that nucleate boiling alters the heat transfer conductance associated with annular flow, as shown in Chapter 3. A second reason is that nucleate boiling ejects liquid from the film and, therefore, increases the entrained liquid. The loss in liquid from the film may lower the quality at which the annular film ends.

From the models of heat transfer in annular flow given in Chapter 3, one would expect that a thick annular film would exhibit nucleate boiling at a lower heat flux than would a thin one: i.e., nucleate boiling would appear at higher flux as the quality increases. One would also expect that a low turbulence film would exhibit nucleate boiling at a lower heat flux than would a very turbulent one; i.e., at fixed quality, a higher flow would require higher flux to bring about nucleation. These trends both appear to be corroborated by the data in Figure 4-13, which are for water-steam at 7 atm taken from Reference 14. The test section for the experiments was a heated rod surrounded by a glass tube to form an annular flow passage.

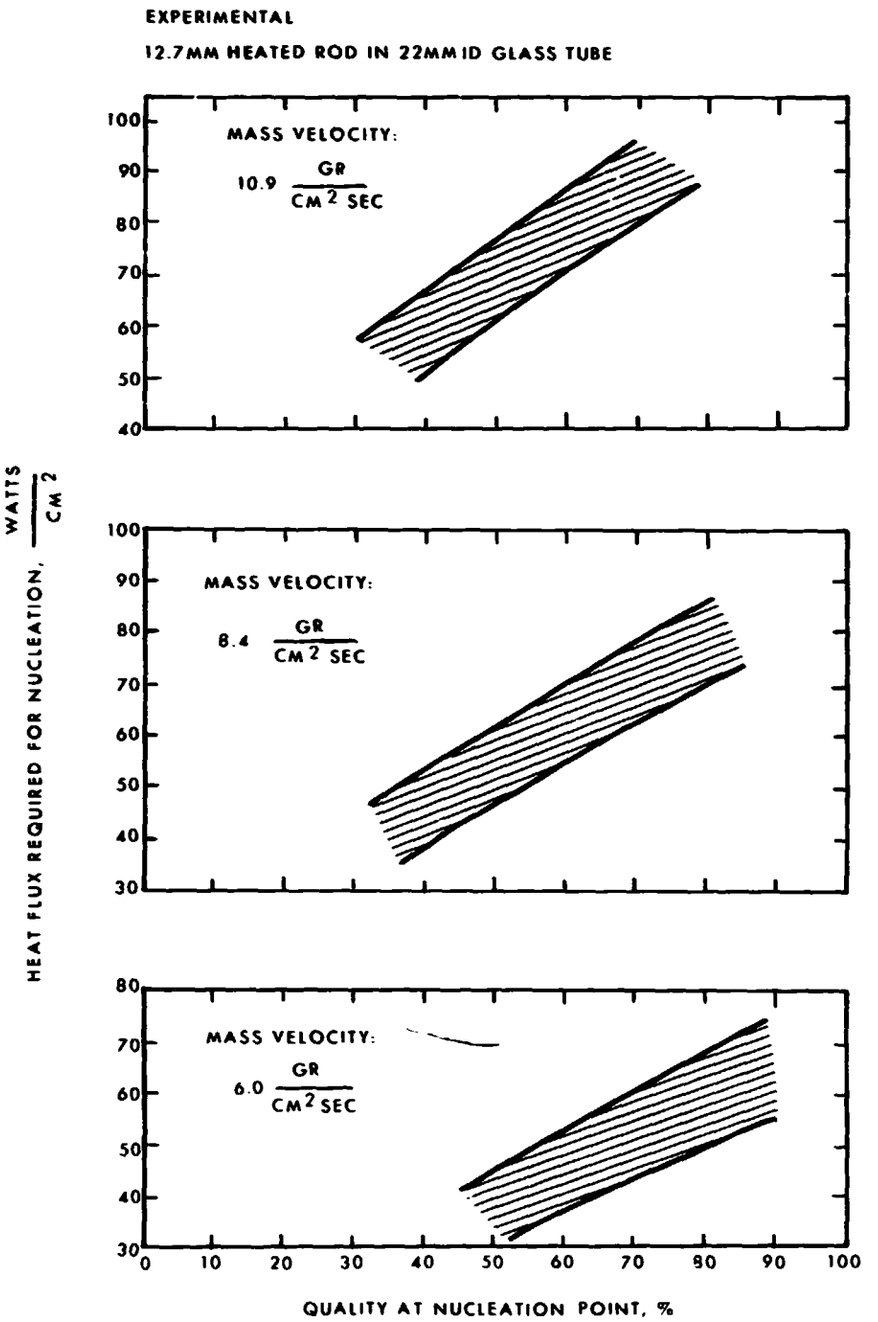

Figure 4-13. Heat flux required for nucleation in a specific water system.

If information is available concerning the amount of wall superheat required to bring about nucleate boiling, then by use of the methods of Chapter 3 the heat flux at which nucleate boiling will occur can be predicted and, in the complete absence of nucleation sites, the liquid superheat predictions of Section A.2 of this chapter are applicable.

As an example, consider the conditions under which nucleation will start in an annular flow of a liquid metal. In the absence of nucleate boiling (which acts as a volume heat sink within the liquid film), all of the heat added to the annular film at the wall must be conducted or convected across the liquid layer to vaporize fluid at the inner surface, which is taken to be at the saturation temperature. Since the liquid metals have very high thermal conductivity, convection may be neglected and the temperature drop across the liquid layer computed on the basis of conduction alone. Nucleation will occur when the heat flux is adequate to maintain the liquid in contact with the wall at the temperature for nucleation given in Section A.2. With this simple model, a graph for the minimum heat flux required to bring on nucleate boiling has been computed for potassium and is shown in Figure 4-14. A similar curve has been constructed for Freon 12, using an arbitrary superheat temperature. The curve for Freon is, of course, hypothetical, since with its low thermal conductivity, turbulent convection in the liquid layer certainly predominates (see Figure 4-15).

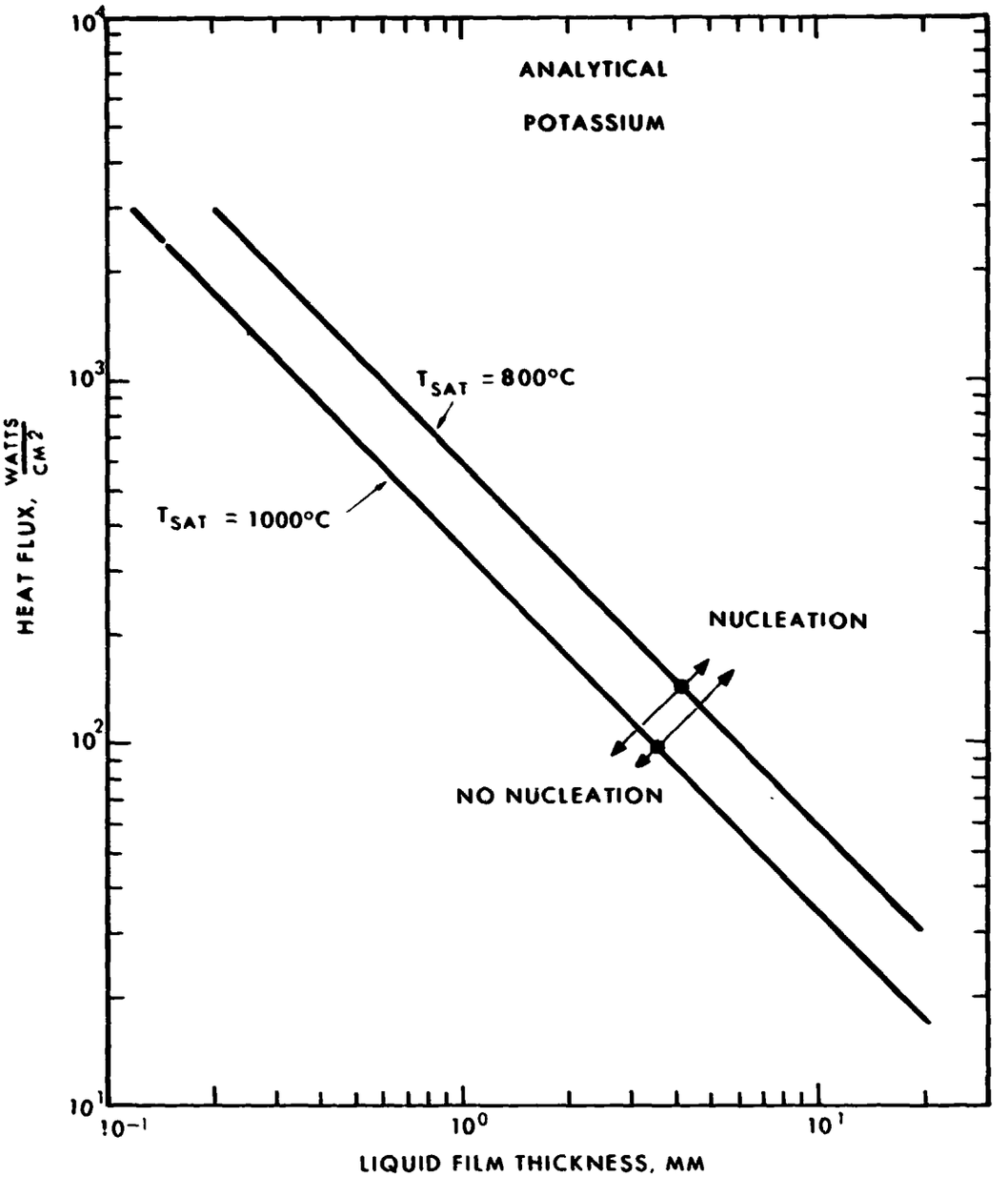

Figure 4-14. Heat flux required to initiate nucleate boiling in an annular flow without nucleation sites.

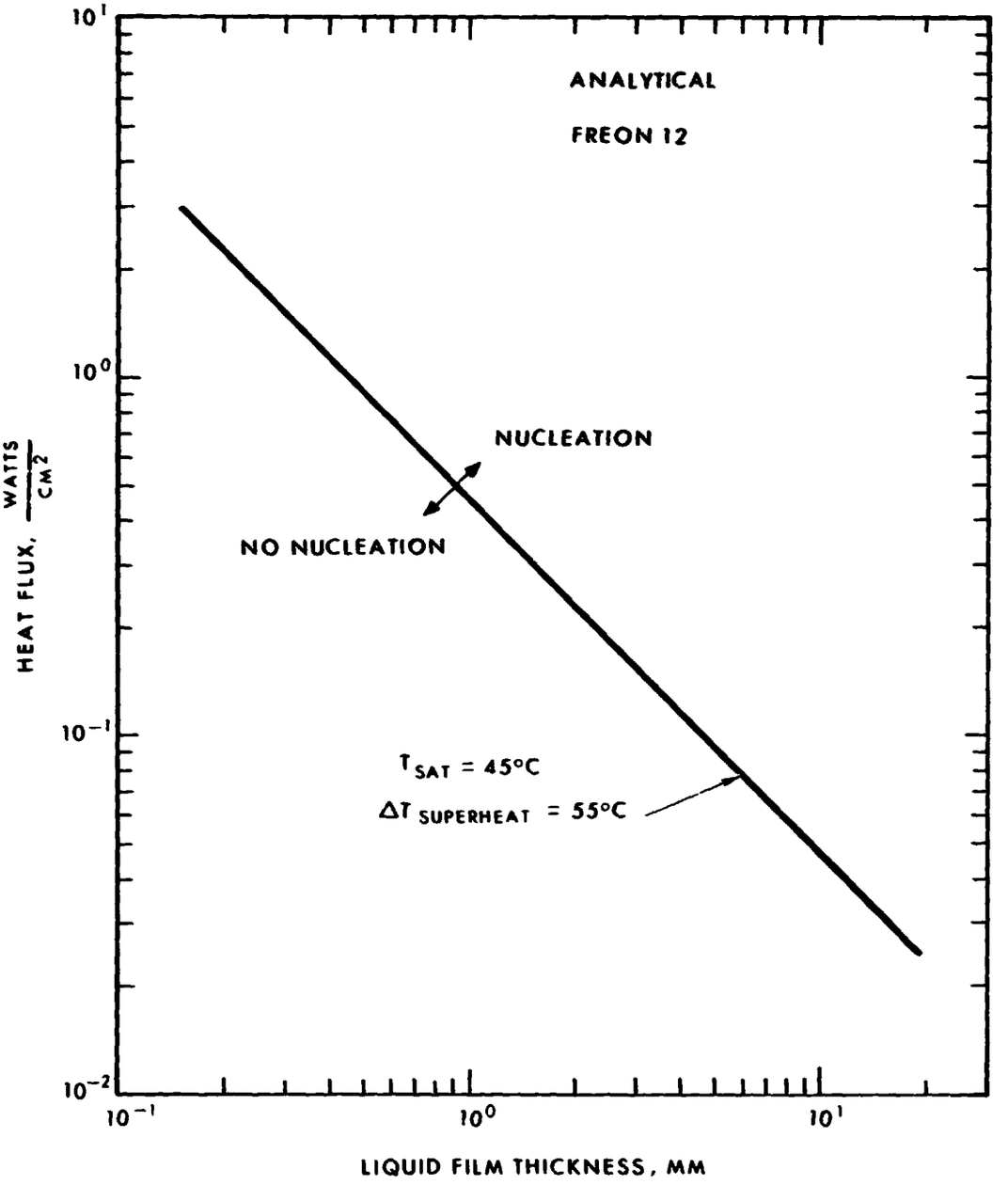

Figure 4-15. Heat flux required to initiate nucleate boiling in an annular flow without nucleation sites.

7. "Burnout," "Boiling Crisis," or "Critical Heat Flux"

If, in an experiment, a boiler with fixed geometry and fixed mass flow rate is subjected to an increasing heat flux, an operating point will be reached at which, for a very small heat flux increase, a large increase in wall temperature will occur. Usually, the wall temperature will not increase suddenly over the entire boiler. If a stable operating point is obtained at this new condition, it will usually be found that at some axial location near the outlet end the wall temperature will change, over a relatively short distance, from a low value of a few tens of degrees to a high value of a few hundreds of degrees. In a system with a uniform heat flux, the boiler tube may fail at this point. There have been many specific experiments investigating this phenomenon, which is commonly referred to as "burnout," "critical heat flux," or, less commonly, "boiling crisis."

Unfortunately, the notion of a "critical heat flux" can lead to some erroneous concepts concerning the phenomena being observed. Several phenomena are actually represented. One of these, film boiling, is described in most heat transfer texts. Factors controlling its onset are described in Section E of this chapter. However, probably the most important of the phenomena associated with "burnout" are dryout of the annular liquid layer on the wall or breakup of the liquid film into rivulets. Of course, a forced convection boiler designed to produce dry vapor at the exit must operate through this region without failure, so the term "burnout" is inappropriate.

Observations made with Freon 11 in a glass test section (Reference 15) support the interpretation of "burnout" as a breakdown of the annular film. These observations, taken under uniform heat flux conditions, demonstrate a very large and discontinuous decrease in heat transfer conductance at an axial location which coincides with the dryout of the annular film.

The rate of change of the liquid flow in the film is determined by a mass balance between the liquid evaporated, the liquid deposited from the vapor, and the liquid entrained from the film. The liquid entrained from the film is usually supposed to be removed from the film by stripping of liquid from wave peaks, and ejection of liquid by breaking of bubbles generated by nucleation in the film. The mechanisms controlling the flow rate in the annular film are, therefore, largely hydrodynamic. One might expect the liquid film flow rate at any point to be determined by the processes occurring upstream; the rates of deposition and entrainment, and the rate of change of vapor velocity all contribute to the liquid film flow. Many different combinations of these processes would give virtually the same liquid flow rate at a particular point. The annular film is very thin near its end so that bubble nucleation and wave motion are probably both suppressed, and the principal mass fluxes in and out of the annular film near its termination are probably due to evaporation and deposition.

When film dryout occurs at a quality less than unity, the remainder of the liquid must certainly be entrained in the vapor flow. Due to diffusion, the fine droplets in the vapor eventually settle out on the walls and evaporate. The longer the boiler, the smaller the entrained flow at the end will be. It is clear that for a fixed flow rate, a low heat flux boiler is a long boiler. If entrainment rates are not too high, a long boiler has proportionately less entrained liquid at a given quality, and one would expect that the end of the annular film would occur at higher quality for a low flux (long) boiler than for a high flux (short) boiler. Regardless of tube diameter, liquid flow rate, or other conditions, the end of the annular film will occur at $X = 1$ for vanishingly small heat flux.

The plot of Figure 4-16 (Reference 13), showing Freon 12 burnout data, indicates a linear relationship between $(q/A)_B$ and X_B over a wide range of test conditions. However, all of the data lines must pass through the point $(q/A)_B = 0$, $X_B = 1$. Since this is the case, only one of the lines in Figure 4-16 can be straight at substantially lower flux than the data cover. All of the remainder must curve at low heat flux. The data of Figure 4-16, plotted on semi-logarithmic coordinates, are shown in Figure 4-17. It is clearer in this plot that the data do tend toward zero heat flux at $X = 1$. The solid lines indicate the actual range of the data. The dotted lines indicate where one might expect data taken over a wider range of heat fluxes to lie. These same data have been replotted

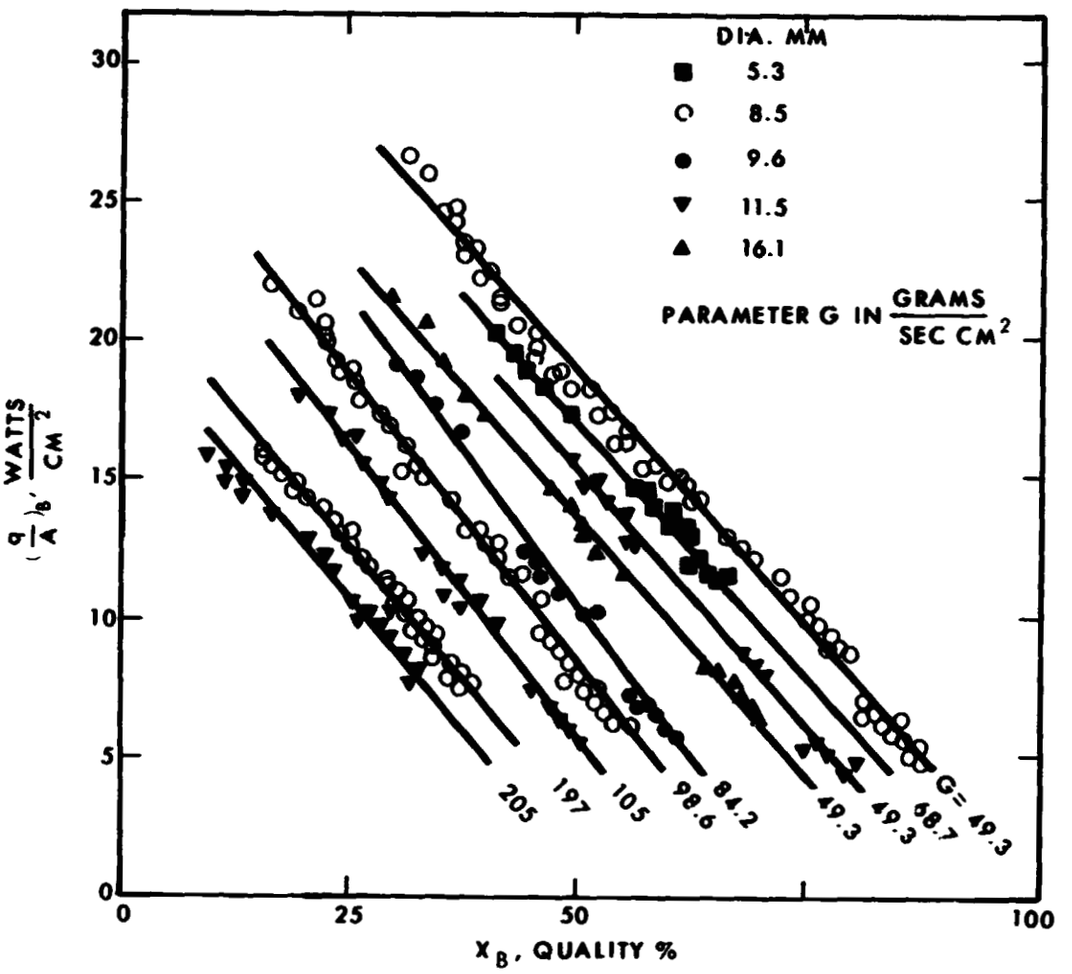

Figure 4-16. Freon 12 linear flow "burnout" data (from reference 13).

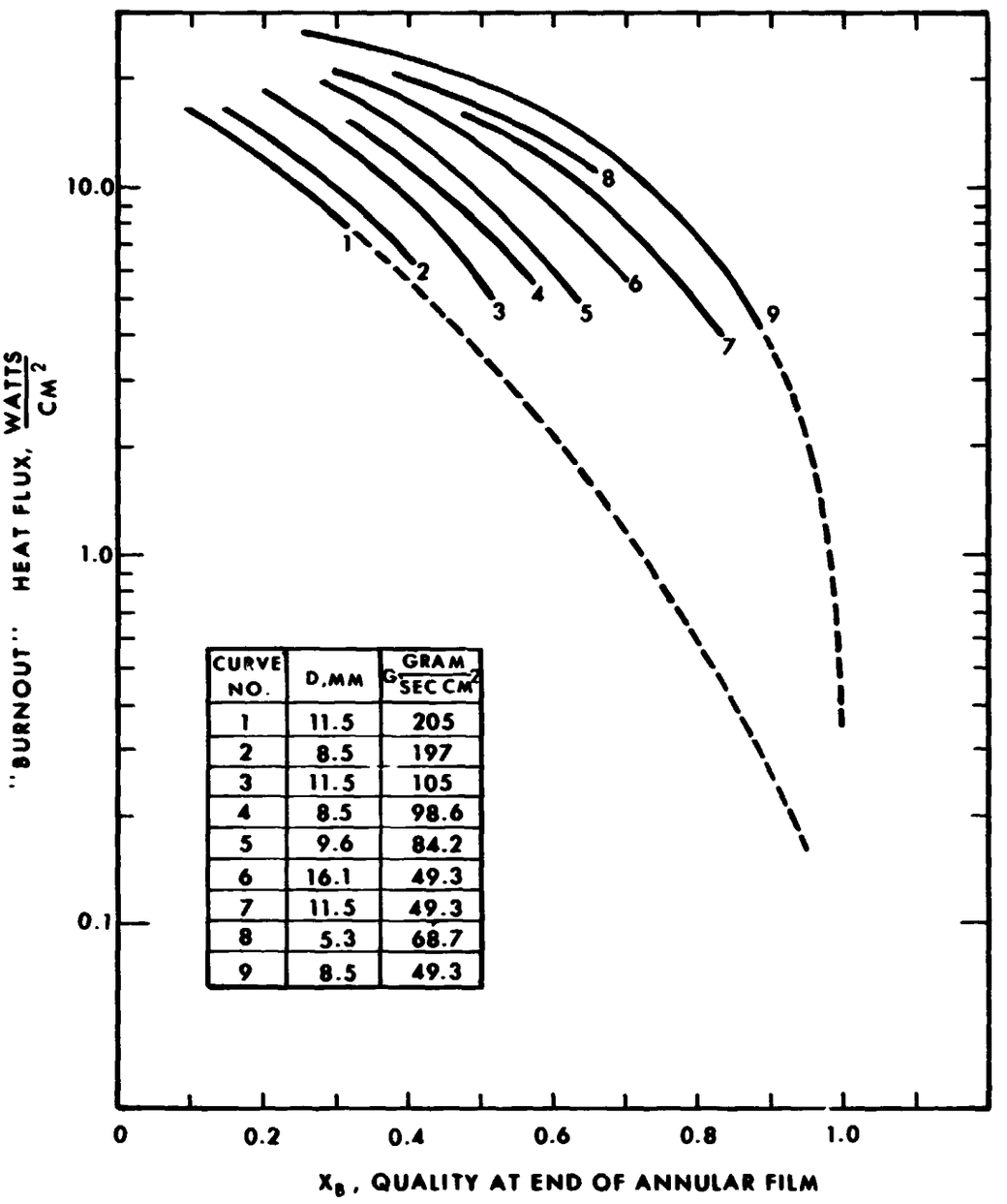

Figure 4-17. Freon 12 linear flow "burnout" data.

as functions of length in Figure 4-18. It may be seen that the boiler length required to maintain the annular film at high quality increases rapidly for high mass flow rates.

As stated earlier, when the wall is no longer wet, all of the remaining liquid is entrained in the vapor. An entrained liquid plot (Figure 4-19) has been constructed from the data of Figure 4-18. It can be seen that for high flows and fluxes, as much as 90 percent of the liquid can be entrained

8. Breakdown of the annular film

Stability Analyses

A number of authors have studied the breakdown of liquid films flowing over heat transfer surfaces. In References 16 and 17, the authors studied the flow of water downward over vertical heated surfaces. They concluded that the development of longitudinal striations (described as "roping") was due to the variation in surface tension with film thickness.

In Reference 18, the author treated analytically the stability of downward flowing films subjected to heat transfer on the basis that the destabilizing mechanism is the nonuniform pressure normal to the surface due to variations in evaporation. The analysis led to definition of a critical heat flux for destabilization, and a prediction of the rate at which dry spots will form after the breakdown process begins.

Although these works are not strictly applicable to forced convection

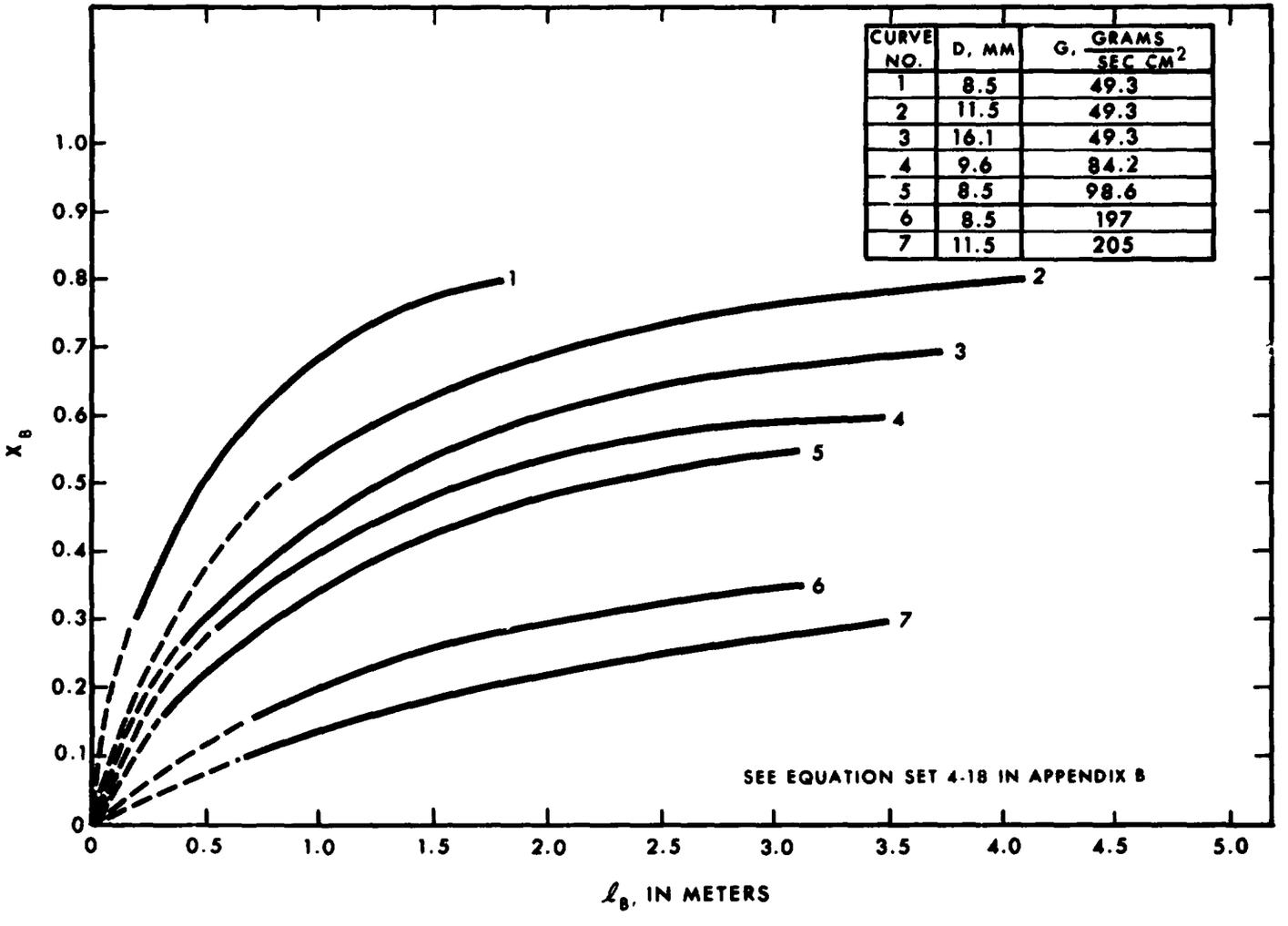

Figure 4-18. Freon 12 linear flow "burnout" data.

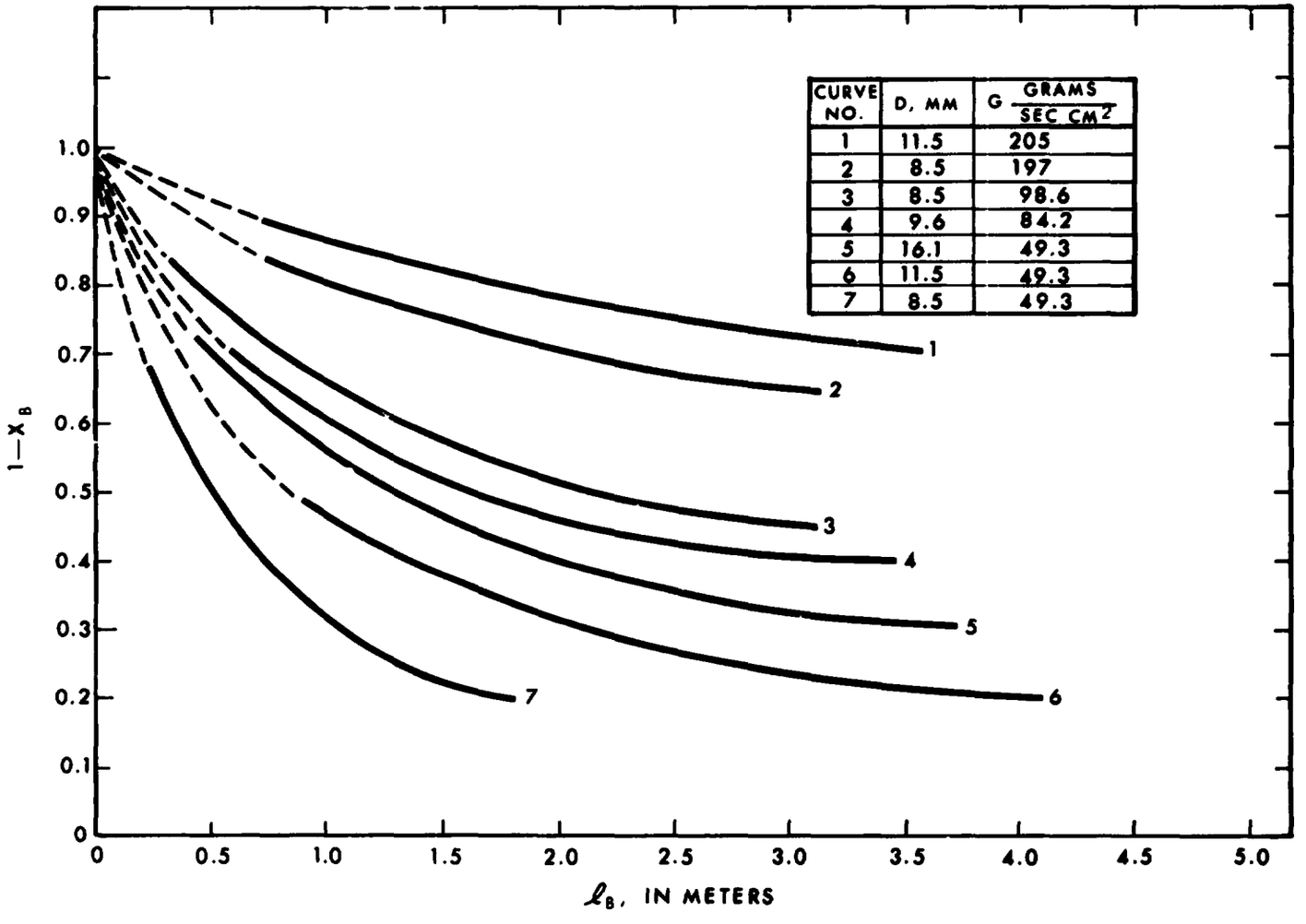

Figure 4-19. Entrained liquid at end of annular film - Freon 12.

boiling since the interface shear present in forced convection boiling does not appear, extension of these approaches to an appropriate case is probably feasible.

Other authors have studied the stability of dry patches on walls in annular flow.[19,20,21,22] An analytical treatment of film stability on unheated walls, given in Reference 21, was compared to adiabatic experimental data in Reference 20. The experiments were performed by blowing an air jet on the annular film to expose the wall and then determining the conditions under which the wall would rewet when the air jet was removed. The rewetting depends strongly upon contact angle between the dry wall and the liquid. The comparison indicates that aerodynamic forces on the edge of the liquid are important. In Reference 19, which treats the dry spot under conditions of heat transfer, it is shown that for liquids with high wettability, the thermal effects become dominant in determining the stability of dry patches and that surface forces dominate in cases of poor wettability. In Reference 5, it is shown that thermal conduction in the wall can be neglected only under conditions in which wall temperature gradients near the boundary of the dry spot are small.

Another approach to the onset of rivulet flow is presented in Reference 5. For this analysis, it is postulated that the vaporizing liquid is in direct contact with the smooth tube

surface and the boiling consists of surface vaporization or some volume boiling but no film boiling. If the contact angle between the liquid and the wall is zero degrees and there is no entrained liquid then, hypothetically, there will be a complete annular liquid film at the wall from qualities ranging from zero to 100 percent. If the contact angle (which is defined by the liquid-vapor, solid-vapor, solid-liquid surface forces) is greater than zero, the width of a liquid rivulet for that particular profile area defined by the contact angle and vapor quality must be compared to the inner circumference of the boiler tube. If the rivulet width is greater than the tube circumference, then the liquid film would not rupture. If the rivulet width is less than the tube circumference, then the liquid film would be separated.

Rough tube surfaces can affect the liquid film in several ways. Surface asperities which are high enough to penetrate the film free surface reduce the liquid film contact area, as do non-homogeneous structures such as oxide deposits, which change the local contact angle.

Finally, film boiling can occur at surface pits or local areas of nonwetting, reducing the wall superheat temperature difference at which surface vaporization ends and transition boiling begins.

In Reference 5, an analysis is presented for the conditions under which rivulets will form on a smooth tube surface. The critical contact angle predicted in this analysis is only

a function of tube radius and thickness of a complete annular liquid film (see Figure 4-20). From the relation between vapor quality and the annular film thickness, it can be shown that the critical contact angle decreases as vapor quality increases. Thus, one would expect the annular film to rupture at vapor qualities less than 100 percent. A specific example showing this effect is given in Figure 4-21.

Film Flow Rate Analyses

In Reference 23, the authors present an analysis of the film flow rate in the presence of vaporization, entrainment and deposition in an annular-dispersed flow. The analysis, which treats the heat transfer term as a perturbation on the adiabatic case, depends upon experimentally-determined adiabatic data for its evaluation. The deposition rate is treated analytically, utilizing the turbulent diffusivity from single phase turbulent flow relationships to establish the deposition flux. Because of the nature of the data with which their comparison is made, the authors use experimentally-determined film end points to predict "burnout heat flux" and then compare that value to the experimental flux. The comparison with selected boiling water data for a variety of heat flux distributions shows that trends are correct, even though the analytical approach is simple.

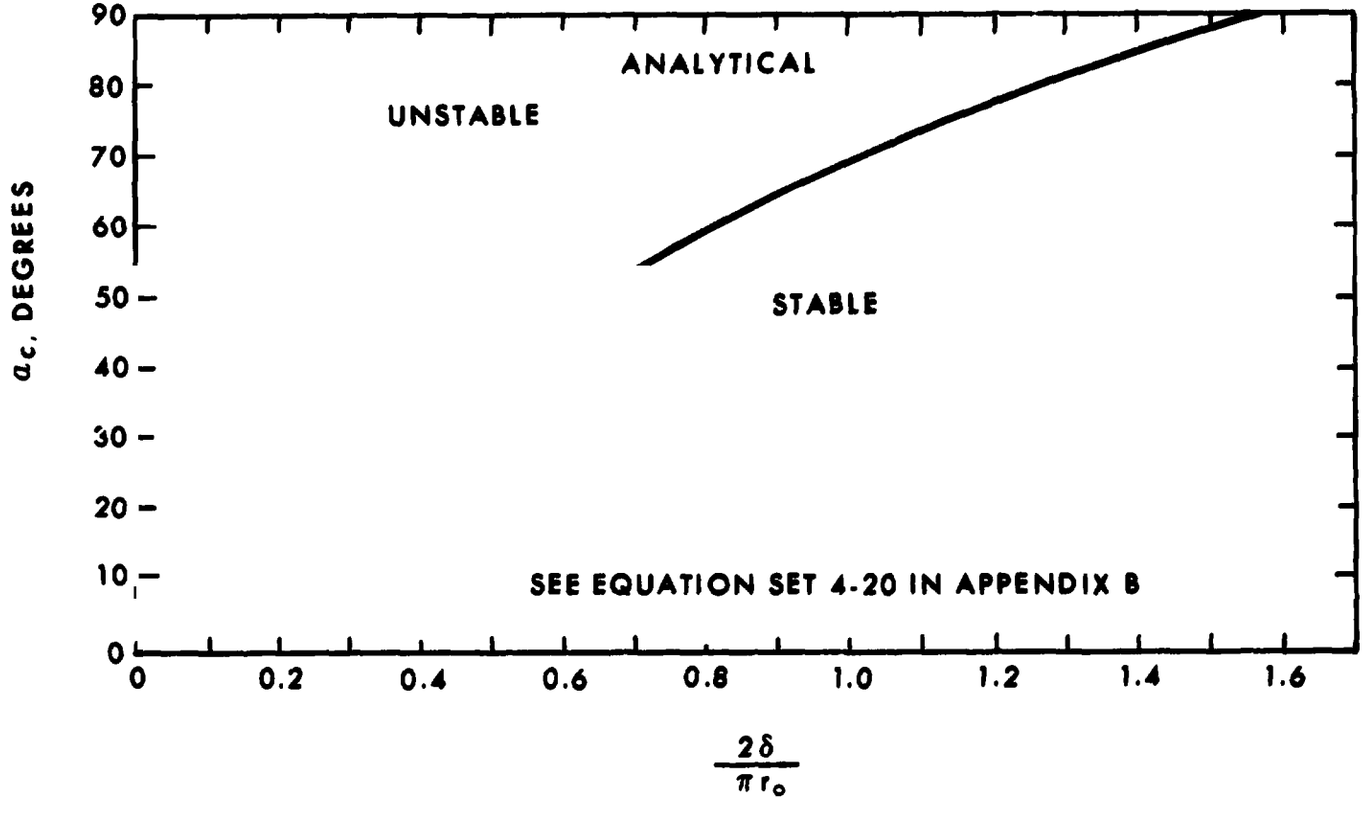

Figure 4-20. Critical contact angle for annular film rupture as a function of film thickness.

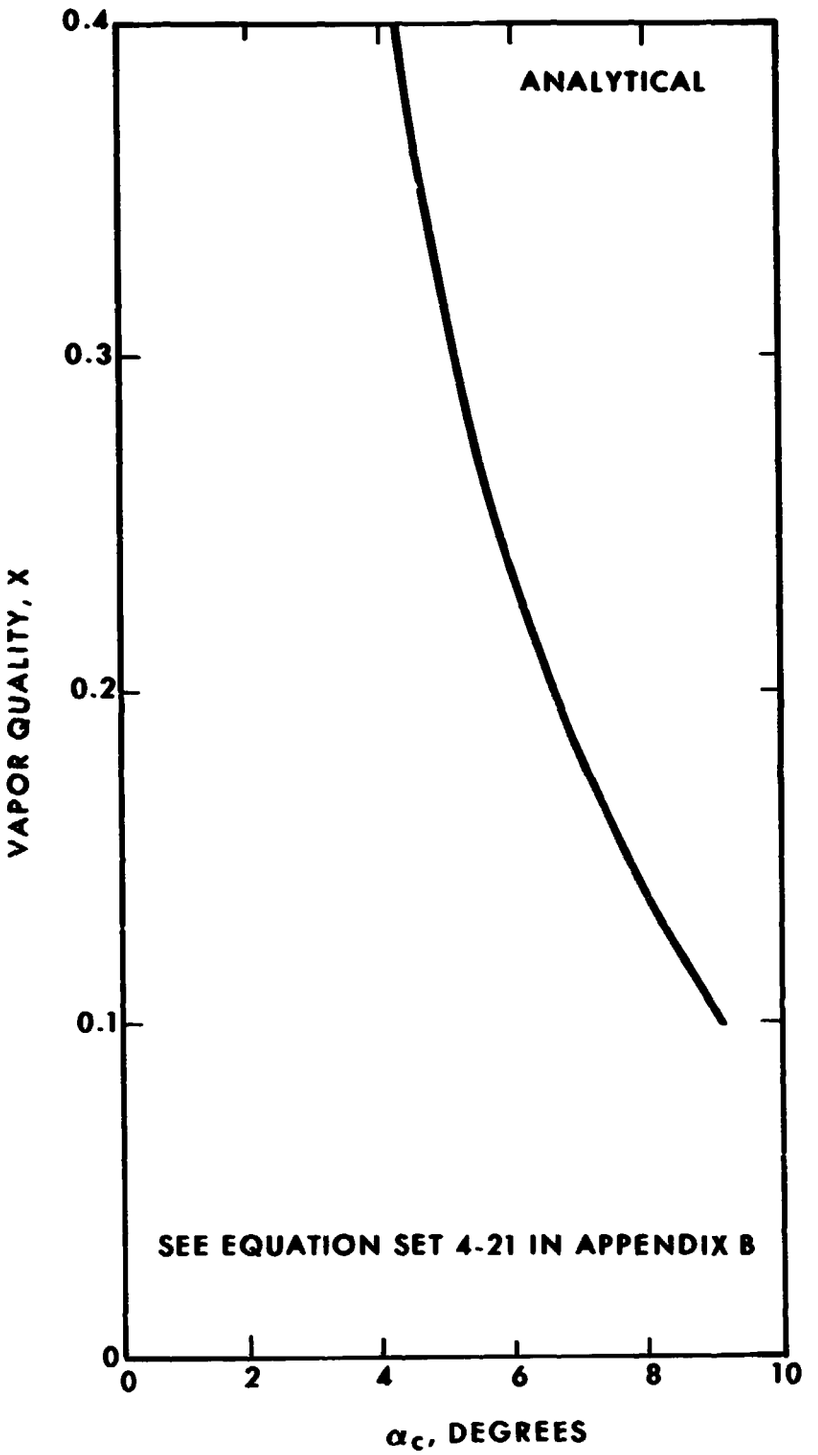

Figure 4-21. Critical contact angle versus vapor quality for a specific potassium system.

B. Fluids Which Do Not Wet the Tube Walls

1. Onset of nonwetting slug flow

Pool boiling mercury in an unwetted glass vessel at reduced pressure exhibits a behavior which is in marked contrast to boiling water, a wetting fluid, under the same conditions. When the mercury reaches the point of incipient boiling, a vapor bubble appears against the glass, then rapidly expands into a thin sheet of vapor against the wall. This sheet of vapor then slides upward along the wall to the surface. It is clear that, under these circumstances, the path of least resistance for the vapor is not through the liquid as a train of bubbles, but along the wall.[24]

Although some of the properties of mercury are somewhat extreme (very high surface tension and density), and the conditions under which the observations were made are unusual, the phenomenon observed must be largely dependent upon the wetting properties of the fluid-wall combination. A somewhat similar "film boiling" may be visualized for the onset of boiling in any nonwetting flow. When vapor is formed, the liquid may be pushed away from a significant portion of the heat transfer surface, so that the flow tends toward agglomerated masses of liquid separated by volumes of vapor. This is the distribution which characterizes nonwetting slug flow. A designer working with nonwetting

fluid-wall combinations can probably conservatively assume that the initiation of slug flow coincides with the onset of phase change and experiments in small diameter tubes with mercury flow confirm this (Reference 15).

2. Transition from slug flow to helical rivulet or droplet flow

Heat transfer conductances for mercury boiling in a tube containing a helical divider are shown in Figure 4-22, taken from Reference 15. It may be seen that at low quality the heat transfer conductances have the same general shape as those for slug flow (Figures 3-7 and 3-8). As the quality and vapor velocity increase, the conductances undergo a change, increasing by an order of magnitude or more. This change is associated with the onset of helical rivulet or droplet flow.

At low vapor velocity, the liquid velocity is very low, and little radial acceleration is provided by the helical divider. As the liquid velocity increases, it spreads out into a film boiling rivulet which is held against the wall by the radial accelerations. The heat transfer conductances after the transition may be predicted from the model of Chapter 3.

The transition is, of course, gradual, since droplets or globules of different sizes have different amounts of slip with regard to the vapor velocity. Experiments in visualization of boiling mercury (Reference 25) have shown

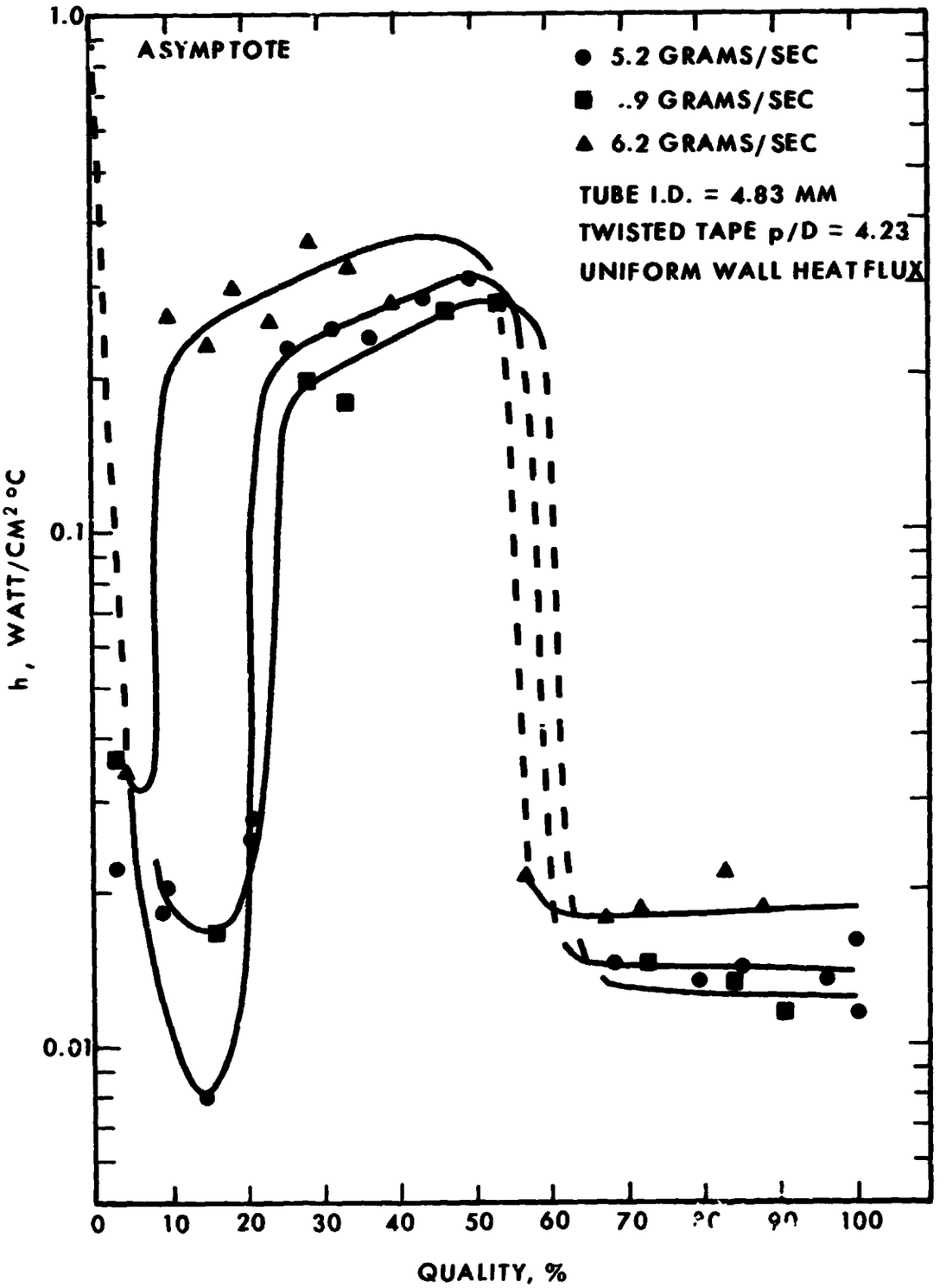

Figure 4-22. Helical flow boiling mercury conductances versus quality.

that range of globule-droplet sizes in upward flow of mercury is quite large. The criterion for the beginning of this transition is that the radial acceleration for the smaller droplets, including slip, must be many times the acceleration of gravity.

C. Boiler Tube Inserts

1. Some aspects of two phase flow in insert transitions

Axial changes in boiler insert type which have been considered for use by designers include: fluted plug to helical vane, fluted plug to helical wire, and helical vane to helical wire. The vane and wire sections may or may not have a centerbody associated with them, and the insert pitch may or may not be the same on both sides of the insert change.

Consider the transition from a fluted plug to a helical vane system. If the pitches of both are the same, then the major difference between the two inserts is in the diameter of the centerbody, and the flow will be similar to a flow into a sudden enlargement. The vapor phase will decelerate rapidly, and there will be a recirculating stall at the base of the plug if the area change is large. The liquid layer on the wall will also tend to lose velocity and thicken, although at a lesser rate than the vapor, and if the quality change with length is high

enough, no significant thickening of the liquid layer will occur. No observable effect of this transition upon the heat transfer performance would be expected.

If the fluted plug and helical vane do not have the same pitch, the liquid layer will be subjected to an acceleration which will thicken it on one side of the channel formed by the next insert and thin it on the other side. The liquid layer flow is similar to the open channel flow around a sharp corner, except that the gravitational field is replaced by a centrifugal acceleration field which may be many times larger than gravity. From experience with open channel flows, one would expect that the major effects of the sharp corner turn would be obliterated within a couple of channel widths.

One would expect a liquid layer on the tube wall to have a deleterious effect upon the flow rotating effectiveness of only the helical wire. If the liquid forms a layer which has appreciable thickness when compared to the diameter of the wire then, as was shown in Chapter 3, the force tending to rotate the fluid will be decreased, and if the liquid layer covers the wires, no force will exist at all. However, the heat transfer downstream from a transition to an ineffective wire coil will not necessarily be poorer than that in a helical vane. As long as the wall is completely covered, liquid-like conductances will prevail. Since centrifugal accelerations are decreasing, more liquid may be entrained in the vapor, and

surface waves will also be deeper. Both of these effects thin the liquid layer and increase turbulent diffusion. If nucleation does not occur, then the vaporization is at the liquid-vapor interface, so that a thin turbulent layer, which has less heat transfer resistance than a thick one, will exhibit a higher heat transfer conductance. Decreased radial acceleration also decreases the pressure rise across the film, which can inhibit nucleation.

As long as the liquid film on the wall remains intact, none of the insert transitions would be expected to cause large changes in the heat transfer or pressure drop characteristics of the boiler.

2. Transition from a helical plug to a helical wire coil

In Chapter 3, relationships were presented for the fully-established flow of a single phase fluid in a helical wire coil. It is, however, under relatively unusual conditions that fully-established flow will be obtained because of the very long entrance lengths required. In Reference 5, an analysis was presented for transition to fully-established flow in a wire coil, starting from an arbitrary initial condition. The model is one of unsteady solid body rotation, with forces exerted on the (solid) fluid cylinder by the wire drag and wall friction.

The analysis leads to relationships for the asymptotic approach to fully-established flow. In order to illustrate the nature of

the results, a specific case is presented in Reference 5. The axial distribution of rotational velocity for this case, which is transition from a helical vane to a helical wire coil, both of which have the same pitch, is shown in Figure 4-23. The characteristic length for this transition is shown in Figure 4-24. As may be seen in the figure, many diameters of tube are necessary for flow accommodation.

3. Interrupted inserts

Many experiments have shown that wetting liquids tend to collect on the centerbodies of helical vane and multi-groove inserts, because of the secondary flows. An analytical investigation of this effect which corroborates experimental results, is presented in Reference 5. Because the centerbody is usually not a heat transfer surface, the accumulated liquid does not readily evaporate, and can run along the centerbody far into the superheat region. For this reason, many designers who have utilized vane systems with centerbodies have interrupted these inserts at intervals in order to return the liquid to the wall. When the liquid comes to the end of the centerbody it is stripped off into the rotating vapor. In order to predict the necessary spacing for these interruptions in the insert, an analysis of the droplet motion has been worked out in Reference 5.

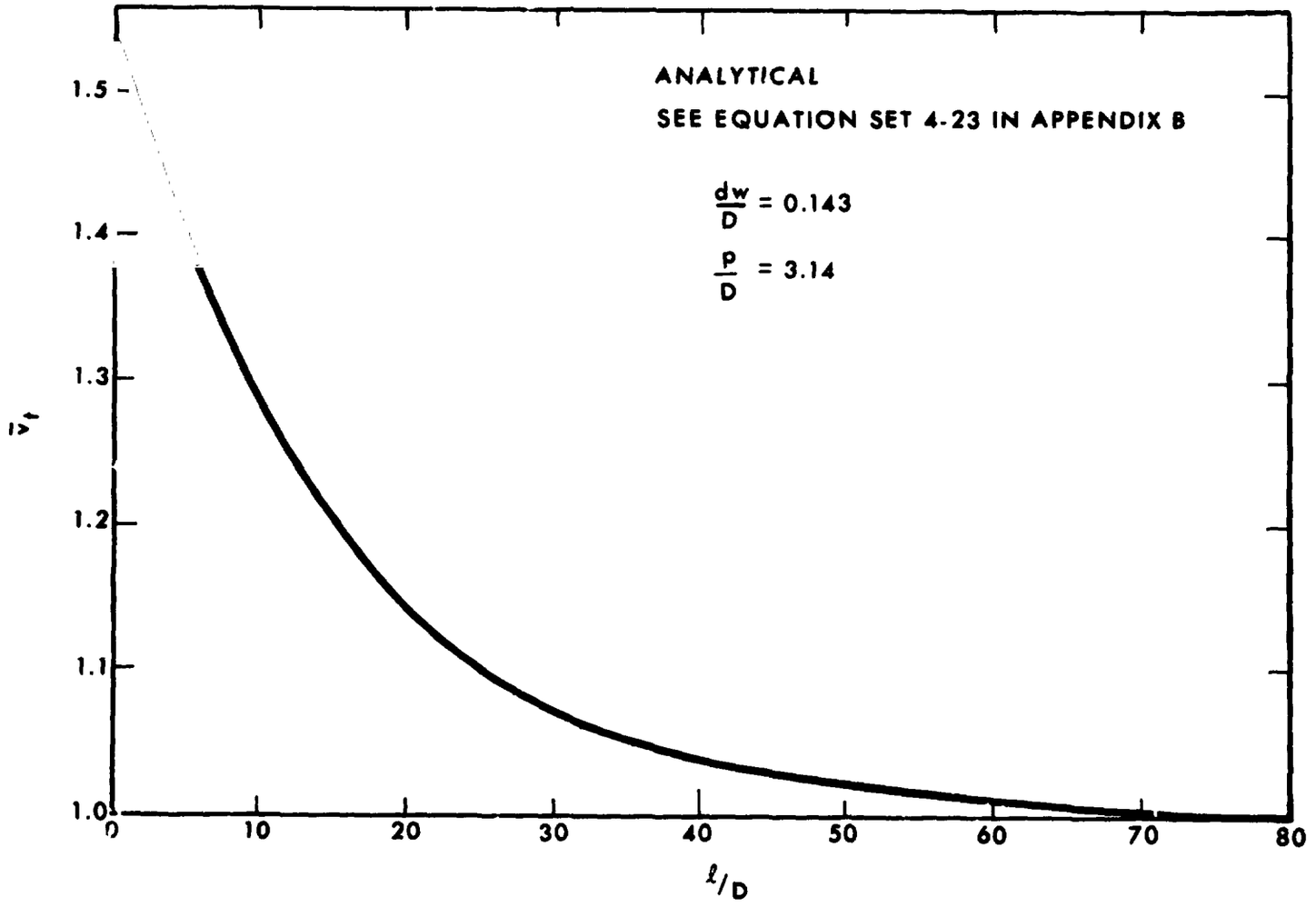

Figure 4-23. Change in rotational velocity of a flow passing from a helical vane insert to a helical wire insert, both of the same pitch.

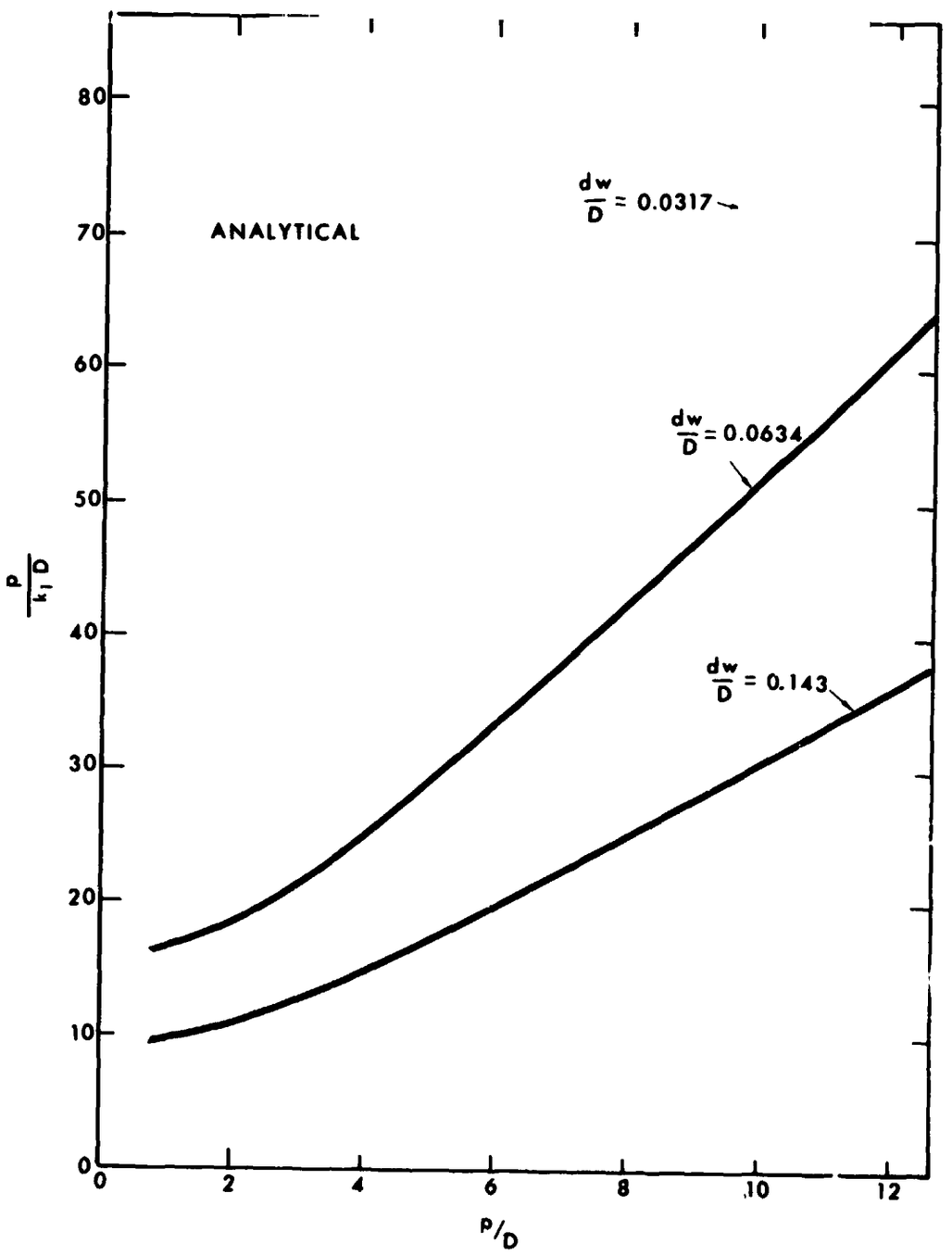

Figure 4-24. Normalized characteristic length.

Several phenomena are taking place simultaneously which affect the droplet motion. The droplets, initially at rest, slip with respect to the vapor in both the axial and rotational motions, and are accelerated in a three-dimensional spiral path due to drag forces. At the same time, the vapor rotation, no longer maintained by the helix, begins to decay due to boiler wall friction, and the vapor axial velocity continues to increase due to vapor addition from vaporization.

In addition, the droplets may be undergoing fragmentation due to internal flow instabilities, vapor shear gradients, or other forces. In order to analyze this complex two-phase flow, a number of restrictions have been made, which are:

(a) The axial vapor velocity field is uniform across the tube, and its change is negligible within the axial length.

(b) The vapor angular velocity change is negligible within the axial length required for the droplets to impact on the wall.

(c) The droplet size is invariant during flight.

(d) The vapor rotational velocity is a linear function of radius (solid body rotation).

(e) The droplet drag coefficient is constant.

A sketch of the geometry of the composite problem is shown in Figure 4-25.

Two limiting cases have been analyzed. In one, appropriate to large droplets, the idealization is made that the droplet velocity is always small compared to the vapor velocity, i.e., the slip is large. In the other case, appropriate to small droplets, the idealization is made that the droplet slip is at all times small. The range of applicability of each of these two solutions has been estimated.

The results of these two analyses are shown in Figure 4-26. It may be seen that the two solutions provide a reasonable bound for the axial travel distance of entrained droplets. The analytical result for the small droplets is given in the Appendix. The result for the large droplets is not in closed form.

A rather striking photograph of the deposition of droplets shed from the interrupted centerbody of a helical insert is shown in Figure 4-27. This photograph, which supports the analysis described above, was taken during the air-water experiments reported in Reference 26.

D. Boiler Tube Thermal Conductivity and Wall Thickness

Many experiments have shown that the onset of film boiling occurs when the wall surface temperature exceeds the liquid saturation temperature by a critical value.

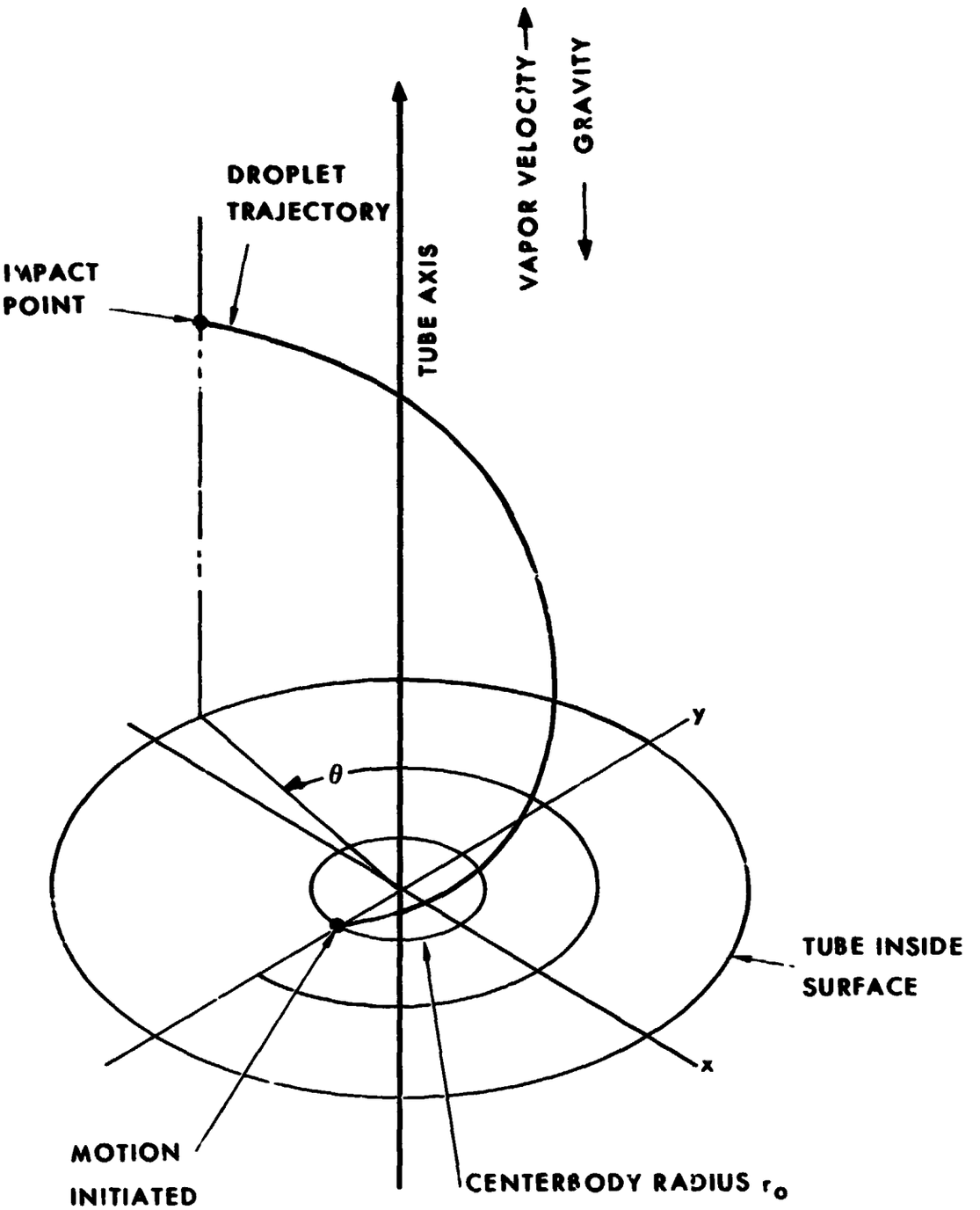

Figure 4-25. Idealized droplet motion at end of centerbody in helical flow.

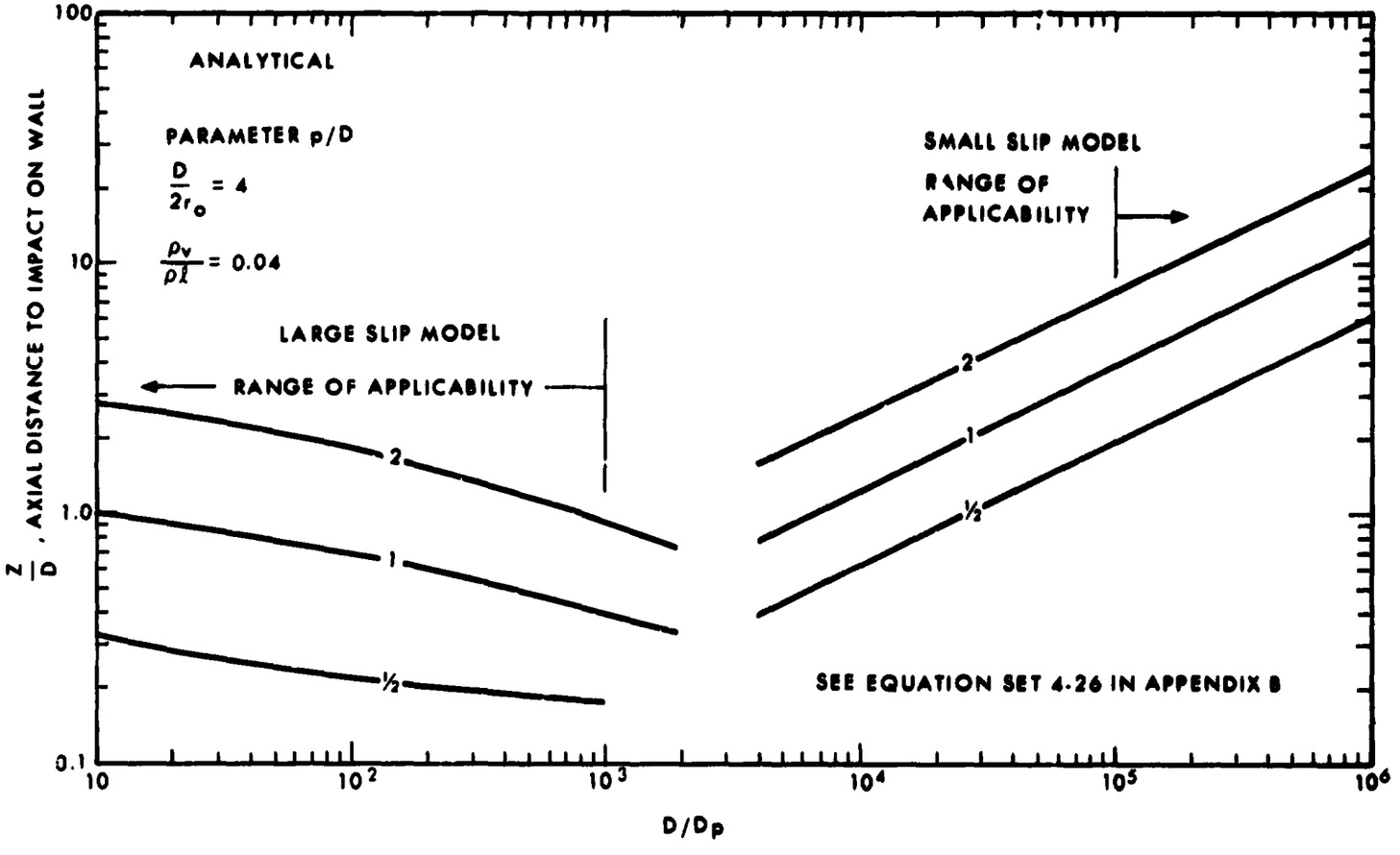

Figure 4-26. Axial distance to impact on wall for droplets in helical flow.

Figure 4-27. Droplet deposition downstream from an interrupted centerbody (photo courtesy of G. E. Missile and Space Division, Cincinnati).

It was shown in Reference 5 that local heat fluxes and wall temperatures are much higher than the average values near discontinuities in the inner wall conductances. The reason for this is that a discontinuous change in conductance is accompanied by a change in inner wall temperature, so that a significant amount of heat flows in the wall from the region of low conductance to the region of high conductance. Figure 4-28 taken from reference 5 indicates this effect for the case of uniform outside wall heat flux. When the surface temperature under the edge of the liquid film rises to a critical level, local "vapor blanketing" occurs (and the end of the liquid film moves upstream).

The closer to the beginning of the boiler the film ends, the higher the droplet concentration in the vapor and the deposition rate onto the wall must be. The impinging droplets may not wet the wall, but they still contribute to the wall cooling, so that the ratio of the 'wetted wall' heat transfer conductance to the 'dry wall' conductance decreases as the end of the film moves toward the boiler inlet. As is shown in Figure 4-28, the decrease in this ratio causes a lowering of the wall temperature at the edge of the film, so that at some point the edge becomes stable and ceases to move. Given a fixed value of wall to saturated fluid temperature difference for which the onset of film boiling occurs, the maximum heat flux for which the end of the annular liquid layer is stable can be computed from the data in the figure and the definition of the heat transfer conductance.

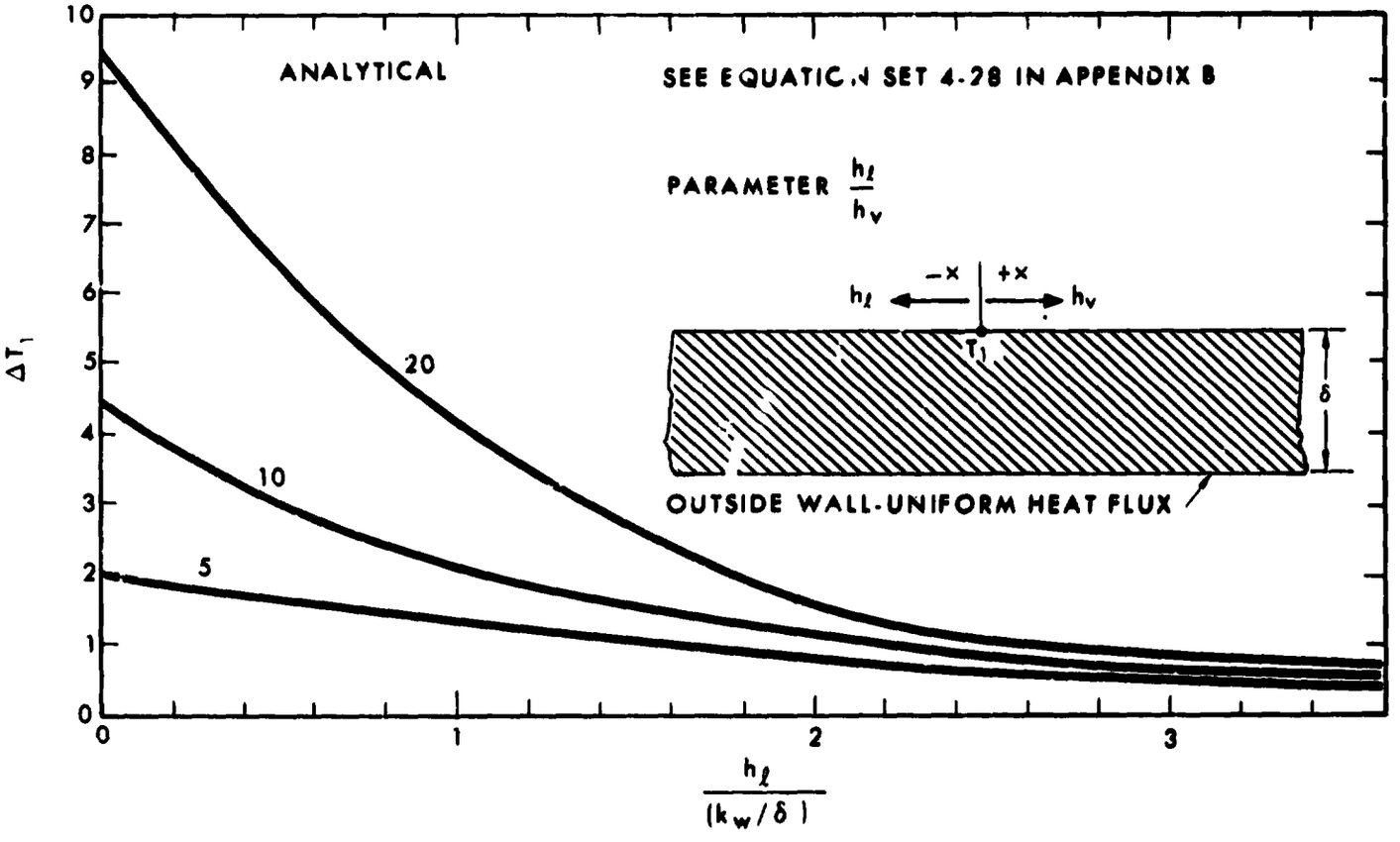

Figure 4-28. Normalized temperature at a conductance discontinuity.

One conclusion that may be drawn from this line of reasoning is that a thick walled or high conductivity boiler decreases the likelihood that the annular liquid layer will be removed by film boiling. Another conclusion is that internal flow regime changes occurring over short distances in a boiler tube would appear to extend over much greater distances if inside wall conductances are inferred from outside wall temperatures. An example of such an interpretation may possibly have occurred in the boiling Freon data of Reference 27. Those data, obtained with a (high conductivity) copper tube, show a change from the maximum near the end of the annular film to the minimum in the fog flow region which is quite gradual, while the data for Freon given in Reference 28, obtained with the aid of flow visualization in a (low conductivity) glass test section show a discontinuous transition between the two regimes. A comparison of these data is shown in Figure 4-29.

E. Boiler Tube Surface Chemistry and Physics

1. Nucleation sites

Several choices which the designer makes strongly effect the availability of nucleation sites in the boiler. Not only are the wall material and tube wall fabrication techniques important, but the methods of cleaning the system and introducing the working fluid affect the nucleation performance. Very small reentrant cavities filled with gas other than the working fluid vapor to form nucleation sites are usually found in profusion

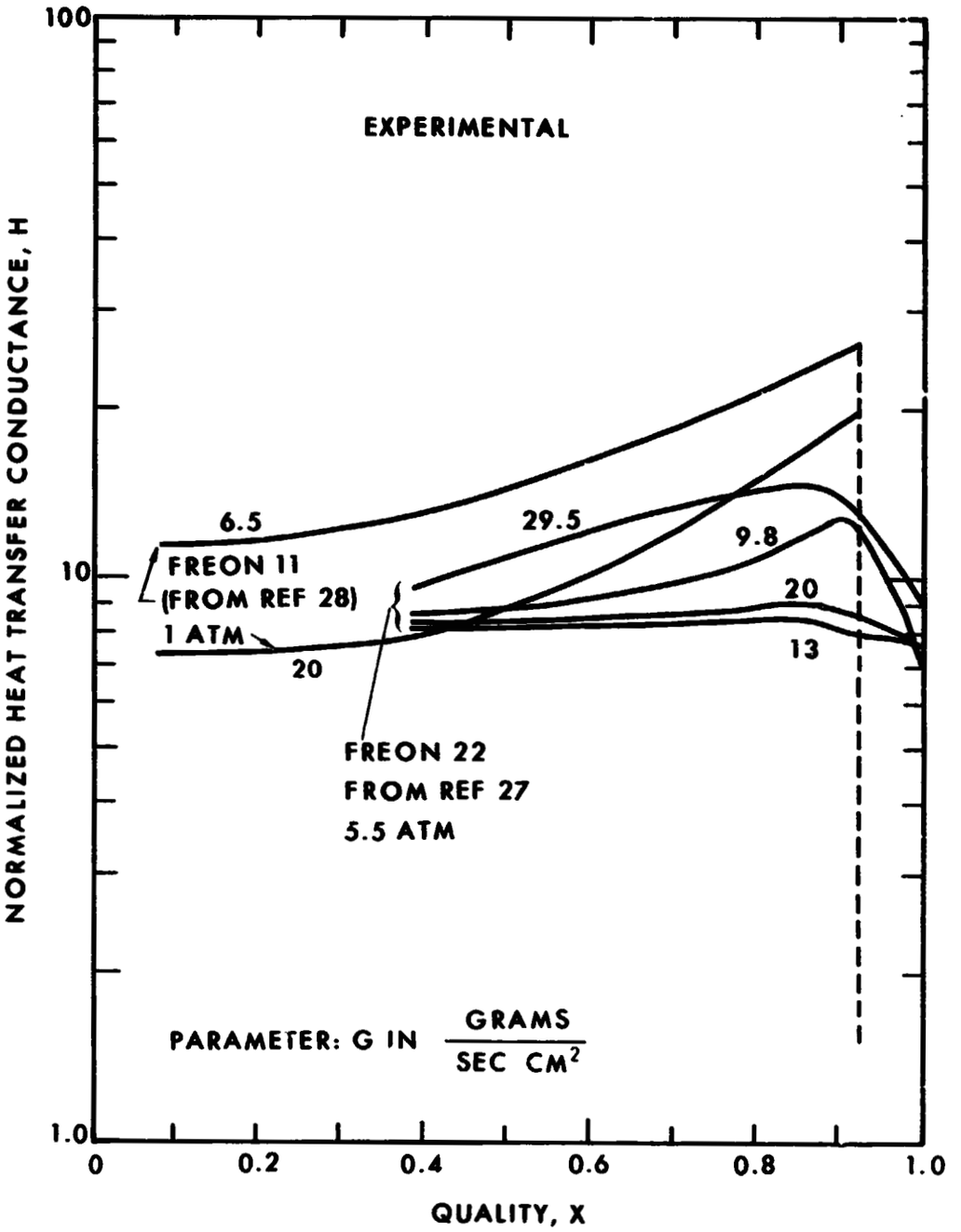

Figure 4-29. Linear forced convection boiling data for Freon 1 and 22.

on normal wrought materials. However, surface preparation can strongly affect them. Figures 4-30 and 4-31 (Reference 29) indicate the magnitudes of the effects which can occur with pool boiling liquid nitrogen. In Reference 39, it was shown that nucleate boiling conductances of Freon 113 on copper could be improved as much as fivefold by surface treatment such as sandblasting, electroetching, etc. It would be expected that some small improvement in liquid metal boiling could also be obtained by such treatments. However, for low Prandtl number fluids, the controlling thermal resistance is usually not in the boundary layer.

Surface material effects are also observed in forced convection boilers. If nucleate boiling does not occur, then heat which is added to an annular film at the wall must be conducted across the liquid layer so that vaporization occurs at the interface between the liquid and the vapor. One would expect that in the absence of nucleation sites, the onset of nucleate boiling would be dependent upon the maximum superheat temperature which the fluid against the wall can sustain without changing phase. In the forced convection experiments of Reference 30, Freon 22 was vaporized in three tubes of identical geometry and under very nearly identical conditions, except that two of the test sections were metal and the third was glass. The glass test section was heated by electrical conduction through a transparent

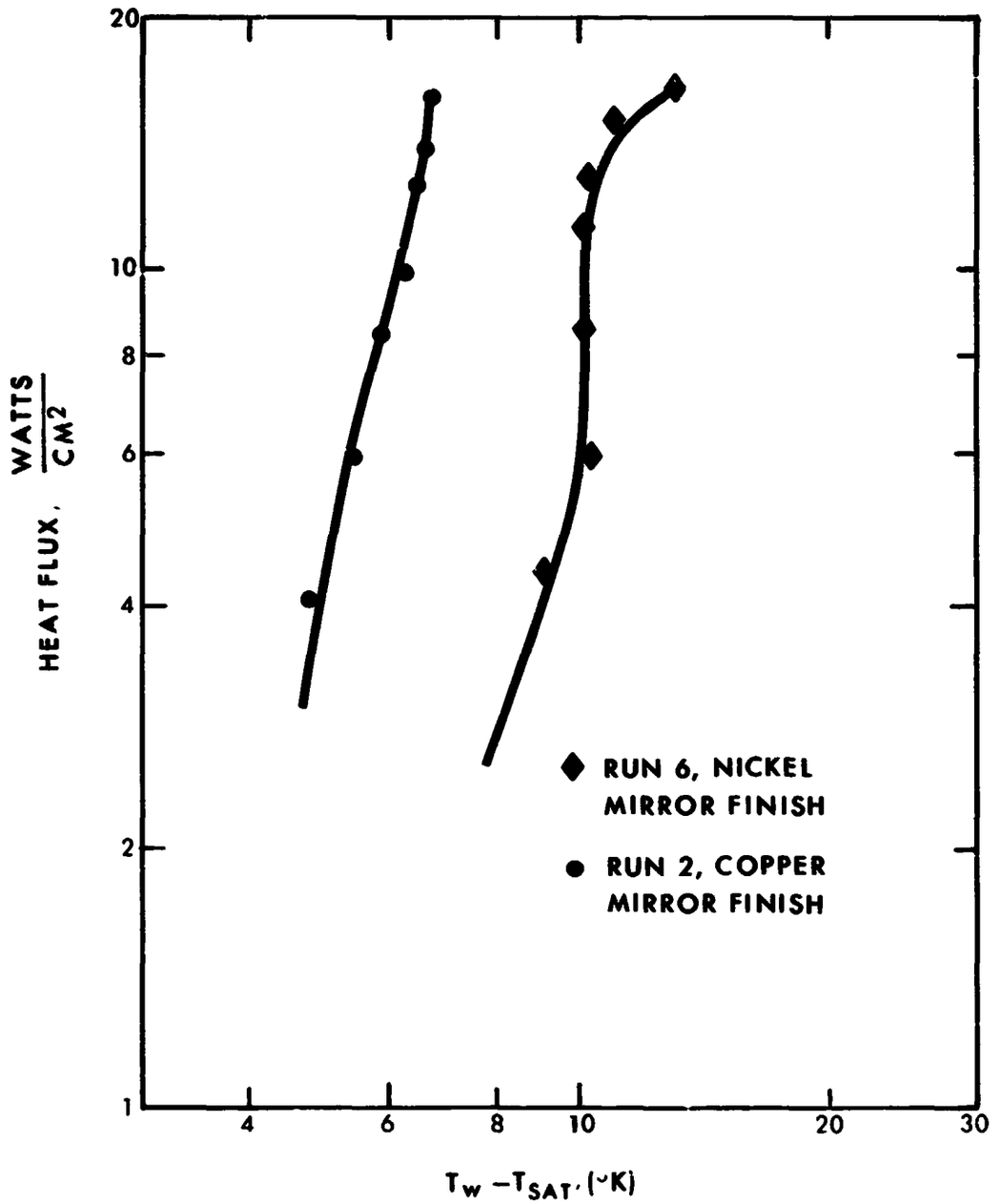

Figure 4-30. Effect of materials on nucleate boiling curve for nitrogen (Reference 29).

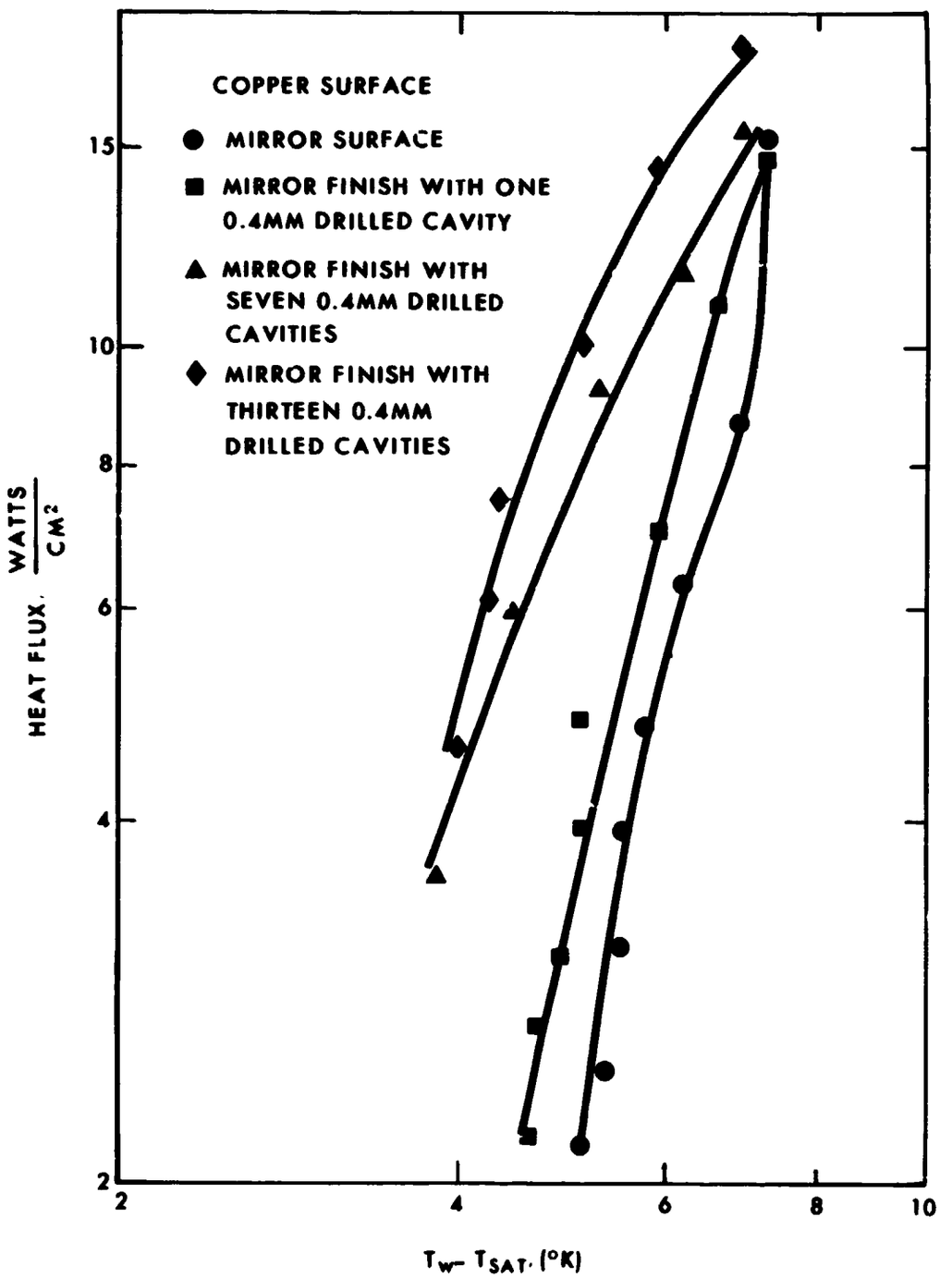

Figure 4-31. Effect of number of drilled cavities on nucleate-boiling curve for nitrogen (Reference 29).

metal film on the inside and was used for flow visualization. Some of the data from these experiments are reproduced in Figures 4-32 and 4-33. In these data the glass exhibited a much lower boiling heat transfer conductance than the two metal tubes. Since the glass test section does not have as many nucleation sites as the metal tube, more superheat of the liquid at the wall is required to bring on vapor generation in the liquid bulk.

The designer can, by choice of surface material, fabrication method, and system filling technique, either enhance or suppress nucleate boiling in forced convection.

2. Droplet vaporization

The chemical and physical nature of the boiler tube surface can control the thermal behavior of vaporizing drops. Therefore, a brief review of the mechanisms in operation and the corresponding transition criteria are presented.*

The lifetime of a droplet on a heated surface, i.e., the length of time from its placement on the surface until it has completely

*Many contributions in the field of droplet vaporization can be found in the literature (see References 32 - 38, for example).

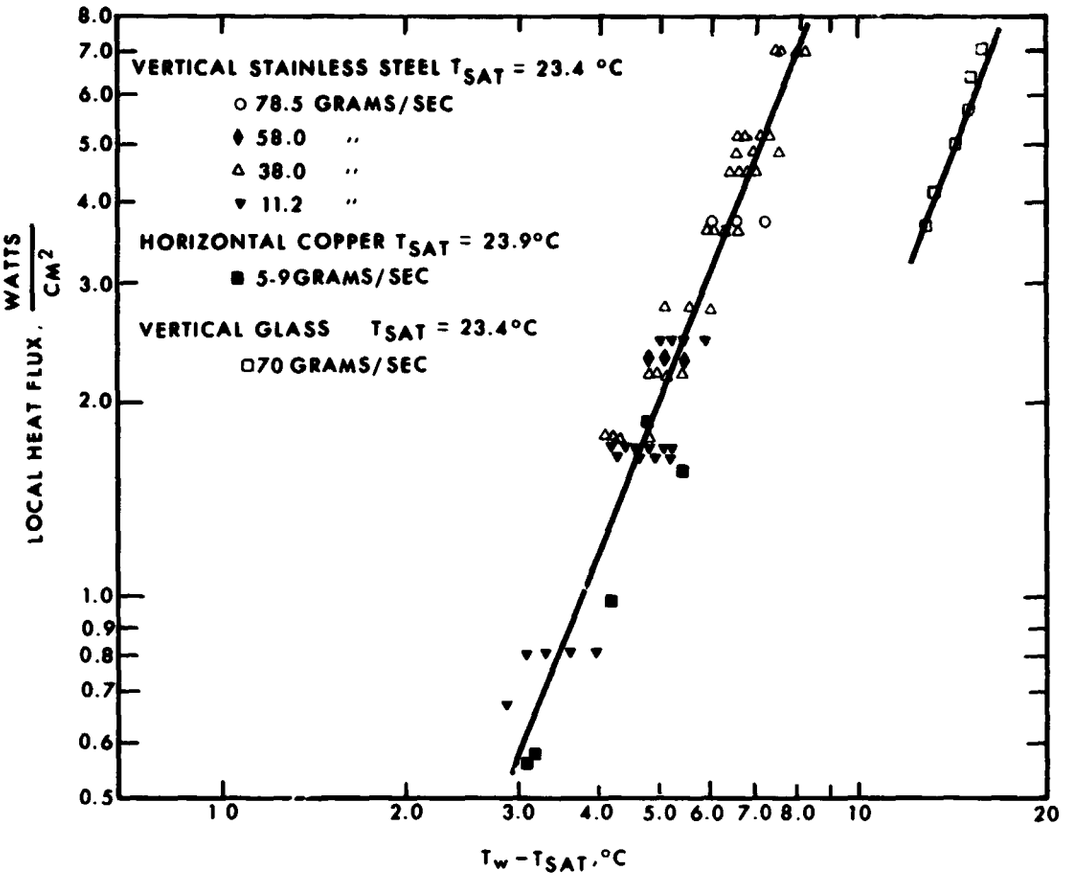

Figure 4-32. Heat transfer data for refrigerant 22 vapor qualities from 0.01 to 0.60.

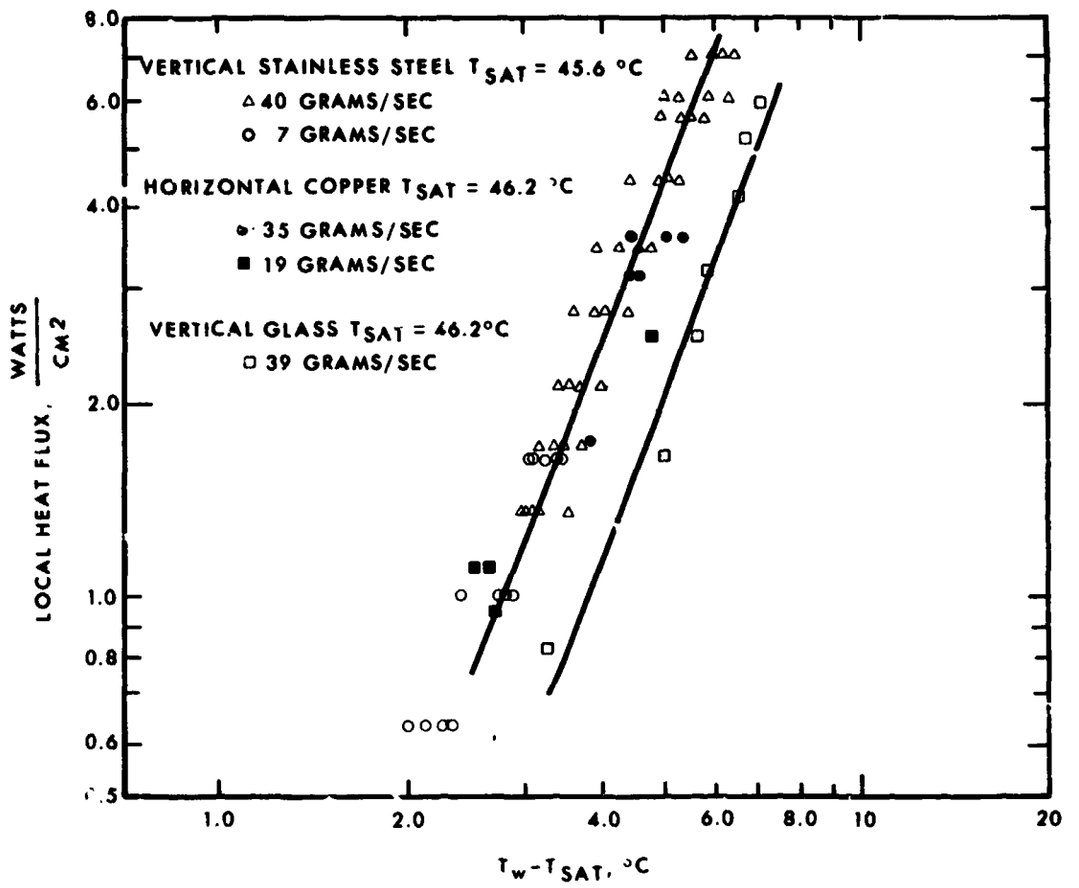

Figure 4-33. Heat transfer data for refrigerant 22 vapor qualities from 0.01 to 0.60.

disappeared, may be divided into three regions, depending upon temperature difference. At low temperature differences, the droplet is in contact with the heated surface, and vaporizes at the free surface. As the temperature difference is increased, the lifetime, which is proportional to the reciprocal of the heat flux, decreases, until it reaches a minimum (end of the surface vaporization region). As the temperature difference is increased beyond this point, the transition region begins in which the droplet is partially supported on a layer of its own vapor. At higher temperature differences, the droplet floats upon a film of its own vapor (like a ground effects machine) with the heat transfer taking place by convection and radiation across the vapor film.

Analyses which describe the direct contact surface vaporization process are given in Reference 35. The lifetime prediction from one of these models describes the vaporization of a droplet idealized as flat disk vaporizing from the upper surface only. Idealizations required in the analysis are that the upper surface is at the saturation temperature, and that the droplet disk diameter does not change during vaporization. The disk simply grows thinner with time. An interface thermal resistance between the droplet and the surface, interpreted as the portion of the disk area which is in direct contact with the surface, is included in the analysis.

If the surface is not microscopically smooth, the pits in the surface will probably not be completely filled with liquid, but will contain a small gas volume. An equation can be written relating the pressure and liquid surface tension forces, which defines the conditions under which the liquid-vapor interface will no longer remain within the pits. Such a relationship is presented in Reference 35, based on the approximation that the liquid vapor pressure is a linear function of the temperature in the range of interest.

Analyses of the film boiling of droplets above heated surfaces under several conditions are also available. In Reference 32, the lifetime of film boiling droplets on smooth surfaces is presented. The film boiling of a droplet on a rough surface, in which some heat is transferred by conduction through roughness elements on the surface, as well as convection through the vapor film, is presented in Reference 34.

Under some conditions, the droplet will spall or fission into several fragments. The lifetimes of the individual fragments differ from the lifetime of the complete droplet. Under some conditions, the droplets oscillate in the film boiling region. It has been shown analytically in Reference 34 that this motion should increase the droplet lifetime.

In Figure 4-34 are shown representative analytical curves for the models describing direct contact surface vaporization on smooth and rough surfaces, film boiling on smooth and rough surfaces, spalling and oscillating droplets.

The presence of dissolved impurities in droplets can change the behavior of droplet vaporization in two ways, depending upon whether the impurities are surface active or inactive. In the first case, the accumulation of surface active impurities (e.g., potassium in mercury) on the droplet surface reduces the vapor pressure or percentage of vaporizing liquid exposed to the heat transfer surface relative to a pure droplet, therefore changing the heat transfer to the droplet.[35] The presence of the surface active impurities effectively increases the lifetime of the droplet. In the second case, the accumulation of dissolved surface inactive impurities (e.g., iron in mercury) upon the droplet surface as a result of impurity saturation in the vaporizing droplet can be visualized to increase the heat transfer. The surface inactive impurity does not accumulate upon the surface until the droplet becomes saturated. When the droplet becomes saturated, the concentration of mercury on the droplet surface is suddenly reduced, thereby causing the droplet to contact the heat transfer surface. Thus, a change in the droplet vaporization mechanism from film boiling to a

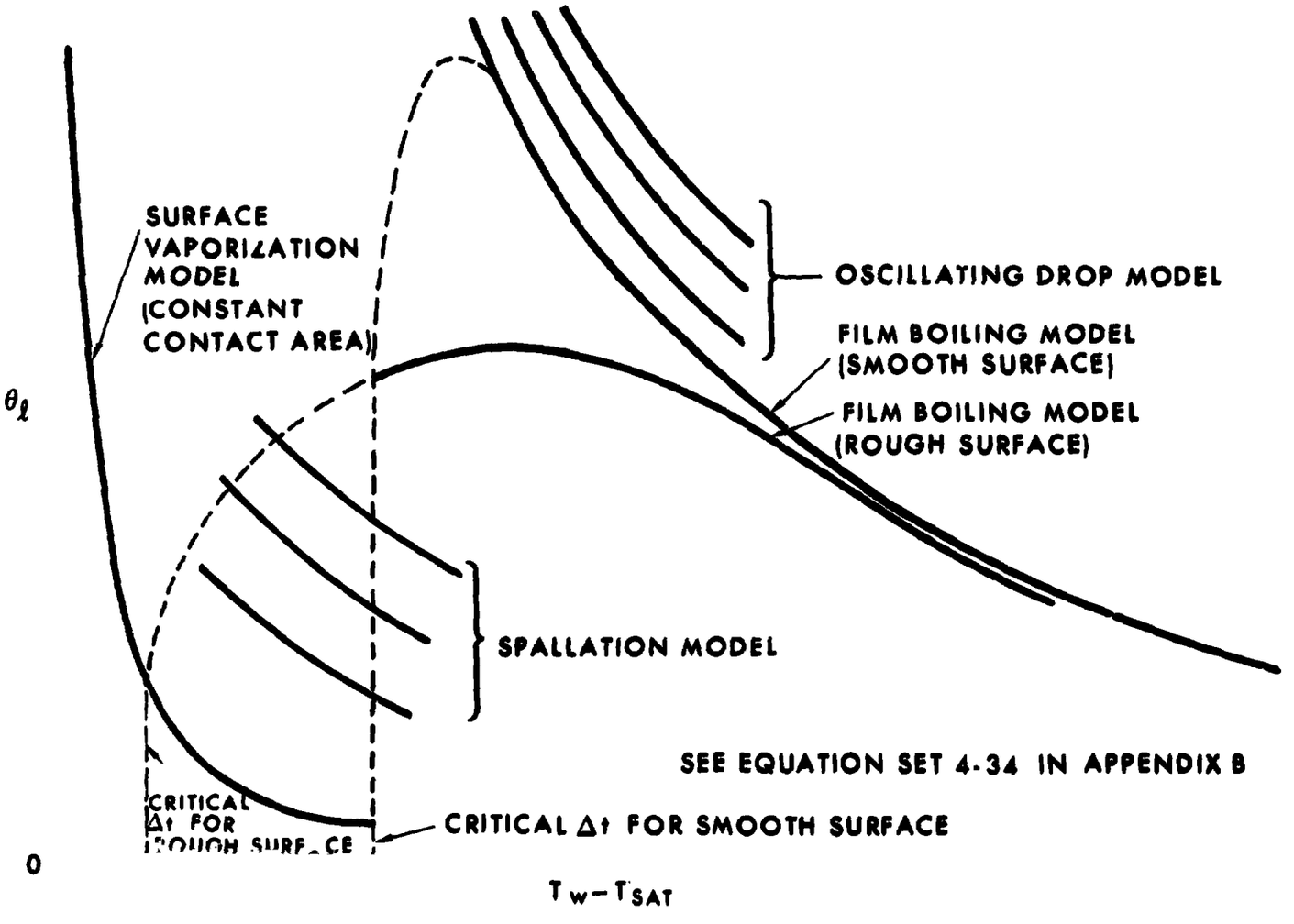

Figure 4-34. Some of the important boiling heat transfer states for droplet vaporization.

direct contact heat transfer type results. (This mode of droplet behavior has been observed in mercury vaporization experiments reported in Reference 35.)

Experimental data for the vaporization lifetime of a variety of different liquids are shown in Figures 4-35, 4-36, and 4-37. In some cases, the theoretical prediction for film boiling on a smooth surface is also included. A series of droplet vaporization experiments is described in Reference 36, to determine the effect of surface contamination (oxide films, decomposed oils) on the vaporization of mercury. Some of these data are reproduced in Figures 4-38 and 4-39.

It may be seen in Figure 4-38 that as the oxide layer on the surface is increased, the maximum temperature difference for the surface vaporization regime decreases.

Many wall materials form microscopic crystalline structures in their surface oxides, which act as roughness elements on the surface. These oxide film structures are not stable on some refractory metals, however. If the metal bulk is not oxygen saturated, oxygen from surface oxides formed over a short period of time tends to diffuse into the metal wall and disappear if the temperature is high and the source of oxygen is removed.

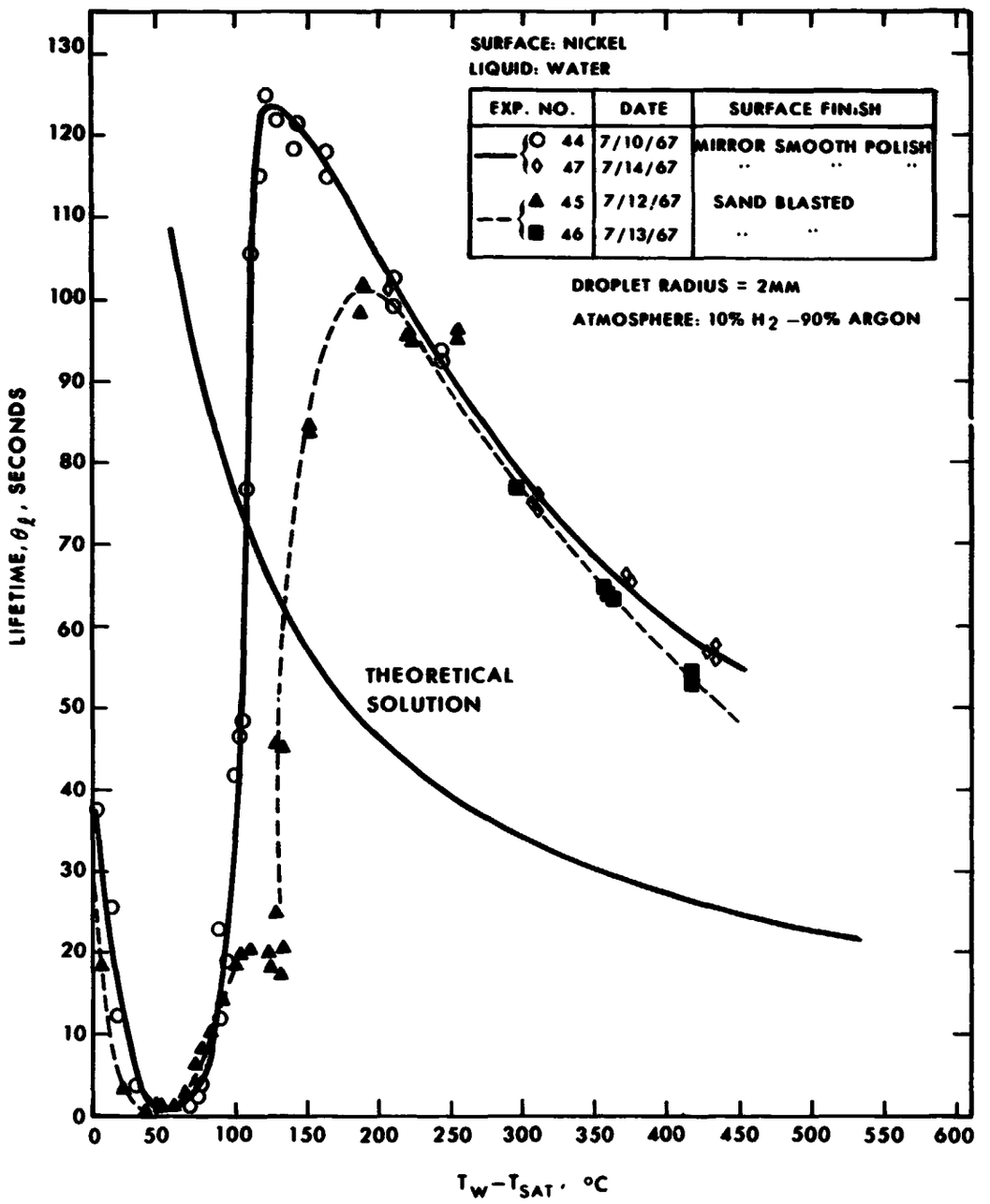

Figure 4-35. The lifetimes for water droplets vaporizing on polished and sand-blasted nickel surfaces.

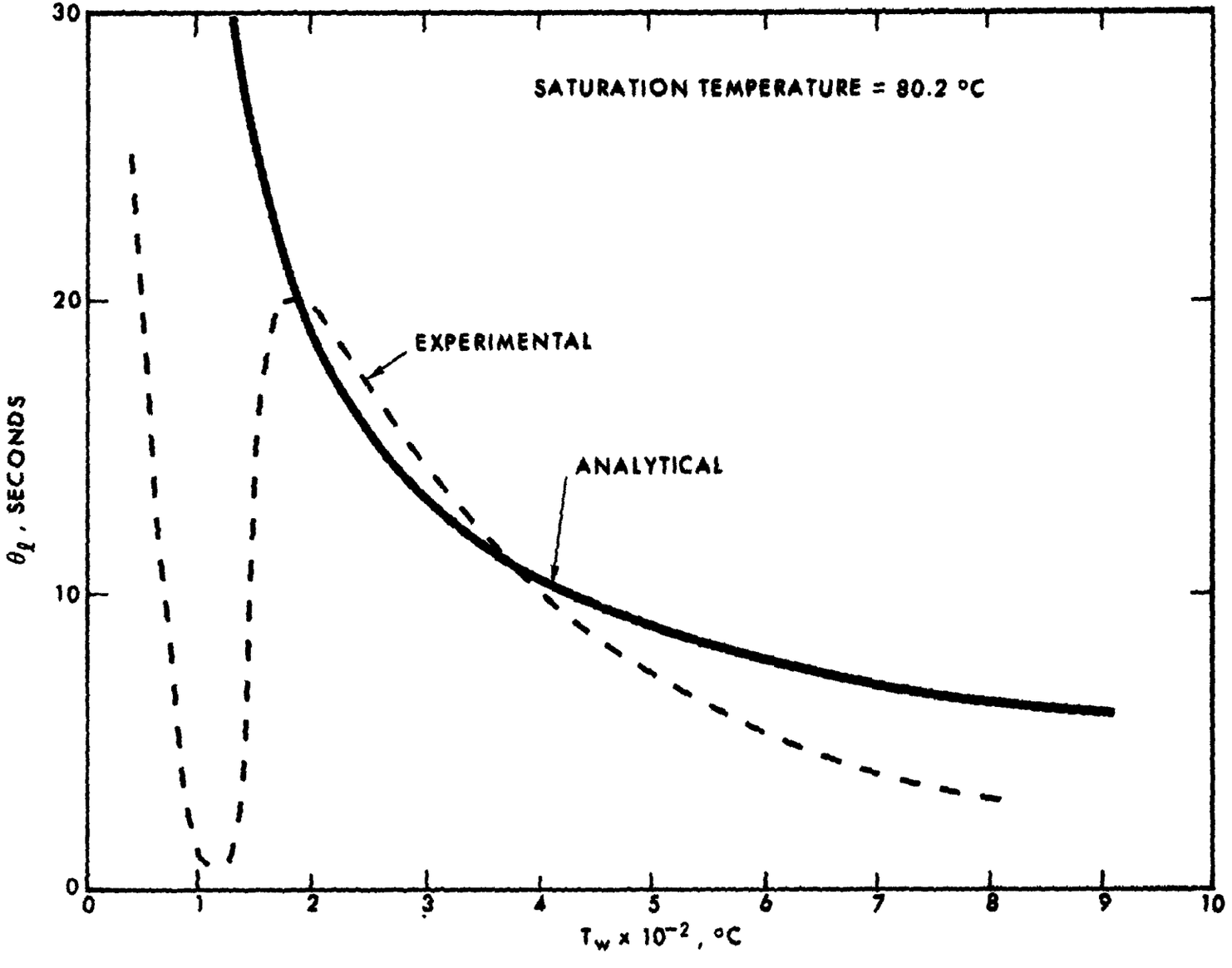

Figure 4-36. The lifetimes for benzene droplets.

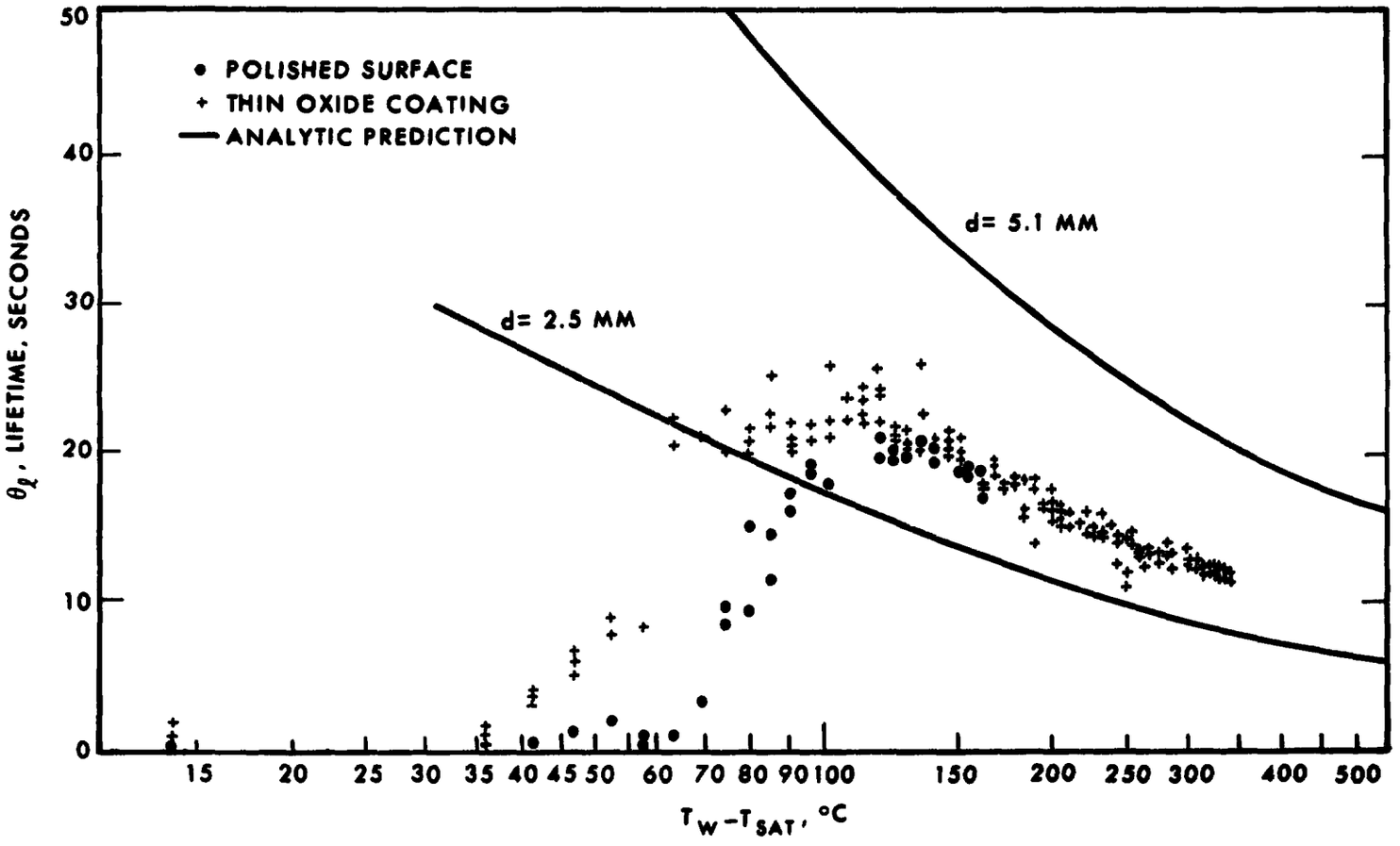

Figure 4-37. The lifetimes for Freon 11 droplets vaporizing on polished and oxidized surfaces.

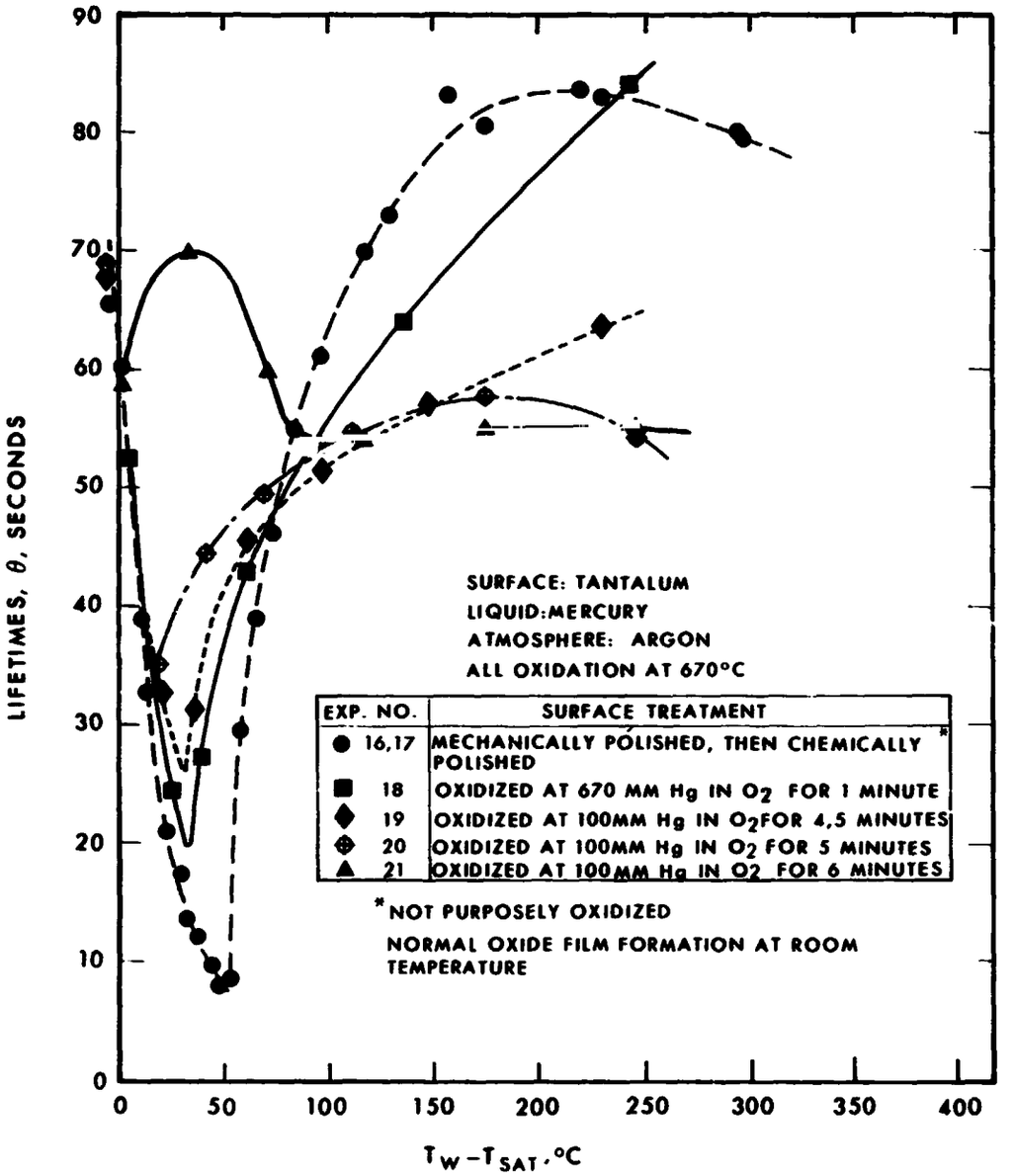

Figure 4-38. The lifetimes of mercury droplets vaporizing on a tantalum surface with various amounts of surface oxidation.

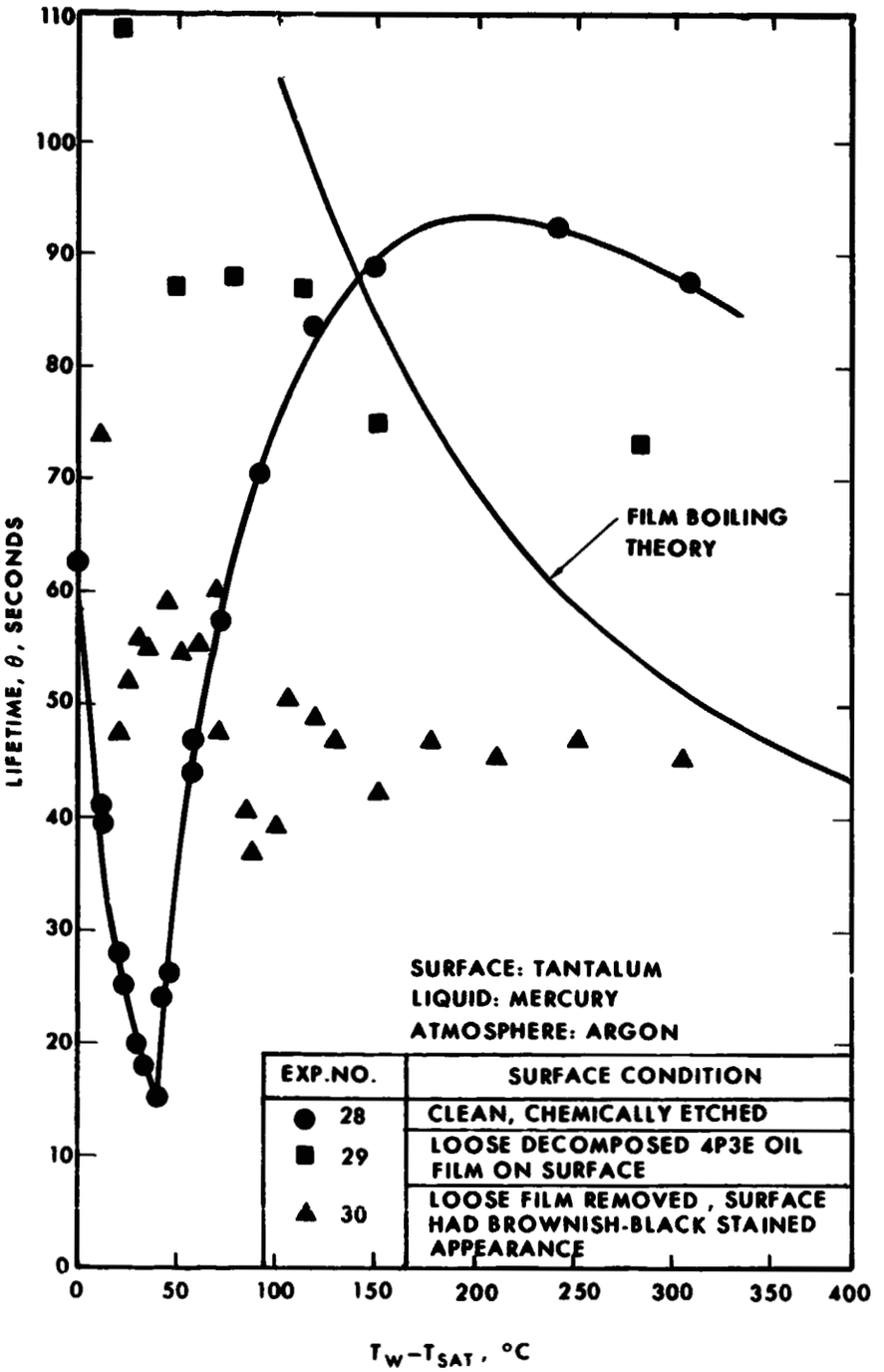

Figure 4-39. The lifetimes of mercury droplets vaporizing on a tantalum surface with various contaminants.

Table 4-I gives an approximate range of temperature differences which bound the three boiling regimes discussed in the text.

Some of the major effects of the chemical and physical features of the boiler tube surface are summarized below:

1. In the surface evaporation region, wetting droplets evaporate as thin films and nonwetting droplets as hemispheres.

2. The value of the wall-fluid temperature difference at which the minimum in the vaporization lifetime occurs decreases with increasing surface roughness.

3. The minimum droplet vaporization lifetime increases with surface roughness.

4. Oscillation of droplets during film boiling increases the vaporization lifetime as much as 50 percent depending upon the type of metal surface and surface temperature. The height of the oscillation increases from approximately five to ten diameters at the beginning to as high as 500 diameters at the end.

5. Roughening a heat transfer surface reduces the heat transfer in the lower portion of the transition region

TABLE 4-I.

APPROXIMATE CRITERIA FOR BOILING REGIME TRANSITION

Fluid	Smooth, clean surface		Rough, clean surface	
	Maximum Temperature difference for surface vaporization	Minimum Temperature difference for film boiling	Maximum Temperature difference for surface vaporization	Minimum Temperature difference for film boiling
	°C	°C	°C	°C
Water	70	120	55	185
Mercury	70	195	35	195
Potassium	110	185	--	---
Freon 11	60	120	35	110
Freon 114	35	55	55	80
Benzine	35	90	--	--

and increases the heat transfer in the upper portion of the transition region.

6. The value of the wall-fluid temperature difference at the maximum vaporization lifetime decreases with increasing surface roughness.

7. The value of the maximum lifetime for vaporizing droplets tends to decrease with surface roughness.

DISCUSSION

This chapter has presented information on transition criteria for the boiler design functions given in Chapter 3. This transition information can be used as a guide for the designer as he makes decisions on which phase distributions exist in particular locations proceeding throughout the boiler tube. Clearly, in many instances, he must use the function which covers the "worst case" because exact criteria on transition are not available

NOMENCLATURE FOR CHAPTER 4

C_o	=	a phase distribution parameter
D	=	tube inside diameter
D_e	=	equivalent diameter of passage
D_p	=	entrained droplet diameter
d	=	droplet diameter
d_w	=	helical wire insert diameter
F_d	=	vapor drag force
F_g	=	gravitational force
F_σ	=	surface tension force
G	=	mass flow rate per unit of passage cross section
g	=	acceleration of gravity
g_c	=	proportionality constant in Newton's second law
g_e	=	acceleration of gravity for earth
H	=	normalized conductance defined by $H = \frac{h}{h_{x = 100\%}}$
h	=	heat transfer conductance
h_l	=	heat transfer conductance between wall and liquid layer

h_v = heat transfer conductance between wall and vapor

k_1 = a dimensionless parameter defined in equation set 4-23

k_w = thermal conductivity of wall material

ℓ = axial tube length

ℓ_B = location in tube where "burnout" occurs

p = helical boiler tube insert pitch

q = heat flux

$(\frac{q}{A})_B$ = "burnout" heat flux

r_o = tube radius, helical insert centerbody radius

T_o = liquid bulk temperature at point of first void formation

T_B = mixed mean (bulk) temperature

T_{sat} = equilibrium saturation temperature

T_w = temperature of the heat transfer surface

u_ℓ = liquid velocity

u_ℓ^* = superficial liquid velocity (mean velocity if liquid only flowed in the tube)

u_v^* = superficial vapor velocity (mean velocity if vapor only flowed in the tube)

V_v = vapor velocity in core of annular flow

$\bar{v}_t$ = normalized velocity component normal to tube axis

x = vapor quality

x_B = quality at location in tube where "burnout" occurs

z = axial distance

z^* = distance from initiation of heated length divided by total heated length

z_o = axial location of first void formation

GREEK SYMBOLS

$\langle \alpha \rangle$ = average void fraction at an axial station

α_c = critical contact angle at film rupture

δ = annular liquid film thickness

δ = tube wall thickness

$\Delta \ell$ = a length scale defined in equation set 4-5

ΔT = heat transfer temperature difference

ΔT_1 = defined in equation set 4-28

$\Delta T_s = T_{sat} - T_o$

$\Delta T_{superheat} = T_{liquid} - T_{sat}$

θ_ℓ = lifetime of liquid droplet on a hot surface

ρ_l = liquid density

ρ_v = vapor density

DIFFERENTIALS

$\frac{\partial p}{\partial z}$ = two phase pressure gradient

REFERENCES

1. Sabin, C. M.; Poppendiek, H. F.; Mouritzen, G.: Meckel, P. T.; Cloakey, J. E.; "Liquid Metal Boiling Inception," NASA CR-2095, Geoscience Ltd GLR-94, Aug 1972.

2. Lewis, J. P.; Groesbelk, D. E.; Christenson, H. H.; "Tests of Sodium Boiling in a Single Tube-in-Shell Heat Exchanger Over the Range 1720° to 1980°K," NASA TN D-5323, July 1969.

3. Staub, F. W.: "Prediction of the Void Fraction in Subcooled Boiling, Annular Flow, and Ideal Bubbly Flow," General Electric, GEAP 5414, San Jose, CA, Jan 1967.

4. Bijwaard, G.; Staub, F. W.; Zuber, N.; "A Program of Two-Phase Flow Investigation, Eleventh Quarterly Report," General Electric, GEAP 5067, Schenectady, N. Y., Dec 1965.

5. Sabin, C. M.; Poppendiek, H. F.: "Heat and Momentum Transfer Model Studies Applicable to Once-Through Forced Convection Potassium Boiling," NASA CR-1896, Geoscience Ltd GLR-71, Sept 1971.

6. Staub, F. W.; Zuber, N.; "A Program of Two-Phase Flow Investigation," Sixth Quarterly Report, General Electric, GEAP 4733, Schenectady, N. Y., p 36, Oct 1964.

7. Griffith, P.; Snyder, G. A.: "The Bubbly-Slug Transition in a High Velocity Two-Phase Flow," MIT TN 5003-29, July 1964.

8. Haberstroh, R. D.: Griffith, P.; "The Transition from the Annular to the Slug Flow Regime in Two-Phase Flow," MIT Tech Rep 5003-28, Dept Mech Eng, June 1964.

9. Wallis, G. B.: "The Transition from Flooding to Upwards Cocurrent Annular Flow in a Vertical Pipe," AE EW-R 142, AEE Winfrith, 1962.

10. Nicklin, D. J.; Davidson, J. F.; "The Onset of Instability in Two-Phase Slug Flow," Symposium on Two-Phase Fluid Flow, Inst Mech Eng, Feb 7, 1962.

11. Griffith, P.; "The Slug-Annular Flow Regime Transition at Elevated Pressure," ANL-6796, Nov 1963.

12. Wallis, G.; Turner, J.; Benberis, I.; Kaufman, D.; "Two-Phase Flow and Boiling Heat Transfer, Dartmouth College, NYO 3114-4, Sept 1964.

13. Kirby, G. J.; "Burnout in Climbing Film Two Phase Flow, A Review of Theories of the Mechanism," AEEW-R470, UK, Atomic Energy Authority, Reactor Group, Winfrith, 1966.

14. Hewitt, G. F.; Kearsey, H. A.; Lacey, P. M. C.; Pulling, D. J.; "Burnout and Nucleation in Climbing Film Flow," Int J Heat Mass Transfer, Vol 8, No. 5, May 1965.

15. Poppendiek, H. F.; Greene, N. D.; Sabin, C. M.; Feigenbutz, L. V.; Mouritzen, G.; MacDonald, F. R.; Livett, R. V.; Chambers, J. E.; Schwartz, P. E.; Connelly, D. J.; Morton, W. A.; "Summary Report on High Acceleration Field Heat Transfer for Auxiliary Space Nuclear Power Systems," Geoscience Ltd GLR-42, AEC Contract No. AT(04-3)-409, SAN-409-29, Jan 1966.

16. Hallett, V.; "Surface Phenomena Causing Breakdown of Falling Liquid Films During Heat Transfer," Int J Heat Mass Transfer, Vol 9, No. 4, April 1966.

17. Norman, W.; McIntyre, V.; "Heat Transfer to Liquid Film on a Vertical Surface," Trans Inst Chem Engrs 38, 301, 1960.

18. Bankoff, S.; "Stability of Liquid Flow Down a Heated Inclined Plane," Int J Heat Mass Transfer, Vol 14, No. 3, Mar 1971.

19. Zuber, N.; Staub, F.; "Stability of Dry Patches Forming in Liquid Films Flowing Over Heated Surfaces," Int J Heat Mass Transfer, Vol 9, No. 9, Sept 1966.

20. Hewitt, G.; Lacey, P.; "The Breakdown of the Liquid Film in Annular Two-Phase Flow," Int J Heat Mass Transfer, Vol 8, No. 5, May 1965.

21. Hartley, D.; Murgatroyd, W.; "Criteria for the Breakup of Thin Liquid Layers Flowing Isothermally Over Solid Surfaces," Int J Heat Mass Transfer, Vol 7, No. 9, 1964.

22. Murgatroyd, W.; "The Role of Shear and Form Forces in the Stability of a Dry Patch in Two-Phase Film Flow," Int J Heat Mass Transfer, Vol 8, No. 2, Feb 1965.

23. Biasi, L.; Clerici, G.; Sala, R.; Tozzi, A.; "A Non-Equilibrium Description of Two-Phase Annular Flow. Applications to the Burn-out Prediction," Int J Heat Mass Transfer, Vol 12, No. 3, Mar 1969.

24. Previously unreported experiments at Geoscience Ltd, 1969.

25. Poppendiek, H. F.; Greene, N. D.; Goddard, W. B.; Sabin, C. M.; "Annual Report on Investigation of Fundamental Mechanisms and Parameters that Influence Steady State and Transient Performance of Rankine Cycle Liquid Metal Systems," AEC Contract No. AT(04-3)-677, SAN-677-29, Geoscience Ltd GLR-64, Period July 1, 1967, through June 30, 1968.

26. Converse, G. L.; et al, "Air-Water Experiments in a Transparent Plastic Tube," General Electric HTC-10, Cincinnati, March 1968.

27. Altman, M.; Norris, R.; Staub, F.; "Local and Average Heat Transfer and Pressure Drop for Refrigerants Evaporating in Horizontal Tubes," J Heat Transfer, pp 189-198, Aug 1960.

28. Poppendiek, H. F.; Greene, N. D.; Sabin, C. M.; Livett, R. K.; MacDonald, F. R.; Feigenbutz, L. V.; "Annual Technical Report on High Acceleration Field Heat Transfer for Auxiliary Space Nuclear Power Systems," AEC Contract No. AT(04-3)-409, SAN-409-12, Geoscience Ltd GLR-27, Period Sept 1, 1963, through Aug 31, 1964.

29. Marto, P. J.; et al, "Nucleate Pool Boiling of Nitrogen with Different Surface Conditions," ASME Paper 68-HT-12, Sept 1968.

30. Bijwaard, C.; Staub, F.; Zuber, N.; "A Program of Two Phase Flow Investigation," Tenth Quarterly Report, General Electric GEAP-4959, San Jose, CA, Oct 1965.

31. Holtz, R.; "The Prediction of Liquid Superheats Required for Initiation of Nucleate Boiling in Liquid Metals," ASME Paper 64-WA/HT-31.

32. Poppendiek, H. F.; Greene, N. D.; Sabin, C. M.; Feigenbutz, L. V.; Mouritzen, G.; MacDonald, F. R.; Livett, R. V.; Chambers, J. E.; Schwartz, P. E.; Connelly, D. J.; Morton, W. A.; "Summary Report on High Acceleration Field Heat Transfer for Auxiliary Space Nuclear Power Systems," AEC Contract No. AT(04-3)-409, SAN-409-29, Geoscience Ltd GLR-42, Jan 1966.

33. Poppendiek, H. F.; Feigenbutz, L. V.; Greene, N. D.; Sabin, C. M.; Connelly, D. J.; "Quarterly Report on Investigation of Fundamental Mechanisms and Parameters that Influence Steady State and Transient Performance of Rankine Cycle Liquid Metal Systems," AEC Contract No. AT(04-3)-677, SAN-677-3, Geoscience Ltd GLR-47, Period July 11 to Sept 30, 1966.

34. Poppendiek, H. F.; Feigenbutz, L. V.; Greene, N. D.; Morton, W. A.; Sabin, C. M.; Connelly, D. J.; "Quarterly Report on Investigation of Fundamental Mechanisms and Parameters that Influence Steady State and Transient Performance of Rankine Cycle Liquid Metal Systems," AEC Contract No. AT(04-3)-677, SAN-677-6, Geoscience Ltd GLR-49, Period Oct 1 to Dec 31, 1966.

35. Poppendiek, H. F.; Feigenbutz, L. F.; Greene, N. D.; Sabin, C. M.; "Quarterly Report on Investigation of Fundamental Mechanisms and Parameters that Influence Steady State and Transient Performance of Rankine Cycle Liquid Metal Systems," AEC Contract No. AT(04-3)-677, SAN-677-15, Geoscience Ltd GLR-55, Period April 1 to June 30, 1967.

36. Poppendiek, H. F.; "SNAP-8 Boiler Performance Degradation and Two-Phase Flow Heat and Momentum Transfer Models," NASA Contract No. NAS 3-11836, CR 72759, Geoscience Ltd GLR-84, Aug 1970.

37. Baumeister, K. J.; Hamill, T. D.; "Creeping Flow Solution of the Leidenfrost Phenomenon," NASA TN D-3133, Dec 1965.

38. Baumeister, K. J.; Hendricks, R. C.; Hamill, T. D.; "Metastable Leidenfrost States," NASA TN D-3226, April 1966.

39. Jakob, M.; Fritz, W.; "Forsch, Giebete Ingenieurw," 2, 434-447, 1931.

CHAPTER 5: BOILER DESIGN EXAMPLES

Quantitative data on forced flow boiling and pressure loss were presented in Chapter 3 and the corresponding flow transition criteria for the important phase distributions were given in Chapter 4. These heat and momentum transfer relations can be used by the engineer to develop boiler designs.

In the following paragraphs, there are found a number of example boiler designs which are based on or can be analyzed with the design functions described in Chapters 3 and 4. The variety of applications and working fluids of the example boilers is one measure of the general applicability of the information presented in Chapters 3 and 4. A brief background for each boiler design is given in addition to the results obtained, including comparisons with actual operating performance. Detailed information about these heat exchangers can be found in the references that are cited.

DESIGN EXAMPLES

A. Design Example No. 1: Double Containment Boiler for SNAP-8 Mercury Rankine Space Power System

An important government program was the SNAP-8 Mercury Rankine cycle nuclear-electric power conversion system for space missions.[1]

The power conversion system was developed by Aerojet Nuclear Systems Company for NASA and the nuclear reactor was developed for the Atomic Energy Commission by Atomics International. A schematic drawing of this 35 kWe system is shown in Figure 5-1. Thermal energy is transferred from the reactor to the power conversion system by a primary eutectic sodium-potassium alloy (NaK) circuit. Mercury is the working fluid in the Rankine cycle circuit. The thermal energy exchange takes place in a counterflow NaK-to-Hg heat exchanger where the mercury is preheated, vaporized, and superheated in a "once-through" boiler configuration. The superheated mercury vapor drives the turbine-alternator assembly to produce electrical power, and then is condensed and pumped back to the boiler. Heat given up by the mercury as it condenses is carried by a secondary NaK heat transfer circuit to a space radiator. Organic fluid in a fourth circuit is pumped to the turbine-alternator assembly for lubrication and cooling, and to the electrical components for cooling.

The once-through boiler concept was selected because of its suitability for operation in zero gravity environment, and mercury was selected because of its modest vapor pressure at the elevated temperature level required in order to radiate waste energy to space. Several versions of this boiler were built and others proposed. The design on which the most operating hours were obtained is described here.

Mercury and NaK are solvents for most ordinary metals. Tantalum is resistant to mercury and to high purity NaK, but it was found impossible to maintain adequate purity level in the NaK circuit, and

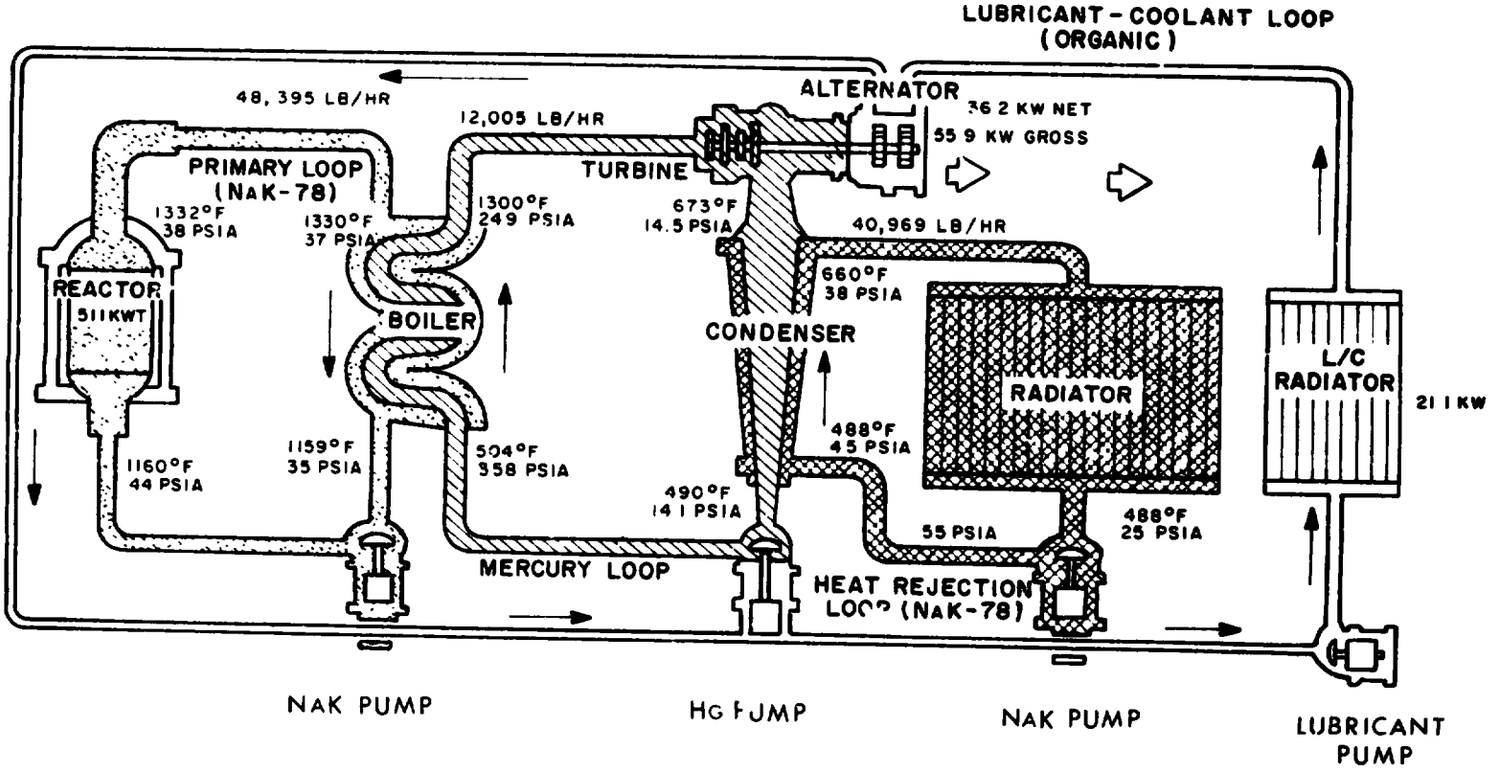

Figure 5-1. SNAP-8 system schematic diagram.

a bimetallic system, using stainless steel in contact with the flowing NaK, was required. The boiler had to be a compact, high flux design, and the uncertain contact resistance between layers of a bimetallic tube lead to the concept of two tubes, spaced apart, with the intervening space filled by stagnant purified NaK, which does not seriously attack tantalum. The outer tube was chosen to be oval, a shape which leads to the lowest average thermal resistance in the NaK layers and still allows for radial tube movement caused by differential thermal expansion when in a coiled configuration.

In order to obtain adequate heat transfer surface and flow cross section, seven tubes in parallel were used and arranged in a bundle within a NaK containment shell. The entire boiler, which was over 20 feet long, had to fit within a 60-inch diameter cylinder, so that this entire assembly was coiled. In order to make the individual tubes in the seven tube bundle of equal length, the tube bundle was twisted one full turn within the shell. The individual boiler tubes contained helically grooved plug inserts, followed by helical wire inserts. Drawings of a few of the details of this assembly are shown in Figure 5-2.

The basic method of analysis[1] was to subdivide the boiler length into a series of small increments and to write the coupling heat transfer and pressure drop relationships for each increment, choosing the relationships on the basis of an assumed phase distribution. The boiler preheat and superheat sections were subdivided by taking equal increments of vapor quality. Solution of the coupling equations at each node provided the local thermal and thermodynamic

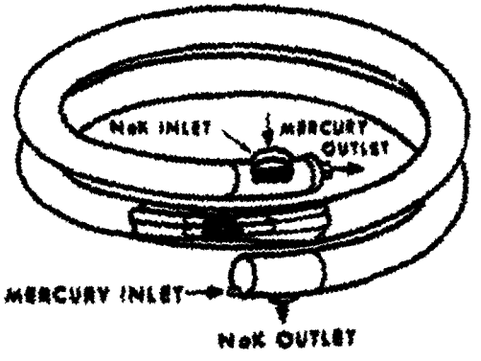

TUBE-IN-TUBE DOUBLE CONTAINMENT

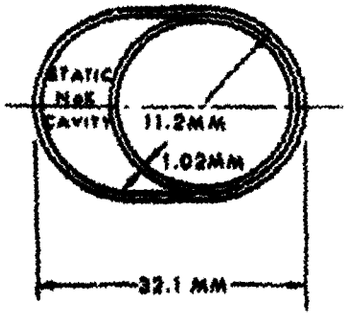

ECCENTRIC MERCURY TUBE POSITION
(DOUBLE CONTAINMENT)

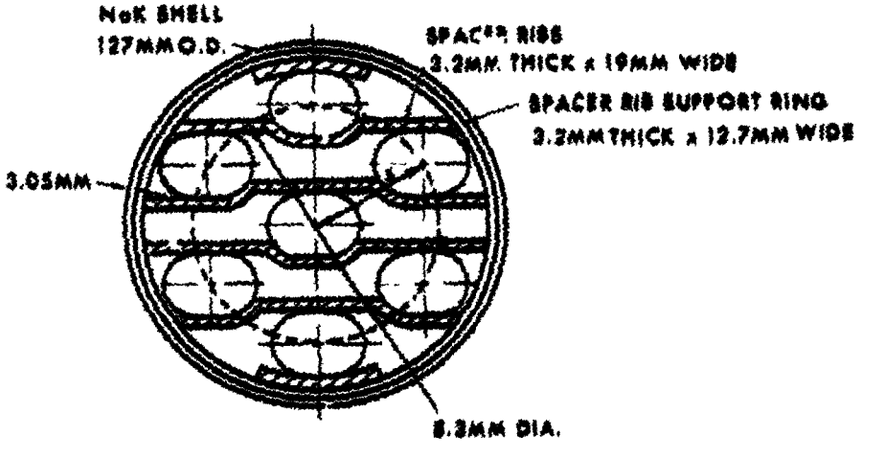

7 TUBE Te-SS CROSS-SECTION SHOWING TUBE BUNDLE SUPPORT

Figure 5-2. SNAP-8 boiler details.

conditions, and increment length. Sequential solution of the nodal equations resulted in an overall boiler performance prediction.

The vapor quality-phase distribution profile, and the location of the inserts, is shown in Figure 5-3. Each boiler tube contained a 36-inch long multigrooved insert plug, which extended from the subcooled liquid region to about 15 percent quality. This section was followed by a helical wire insert of p/D = 3.1, which extended to the end of the boiler tube. Appropriate phase distributions are referred to in Figure 5-3, together with references to the heat transfer and pressure drop relationships used in these regions.

The validity of these boiler designs was successfully supported by the test results of experimental single tube and full-scale tantalum-stainless steel boilers. Comparison of test data with design predictions is depicted in Figure 5-4. The analytical mercury temperature prediction (T_{Hg}) shows the sensible heat addition up to the preheat length termination point (ΔT_{pp}). In the two phase region, T_{Hg}) is the vapor saturation temperature, a function of the local pressure, and thereafter it represents the vapor superheat temperature. In the boiler tests, mercury temperatures were measured only at the ends, so no experimental points are found along the curve of mercury temperature. In counterflow heat exchanger-type boilers the minimum, or "pinch-point," temperature difference lies at the point of boiling inception.

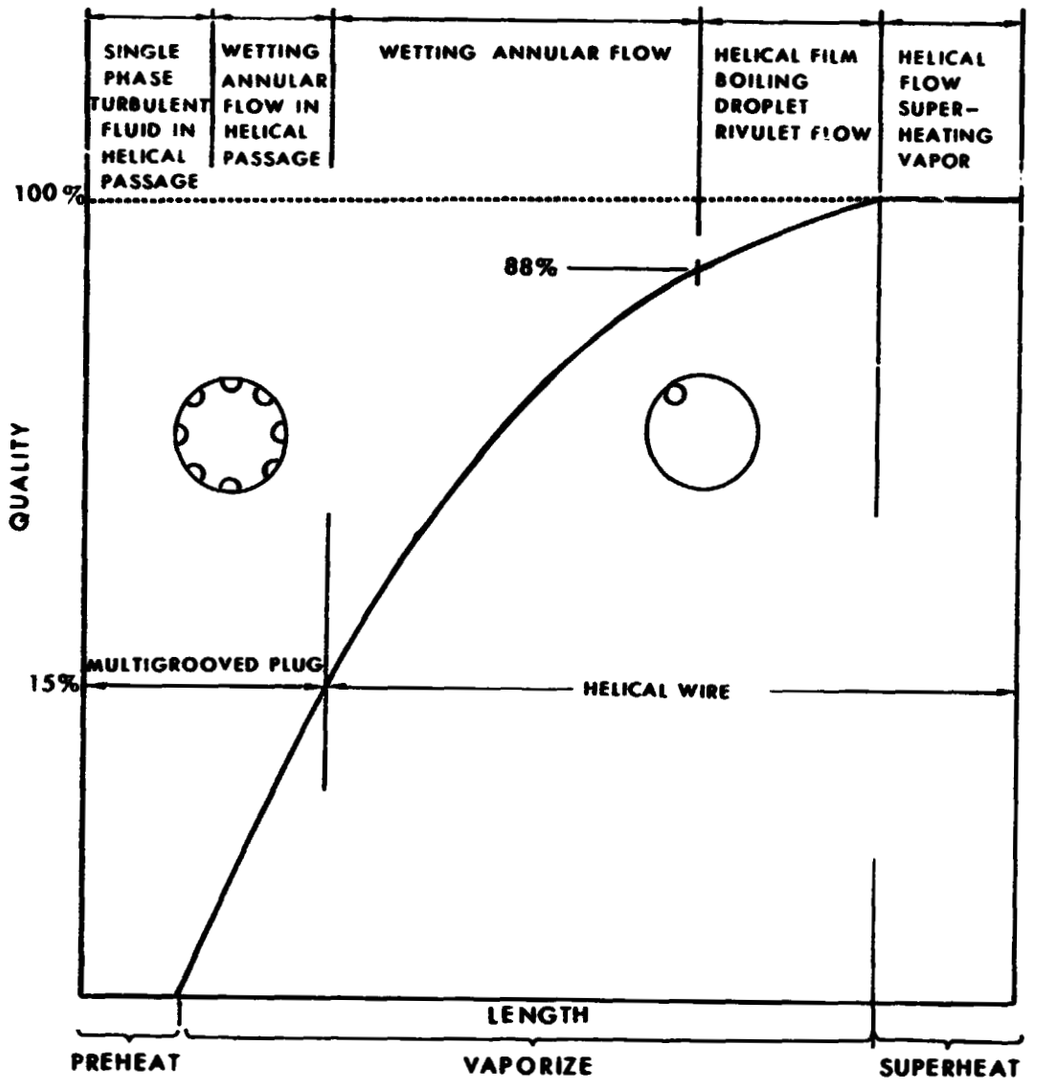

Figure 5-3. Quality versus length in mercury boiler.

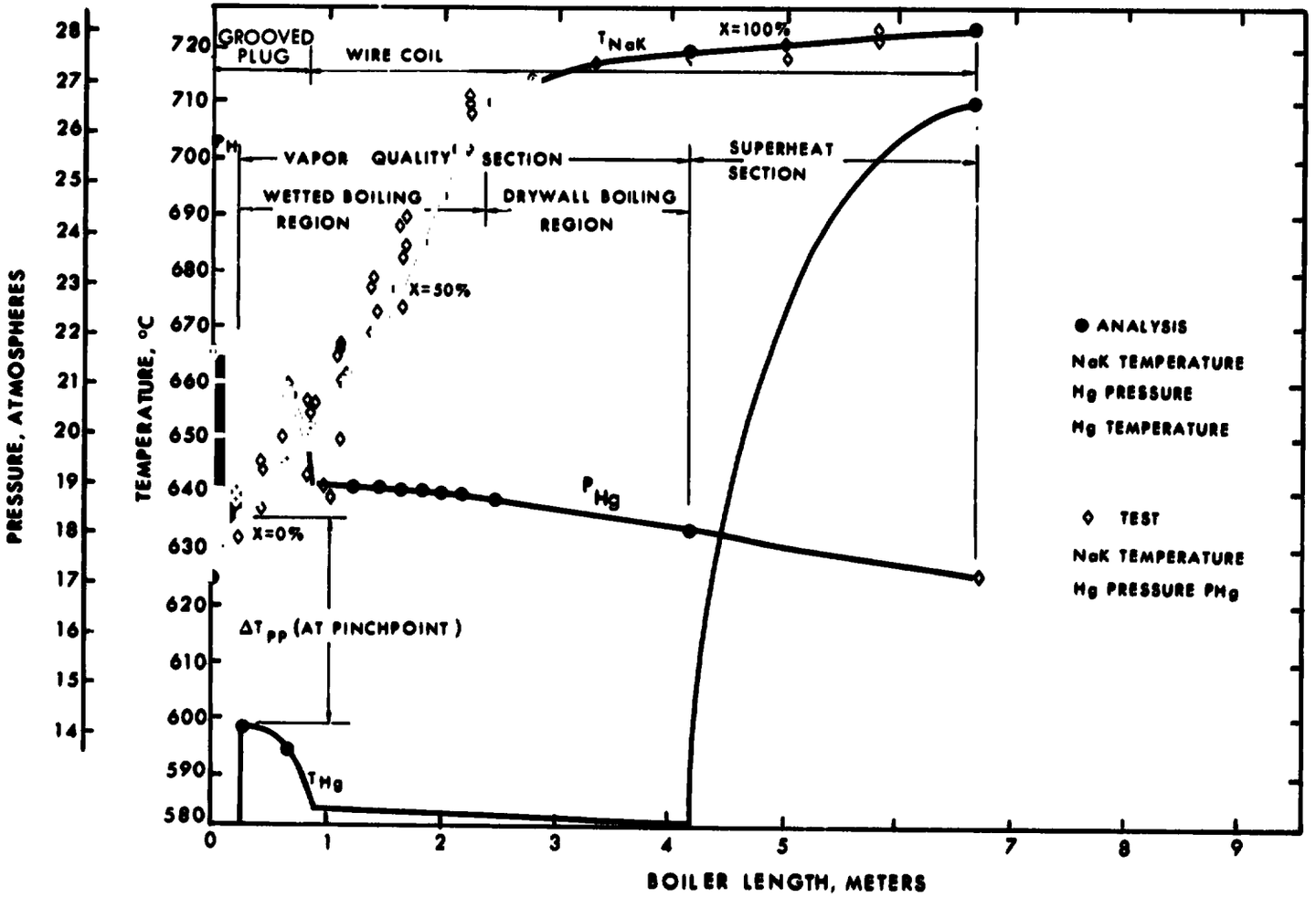

Figure 5-4. Typical SNAP-8 boiler temperature and pressure profiles.

The first series of tantalum-stainless steel boilers (denoted by BRDC Nos. 1, 2, and 3), were significantly longer than the one described in Figures 5-2, 5-3, and 5-4. These were designed with a four foot long multipassage plug insert and had an overall length of 37 feet. BRDC Boiler No. 1 was employed in system and endurance tests at a NASA facility and at a General Electric, Evendale, Ohio, test facility. A total test time of 15,125 hours and six startups were accumulated on this boiler. BRDC Boiler No. 2 was operated with a breadboard power conversion system for over 8700 hours and accumulated 27 startups. BRDC Boiler No. 3 operation in the NASA test facility resulted in 135 startups and a total test time of 157 hours. The performance characteristics of these boilers ranged from poor to excellent and were dependent on the boiler contamination state. The effects of boiler contamination ("deconditioning") were experienced primarily in combined systems testing, and were attributed to oil influx into the mercury loop and decomposition in the boiler. This was the most serious problem encountered in the boiler during combined systems operation. At the operating temperature of the SNAP-8 system, mercury wets clean tantalum and the decomposed organic coolant apparently caused the wall to dewet. A more complete discussion of the mechanisms of boiler performance degradation and their analytical interpretations are provided in Reference 2.

B. Design Example No. 2: Boiler for Potassium Rankine Space Power System

NASA Lewis Laboratory has had significant interest in space Rankine cycle power systems where the working fluid is potassium. As a result of this interest, a test facility for potassium Rankine cycle power plant development was constructed and operated by the Space Power Division of the General Electric Company.[3] The system consisted of three flow circuits interconnected by heat exchangers. These were lithium-heating, potassium-boiling, and NaK heat-rejection circuits. The lithium flowed from an electromagnetic pump through a flowmeter, a 400-kW capacity AC electrical heater which simulated a nuclear reactor, and into the shell-side of the single-tube boiler; from the exit of the boiler, the lithium was returned to the suction side of the pump for recirculation. Liquid potassium flowed from a second electromagnetic pump through a flowmeter, a liquid throttle valve, a 30-kW capacity AC electrical preheater, and into the tube side of the boiler. From the boiler, the potassium vapor entered a radiant desuperheater and vapor throttle valve which, in combination, simulated the turbine of the power plant. Expanding through the throttle valve, the vapor then flowed into a three-tube condenser, where heat was removed from the vapor and transferred to the condenser coolant, NaK. The potassium in the liquid state then returned to the potassium pump for recirculation to the boiler. The NaK coolant flowed from a third electromagnetic pump through a flow-meter and into the shell-side of the condenser. From the condenser, the NaK entered an air-cooled heat exchanger and then returned to the pump.

Both the lithium and potassium circuits were fabricated of the tantalum-based refractory alloy, T-111, and were contained in a vacuum chamber about 5.5 meters tall and 1.8 meters in diameter. This chamber was capable of extremely low pressures and was equipped with bake-out heaters and cooling coils. The NaK loop was fabricated of Type 321 stainless steel. Most of this circuit was outside of the vacuum containment.

A schematic diagram of the boiler is shown in Figure 5-5. The curved test boiler consisted of an outer and inner tube, both approximately 2.29 meters long, to which were attached appropriate fittings for welding into the liquid metal circuits. The inner tube, in which the potassium vaporized, had an inside diameter of 1.7 cm. The lithium flowed countercurrent to the potassium in the 0.45 cm annulus formed by the two tubes. Pressure gauges and thermocouple immersion wells were located near the entrances and exits of the lithium and potassium passages. The boiler tube contained a composite swirl-generating insert for enhancing the heat transfer to the potassium. The initial 1.4 meters of the insert consisted of a single helical vane wrapped about and spotwelded to a 0.635-cm-diameter hollow centerbody. The remaining 0.89-meter length of the insert consisted of a helical wire coil. The ratio of pitch to the tube-inner-diameter for the composite insert was about 3.0. The centerbody of the helical-vane portion of the insert served as an immersion well into which seven thermocouples were placed for measuring potassium fluid temperatures. Seven additional thermocouples were placed in a similar tube in the region

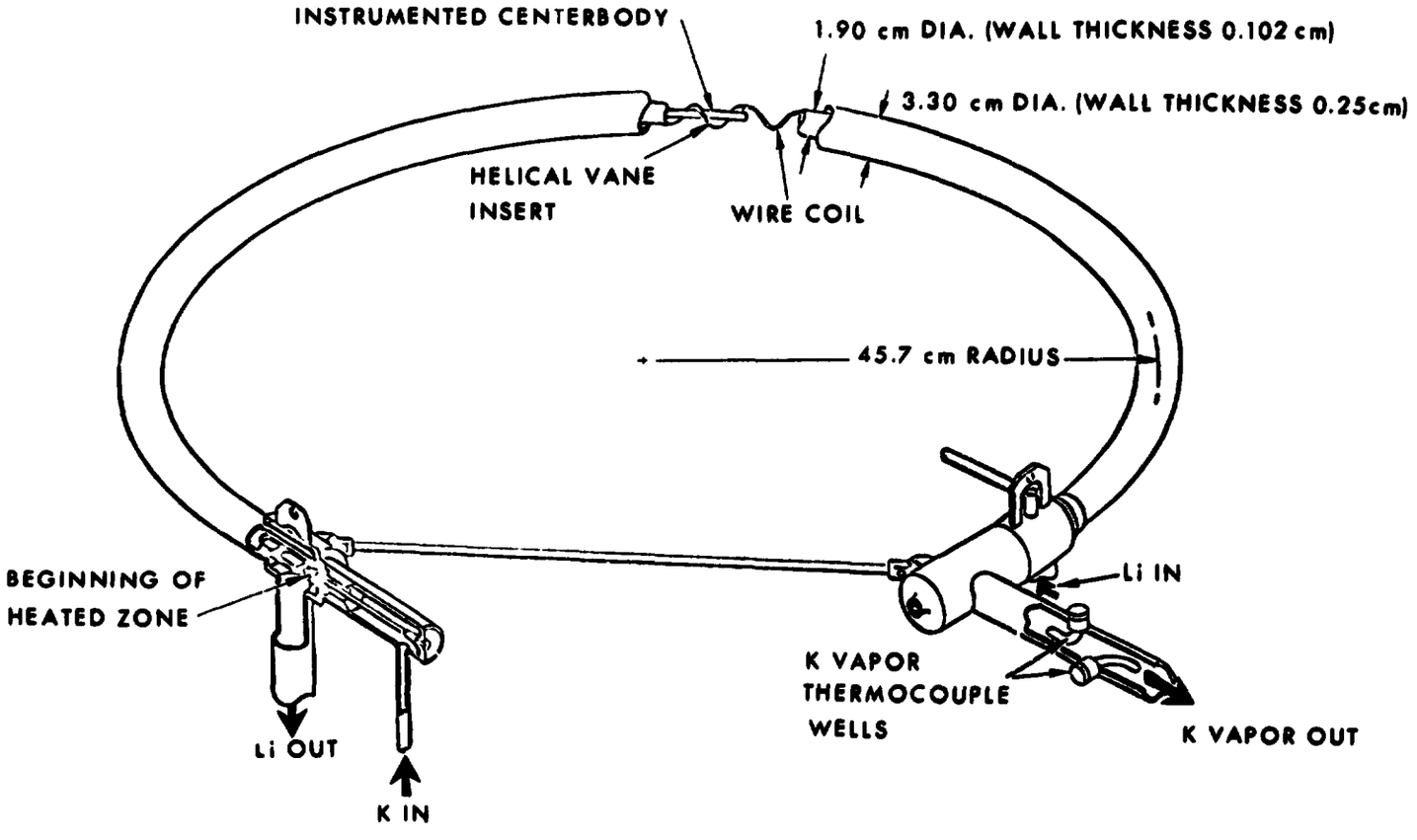

Figure 5-5. Schematic drawing of single-tube boiler.

of the boiler which contained the wire coil. The lithium temperature distribution was measured by four thermocouples distributed uniformly around the shell periphery at each of 15 axial stations.

Figure 5-6 presents experimental temperature data for this boiler, for the inlet and outlet conditions given in Table 5-I. Table 5-I also lists the inlet and outlet conditions for the boiler at the nominal design point of the advanced Rankine system. From this table, it is clear that the run shown in Figure 5-6 closely matches the nominal operating condition required for the system. From the temperature profile shown in Figure 5-6, the liquid, two-phase, and superheat regions of the potassium can readily be identified. The liquid region extends from the beginning of the heated zone to a point about 0.15-meter downstream of the inlet. Within this very short length, the potassium temperature rises from about 1040°K to the local saturation temperature of 1387°K. The two-phase region starts at the 0.15-meter point within the heated zone and extends to the 1.5-meter point. From the end of this region to the boiler exit is the superheated-vapor region.

Several phase distribution regimes would be expected in this boiler. These are: single phase liquid superheating, wetted wall annular flow, and entrained flow with a dry wall. The latter phase distribution probably extends into the net vapor superheat region where superheated vapor carrying droplets of saturated liquid exist in such proportion that the mixed mean temperature is superheated. The design relationships for flow through a helical vane and helical wire would be appropriate. In the high quality and superheat regions,

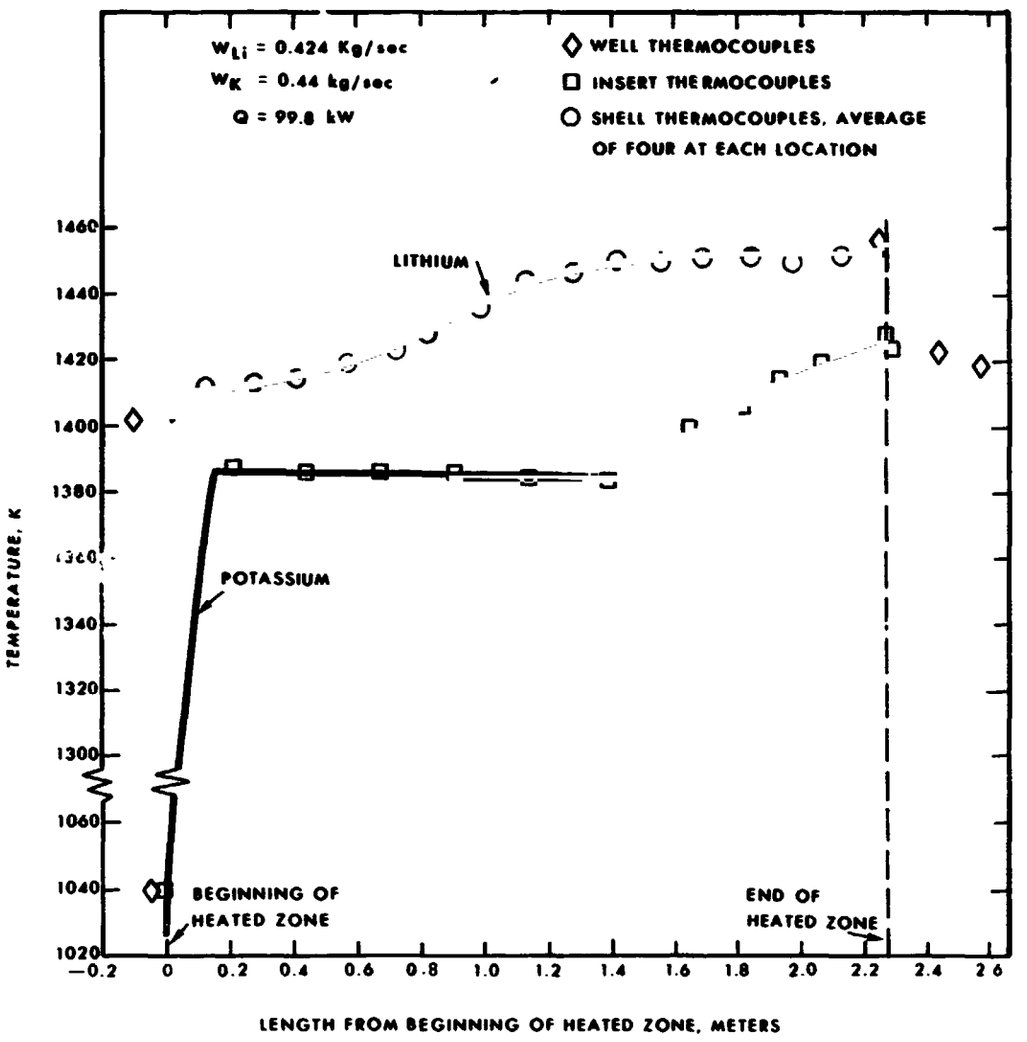

Figure 5-6. Boiler temperature distribution.

TABLE 5-I.

Comparison of Boiler Inlet and Outlet Conditions

At the Nominal Operating Point of the Potassium

Rankine System With Those for Run Shown in Figure 5-6.[3]

Parameter	Nominal Operating Point of Potassium System	Test Conditions for Run Shown in Figure 5-6.
Lithium inlet temperature, K	1477	1456
Potassium inlet temperature, K	928	1039
Potassium exit temperature, K	1422	1423
Potassium exit pressure, N/cm^2	112	109
Potassium exit superheat, K	40	47.8

the functions for helical nonwetting droplet flow would be applicable.

A plot of the pressure losses across the boiler as a function of potassium flow rate is given in Figure 5-7. These data were obtained during runs in which the potassium-exit pressure (exit saturation temperature) and the potassium-inlet temperature were held constant. The flow rate and the heat input were varied to achieve an exit quality of 1.0 and two levels of exit superheat. The pressure losses, as shown in this figure, are substantially larger for the boiler operating with a modest exit superheat. This increased pressure loss is due to the longer vapor path lengths present within the boiler tube and to large momentum pressure losses.

C. Design Example No. 3: Rankine Cycle Boiler for an Organic Working Fluid

The Army has undertaken the development of several Rankine cycle engines utilizing organic working fluids. These engines are intended as silent prime movers for electrical power generators. The boiler for one of these engines[4] is described in the following paragraphs.

Because of the low noise requirement, the combustion heat source for this boiler was of unusual design and recycled a portion of the exhaust gases into the intake. The burner was, therefore, integrated with the boiler. A typical burner/boiler module is shown in Figure 5-8.

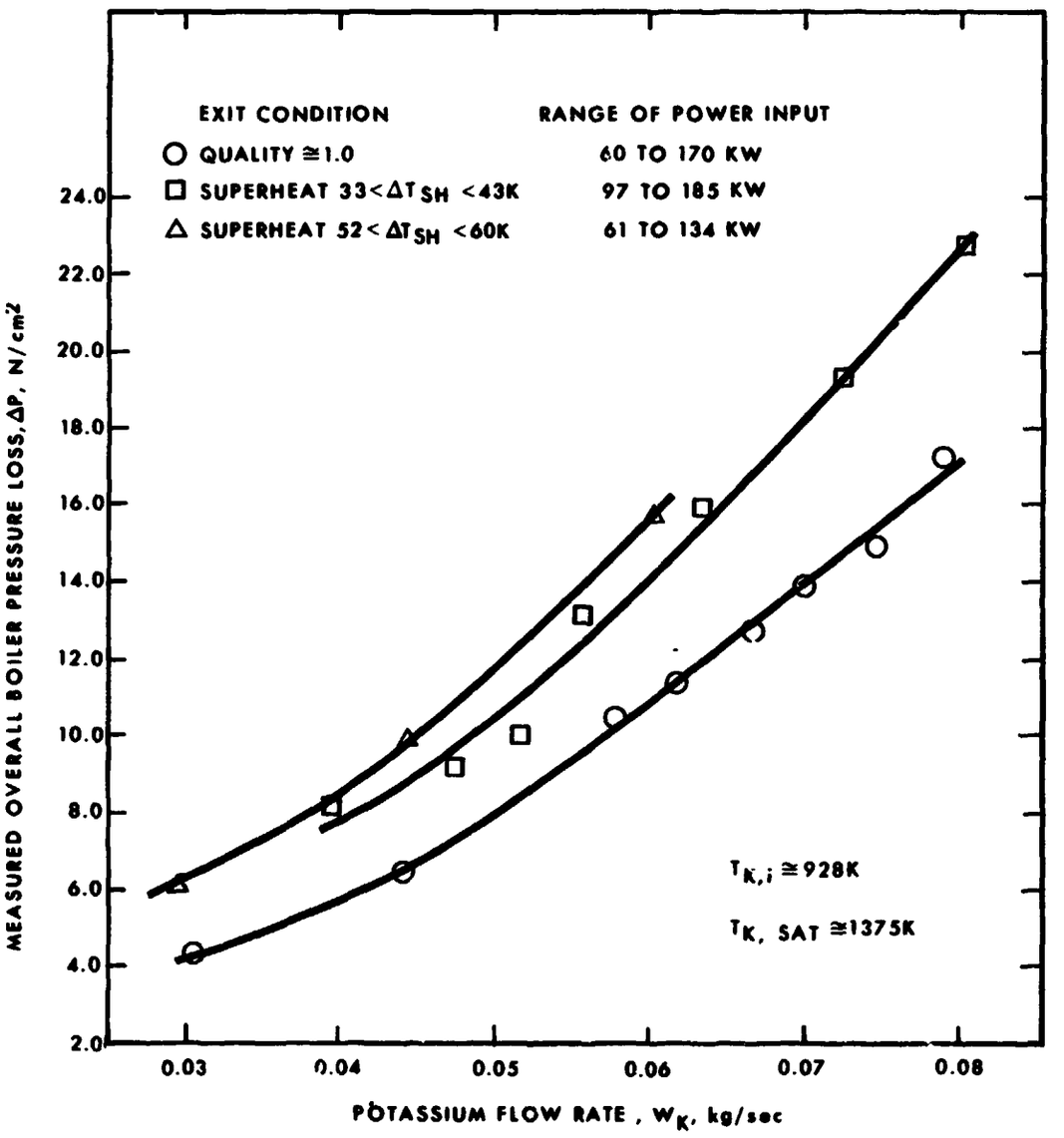

Figure 5-7. Effect of exit quality and vapor superheat on boiler overall pressure loss.

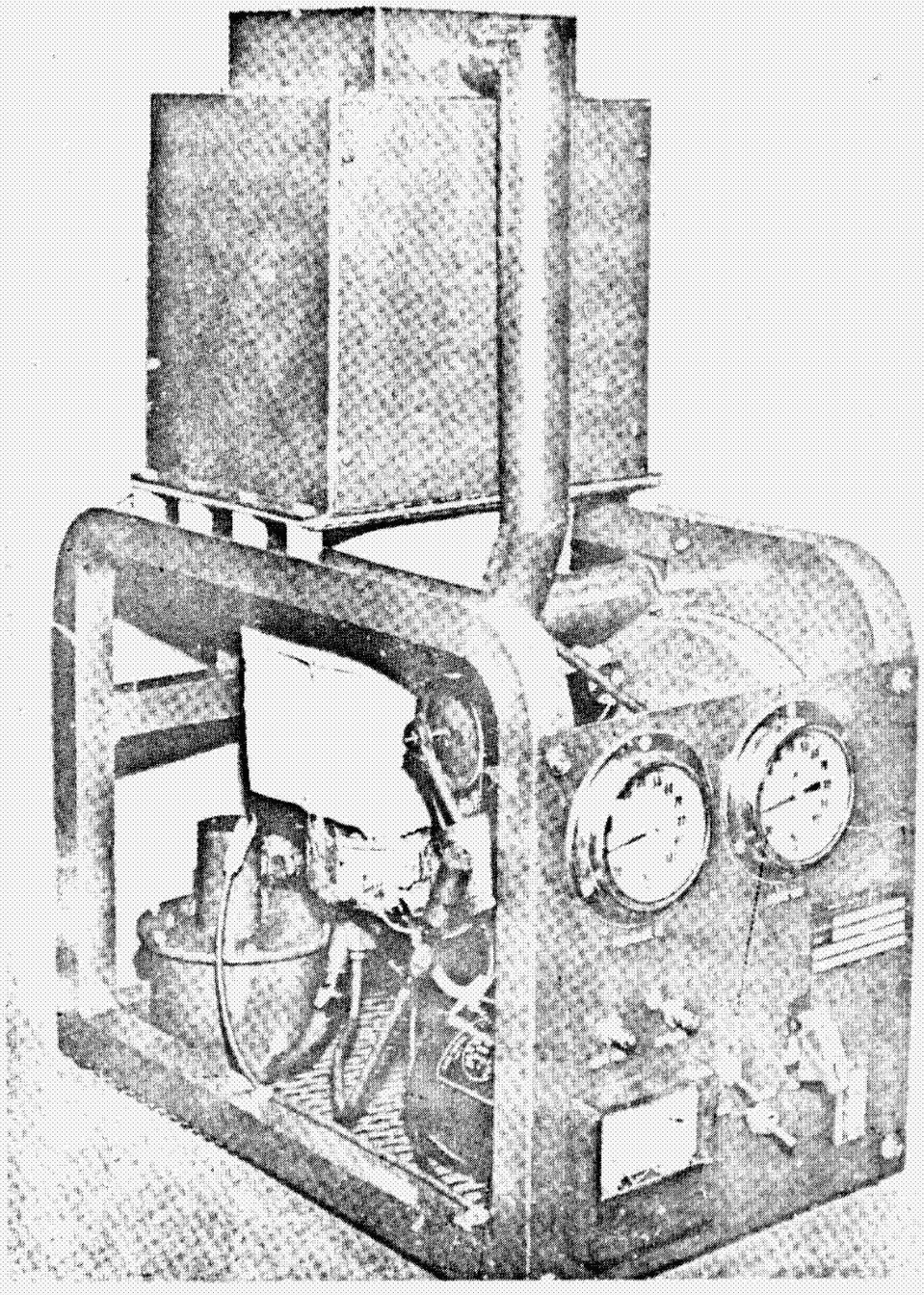

Figure 5-8. Assembled boiler/burner module.

In addition to the burner and primary heat exchanger, the unit also contained control equipment and instrumentation appropriate to this application. Figure 5-9 is a schematic diagram of the module.

The organic vapor temperature was monitored by a thermocouple probe, which operated a temperature controller. The temperature controller regulated the combustion rate (by means of the fuel pump motor speed) to maintain a constant organic vapor outlet temperature of the boiler, despite variations in organic fluid flow rate.

The heat exchanger consisted of two staggered tube arrays of stainless-steel finned stainless steel tubing. The lower of the two banks, next to the combustor, was the boiler, and the preheater was directly above it. The tube size was somewhat larger in the boiler unit to accommodate vapor flow without excessive pressure drop, and a single-tube design was used. The preheater section was a counterflow unit and the boiler was a parallel flow unit. Parallel flow was found to be desirable in limiting tube wall temperatures at the boiler exit. A drawing of this array is shown in Figure 5-10, and a photograph in Figure 5-11. The important dimensions, calculated heat transfer rates, conductances, and pressure drops are given in Table 5-II.

The organic fluid used in this unit, mono-isopropyl-biphenyl, is temperature sensitive, and it was determined that if the tube wall temperature was limited to 850°F, adequate system lifetime was attained. It may be seen from information in the table that the calculated highest temperature was on the front side of the final

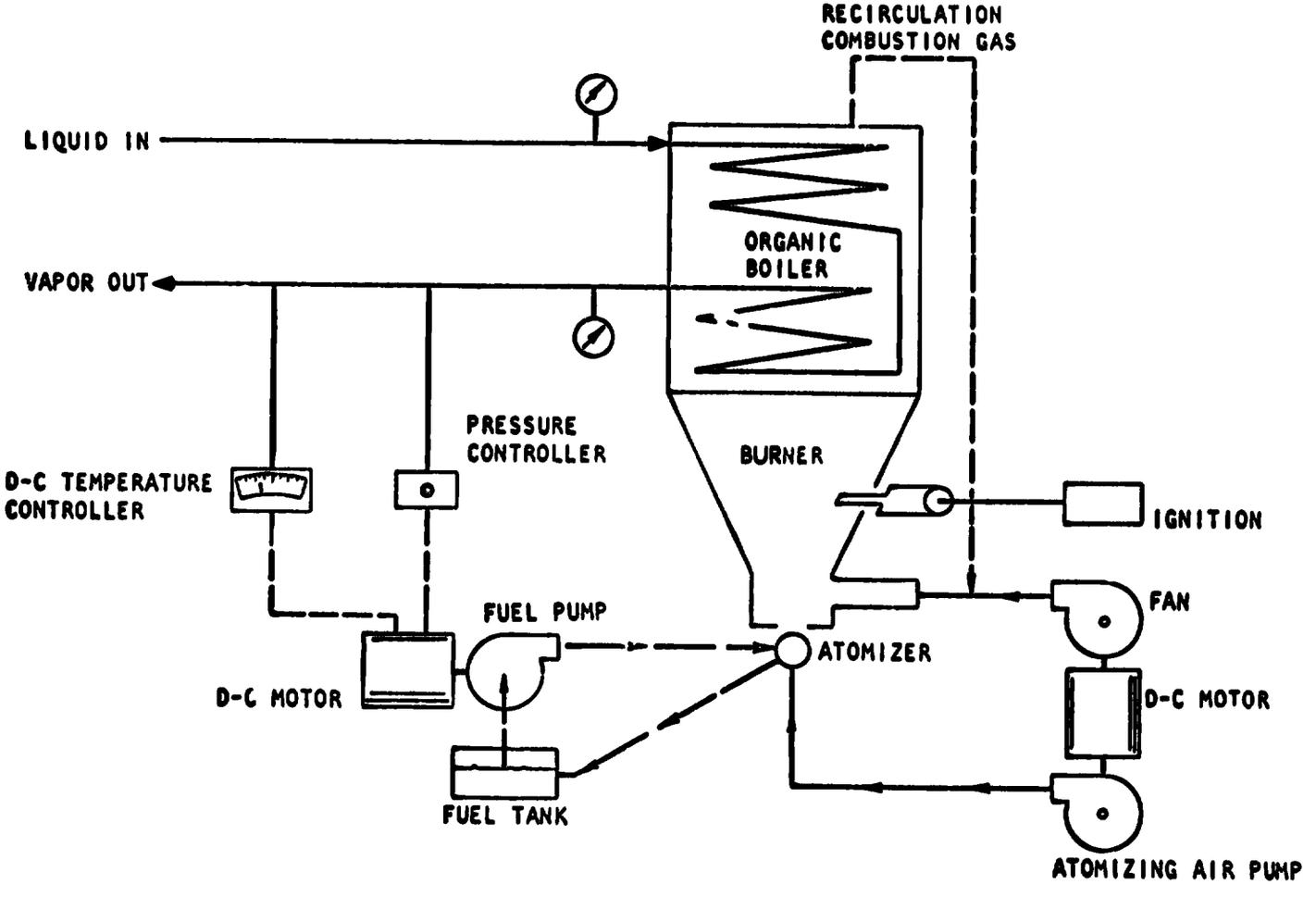

Figure 5-9. Burner/boiler functional schematic.

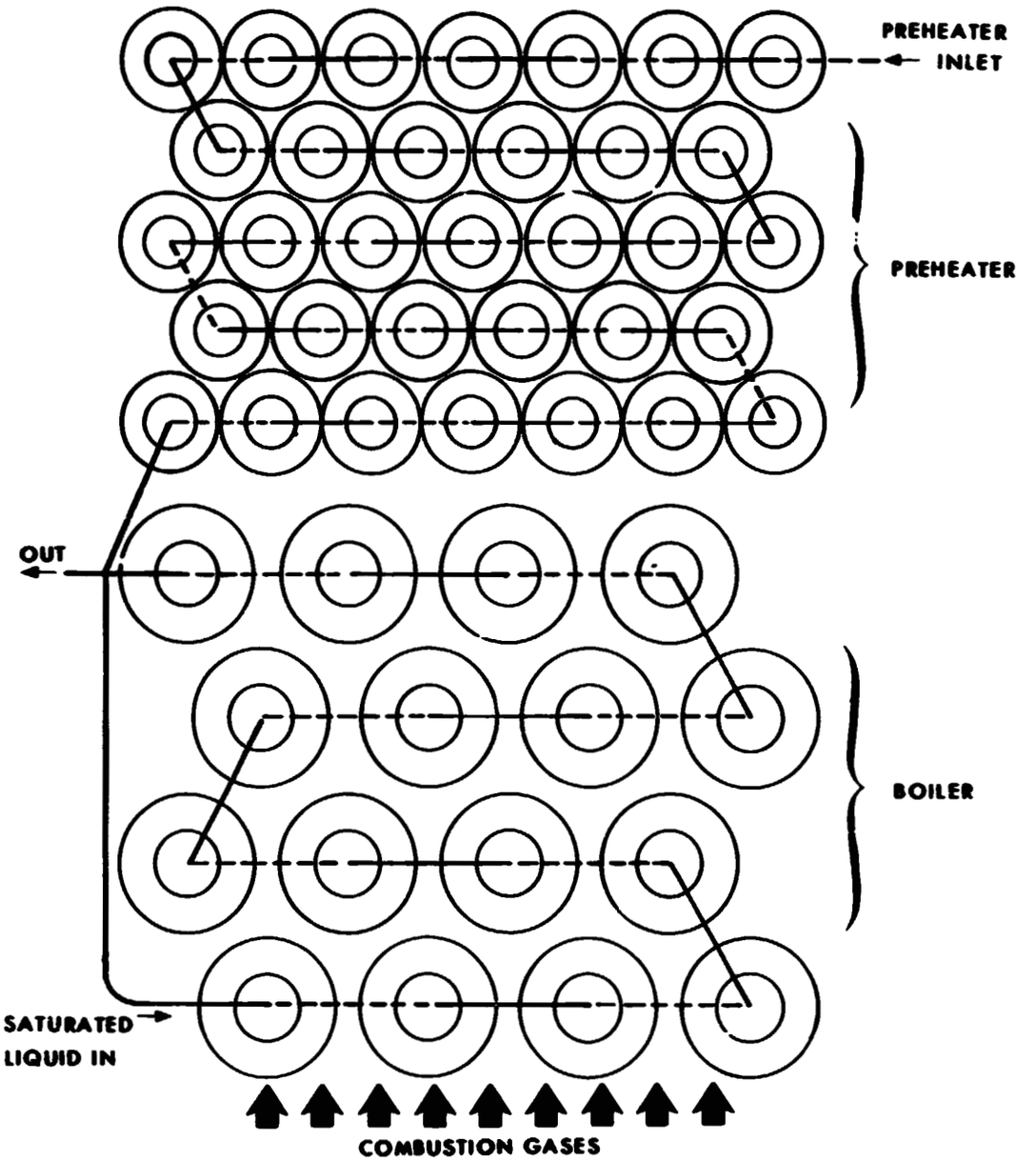

Figure 5-10. Section through organic fluid preheater vaporizer assembly.

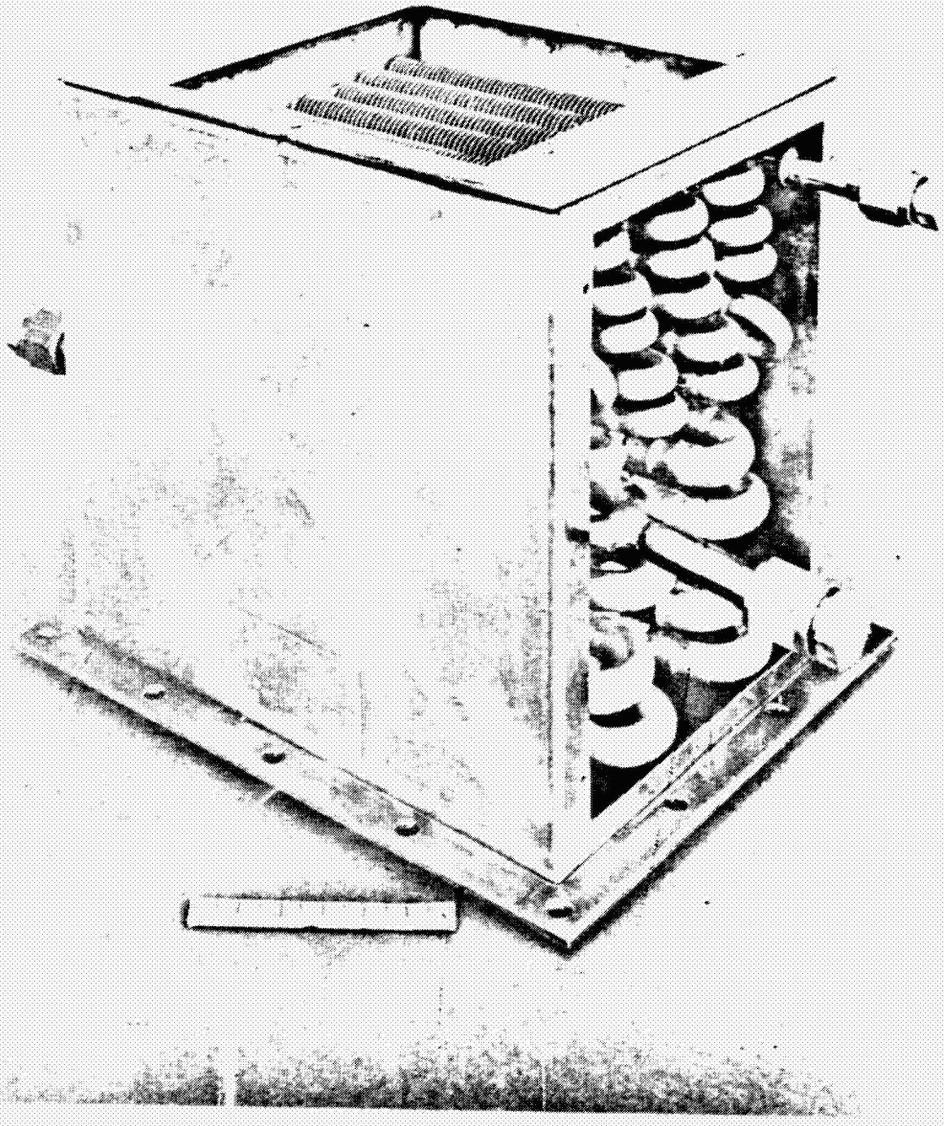

Figure 5-11. Boiler assembly.

TABLE 5-II.

CHARACTERISTICS OF ROCKETDYNE ORGANIC FLUID PREHEATER-BOILER-FINAL CONFIGURATION

Characteristics based on gas flow rate 136 lb/hr

Gas temperature	2000°F
Organic flow rate	290 lb/hr
Organic saturation temperature	700°F
Organic outlet condition	10°F superheat

A. Thermal Characteristics	Boiler	Preheater
1. Temperatures (°F)		
Organic inlet	700	568
Organic outlet	710	700
Maximum wall temperature, organic side	787 mean outlet 831 outlet front side	---
Outlet gas	1245	700
2. Temperature Differences (°F)		
Gas to organic, mean	920	340
Gas to organic, maximum	1300	545
3. Heat Fluxes (Btu/hr ft^2)		
Mean	33,300	14,700
Maximum	45,100	---
Minimum	23,200	---
4. Conductances (Btu/hr ft^2 °F) (based on inside area except as noted)		
Inside tube wall to organic, mean	1200	313
Inside tube wall to organic, minimum	266 outlet	286
Gas to organic, mean	37.9	56.7
Gas to organic minimum	34.1	55.8
Gas side to fins, mean (based on gas side area)	8.83	15.68

TABLE 5-II (continued)

	Boiler	Preheater
B. Flow Characteristics		
1. Pressure Drops		
Gas side	0.025 in/H_2O	0.112 in/H_2O
Organic side	6.5 lb/in^2	0.84 lb/in^2
Minimum gas side flow area	0.128 ft^2	0.087 ft^2
C. Dimensional Characteristics (inches except where noted)		
Tubing O.D.	1/2	3/8
Tubing wall thickness	0.020	0.016
Fin diameter	0.900	0.650
Fin thickness	0.018	0.018
Fin pitch (fins per inch)	6.5	10.5
Heated area (gas side)	4.46 ft^2	7.20 ft^2
Heated area (organic side)	0.907 ft^2	1.38 ft^2
Heated length	7.47 ft	15.4 ft
Total length	11.2 ft	23.3 ft
Number of tubes (total)	16	33
Number of rows	4	5
Arrangement	Staggered	Staggered
	4-4-4-4	7-6-7-6-7

Weight of tubing and fins	10.46 lbs
Weight of tube sheets and side panels	3.60 lbs
Weight of housing and flanges	4.024 lbs
Total weight	18.2 lbs

Material: Stainless steel. All flow passages type 347 with nicrobrazed joints.

row of tubes in the boiler. The thin walled stainless steel tubing did not conduct a significant amount of heat around the periphery of the tube, so that nonuniform heat transfer from the gas to the fin was not equalized. This local hot zone was determined to be acceptable for the application, which required only a relatively short service life. Conductances were computed for this preheater-boiler system on the basis of turbulent single phase flow for the preheater, wetting annular flow with a turbulent film in the two phase region from boiling inception to 85 percent quality, single phase flow vapor heating with a variable flow rate to 100 percent quality, and single phase flow of the vapor in the very short superheat region.

The computed local two phase pressure gradient is shown in Figure 5-12, together with the gradient as predicted by the Martinelli correlation.

Operating experience with this unit indicated that its performance was quite close to the design calculations.[4]

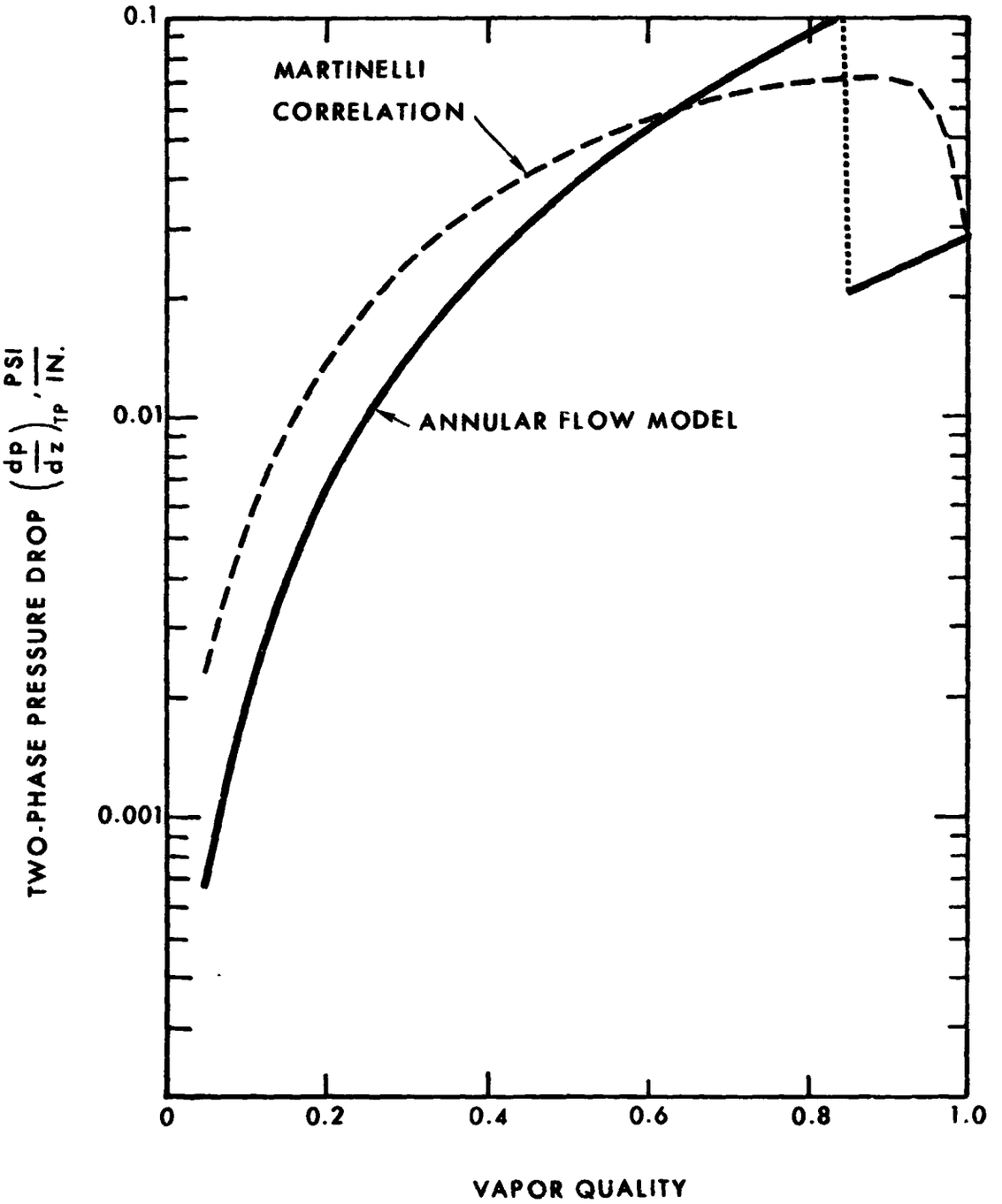

Figure 5-12. Two-phase flow pressure gradient in organic boiler.

D. Design Example No. 4: A Liquid Hydrogen Boiler

A small liquid hydrogen vaporizer using a flow of liquid hydrogen as the heat source was designed and constructed for a special application. The arrangement employed was a counterflow heat exchanger, with vaporization taking place in a central tube surrounded by an annular passage containing the hot side fluid. The general requirements for this boiler are given in Table 5-III.

TABLE 5-III.

General Characteristics of Hydrogen Boiler

	Cold Side	Hot Side
Flow rate	0.44 gm/sec	150 gm/sec
Inlet temperature	17.2 °K	20.8
Outlet temperature	20°K	20.7
Inlet pressure	0.34 atm	1.16 atm
Pressure drop	0.027	0.0027 atm

The heat flows required to accomplish this performance are 200 watts in the boiling section, and 13 watts in the superheater.

It may be shown by means of standard heat exchanger calculations,* that the specified conditions require an overall conductance-heat transfer area product for the vaporization section of UA = 47.1 watts/°C, and for the superheat section of UA = 6.0 watts/°C.

Liquid hydrogen is a low surface tension fluid which wets metal surfaces readily. For the small overall temperature differences in this application, no possibility of film boiling existed. The phase distributions expected were turbulent liquid preheating, annular flow throughout most of the vaporization region, and dry vapor in the superheater. Because of the very small vapor velocities and heat flows, no entrainment was expected, so that the wetted wall condition would extend all the way to 100 percent quality. Round 0.81 cm inside diameter tubing was chosen for the boiler tube.

The hot side duct was an annular passage with an equivalent diameter of 2.5 cm. In Table 5-IV are presented the principal calculated performance data for this unit.

---

*See, for example, Reference 5.

TABLE 5-IV.

Computed Performance of Hydrogen Vaporizer

Vaporization in annular flow at 70 percent quality		
Void fraction	0.87	
Liquid film thickness	0.25 min	
Heat transfer conductance:		
Based on turbulent film, no nucleation		23.9 watts/cm^2 °C
Based on laminar film, no nucleation		3.7 watts/cm^2 °C
Liquid preheating:		
Heat transfer conductance (turbulent flow, Re = 4400)		2.6 watts/cm^2 °C
Superheating of vapor:		
Outlet vapor conductance (turbulent flow, Re = 54,000)		2.0 watts/cm^2 °C
Outlet vapor velocity		2380 cm/sec
Integrated two phase pressure drop, for annular flow	0.012 atm	
Hot side conductance (turbulent flow, Re = 455,000)	31.1 watts/cm^2 °C	

It is rather difficult to test a heat exchanger under the conditions specified for this design. The temperature differences and flows are very small, and accurate measurements of liquid hydrogen flows are not simply made. Therefore, a proof test of this unit was made using Freon 11 (another wetting fluid) as the vaporizing flow, and warm water as the hot side fluid. It was possible to perform these heat exchanger tests with very large water flows, so that the mean vaporization side conductances could be extracted from the data. Results of these tests with a Freon 11 flow and temperature differences chosen to match inlet Reynolds number and heat flow, yielded a mean vaporizing conductance of 29.6 watts/cm^2 °C. The predicted mean vaporizing conductance for Freon, utilizing the model of a turbulent annular film without nucleation, was 26.1 watts/cm^2 °C.

E. Design Example No. 5: Rankine Cycle Automobile Engine Vapor Generator

The design techniques discussed in Chapters 3 and 4 are also being used to design vapor generators for "steam" automobiles now under development. The working fluids for these engines include several very specialized organic fluids and organic fluid mixtures, and water.

This section is divided into two parts, which are;

1. A general discussion of automobile vapor generator design considerations, and
2. A specific example.

1. Rankine Cycle Automobile Vapor Generator Considerations

Some of the considerations which the vapor generator designer working on this application must take into account are itemized below:

(a) The timelag from an increase in water flow to an increase in steam flow must be short, in order that the vehicle can respond rapidly to changes in power demand. There must be no significant energy storage in a boiler for this application so that water flow, steam flow, and heat input (combustor output level) must match closely, even during rapid transients. Some modern designs use several parallel paths in the two phase and superheater portions of the vapor generator to

minimize transit time in this region. The multitube design shortens response time but can introduce flow instabilities. The Doble steam automobiles, which were manufactured commercially for many years, used a monotube boiler with a great length of tubing and a long flow transit time. These boilers employed a "normalizer" system to more closely match steam conditions with steam demand than would have been possible with water input to the preheater only. The normalizer was a second water input near the inlet to the superheater which introduced water to trim superheater output conditions. This water flow, being much closer in both distance and time to the expander inlet, provided the necessary fast response. This system is also used in the steam powered bus constructed by Brobeck Associates for the State of California.

(b) The heat fluxes in the vaporizing and superheating sections must be chosen so that tube wall temperatures are well controlled. For example, it has been shown in Chapter 4 that a large change in boiling side heat transfer conductance occurs when the wall is no longer wetted by the working fluid, and the vapor quality at which this occurs depends upon a number of complex interrelationships in geometry, flow rate, and fluid properties. Although an automotive

steam generator must be a high average heat flux design for compactness, the transition cited above and all the regions downstream must be in a low flux region to prevent tube failure.

(c) Stored energy and liquid holdup in the boiler must be small to prevent serious accidents in the case of tube rupture or vehicle collision, and also to minimize start up time. Fuel economy on short runs can be seriously affected by energy required to bring the boiler to operating temperature.

(d) Lubricants finding their way into the boiler must not be decomposed on the heat transfer walls to form thermally insulating or nonwetting layers. A typical historical solution to this problem has been to limit wall temperatures to levels which the lubricants can tolerate. Other solutions proposed to keep oils from the boiler include oil separators at the boiler inlet, and dry lubricants, or self-lubricating surfaces in the expander and pump.

2. A Specific Automotive Vapor Generator Example

A Rankine cycle automotive engine vapor generator for an engine of approximately 100 bhp is described in the following paragraphs.

As was commented on in item (b), heat fluxes must be controlled to prevent tube wall overheating. In many modern designs, the technique for accomplishing this is to place the vaporizer closest to the combustor, with the low quality vaporization region in cross-parallel flow, then introduce the superheater into the hot gas stream, operated cross counterflow, follow with a few rows of high quality vaporizer section (sometimes called the "dryout region"), and place the liquid preheater farthest from the combustor. Such a flow path is shown in Figure 5-13. The example design presented here approaches the problem of heat flux control in a different manner, specifically, by employing tubing coating where necessary with a thermal insulator. Thermally resistive coatings have been utilized in portions of organic boilers presently in service to protect the working fluid, so the general technique has been tested successfully. The adoption of such a system for the example water vaporizer allows the use of a simple counterflow design. The flow path and typical conditions are shown in Figure 5-14. Table 5-V presents some salient characteristics of this design.

It may be seen that with a superheater of two channels, that the maximum wall temperature is in the order of 632°C. If, for strength and corrosion resistance, the outlet wall temperature were to be limited to 593°C (for example), some thermal insulation would be required at the superheater outlet. This could take the

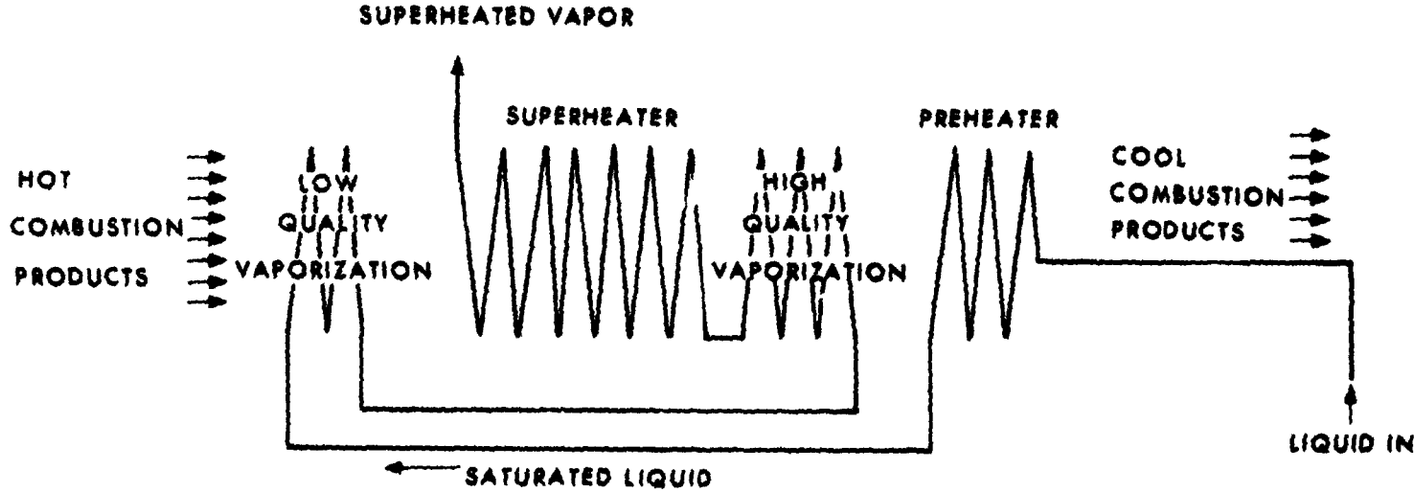

Figure 5-13. Flow path in typical modern automotive forced convection vapor generator.

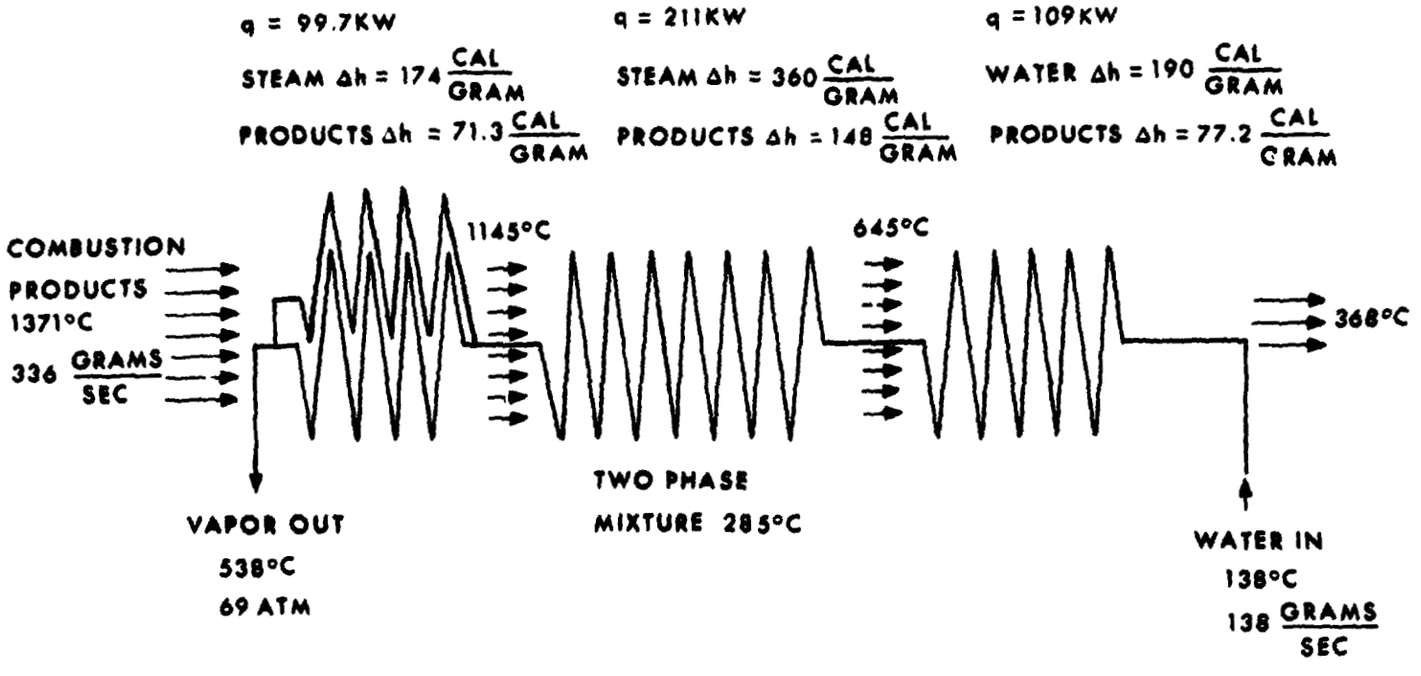

Figure 5-14. Flow path and stream conditions in example boiler.

TABLE 5-V

Combustor heat rate	0.525×10^6 watts
Steam heat rate	0.42×10^6 watts
Thermal efficiency	80 percent

Characteristic	Superheater	Vaporizer	Preheater
Heat transfer effectiveness	0.208	0.581	0.518
Arrangement	multipass cross counterflow	multipass cross counterflow	multipass cross counterflow
Stream capacity rate ratio $\frac{C_{min}}{C_{max}}$	0.75	0	0.62
Conductance-heat transfer area product UA watts/°C	51.6	280	274
Gas side conductance watts/cm^2 °C	0.0169	0.0159	0.0159
Water side conductance watts/cm^2 °C	0.133	variable with location	1.42
Overall conductance (without insulation) watts/cm^2 °C	0.0153	0.0142	0.0156
Maximum temperature difference °C	816	843	343
Heat flux watts/cm^2	16.4	15.6	7.2
Wall temperature C	632	393	289
Tube diameter (bare) mm	19.1	19.1	12.7
Tube spacing transverse mm	23.9	23.9	16.0
Tube spacing longitudinal mm	23.9	23.9	16.0
Number of parallel channels	2	1	1

form of a ceramic coating, or a metal foil wrap spaced from the tube by dimpling, or some other simple device. Inspection of the wall temperatures row by row would be necessary for this arrangement, particularly under off design or transient conditions.

This design, utilizing a single vaporization path and two parallel superheater paths, is not particularly compact. A significant saving in tube length can be realized in the cooler portions of the assembly by use of finned tubing, rather than the close-spaced bare tubing of the example.

This application is interesting in that the gas side conductance controls the heat flux and the boiling conductance variations do not affect the design. Only the superheated vapor conductance needs to be computed accurately. This is not the case for the geometry in which the vaporization takes place in the tubes next to the combustor. For that case, boiling conductance heat fluxes and wall temperatures must be evaluated carefully to prevent tube overheating.

CONCLUDING REMARKS

It has been shown that the heat transfer and pressure drop functions presented in Chapters 3 and 4 have been used successfully to design boilers whose measured performance characteristics are in satisfactory agreement with predicted values.

Results of the NASA SNAP-8 mercury boiler program have shown that if the mercury is kept free of foreign materials such as oxygen and organics and if optimized designs (based on helical flow) are used, mercury boilers with good heat transfer and fluid flow performance characteristics can be built and successfully used in industry. It has also been demonstrated in NASA's potassium Rankine cycle program that efficient potassium boilers can be designed, fabricated and operated. In addition, working fluid purity levels required have been established. These high temperature boilers can be used to extend the thermodynamic efficiency beyond that attainable with mercury.

The major limitation in organic boilers is the degradation of these fluids at elevated temperatures. When an organic working fluid is exposed to high temperature levels, the chemical composition of the fluid changes and the degree depends upon container metal, time, as well as temperature levels. The boiler designer must consider these processes and the system thermal efficiency to determine how they influence the overall economics involved.

The major reason for the development of a Rankine cycle automobile engine is that the external combustion process can be optimized to reduce generation of the pollutants formed in an internal combustion engine. The Environmental Protection Agency, the State of California, and several industrial organizations are constructing Rankine cycle automotive engines using a variety of working fluids.

REFERENCES

1. Sellers, A. J.; "Thermal Design of the SNAP-8 Tantalum Stainless Steel Boiler," NASA CR-72760, June 1971.

2. Poppendiek, H. F.; "SNAP-8 Boiler Performance Degradation and Two-Phase Flow Heat and Momentum Transfer Models," Geoscience Ltd GLR-84, NASA CR 72759, Aug 1970.

3. Gutstein, M. U.: Bond, J. A.; "Preliminary Results of Testing a Single-Tube Potassium Boiler for the Advanced Rankine System," NASA TM X-52996.

4. Hagel, J. A.; Baughman, J. R.; "Burner/Boiler Module Final Technical Report," Rocketdyne Rep R-7740, for USAMERDC Contract DAAK02-68-C-0574.

5. Kays, William; London, A. L.; "Compact Heat Exchangers," Second Edition, McGraw-Hill Book Co., 1964.

CHAPTER 6: BOILER APPLICATIONS

Five example boiler designs were presented in Chapter 5 to illustrate how the design functions and transition criteria presented in Chapters 3 and 4 can be utilized. These examples also illustrate some applications of forced flow and once-through boilers to technologies other than space technology. It is possible to envision additional boiler requirements and applications, some of which are summarized in the following paragraphs.

A. Mobile Propulsion Systems

An example of a forced flow boiler application to future mobile propulsion systems (namely, the automotive steam car) was noted in the previous chapter. Interest has been developed in this system because the external combustion process associated with it appears to have excellent potential for reducing combustion gas emissions. It is believed that mobile power plants which utilize forced flow boilers could also be used in trains, trucks, and buses. In such systems, high specific power densities and good operating performance characteristics can be achieved.

B. Topping Cycles for Power Plants

The concept of using a topping cycle in a power plant to increase the overall thermodynamic efficiency is an old one. However, this

approach is now more appealing because the technology of high temperature, low pressure working fluids (such as the liquid metals) has now been developed in addition to the forced flow and once through boiler concept. Potassium is of particular interest because it has high temperature capabilities, has good thermal properties, and its cost is not excessive.

C. Bottoming Cycles for Power Plants

It is thought that there may be some advantages in including a low temperature Rankine cycle system in a power plant to utilize some of the associated waste heat. There are a number of organic working fluids whose thermal properties are sufficiently good and whose decomposition rates are negligible at low temperatures so that such bottoming cycles may modestly increase overall power plant efficiencies.

D. Auxiliary Power Plants

As new land areas throughout the world are developed (particularly in remote regions where it is difficult and expensive to route electric power lines), it will probably be important to construct auxiliary power plants whose heat source may be either nuclear or fossil fuel types. In order to keep the capital costs for such systems to a minimum, the designers will clearly desire to have compact systems; optimized boilers would be of particular importance.

E. Advanced Refrigeration System

In order to reduce the fuel and energy requirements for large refrigeration systems, more advanced refrigeration systems will be required. Most modern refrigeration system evaporators operate on a semi-forced flow basis in that the boiling process is more accurately defined by a natural convection type requiring large volumes. It is believed that more efficient and compact evaporators, based on forced flow boiling, may help in obtaining increased system efficiency and reduced component sizes.

F. Boiling Nuclear Reactors

Nuclear reactor designers have considered the advantages of systems that contain boiling working fluids. Boiling water reactors have, of course, already been built and are in operation. It is felt that the use of forced helical flow boiling in such nuclear reactor cores will not only yield high power density systems but reduce the possibilities of slug flow thereby increasing fluid flow and reactor stability.

G. Solar Evaporation Boilers

There is a great interest in utilizing solar energy as a prime source because of the national objective of conserving fossil fuels. One type of conversion process involves the evaporation of a working fluid, which is then used in a Rankine cycle system. In such a concept, forced flow boiling again would have a significant advantage.

H. Geothermal Power Systems

The government has identified our geothermal heat sources as having great energy value. Hot fluids pumped through fractured geothermal strata would change phase at points of pressure reduction near the surface of the earth where wet steam would be transferred to some type of expander or turbine. In order to prevent mechanical erosion by the wet steam, a high vapor quality boiler and superheater would have to be interposed between the geothermal steam source and the prime mover. Again, forced flow boiling in this component would be used.

I. Process Heat Exchangers Involving Change of Phase

The process industry utilizes a variety of evaporative heat exchangers and many different working fluids. The forced convection boiling technology presented here can be applied to such heat exchangers to provide better temperature control (by preventing hot spot regions) and to reduce capital costs (by optimizing size and pumping power requirements).

APPENDIX A: THERMAL PROPERTIES OF SOME OF THE IMPORTANT WORKING FLUIDS

Figures A-1 through A-7 contain thermal conductivity, specific heat, viscosity, density, Prandtl number, vapor pressure and surface tension data as functions of temperature level for some of the important working fluids in the liquid and saturated vapor states. These data are presented for the convenience of the boiler designer.

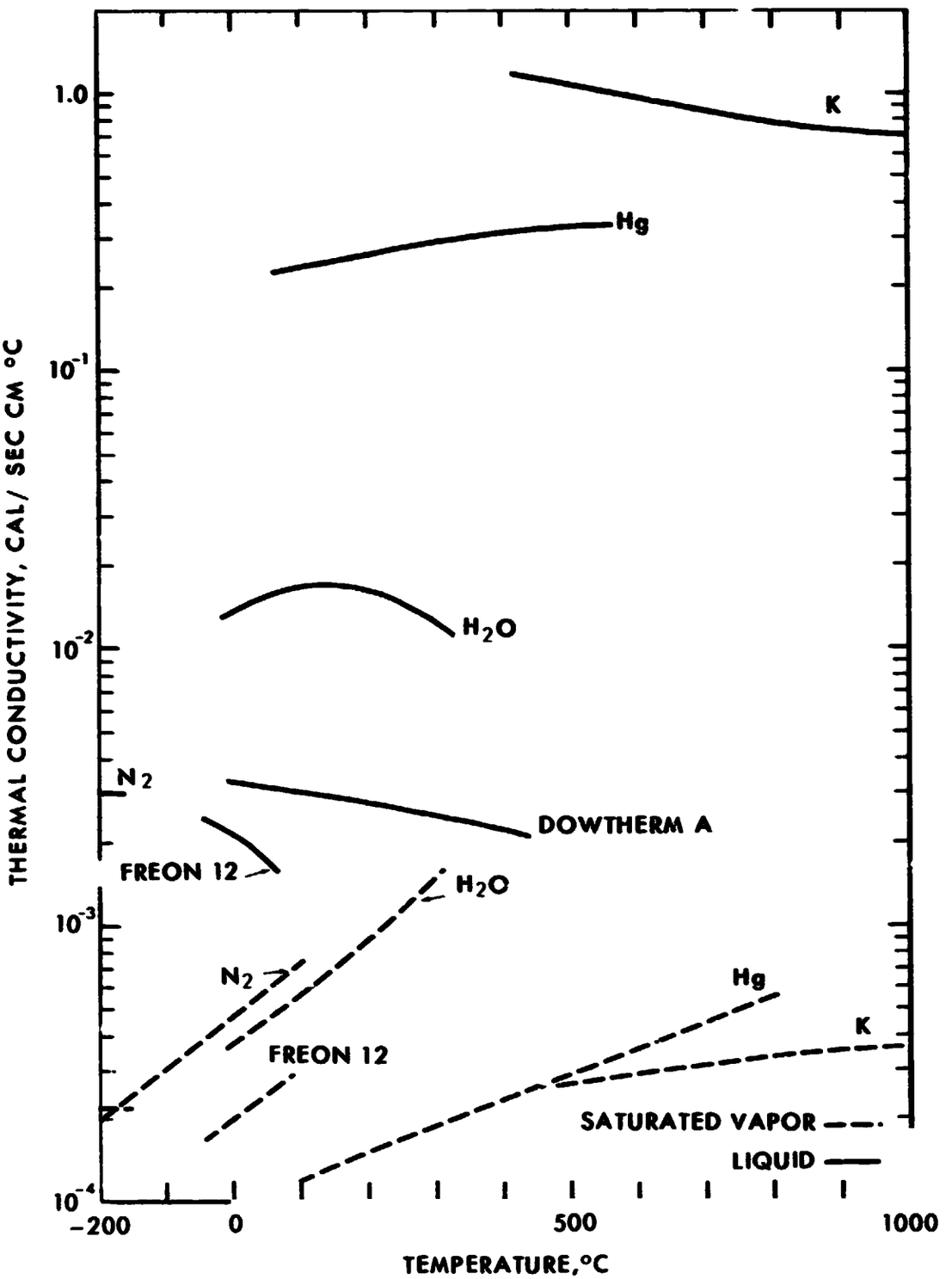
THERMAL CONDUCTIVITY, CAL/ SEC CM °C
1.0
10^{-1}
10^{-2}
10^{-3}
10^{-4}
K
Hg
H_2O
N_2
DOWTHERM A
FREON 12
H_2O
N_2
FREON 12
Hg
K
SATURATED VAPOR
LIQUID
-200
0
500
1000
TEMPERATURE,°C

Figure A-1.

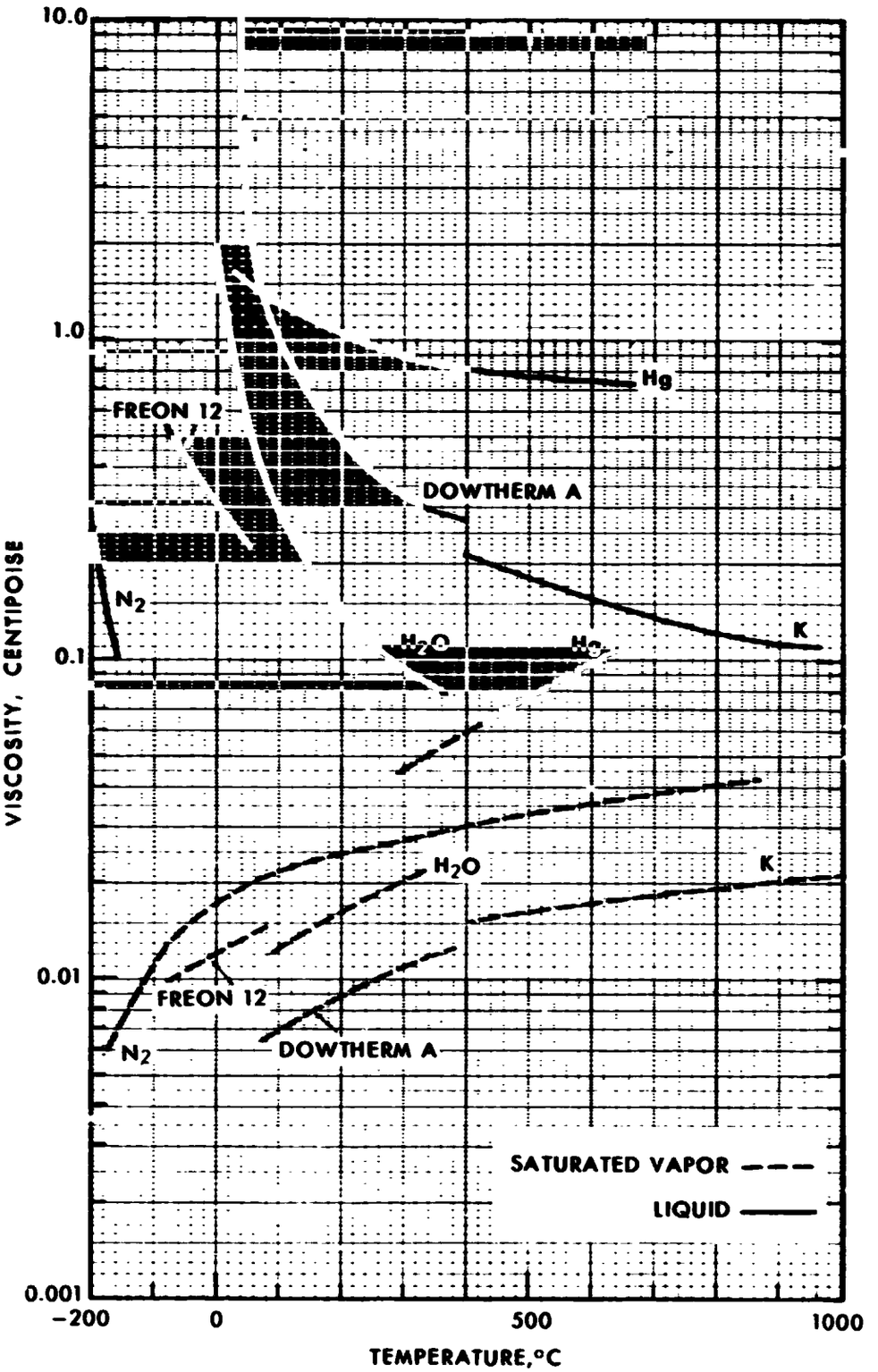
10.0
1.0
0.1
0.01
0.001
VISCOSITY, CENTIPOISE
Hg
FREON 12
DOWTHERM A
N_2
H_2O
K
H_2O
K
FREON 12
N_2
DOWTHERM A
SATURATED VAPOR
LIQUID
−200
0
500
1000
TEMPERATURE,°C

Figure A-2.

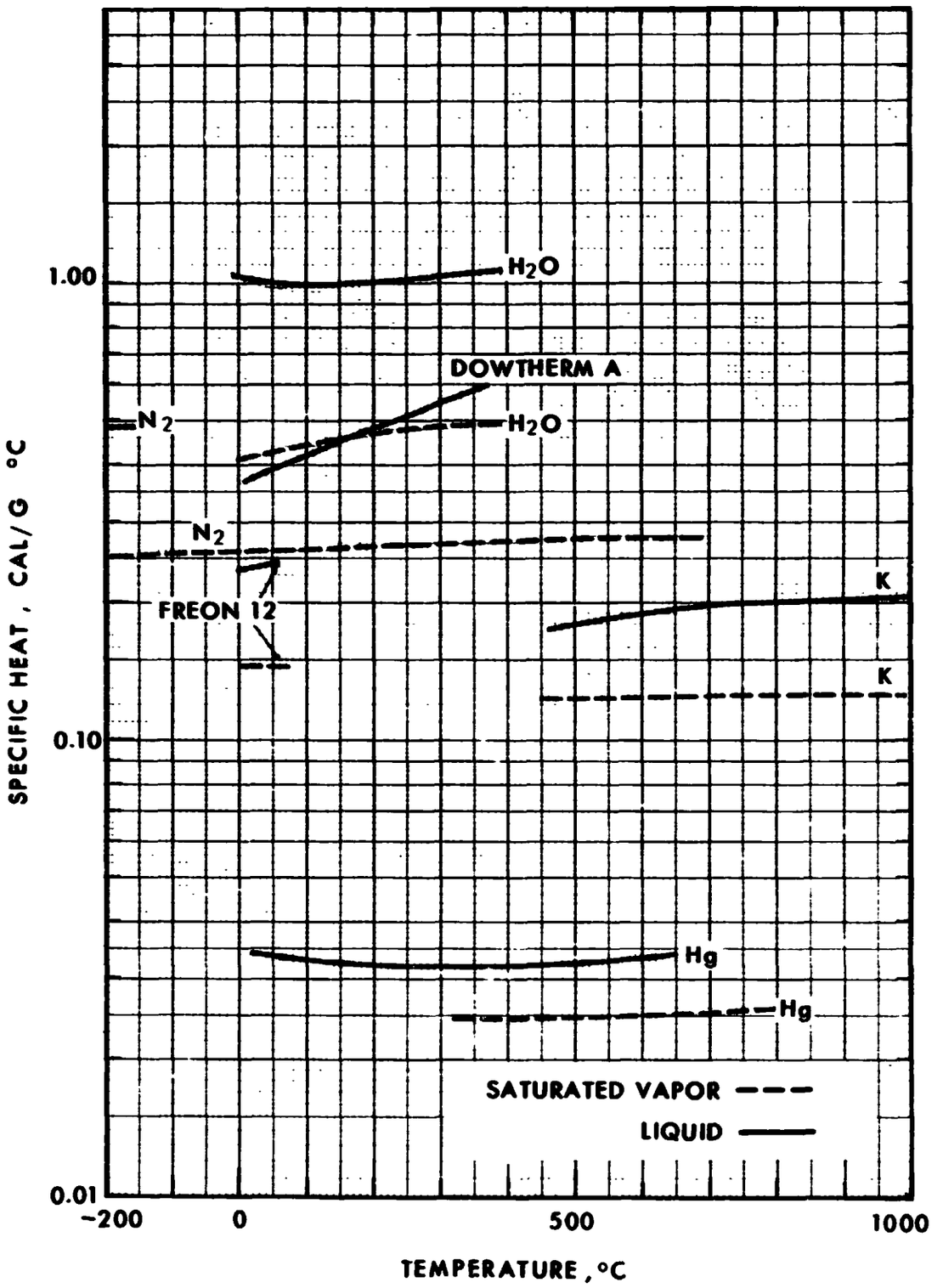
1.00
0.10
0.01
SPECIFIC HEAT , CAL/G °C
H_2O
DOWTHERM A
N_2
H_2O
N_2
FREON 12
K
K
Hg
Hg
SATURATED VAPOR
LIQUID
-200
0
500
1000
TEMPERATURE , °C

Figure A-3.

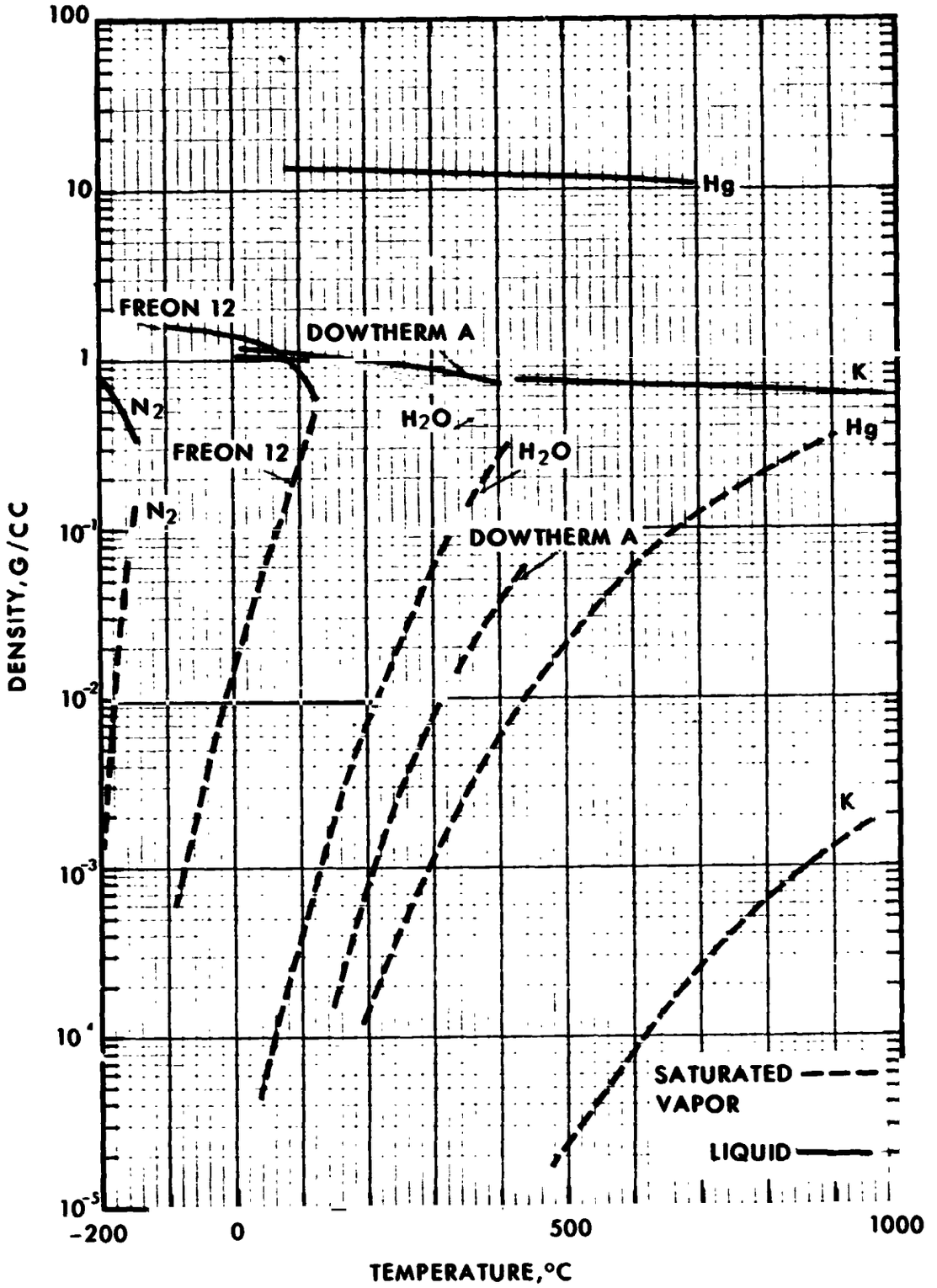
100
10
1
10^{-1}
10^{-2}
10^{-3}
10^{-4}
10^{-5}
DENSITY, G/CC
Hg
FREON 12
DOWTHERM A
K
N_2
H_2O
FREON 12
H_2O
Hg
N_2
DOWTHERM A
K
SATURATED VAPOR
LIQUID
-200
0
500
1000
TEMPERATURE, °C

Figure A-4.

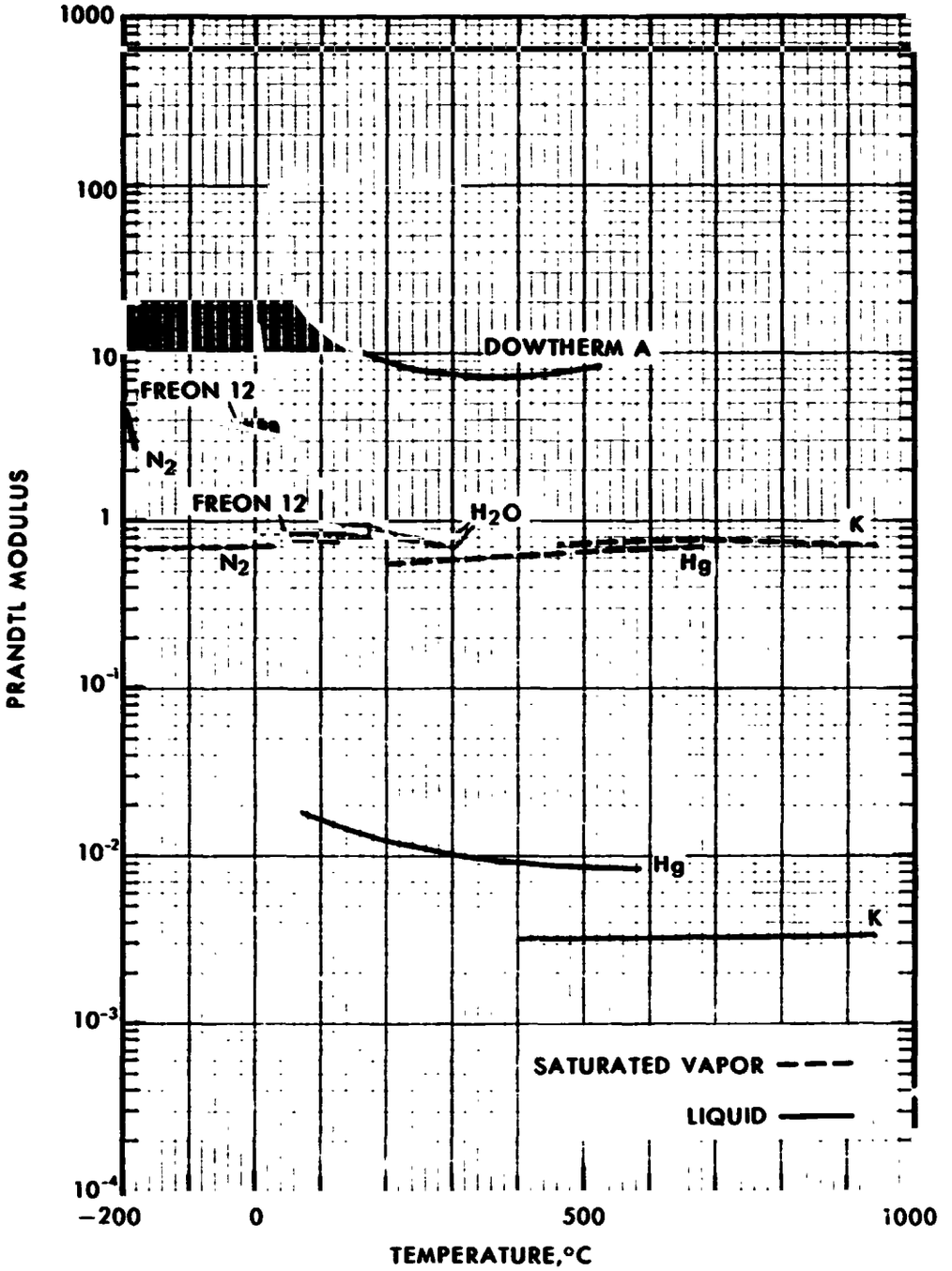
1000
100
10
1
10^{-1}
10^{-2}
10^{-3}
10^{-4}
PRANDTL MODULUS
DOWTHERM A
FREON 12
N_2
FREON 12
H_2O
K
N_2
Hg
Hg
K
SATURATED VAPOR
LIQUID
−200
0
500
1000
TEMPERATURE,°C

Figure A-5.

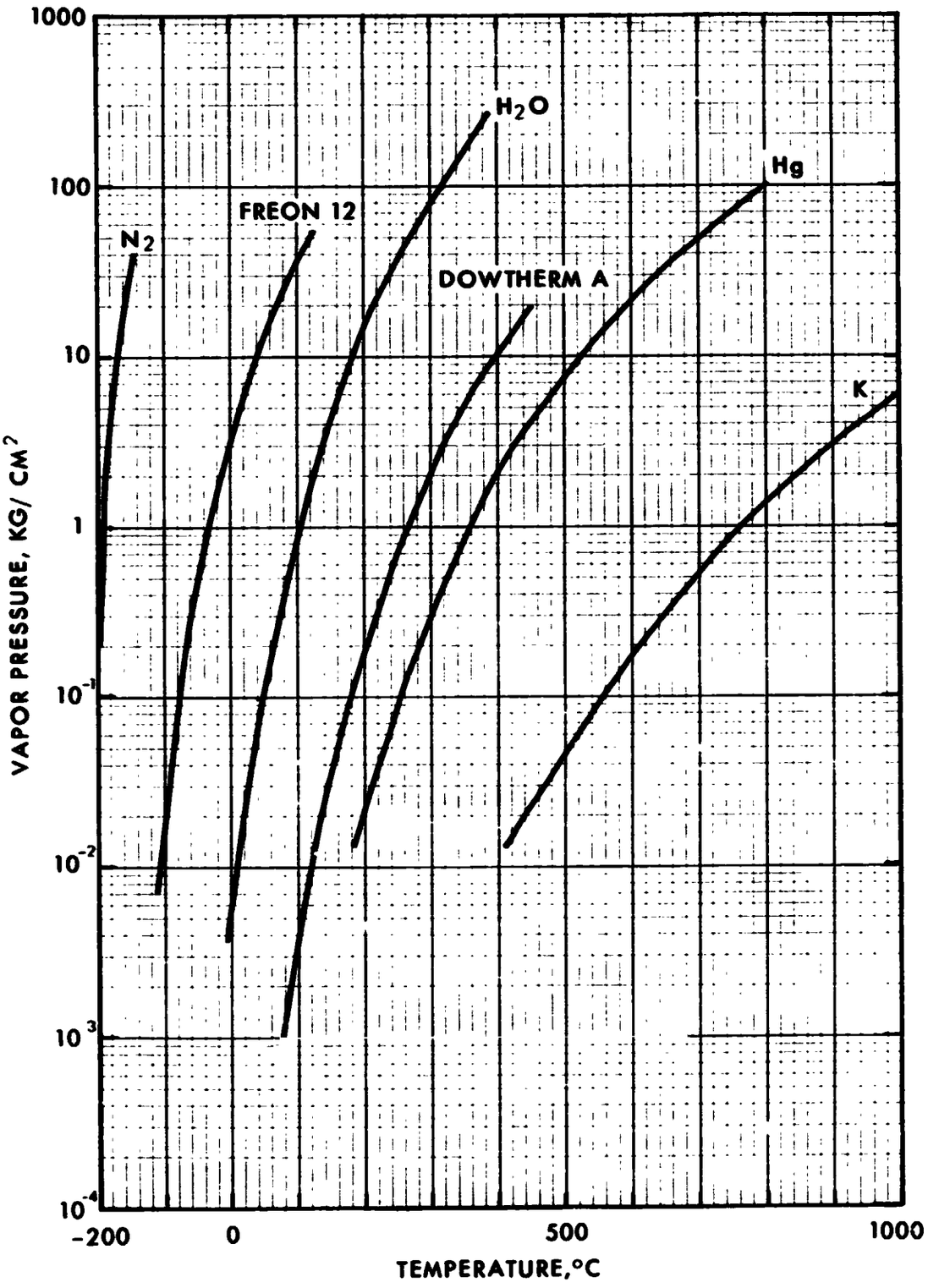
1000
100
10
1
10^{-1}
10^{-2}
10^{-3}
10^{-4}
VAPOR PRESSURE, KG/ CM^2
H_2O
Hg
FREON 12
N_2
DOWTHERM A
K
-200
0
500
1000
TEMPERATURE,°C

Figure A-6.

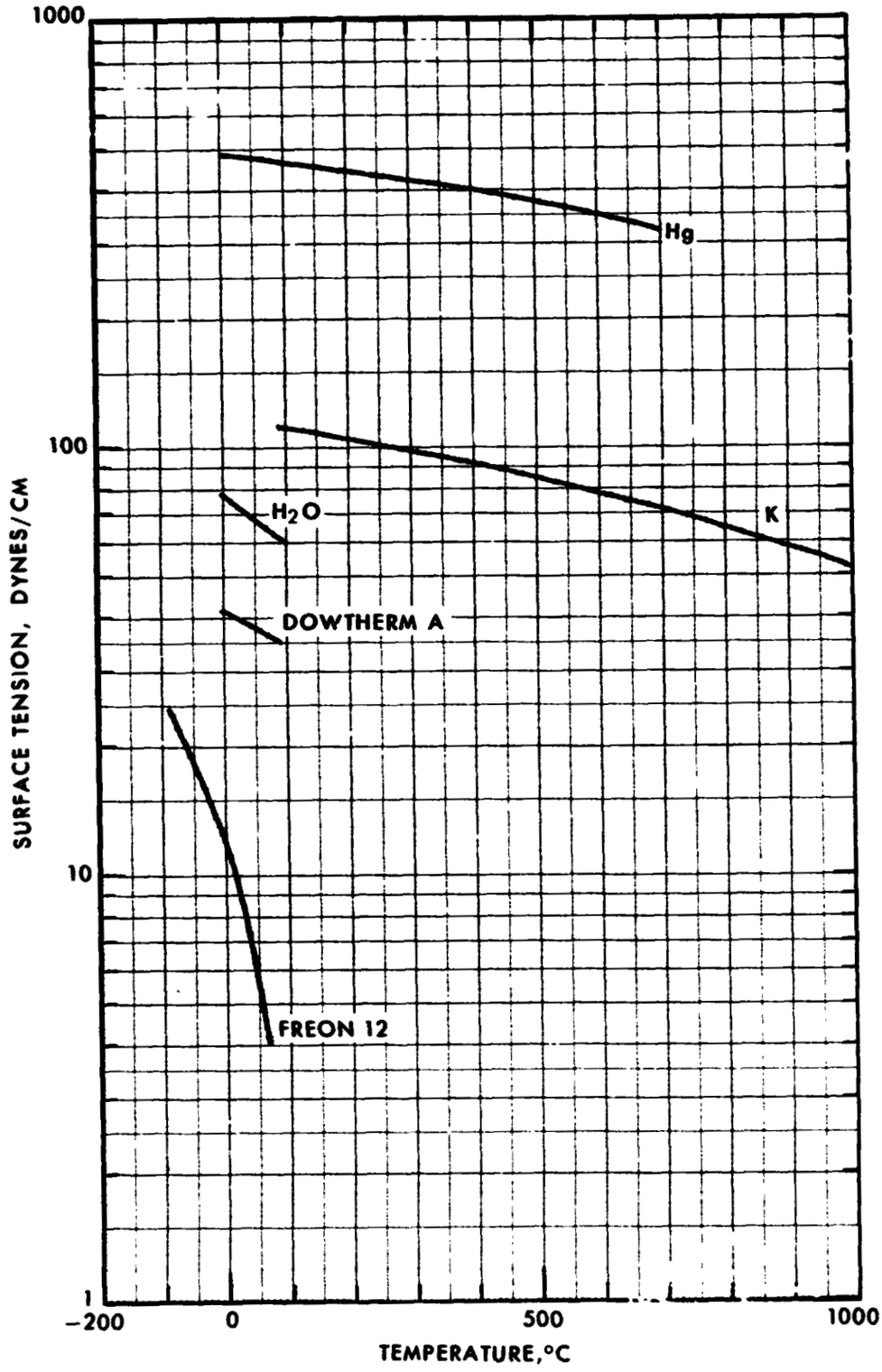
1000
100
10
1
SURFACE TENSION, DYNES/CM
Hg
K
H_2O
DOWTHERM A
FREON 12
−200
0
500
1000
TEMPERATURE, °C

Figure A-7.

APPENDIX B:

EQUATION SETS FOR CHAPTER 3

The experimental semi-empirical and analytical information presented in the figures in Chapter 3 are defined by functions that represent the heat transfer and pressure drop design functions in this monograph. These functions are presented in this Appendix in the form of equation sets that are numbered in conformance with the figures in Chapter 3.

Equation Set 3-1:

$$\zeta = \frac{64}{Re}, \text{ analytical and experimental}$$

$$\zeta = \frac{0.023}{Re^{0.2}}, \text{ experimental}$$

Equation Set 3-2:

Turbulent single phase

$$Nu = 0.023\, Re^{0.8}\, Pr^{0.4}, \text{ experimental and semi-empirical}$$

Equation Set 3-3:

Turbulent single phase

$$Nu = 7 + 0.025\ Pe^{0.8}, \text{ analytical}$$

$$Nu = 0.625\ Pr^{0.4}, \text{ experimental and semi-empirical}$$

Equation Set 3-4:

Turbulent single phase (analytical)

$$Nu = \frac{\gamma \sqrt{\frac{\zeta}{8}}\ \frac{\Delta T_c}{\Delta T_m}\ Re\ Pr}{5\left[\gamma Pr + \ln(1 + 5\gamma Pr) + 0.5\ F_o \ln \frac{Re}{60}\sqrt{\frac{\zeta}{8}}\right]}$$

F_o = A function of γ, Pr, Re, and ζ.

Equation Set 3-6:

Nonwetting slug flow

$$\frac{\Delta p_{TP}}{\Delta p\ (x = 1)} = \frac{\rho_v}{\rho_\ell}\left[\frac{1}{x^2_{exit}} + \frac{\left(\frac{\rho_\ell}{\rho_v} - 1\right)}{2\ x_{exit}}\right], \text{ analytical}$$

Equation Set 3-8:

Nonwetting slug flow

Laminar flow

$$H = \left[\frac{k_\ell}{k_v} - 1\right]\left[\frac{1 - x}{1 + \left(\frac{\rho_\ell}{\rho_v} - 1\right)x}\right] + 1 \quad \text{, analytical}$$

Turbulent flow

$$H = \frac{190\, k_\ell}{k_v \left[Re_v\,(x = 1)\right]^{0.8} Pr_v^{0.4}} \left[\frac{1 - x}{1 + \left(\frac{\rho_\ell}{\rho_v} - 1\right)x}\right]$$

$$+ x^{0.8} \left[1 - \frac{1 - x}{1 + \left(\frac{\rho_\ell}{\rho_v} - 1\right)x}\right] \quad \text{, analytical}$$

Equation Set 3-9:

Wetting slug flow

$$\alpha = \frac{u_v}{1.2\,(u_\ell + u_v) + 0.35\sqrt{gD}} \quad \text{, analytical}$$

Equation Set 3-10:

Upward annular flow, analytical

$$\alpha = \left(\frac{r_i}{r_o}\right)^2$$

$$\frac{8\pi}{\zeta}\left(\frac{r_o \mu_v}{w_v}\right)\left(\frac{w_\ell \mu_\ell \rho_v}{w_v \mu_v \rho_\ell}\right)\left(\frac{r_i}{r_o}\right)^5 - \frac{1}{4}\left(\frac{r_i}{r_o}\right)^4 + \frac{1}{2}\left(\frac{r_i}{r_o}\right)^2 - \frac{1}{4} = 0$$

Equation Set 3-14:

Viscous-turbulent annular flow, analytical

$$\frac{\frac{\partial p}{\partial z}}{\left(\frac{\partial p}{\partial z}\right)_v} = \frac{\zeta}{\zeta_p}\left(\frac{r_o}{r_i}\right)^5 \left\{1 + \frac{2 r_i^2 \left(\frac{r_i^2}{2} - \frac{r_o^2}{2}\right)}{\left[-\left(\frac{r_o^4}{4} - \frac{r_i^4}{4}\right) + r_o^2\left(\frac{r_o^2}{2} - \frac{r_i^2}{2}\right)\right]} \frac{\rho_v}{\rho_\ell}\frac{w_\ell}{w_v} + \right.$$

$$\left. \frac{r_i^4 \left(\frac{r_i^2}{2} - \frac{r_o^2}{2}\right)^2}{\left[-\left(\frac{r_o^4}{4} - \frac{r_i^4}{4}\right) + r_o^2\left(\frac{r_o^2}{2} - \frac{r_i^2}{2}\right)\right]^2} \left(\frac{\rho_v}{\rho_\ell}\frac{w_\ell}{w_v}\right)^2 \right\}$$

Equation Set 3-15:

Void fraction versus pressure drop

$$\phi_{\ell tt} = \frac{1}{\left(1 - \sqrt{\alpha}\right)\left(1 + \frac{8}{7}\sqrt{\alpha}\right)^{7/8}} \quad \text{, analytical, Reference 19*}$$

$$\phi_{\ell tt} = \frac{1}{\left(1 - \sqrt{\alpha}\right)^{1/2}\left(1 + \frac{8}{7}\sqrt{\alpha}\right)^{7/8}} \quad \text{, analytical, Reference 22*}$$

Equation Set 3-16:

Turbulent annular film

$$k_t = 0.0131 \frac{w_\ell \, c_{p_\ell}}{\pi \, r_o} \quad \frac{1}{1 + 1.14\left(\frac{r_i}{r_o}\right)} \quad \text{, analytical}$$

*References are listed at the end of Chapter 3.

Equation Set 3-17:

Wetted rivulet flow, analytical

$$\frac{h_b}{h_v} = \frac{h_{an\ film}}{h_v} F^2 + (1 + F)$$

$$F = \frac{\sin\alpha}{\pi r_o} \sqrt{\frac{2\pi r_o \delta}{\alpha - \frac{1}{2}\sin 2\alpha}} \quad \text{for } \alpha_c < \alpha < 90°$$

$$F = \frac{\sin(\pi - \alpha)}{\pi r_o} \sqrt{\frac{2\pi r_o \delta}{\alpha + \frac{1}{2}\sin(\pi - \alpha)}} \quad \text{for } 90 < \alpha < 180°$$

Equation Set 3-19:

Annular flow with entrainment, analytical

(1) $$F' = \left[\frac{\left(-\frac{\partial p}{\partial z}\right)\left(\frac{r_o}{2}\right)}{\rho_f} \right] \frac{\rho_v}{G_v} \; R \left[\frac{g \rho_f}{-\frac{\partial p}{\partial z}} \right]^{-n}$$

(2) $$R = \left(\frac{\rho_f}{\rho_v}\right)^{1/3} \text{ for } 1 < \frac{\rho_f}{\rho_v} < 200$$

$$n = 0 \text{ for } -\frac{\partial p}{\partial z} \geqslant g \rho_f$$

$$n = 1/3 \text{ for } -\frac{\partial p}{\partial z} \leqslant g \rho_f$$

(3) $$\tau_w = \left[\left(-\frac{\partial p}{\partial z}\right) - g \rho_f \left(1 - \frac{r_i^2}{r_o^2}\right) \right] \frac{r_o}{2}$$

(4) $$w_f = \frac{2}{r_o} \mu_f F(y^+)$$

(5) $F(y^+) = 3y^+ + 2.5y^+ \ln y^+ - 64$ for $y^+ > 30$

$F(y^+) = 12.5 - 8.05y^+ + 5y^+ \ln y^+$ for $5 < y^+ < 30$

$F(y^+) = 0.5y^{+2}$ for $y^+ < 5$

$$y^+ = y\sqrt{\left(\frac{\tau_w}{\rho_\ell}\right)\frac{\rho_\ell}{\mu_\ell}}$$

Equation Set 3-21:

Single phase turbulent

$$\frac{Nu_b}{Re_b^{0.8}\, Pr_b^{0.4}} = C\,\phi_1\left(\frac{\ell}{D}\right)\,\phi_2\,(T_w, T_b)$$, semi-empirical

$C\,\phi_1 = 0.021\left[1 + \left(\frac{\ell}{D}\right)^{-0.7}\right]$, semi-empirical, References 33, 39

$C\,\phi_1 = 0.034\left(\frac{L}{D}\right)^{-0.1}$, semi-empirical, References 32, 38

Equation Set 3-23:

Single phase turbulent

$$\frac{\zeta}{\zeta_{ad}} = \left[\frac{1}{2}\left(1 + \frac{T_w}{T_b}\right)\right]^{-\frac{1}{2}} \quad \text{, semi-empirical}$$

Equation Set 3-24:

Helical flow single phase

$$\frac{\zeta_h}{\zeta} = \left[1 + \left(\frac{\pi}{p/D}\right)^2\right]^{1.5} \frac{D_\ell}{D_h} \quad \text{, analytical}$$

Equation Set 3-25:

Helical flow single phase

$$\frac{Nu_{forced}}{Nu_\ell} = \left[1 + \left(\frac{\pi}{p/D}\right)^2\right]^{0.4} \left(\frac{D_h}{D_\ell}\right)^{0.8} \quad \text{, analytical}$$

$$\frac{Nu_{free}}{Nu_{\ell}} = 7.1 \frac{(\beta \Delta T)^{1/3}}{Re_{\ell}^{0.13}\ Pr^{0.07}} \left(\frac{\pi}{p/D}\right)^{2/3} \left(\frac{D_t}{D_{\ell}}\right)^{2/3}$$

$$\frac{Nu_h}{Nu_{\ell}} = \frac{Nu_{forced}}{Nu_{\ell}} + \frac{Nu_{free}}{Nu_{\ell}}$$

$$D_{\ell} = D_h = D_t$$

} analytical

Equation Set 3-26:

Helical wetted rivulet flow, analytical

$$\frac{h_{vap}}{|F_1|} = (1 - x)^{8/15} x^{1/5}$$

$$|F_1| = \left[\frac{6.6\ L^{0.4}\ k_v^{0.6}\ w^{1.2}}{8^{8/15}\ \Delta T^{0.4}\ (\frac{2}{D})^{1.2}\ (\frac{D^2}{2})^{1.2}\ D\ \rho_v^{1.2}} \frac{\rho_{\ell}^{0.2}\ \rho_v^{0.2}}{(g)^{0.4}}\right] \left(\frac{\rho_v}{\rho_{\ell}}\right)^{8/15}$$

Equation Set 3-28: analytical:

$$\frac{D_h}{D} = \frac{\sqrt{1 + \left(\frac{\pi D}{p}\right)^2} - 1}{\left(\frac{\pi D}{p}\right)^2 \left[\frac{1}{2\sqrt{1 + \left(\frac{\pi D}{p}\right)^2}} + \frac{\frac{\pi D}{p}}{2\left[1 + \left(\frac{\pi D}{p}\right)^2\right]} + \frac{1}{m\pi} \right]}$$

m = 1 for twisted tape

m = 2 for helical vane

Equation Set 3-32:

Helical wires single phase, analytical, Reference 25

$$\frac{\zeta_{hw}}{\zeta_p} = \left\{ 1 + \frac{\left(\frac{\pi D}{p}\right)^2}{\left[\kappa\left(1+\left(\frac{\pi D}{p}\right)^2\right)\right]^{1/2}+1} \right\}^{3/2} + \frac{\left(\frac{\pi D}{p}\right)^3}{\left\{\left[\kappa\left(1-\left(\frac{\pi D}{p}\right)^2\right)\right]^{1/2}-1\right\}^2}$$

$$\kappa = \frac{\pi \zeta_p D}{4 C_{D_m} d_w}$$

$$C_{D_m} = 1.41\left(\frac{d_w}{D}\right)^{2/7} C_{D_w}$$

For round wires, $C_{D_w} \sim 1.0$

Equation Set 3-33:

Helical wires single phase, analytical, Reference 25

$$\frac{v}{v_{\text{without slip}}} = \frac{1}{\left\{\kappa\left[1+\left(\frac{\pi D}{p}\right)^2\right]\right\}^{1/2}+1}$$

κ is defined in Equation Set 3-32.

APPENDIX B:

EQUATION SETS FOR CHAPTER 4

The experimental, semi-empirical, and analytical equation sets for Chapter 4 are presented below.

Equation Set 4-3: Analytical

$$y_d^+ = \frac{D_d}{2} \frac{\rho_\ell u_\ell \sqrt{\frac{f}{8}}}{\mu_\ell}$$

$$\frac{f \rho_\ell u_\ell^2 D_d}{32 g_c \sigma \phi} + \frac{D_d^2 (\rho_\ell - \rho_v) g}{12 \sigma \phi g_c} = 1$$

For $y_d^+ < 5$

$$\frac{T_{sat} - T_B}{q} \left[c_p \rho_\ell u_\ell\right] = \frac{1}{\sqrt{\frac{f}{8}}} \left\{ P_r \left(5 - y_d^+\right) + 5 \ln (1 + 5 Pr) + 2.5 \left[\frac{\ln \frac{y_{CL}^+}{30}}{1 - \frac{30}{y_{CL}^+}} - 1 \right] \right\}$$

For $30 < y_d^+$

$$\frac{T_{sat} - T_B}{q} \left[c_p \rho_\ell u_\ell\right] = \frac{2.5}{\sqrt{\frac{f}{8}}} \left[\frac{\ln \frac{y_{CL}^+}{y_d^+}}{1 - \frac{y_d^+}{y_{CL}^+}} - 1 \right] \left[1 - \frac{y_d^+}{y_{CL}^+}\right]$$

$0.02 < \phi < 0.03$

Equation Set 4-5: Semi-Empirical

$$F_1 = \frac{T_w - T_o}{\Delta T_s} = \tanh\left(\frac{z - z_o}{\Delta \ell}\right)$$

Length required to heat liquid to saturation in the absence of boiling:

$$\Delta \ell = \frac{A_c}{\xi_h q} \rho_\ell u_\ell c_p (T_s - T_o)$$

Equation Set 4-6:

$$\langle\alpha\rangle = \frac{\frac{q}{\rho_\ell L}\frac{\xi_h}{A_c}(z - z_o) - u_{\ell_i}\frac{\rho_\ell c_p \Delta T_s}{\rho_v L}F_1}{C_o\left\{\frac{q}{\rho_\ell L}\left(\frac{\xi_h}{A_c}(z - z_o)\right) - \frac{u_{\ell_i}\rho_\ell c_p \Delta T_s F_1}{\rho_v L}\right\}\left\{\frac{\rho_\ell - \rho_v}{\rho_\ell}\right\} + \left\{c_p u_{\ell_i} + F_2\right\}\left\{1 + \frac{c_p \Delta T_s (1 - F_1)}{L}\right\}}$$

$$F_1 = \frac{T_w - T_o}{\Delta T_s} \quad \text{(from Equation Set 4-5)}$$

$$F_2 = 1.18\left[\frac{\sigma g (\rho_\ell - \rho_v)}{\rho_\ell^2}\right]^{1/2}$$

The initial point of vapor generation for water has been found empirically to be approximated by

$$\frac{T_s - T_o}{q} u_{\ell_i} = 14 + 0.1p$$

where u_{ℓ_i} is given in $\frac{cm}{sec}$

and p is in atmospheres.

Equation Set 4-7: **Semi-Empirical**

$$u_\ell^* > 1.5$$

$$u_v^* = \frac{\left(7 + 0.06 \frac{\rho_\ell}{\rho_v}\right)}{\sqrt{\frac{\rho_\ell}{\rho_v}}} u_\ell^*$$

$$u_\ell^* < 1.0$$

$$u_v^* = 0.9 + 0.6\, u_\ell^*$$

Equation Set 4-11 **Analytical**

$$V_v = \frac{2\sqrt{3}}{3} \left\{ \frac{g_e \frac{\rho_\ell}{\rho_v} D_p + \frac{6\sigma g_c}{\rho_v D_p}}{C_D} \right\}^{1/2}$$

Equation Set 4-18: Analytical

$$X_B = \frac{\left(\frac{q}{A}\right)_B \pi D \ell}{w_t L}$$

Equation Set 4-20: Analytical

$$\frac{2\delta}{\pi r_o} = \frac{\alpha_c - \frac{1}{2}\sin 2\alpha_c}{(\sin \alpha_c)^2}$$

Equation Set 4-21: Analytical

(1) Viscous-viscous annular flow (Chapter 3)

(2) Equation Set 4-20

Equation Set 4-23: **Analytical**

$$\bar{v}_t = \frac{1}{1-\mu}\left\{1-\mu\,\frac{(1+\mu)-(1-\mu)e^{-k_1\bar{\ell}}}{(1+\mu)+(1-\mu)e^{-k_1\bar{\ell}}}\right\}$$

$$\kappa_1 = 4\sqrt{\frac{\pi\zeta C_{D_m} d_w}{D\left[1+\left(\frac{\pi D}{p}\right)^2\right]}}$$

$$\mu = \sqrt{\kappa\left[1+\left(\frac{\pi D}{p}\right)^2\right]}$$

$$\kappa = \frac{\pi\zeta D}{4\,C_{D_m} d_w}$$

$$\bar{\ell} = \frac{\ell_a}{p}$$

$$\bar{v}_t = \frac{v_t}{v_{t_f}}$$

Equation Set 4-26: Analytical

Small Slip Model:

$$\frac{z}{D} = \frac{p}{D\pi}\left[\frac{3}{8} C_D \frac{D}{D_\rho} \frac{\rho_v}{\rho_\ell}\right]^{1/2}\left[1 - \left(\frac{2 r_o}{D}\right)^{1/2}\right]$$

The large slip model is not easily represented in closed form. See Reference 5 for computational details.

Equation Set 4-28.

The analysis does not yield a result in closed form. The definition of ΔT_1 is

$$\Delta T_1 = \frac{\left(T_1\right) - \left(T_{\text{inside wall at } -\infty}\right)}{\left[\left(T_{\text{outside wall}}\right) - \left(T_{\text{inside wall}}\right)\right]_{-\infty}}$$

Equation Set 4-34 **Analytical**

Surface vaporization (constant contact area), Reference 35.

$$\theta_\ell = \frac{8 \rho_\ell L r_s^2 g_c}{9 k_\ell (T_w - T_s) f_c g} \left(\frac{r_s}{r_d}\right)^4$$

Surface temperature for minimum vaporization lifetime for surface vaporization

$$\Delta p_v = \frac{2 \sigma \cos \alpha}{r_p}$$

Change in lifetime with spallation

$$\frac{\theta_{\ell_n}}{\theta_{\ell_{n=1}}} = \left(\frac{\text{volume of divided droplet}}{\text{volume of undivided droplet}}\right)^{7/15} = \left(\frac{1}{n}\right)^{7/15}$$

Film boiling on a smooth surface

$$\theta_{\ell} = \frac{30\zeta^{1/5}}{7(160)^{1/5}} \frac{\rho_{\ell}^{4/5} L^{3/5} r_{d_o}^{7/5}}{\rho_v^{1/5} (T_w - T_s)^{3/5} k_v^{3/5} g^{1/5}}$$

The relationships for oscillating droplets and for film boiling are not in closed form. Derivations and results may be found in Reference 35.

NOMENCLATURE FOR APPENDIX B

A_c	=	flow cross section
C_0	=	a phase distribution parameter
C_D	=	drag coefficient
C_{D_m}	=	drag coefficient for a wire against a wall, modified for tube boundary layer
c_p	=	liquid specific heat
D	=	tube inside diameter
D_d	=	vapor bubble diameter at departure from wall
D_e	=	equivalent diameter of passage
D_p	=	entrained droplet diameter
d	=	droplet diameter
d_w	=	helical wire insert diameter
F_1	=	functions defined in equation set 4-6
F_2	=	functions defined in equation set 4-6
F_d	=	vapor drag force
F_g	=	gravitational force

F_σ = surface tension force

f = friction factor

f_c = fraction of droplet base area in direct contact with surface

G = mass flow rate per unit of passage cross section

g = acceleration of gravity

g_c = proportionality constant in Newton's second law

g_e = acceleration of gravity for earth

H = normalized conductance defined by $H = \frac{h}{h_{x = 100\%}}$

h = heat transfer conductance

h_ℓ = heat transfer conductance between wall and liquid layer

h_v = heat transfer conductance between wall and liquid vapor

k_1 = a dimensionless parameter defined in equation set 4-23

k_ℓ = thermal conductivity of liquid

k_v = thermal conductivity of vapor

k_w = thermal conductivity of wall material

L = latent heat of vaporization

ℓ = axial tube length

$\bar{\ell}_1$ = normalized length defined in equation set 4-23

ℓ_a = axial length in tube

ℓ_B = location in tube where "burnout" occurs

P_r = Prandtl modulus of liquid

p = helical boiler tube insert pitch

q = heat flux

$(\frac{q}{A})_B$ = "burnout" heat flux

r_0 = tube radius, helical insert centerbody radius

r_d = radius flat disk with volume equal to that of round drop

r_{d_o} = initial drop radius

r_p = meniscus radius of liquid-vapor interface in surface cavity

r_s = radius of round drop

T_0 = liquid bulk temperature at point of first void formation

T_1 = temperature on the heat transfer wall at a conductance discontinuity

T_B = mixed mean (bulk) temperature

T_{sat} = equilibrium saturation temperature

T_w = temperature of the heat transfer surface

u_ℓ = liquid velocity

u_{ℓ_i} = liquid inlet velocity

u_ℓ^* = superficial liquid velocity (mean velocity if liquid only flowed in the tube)

u_v^* = superficial vapor velocity (mean velocity if vapor only flowed in the tube)

V_v = vapor velocity in core of annular flow

v_t = transverse velocity component at the wall in helical flow, assuming solid body rotation

$\bar{v}_t$ = normalized velocity component normal to tube axis

v_{t_f} = helical flow transverse velocity component for fully established flow

W_t = total mass flow in tube

x = vapor quality

x_B = quality at location in tube where "burnout" occurs

y^+_{CL} = y^+ evaluated with the tube radius rather than the bubble radius

y^+_d = defined in equation set 4-3

z = axial distance

GREEK SYMBOLS

α = contact angle

$\langle\alpha\rangle$ = average void fraction at an axial station

α_c = critical contact angle at film rupture

δ = annular liquid film thickness

δ = tube wall thickness

$\Delta\ell$ = a length scale defined in equation set 4-5

Δp_v = excess pressure above liquid saturation pressure at local temperature in cavity

ΔT = heat transfer temperature difference

ΔT_1 = defined in equation set 4-28

$\Delta T_s = T_{sat} - T_o$

$\Delta T_{superheat} = T_{liquid} - T_{sat}$

ζ = friction factor for a smooth tube

θ_ℓ = lifetime of liquid droplet on a hot surface

$\theta\ell_n$ = lifetime of one of n equal droplets resulting from spallation

κ = a parameter in equation set 4-23

μ = a parameter in equation set 4-23

μ_ℓ = liquid viscosity

ξ_h = heated perimeter

ρ_ℓ = liquid density

ρ_v = vapor density

σ = surface tension

ϕ = an experimentally evaluated bubble contact angle function

DIFFERENTIALS

$\frac{\partial p}{\partial z}$ = two phase pressure gradient

APPENDIX C: ILLUSTRATIVE HEAT TRANSFER AND PRESSURE DROP DERIVATIONS

1. Linear, Nonwetting Slug Flow Heat Transfer

It is postulated that alternate slugs of liquid and vapor flow through the boiler tube; the vapor slugs have dry walls. It is presumed that heat transfer from the boiler tube to the liquid and vapor slugs is defined in terms of the wall-to-saturation temperature difference and liquid and vapor convective conductances. It is postulated that the mixed mean or bulk temperature of a vapor slug is equal to the saturation temperature. The mean heat transfer conductance is then defined as

$$h(x) = h_{\ell}(x)\, y_{\ell}(x) + h_{v}(x)\, y_{v}(x) \qquad \text{(a)}$$

where h_{ℓ} and h_{v} are the liquid and vapor slug conductances, respectively, y_{ℓ} and y_{v} are the liquid and vapor volume fractions respectively, and x is the vapor quality.

The relation between vapor quality and the volume fraction for this flow type is,

$$x = \frac{1}{1 + \frac{w_\ell}{w_v}\frac{y_\ell}{y_v}} = \frac{1}{1 + \frac{w_\ell}{w_v}\left(\frac{y_\ell}{1 - y_\ell}\right)} \qquad \text{(b)}$$

where w_ℓ and w_v are the liquid and vapor weight densities, respectively.

The convective conductance for the liquid slugs in Equation (a) can be expressed in terms of the classical Nusselt viscous flow equation with uniform wall heat addition,

$$h_\ell = \frac{48}{11}\frac{k_\ell}{D} \qquad \text{(c)}$$

where k_ℓ is the thermal conductivity of the liquid and D is the tube diameter.

The convective conductance for a vapor slug under viscous flow is

$$h_v = \frac{48}{11}\frac{k_v}{D} \qquad \text{(d)}$$

The corresponding function for turbulent flow is

$$h_v = h_v(x = 1)\left(\frac{W_v(x)}{W_v(x = 1)}\right)^{0.8}$$

$$= h_v(x = 1)\,(x)^{0.8} \qquad \text{(e)}$$

where

$$h_v(x=1) = 0.023 \frac{k_v}{D} Re_v^{0.8}(x=1)\, Pr_v^{0.4} \qquad (f)$$

The quantity W_v is the vapor flow rate, k_v is the vapor thermal conductivity, Re_v is the vapor Reynolds modulus and Pr_v is the vapor Prandtl modulus.

The substitution of Equations (b) to (f) into Equation (a) yields

$$\frac{h(x)}{h_v(x=1)} = H = \frac{190}{k_v/k_\ell\, Re_v^{0.8}(x=1)\, Pr_v^{0.4}} \left(\frac{1-x}{1+\left(\frac{w_\ell}{w_v} - 1\right) x} \right)$$

$$+ x^{0.8} \left(1 - \frac{1-x}{1+\left(\frac{w_\ell}{w_v} - 1\right) x} \right) \qquad (g)$$

for turbulent gas flow.

The corresponding substitutions yield

$$H = \left(\frac{k_\ell}{k_v} - 1 \right) \left(\frac{1-x}{1+\left(\frac{w_\ell}{w_v} - 1\right) x} \right) + 1 \qquad (h)$$

for viscous gas flow.

Equations (g) and (h) have been evaluated for properties that are representative of mercury in Figure 3-8 of Chapter 3.

2. Annular Flow Pressure Drop (for Viscous-Turbulent Flow)

Consider the case of a viscous annulus contiguous to the tube wall with an inner turbulent core. The pressure drop for the turbulent core ($0 < r < r_1$) is,

$$\frac{\partial p}{\partial x} = \frac{\zeta w_1}{2 r_1} \frac{V^2}{2g} \tag{i}$$

where

r , radial distance

r_1 , radius of the turbulent core

p , pressure

x , axial distance

ζ , Weisbach friction factor

w_1 , density of turbulent fluid

V , average velocity of turbulent fluid with respect to the moving interface

The mass flow rate of the turbulent core is

$$G_1 = \pi r_1^2 w_1 (v_1 + V) \tag{j}$$

where the velocity of the moving interface at $r = r_1$ is v_1.

The quantity v_1 is obtained by equating the shear stress-pressure drop function,

$$\tau = \frac{\partial p}{\partial x} \frac{r}{2} \tag{k}$$

to the shear stress-shear strain function,

$$\tau = - \mu \frac{du}{dr} \tag{l}$$

The result is

$$v_1 = - \frac{1}{2 \mu_o} \frac{\partial p}{\partial x} \left(\frac{r_1^2}{2} - \frac{r_o^2}{2} \right) \tag{m}$$

where

μ_o , viscosity of viscous fluid

r_o , inside pipe radius

The substitution of Equations (j) and (m) into Equation (i) yields,

$$\frac{\partial p}{\partial x} = \frac{\partial p}{\partial x_{TP}} = \frac{\zeta w_1}{4 r_1 g} \left[\frac{G_1^2}{\pi^2 r_1^4 w_1^2} \right.$$

$$+ \frac{1}{\mu_o} \frac{\partial p}{\partial x} \left(\frac{r_1^2}{2} - \frac{r_o^2}{2} \right) \frac{G_1}{\pi r_1^2 w_1}$$

$$\left. + \frac{1}{4 \mu_o^2} \left(\frac{\partial p}{\partial x} \right)^2 \left(\frac{r_1^2}{2} - \frac{r_o^2}{2} \right)^2 \right] \qquad \text{(n)}$$

If the turbulent fluid in the core fills the whole pipe, the pressure drop function would be

$$\left(\frac{\partial p}{\partial x} \right)_{1p} = \frac{\zeta_p G_1^2}{4 \pi^2 g r_o w_1} \qquad \text{(o)}$$

where the subscript 1p refers to the inner turbulent fluid.

Upon dividing Equation (n) by Equation (o) there results,

$$\frac{\left(\frac{\partial p}{\partial x}\right)_{TP}}{\left(\frac{\partial p}{\partial x}\right)_{lp}} = \frac{\zeta}{\zeta_p}\left(\frac{r_o}{r_1}\right)^5 \left[1 + \frac{2 r_1^2 w_1 \left(\frac{r_1^2}{2} - \frac{r_o^2}{2}\right)}{w_o\left[-\left(\frac{r_o^4}{4} - \frac{r_1^4}{4}\right) + r_o^2\left(\frac{r_o^2}{2} - \frac{r_1^2}{2}\right)\right]}\frac{G_o}{G_1}\right.$$

$$\left. + \frac{r_1^4 w_1^2 \left(\frac{r_1^2}{2} - \frac{r_o^2}{2}\right)^2}{w_o^2\left[-\left(\frac{r_o^4}{4} - \frac{r_1^4}{4}\right) + r_o^2\left(\frac{r_o^2}{2} - \frac{r_1^2}{2}\right)\right]^2}\left(\frac{G_o}{G_1}\right)^2\right] \quad (p)$$

where

$$G_o = 2\pi w_o \left[-\frac{1}{4\mu_o}\frac{\partial p}{\partial x}\left(\frac{r_o^4}{4} - \frac{r_1^4}{4}\right) + \frac{r_o^2}{4\mu_o}\frac{\partial p}{\partial x}\left(\frac{r_o^2}{2} - \frac{r_1^2}{2}\right)\right]$$

(q)

Upon equating the pressure drop terms in the two fluids, a complicated algebraic equation for r_1/r_o results (not shown here) in terms of ζ and the dimensionless moduli

$$\frac{g r_o \mu 1}{G_1} \quad , \quad \frac{G_o w_1}{G_1 w_o} \quad , \text{ and } \frac{G_1 \mu_1 w_o}{G_o \mu_o w_1} \; ;$$

thus, the two phase flow pressure drop ratio in Equation (p) is also a function of these moduli.

APPENDIX D: COMMENTS ON SOME ASSOCIATED TOPICS

There are a number of associated technical topics that the boiler designer should be aware of, and several of them are briefly outlined below:

1. Fluid Flow Stability in Boilers

   The boiler designer should have some understanding of fluid flow stability in single and multitube boilers. The flow dynamics in both cases are related to such parameters as nonuniform tube heating, liquid superheating, differences between the densities of the liquid and vapor, differences in pressure drop with flow regime type, and others.

   On a practical basis, flow restrictors in the form of orifices are used in multitube systems to assist in balancing the nonuniform flow patterns. There are a number of references in the literature for the reader if further information on this topic is desired (see references 1 to 4, for example).

2. Nonequilibrium Effects

   There are some working fluids that can sustain significant amounts of liquid superheat; this phenomenon can occur even in forced flow systems. One working fluid that exhibits a significant amount of superheat prior to flashing into steady state boiling is potassium.[5] Although this problem

is generally not a critical one, the boiler designer should be cognizant of the fact that a sudden change in boiling state can occur with some working fluids, resulting in sudden changes in pressure and fluid flow. Likewise, techniques have been developed to overcome this phenomenon wher it does occur such as the use of boiling initiators, artificial cavities, and local high temperature surfaces.

3. Working Fluid Stability

The power plant designer must make a choice of the working fluids to be used in his system; the choice is usually based on a number of considerations. Ideally, it is desirable to have a working fluid that has good thermal properties so that optimum heat transfer performance can be obtained. In addition, it is necessary that the thermodynamic properties are also optimum (to yield good cycle performance). For many applications, the working fluid should be nontoxic, nonflammable, noncorrosive, and of low cost.

A final criterion is that the working fluid should have good chemical stability over the range of operating temperatures so that the fluid properties do not change with time or so that the decomposition products do not foul the prime heat transfer surfaces. It is suggested that the designer consult references on fluid decomposition, such as 6 and 7, for further information on this topic.

4. "Boiler Conditioning"

There are certain working fluids (primarily the liquid metals) which can exhibit heat transfer performance changes with time. Such fluids

must operate in very clean environments and the fluids themselves must be fairly pure. Oxygen, nitrogen, and lubricating oil leaks must not occur; if such foreign materials do enter the system, the surface physics and chemistry can change significantly so that a normally wetting fluid-wall system can be transformed to a partially or totally nonwetting system, thereby changing phase distributions and boiler performance. It is suggested that the boiler designer consult reference 8 which provides more information on this topic.

References

1. Quartd, E. R.: "Analysis of Parallel Channel Transient Response and Flow Oscillations," WAPD-AD-TH-489, April 1959.

2. Wallis, G. B.; Heasley, J. H.; "Oscillations in Two-Phase Flow Systems," J Heat Transfer, pp 363-369, Aug 1961.

3. Hooper, J. R.; Kung, H. R.: "Experimental Investigation of Heat Rejection Problems in Nuclear Space Power Plants," Vol 3, Space Power Plant Startup and Transient Operation Simulation, PWA 2227, June 1, 1962 to March 31, 1963.

4. Hess, H. L.: Hooper, J. R.: Organ, S. L.: "Analytical and Experimental Study of the Dynamics of a Single-Tube Counterflow Boiler," NASA CR-1230, Feb 1969.

5. Sabin, C. M.: Poppendiek, H. F. "Liquid Metal Boiling Inception," NASA CR-2095, Aug 1972.

6. Voorhies, Alexis, Jr.: "Carbon Formation in Catalytic Cracking," Industrial and Engineering Chemistry, Vol 37, Part 1, 1945.

7. Gunderson, R. C.: Hart, A. W.: "Synthetic Lubricants," Reinhold Publishing Company, 1962.

8. Poppendiek, H. F.: " SNAP-8 Boiler Performance Degradation and Two-Phase Flow Heat and Momentum Transfer Models," NASA CR 72759, Geoscience Ltd GLR-84, Aug 1970.